1995

Theory Of Spin Waves In Heisenberg Ferromagnetic And Antiferromagnetic Thin Films With Nonuniaxial Single-ion Anisotropy

Paula R. Heron

NOTICE

The quality of this microform is heavily dependent upon the quality of the original thesis submitted for microfilming. Every effort has been made to ensure the highest quality of reproduction possible.

If pages are missing, contact the university which granted the degree.

Some pages may have indistinct print especially if the original pages were typed with a poor typewriter ribbon or if the university sent us an inferior photocopy.

Reproduction in full or in part of this microform is governed by the Canadian Copyright Act, R.S.C. 1970, c. C-30, and subsequent amendments.

AVIS

La qualité de cette microforme dépend grandement de la qualité de la thèse soumise au microfilmage. Nous avons tout fait pour assurer une qualité supérieure de reproduction.

S'il manque des pages, veuillez communiquer avec l'université qui a conféré le grade.

La qualité d'impression de certaines pages peut laisser à désirer, surtout si les pages originales ont été dactylographiées à l'aide d'un ruban usé ou si l'université nous a fait parvenir une photocopie de qualité inférieure.

La reproduction, même partielle, de cette microforme est soumise à la Loi canadienne sur le droit d'auteur, SRC 1970, c. C-30, et ses amendements subséquents.

Canada

THEORY OF SPIN WAVES
IN HEISENBERG FERROMAGNETIC AND ANTIFERROMAGNETIC THIN FILMS
WITH NONUNIAXIAL SINGLE-ION ANISOTROPY

by

Paula R.L. Heron

Department of Physics

Submitted in partial fulfilment
of the requirements for the degree of
Doctor of Philosophy

Faculty of Graduate Studies
The University of Western Ontario
London, Ontario
July 1995

ISBN 0-612-03459-3

Name Paula R L. Heron

Dissertation Abstracts International is arranged by broad, general subject categories. Please select the one subject which most nearly describes the content of your dissertation. Enter the corresponding four-digit code in the spaces provided.

Physics - Solid State
SUBJECT TERM

0611
SUBJECT CODE

U·M·I

Subject Categories

THE HUMANITIES AND SOCIAL SCIENCES

COMMUNICATIONS AND THE ARTS
- Architecture 0729
- Art History 0377
- Cinema 0900
- Dance 0378
- Fine Arts 0357
- Information Science 0723
- Journalism 0391
- Library Science 0399
- Mass Communications 0708
- Music 0413
- Speech Communication 0459
- Theater 0465

EDUCATION
- General 0515
- Administration 0514
- Adult and Continuing 0516
- Agricultural 0517
- Art 0273
- Bilingual and Multicultural 0282
- Business 0688
- Community College 0275
- Curriculum and Instruction 0727
- Early Childhood 0518
- Elementary 0524
- Finance 0277
- Guidance and Counseling 0519
- Health 0680
- Higher 0745
- History of 0520
- Home Economics 0278
- Industrial 0521
- Language and Literature 0279
- Mathematics 0280
- Music 0522
- Philosophy of 0998
- Physical 0523
- Psychology 0525
- Reading 0535
- Religious 0527
- Sciences 0714
- Secondary 0533
- Social Sciences 0534
- Sociology of 0340
- Special 0529
- Teacher Training 0530
- Technology 0710
- Tests and Measurements 0288
- Vocational 0747

LANGUAGE, LITERATURE AND LINGUISTICS
- Language
  - General 0679
  - Ancient 0289
  - Linguistics 0290
  - Modern 0291
- Literature
  - General 0401
  - Classical 0294
  - Comparative 0295
  - Medieval 0297
  - Modern 0298
  - African 0316
  - American 0591
  - Asian 0305
  - Canadian (English) 0352
  - Canadian (French) 0355
  - English 0593
  - Germanic 0311
  - Latin American 0312
  - Middle Eastern 0315
  - Romance 0313
  - Slavic and East European 0314

PHILOSOPHY, RELIGION AND THEOLOGY
- Philosophy 0422
- Religion
  - General 0318
  - Biblical Studies 0321
  - Clergy 0319
  - History of 0320
  - Philosophy of 0322
- Theology 0469

SOCIAL SCIENCES
- American Studies 0323
- Anthropology
  - Archaeology 0324
  - Cultural 0326
  - Physical 0327
- Business Administration
  - General 0310
  - Accounting 0272
  - Banking 0770
  - Management 0454
  - Marketing 0338
- Canadian Studies 0385
- Economics
  - General 0501
  - Agricultural 0503
  - Commerce-Business 0505
  - Finance 0508
  - History 0509
  - Labor 0510
  - Theory 0511
- Folklore 0358
- Geography 0366
- Gerontology 0351
- History
  - General 0578
  - Ancient 0579
  - Medieval 0581
  - Modern 0582
  - Black 0328
  - African 0331
  - Asia, Australia and Oceania 0332
  - Canadian 0334
  - European 0335
  - Latin American 0336
  - Middle Eastern 0333
  - United States 0337
- History of Science 0585
- Law 0398
- Political Science
  - General 0615
  - International Law and Relations 0616
  - Public Administration 0617
- Recreation 0814
- Social Work 0452
- Sociology
  - General 0626
  - Criminology and Penology 0627
  - Demography 0938
  - Ethnic and Racial Studies 0631
  - Individual and Family Studies 0628
  - Industrial and Labor Relations 0629
  - Public and Social Welfare 0630
  - Social Structure and Development 0700
  - Theory and Methods 0344
- Transportation 0709
- Urban and Regional Planning 0999
- Women's Studies 0453

THE SCIENCES AND ENGINEERING

BIOLOGICAL SCIENCES
- Agriculture
  - General 0473
  - Agronomy 0285
  - Animal Culture and Nutrition 0475
  - Animal Pathology 0476
  - Food Science and Technology 0359
  - Forestry and Wildlife 0478
  - Plant Culture 0479
  - Plant Pathology 0480
  - Plant Physiology 0817
  - Range Management 0777
  - Wood Technology 0746
- Biology
  - General 0306
  - Anatomy 0287
  - Biostatistics 0308
  - Botany 0309
  - Cell 0379
  - Ecology 0329
  - Entomology 0353
  - Genetics 0369
  - Limnology 0793
  - Microbiology 0410
  - Molecular 0307
  - Neuroscience 0317
  - Oceanography 0416
  - Physiology 0433
  - Radiation 0821
  - Veterinary Science 0778
  - Zoology 0472
- Biophysics
  - General 0786
  - Medical 0760

EARTH SCIENCES
- Biogeochemistry 0425
- Geochemistry 0996
- Geodesy 0370
- Geology 0372
- Geophysics 0373
- Hydrology 0388
- Mineralogy 0411
- Paleobotany 0345
- Paleoecology 0426
- Paleontology 0418
- Paleozoology 0985
- Palynology 0427
- Physical Geography 0368
- Physical Oceanography 0415

HEALTH AND ENVIRONMENTAL SCIENCES
- Environmental Sciences 0768
- Health Sciences
  - General 0566
  - Audiology 0300
  - Chemotherapy 0992
  - Dentistry 0567
  - Education 0350
  - Hospital Management 0769
  - Human Development 0758
  - Immunology 0982
  - Medicine and Surgery 0564
  - Mental Health 0347
  - Nursing 0569
  - Nutrition 0570
  - Obstetrics and Gynecology 0380
  - Occupational Health and Therapy 0354
  - Ophthalmology 0381
  - Pathology 0571
  - Pharmacology 0419
  - Pharmacy 0572
  - Physical Therapy 0382
  - Public Health 0573
  - Radiology 0574
  - Recreation 0575
  - Speech Pathology 0460
  - Toxicology 0383
- Home Economics 0386

PHYSICAL SCIENCES

Pure Sciences
- Chemistry
  - General 0485
  - Agricultural 0749
  - Analytical 0486
  - Biochemistry 0487
  - Inorganic 0488
  - Nuclear 0738
  - Organic 0490
  - Pharmaceutical 0491
  - Physical 0494
  - Polymer 0495
  - Radiation 0754
- Mathematics 0405
- Physics
  - General 0605
  - Acoustics 0986
  - Astronomy and Astrophysics 0606
  - Atmospheric Science 0608
  - Atomic 0748
  - Electronics and Electricity 0607
  - Elementary Particles and High Energy 0798
  - Fluid and Plasma 0759
  - Molecular 0609
  - Nuclear 0610
  - Optics 0752
  - Radiation 0756
  - Solid State 0611
- Statistics 0463

Applied Sciences
- Applied Mechanics 0346
- Computer Science 0984
- Engineering
  - General 0537
  - Aerospace 0538
  - Agricultural 0539
  - Automotive 0540
  - Biomedical 0541
  - Chemical 0542
  - Civil 0543
  - Electronics and Electrical 0544
  - Heat and Thermodynamics 0348
  - Hydraulic 0545
  - Industrial 0546
  - Marine 0547
  - Materials Science 0794
  - Mechanical 0548
  - Metallurgy 0743
  - Mining 0551
  - Nuclear 0552
  - Packaging 0549
  - Petroleum 0765
  - Sanitary and Municipal 0554
  - System Science 0790
- Geotechnology 0428
- Operations Research 0796
- Plastics Technology 0795
- Textile Technology 0994

PSYCHOLOGY
- General 0621
- Behavioral 0384
- Clinical 0622
- Developmental 0620
- Experimental 0623
- Industrial 0624
- Personality 0625
- Physiological 0989
- Psychobiology 0349
- Psychometrics 0632
- Social 0451

The UNIVERSITY *of* WESTERN ONTARIO

Faculty of Graduate Studies

In the interests of facilitating research by others at this institution and elsewhere, I hereby grant a licence to:

THE UNIVERSITY OF WESTERN ONTARIO

to make copies of my thesis

SPIN WAVES IN ANISOTROPIC MAGNETIC FILMS

or substantial parts thereof, the copyright which is invested in me, provided that the licence is subject to the following conditions:

1. Only single copies shall be made or authorized to be made at any one time, and only in response to a written request from the library of any University or similar institution on its own behalf or on behalf of one of its users.
2. This licence shall continue for the full term of the copyright, or for so long as may be legally permitted.
3. The Universal Copyright Notice shall appear on the title page of all copies of my thesis made under the authority of this licence.
4. This licence does not permit the sale of authorized copies at a profit, but does permit the collection by the institution or institutions concerned of charges covering actual costs.
5. All copies made under the authority of this licence shall bear a statement to the effect that the copy in question "is being made available in this form by the authority of the copyright owner solely for the purpose of private study and research and may not be copied or reproduced except as permitted by the copyright laws without written authority from the copyright owner."
6. The foregoing shall in no way preclude my granting to the National Library of Canada a licence to reproduce my thesis and to lend or sell copies of the same.

R. Cordeiro — *(signature of witness)*

(signature of student)

September 11, 1995	Ph.D.	Physics
(date)	*(degree)*	*(department of student)*

THE UNIVERSITY OF WESTERN ONTARIO

FACULTY OF GRADUATE STUDIES

CERTIFICATE OF EXAMINATION

Chief Advisor

M. G. Cottam

Examining Board

Advisory Committee

P.R. Norton

James D. Talman

M Singh.

The thesis by
Paula R.L. Heron

entitled

Theory of Spin Waves in Heisenberg Ferromagnetic and Antiferromagnetic Thin Films with Nonuniaxial Single-ion Anisotropy

is accepted in partial fulfilment of the requirements for the degree of Doctor of Philosophy

Date September 5, 1995

David Bellhouse

Chair of the Examining Board

ABSTRACT

This thesis describes the microscopic, quantum mechanical theory of exchange-dominated spin waves in Heisenberg ferromagnetic and antiferromagnetic thin films including the effects of *nonuniaxial* single-ion anisotropy. The results constitute a generalization of previous theoretical studies on spin waves in thin films with uniaxial anisotropy and in semi-infinite ferromagnets with nonuniaxial anisotropy.

A spin Hamiltonian containing nearest-neighbour exchange terms, Zeeman terms, and single-ion anisotropy terms is used. The films may be asymmetric with respect to surface exchange and anisotropy parameters which are also assumed to be perturbed from the bulk values. The results apply both to cases in which the nonuniaxial anisotropy is an intrinsic aspect of the material and where it arises only at the surfaces as a consequence of lowered symmetry for those sites. Low temperatures are assumed where the linear spin-wave approximation is valid. The formalism is developed for arbitrary film thickness, arbitrary quantum spin number S, and perpendicular magnetization. Simple cubic (001) ferromagnetic systems and body-centered tetragonal (001) antiferromagnetic systems are specifically examined with extensions to other situations outlined.

A theoretical approach based on the equation-of-motion method is used to find Green functions which provide expressions for the dispersion relations for surface and quantized bulk spin waves, the associated

spectral intensities, transverse spin correlation functions, and the dynamic response of the system in, for example, light scattering and spin wave resonance experiments. Representative numerical examples are provided for the dispersion relation results, some thermodynamic properties related to the mean-squared amplitude and ellipticity of spin precession, and the static magnetization. The use of the Green function results in calculating the light scattering cross-sections and absorption strength in spin wave resonance is outlined. Procedures developed to manage the increased mathematical complication associated with the nonuniaxial anisotropy are described.

ACKNOWLEDGMENTS

I am grateful to my supervisor Michael G. Cottam for his guidance throughout my studies at Western and in the preparation of this thesis.

I wish also to thank Dr. Peter Norton and Dr. Martin Zinke-Allmang for their work as members of my advisory committee. Financial support from NSERC, in the form of a post-graduate scholarship, and from the University of Western Ontario is gratefully acknowledged.

Finally, I wish to thank my family for always supporting and encouraging me in the pursuit of my goals.

TABLE OF CONTENTS

CHAPTER 1

INTRODUCTION

Magnetic thin films and related structures such as superlattices are currently the focus of a great deal of theoretical and experimental study. This interest is motivated in part by the commercial potential of applications in, for example, the magnetic recording industry. These so-called nano-scale structures exhibit some novel properties which have no analogue in bulk samples, one example being the giant magnetoresistance effect (Baibich *et al* 1988, Binasch *et al* 1989). Falicov *et al* (1990) review the field of thin film magnetism, addressing the topics of fabrication, characterization, and applications while a special issue of *Physics Today* (1995) highlights recent developments in thin film magnetoelectronics.

In this thesis we are concerned with ferromagnets and antiferromagnets, materials which spontaneously order below some critical temperature. Far from the critical point, where there is a high degree of long-range order, magnetic properties can be understood in terms of the low-lying magnetic excitations which are *spin waves*. In Heisenberg ferromagnetic and antiferromagnetic thin films there are localized *surface* spin waves and *standing* bulk spin waves, excitations not occurring in effectively infinite samples. The microscopic quantum-mechanical theory of such spin waves has been reviewed by Puszkarski (1970, 1972), Wolfram and DeWames (1972) and more recently by Cottam and Slavin (1994). Cottam and Kontos (1980) have employed a Green-function approach to study spin waves in thin ferromagnetic films using a Heisenberg Hamiltonian in

Heisenberg Hamiltonian in which uniaxial single-ion anisotropy is included and the dipole-dipole interactions are assumed to be negligible.

The present project extends such calculations to the more complicated case of *nonuniaxial* single-ion anisotropy in which a preferred *plane* for the magnetization vector exists, rather than a preferred *axis*. It occurs as a bulk effect in, for example, ferromagnets such as $CrBr_3$ and antiferromagnets such as NiO, NiF_2, and K_2FeF_4. Also, De Jongh and Miedema (1974) catalogue many other nonuniaxial magnetic compounds including K_2CuF_4, Rb_2CuCl_4, $CoCl_2 \cdot 6H_2O$, $CoBr_2 \cdot 6H_2O$, $CrCl_3$, $CsMnCl_3 \cdot 2H_2O$, and $AgCrSe_2$. This type of anisotropy has previously been considered theoretically in the case of effectively infinite (bulk) ferromagnets (e.g. see Kitaev et al 1974, Cottam and Latiff-Awang 1977, and Balucani et al 1980 (a) for microscopic Green-function treatments). An extension to semi-infinite ferromagnets was made by Gopalan and Cottam (1990), who found that the spectrum consists of (at most) one surface mode and a continuum of bulk modes.

In this thesis, by contrast, we find for a nonuniaxial thin film that there may be additional surface modes (up to two) and a series of discrete standing bulk modes, instead of a bulk continuum. Also we show that the inclusion of nonuniaxial anisotropy leads to a spin wave spectrum which differs quantitatively from that found by Cottam and Kontos (1980) for a uniaxial film. In addition, the spin precession (corresponding to the semi-classical depiction of a spin wave) is found to be elliptical as is characteristic of nonuniaxial systems, rather

than circular as for the simple uniaxial case (e.g. see Phillips and Rosenberg 1966).

In our calculations we allow for *surface anisotropy* or surface *pinning* (Kittel 1958). In brief, lowered symmetry of the local environment for spins on the surface may result in anisotropy effects which are different from those found in bulk samples (e.g. see Néel 1954, Rado 1982, 1989, Heinrich and Cochran 1993). In some cases the anisotropy coefficients at the surface may simply be modified in value while in other cases new anisotropy terms may be allowed. An important example for the present study is found in single-crystal (110) Fe films in which the surface exhibits nonuniaxial anisotropy while the bulk does not (Prinz *et al* 1982 and Gradmann *et al* 1986). Early observations of giant magnetoresistance occurred in Fe-Cr-Fe systems (Binasch *et al* 1989) in which these films form the ferromagnetic layers. Mills (1989) and Gopalan and Cottam (1990) have made theoretical studies of surface spin waves in such a case in semi-infinite systems. Falicov *et al* (1990) describe the significance of surface anisotropy for potential applications. For example, the ability to manipulate anisotropy though the combination of bulk and surface (or interface) effects has implications for the introduction of magnetic films into integrated circuit devices and for magneto-optical recording media.

Another surface-related aspect of films is the perturbation at the surface of parameters relating to exchange and any uniaxial anisotropies (e.g. see Lévy 1981). Generally both the number and type of surface spin wave modes are sensitive to the ratio of surface and bulk

parameters (e.g. see Wolfram and Dewames 1972). A magnetic film on a (nonmagnetic) substrate may be asymmetric if the conditions on the two surfaces are different as is the case in many experimental situations. For example the film may have one free surface; the substrate and an overlayer may be of different species; or there may be growth-dependent effects. Previous studies on uniaxial films (e.g. see Puszkarski 1972, Kontos 1985) have shown that asymmetric boundary conditions affect both the bulk and surface spin wave modes. We have included this possibility in our theoretical model in order to model realistic thin film situations.

Nonuniaxial anisotropy in both semi-infinite antiferromagnets and finite-thickness antiferromagnetic films is also studied here, extending previous calculations on *uniaxial* semi-infinite systems (see e.g. Wolfram and DeWames 1972). Nonuniaxial effects in *infinite* antiferromagnets have previously been studied using Green function methods by Cottam and Latiff-Awang (1979) (a).

In this introductory chapter we will discuss the nature of the model chosen to represent these magnets, the particular magnetic properties of interest, and the methodology to be used. In particular some pertinent background material on spin waves is supplied. Relevant experimental techniques are also briefly reviewed. The thesis contents are outlined below where we establish the scope of the project, including some limitations.

1.1 Outline of the Thesis

The choice of Hamiltonian is a central, defining issue in a microscopic quantum-mechanical study such as that described in this thesis. We include Heisenberg exchange and Zeeman terms as well as the single-ion anisotropy terms. The ferromagnetic Hamiltonian is discussed in detail in Section 1.2 while the analogous antiferromagnetic Hamiltonian is presented later in Chapter 5. As in the studies of Cottam and Kontos (1980) and Gopalan and Cottam (1990) the classical magnetic dipole-dipole interaction is not considered here. In most materials it is at once much weaker and much longer range than the exchange interaction which typically affects near neighbours only (e.g. see Wolfram and DeWames 1972). The dipole-dipole interaction is the dominant one for long-wavelength spin waves (*magnetostatic* modes) and is important for experimental techniques which probe this region. However such excitations comprise only a very small part of the Brillouin zone (typically for wavevectors less than about 10^6 cm^{-1} compared with a zone boundary around 10^8 cm^{-1}) and at most temperatures they have little contribution to the static magnetic and thermodynamic properties (see e.g. Wolfram and DeWames 1972). Cottam and Slavin (1994) review spin-wave theory in thin films for cases in which dipole-dipole interactions are included in place of or in addition to exchange.

We have restricted our attention to low temperatures compared with the magnetic transition temperature where, as we have noted, the excitations are spin waves. Hence critical phenomena, spin-wave interactions and other non-linear effects may be neglected (see e.g Phillips and Rosenberg 1966, Keffer 1966, and Callaway 1991). Spin waves in

ferromagnets are discussed briefly in Section 1.4. Chapter 5 contains the corresponding discussion of spin waves in antiferromagnets.

In this thesis the films are considered to be infinite in extent in two dimensions (the x and y directions) and composed of N layers in the z direction. The films may have as few as three layers for ultrathin samples but we have developed the theory for arbitrary $N \geq 3$. A static applied magnetic field in the positive z direction is assumed. In the case of ferromagnets the calculations are carried out explicitly for a simple cubic (001) film with the crystal axes coinciding with the x, y and z axes. Other crystal symmetries and surface orientations may be assumed using the same general formalism and a prescription for doing so is provided in Appendix I. Section 1.3 contains a detailed description of the model of the thin film and the general assumptions made concerning the relative values of exchange and anisotropy parameters for various sites within the film.

In this thesis we make use of standard many-body theory techniques such as the operator equation-of-motion method and the Green function equation-of-motion method, both of which are briefly described in Section 1.5. The Green-function method is used here to determine spin-spin correlation functions and provides a powerful means of investigating the spin fluctuations in the system. We are therefore able, in principle, to study dynamic properties such as light scattering which are not accessible using simple approximations such as molecular field theory (also known as mean field or effective field theory) which neglect fluctuations (see e.g. Kittel 1987, Callaway 1991). We may also

readily calculate static properties such as magnetization which are affected by fluctuations. Finally, Section 1.6 contains a brief discussion of some relevant experimental techniques for studying spin waves in thin films.

The application of the operator equation-of-motion method to ferromagnetic thin films with nonuniaxial anisotropy is described in Chapter 2. A number of special cases are considered and formal results for spin-wave frequencies are derived. Comparisons with previous calculations are made where appropriate. In Chapter 3 the numerical evaluation of spin wave dispersion relations using the formal expressions of Chapter 2 is discussed and results for some specific examples are presented. These results are used to illustrate the effects of film thickness, film asymmetry and relative strength of the anisotropy parameters, etc., on the spin-wave energies.

In Chapter 4 the Green function equation-of-motion method is used to find spin-wave contributions to the spectral intensities and correlation functions. The Green functions also give the dispersion relations which are shown to be identical to those of Chapters 2 and 3. Some static properties (e.g. mean-square amplitude of transverse spin components) are calculated as a function of distance from the surface. Again, comparison with previous results is made where possible and the effects of film thickness and anisotropy parameters etc. on the spin-wave intensities are illustrated with specific numerical examples.

General discussion of the anisotropic antiferromagnets appears in Chapter 5 in which the Green function technique is applied in the case of semi-infinite systems. Numerical dispersion relation and amplitude results for some special cases are presented. The corresponding study of finite-thickness models is the subject of Chapter 6.

Discussion and conclusions follow in Chapter 7. A number of appendices are included. As mentioned above, modifications of the approach to include different crystal lattices, anisotropic exchange, etc., are discussed in Appendix I. Other appendices deal with calculational details.

1.2 The Ferromagnetic Hamiltonian with Single-Ion Anisotropy

The Hamiltonian used is a generalized Heisenberg Hamiltonian divided, for convenience, into two parts $\mathcal{H} = \mathcal{H}_H + \mathcal{H}_A$

$$\mathcal{H}_H = - g\mu_B H_0 \sum_i S_i^z - \frac{1}{2} \sum_{ij} J_{ij}\, \mathbf{S}_i \cdot \mathbf{S}_j$$

$$\mathcal{H}_A = - \sum_i D_i (S_i^z)^2 - \sum_i F_i [(S_i^x)^2 - (S_i^y)^2] \qquad (1.2.1)$$

where the first part contains the Zeeman and exchange terms, and the second contains the single-ion anisotropy terms. In the Zeeman term g is the Landé g-factor, μ_B is the Bohr magneton, and H_0 is an applied field along the positive z axis (i.e. parallel to the film normal). S_i^z is the z component of the spin at site i, which may assume the eigenvalues S, S - 1,..-S. Our formalism applies to general S. However for S = 1/2 $\mathcal{H}_A$ reduces to a constant and so single-ion anisotropy only occurs for systems where $S \geq 1$. Orbital angular momentum is considered to be quenched (see e.g Bleaney and Stevens 1953, Caspers 1989) and so

does not appear explicitly in the Hamiltonian. The Zeeman term describes the energy advantage of the independent alignment of each spin with the applied field so that here the thermal average $\langle S^z \rangle$ with respect to $\mathcal{H}_H$ tends to S in the limit that $T \to 0$. The simple extension to the case where H_0 and the static magnetization are parallel to the surface is discussed in Appendix I.

In the exchange coupling term in (1.2.1) the indices i and j range over all lattice sites, and hence the factor of 1/2 is included to avoid double counting of spin pairs. J_{ij} is the exchange constant (or exchange integral) for the interaction between the spins at sites i and j. If J_{ij} is positive for all i,j then parallel spin alignment is favoured and the material is ferromagnetic. If J_{ij} is negative for nearest neighbours then an antiparallel arrangement is favoured and the material is antiferromagnetic. A simple antiferromagnetic material is generally described in terms of two or more inter-penetrating sublattices (see Chapter 5) which usually contain spins of different orientation so that nearest neighbours are antiparallel.

The exchange interaction is of quantum mechanical origin and is related to overlap integrals between the electronic wavefunctions of neighbouring spins. A brief account may be found in many standard texts, e.g. Callaway (1991). Several different types of exchange occur. In insulators (e.g. many ferromagnets and most antiferromagnets) the mechanism is direct exchange or, more usually, superexchange (or indirect exchange) both of which are well described by the Heisenberg Hamiltonian. Anderson (1963) provides a detailed discussion of exchange

in insulators. Magnetic metals contain non-localized electrons as well as (possibly) localized electrons. This more complicated situation is usually described in terms of itinerant theories of exchange as reviewed by Herring (1966). Therefore for the description of some features of metallic ferromagnets (e.g. electrical conductivity) the use of the localized-moment model is inappropriate. However for the study of spin waves in many metals (e.g. Fe) an effective Heisenberg Hamiltonian is used successfully in a phenomenological sense with the exchange constants generally derived from experimental results (e.g. see Keffer 1966).

The Hamiltonian $\mathcal{H}_A$ in (1.2.1) contains magnetocrystalline anisotropy terms in which the energy depends on the orientation of the spins relative to the crystal field. The origin of these terms will not be discussed in detail here but the reader is directed to, e.g., Bleaney and Stevens (1953) and Stevens (1963). In brief, in a crystal lattice the electrons (whose spins give rise to the magnetic moments) may have their orbital wave-functions influenced by the electric fields of neighbouring ions. The symmetry properties of the local environment are then communicated to the spins via the spin-orbit coupling. The energy associated with this may be calculated using perturbation theory in terms of the spin-orbit interaction. This effect may be significant despite near quenching of orbital moments (see e.g. Van Vleck 1937). The exact theory is sufficiently complicated that in practice an effective spin Hamiltonian is used in which the anisotropy energy is represented by an expansion in powers of the spin operators (arising from the spin-orbit interaction) with higher order terms neglected (see

e.g. Akhiezer *et al* 1968). Symmetry arguments, which may be different for surface and bulk sites, are then used to eliminate various lower order terms. For example, in cases of purely cubic symmetry, fourth-order terms are the only ones which remain. For situations of lower symmetry (e.g. tetragonal or hexagonal) terms like those in (1.2.1) occur in lowest order. The first of these is the uniaxial term. It is sometimes also referred to as the easy-axis term since, for $D_1 > 0$, it describes the energy advantage for each individual spin of alignment along the z axis, in either direction. The minimum energy is achieved when $S^z = \pm S$. As mentioned above, systems with such anisotropy have been considered in some previous Green-function theories for thin films (e.g. Cottam and Kontos 1980). Uniaxial anisotropy is frequently represented by an effective field, but this approximation will not be necessary for the calculations we perform.

The second term in $\mathcal{H}_A$ deals with anisotropy in the plane perpendicular to the magnetization. For $F_1 > 0$ the x axis is preferred over the y axis. The result of combining the two terms in $\mathcal{H}_A$ is a preference for the xz plane. This is known as easy-plane or nonuniaxial anisotropy. In some experimental accounts and in macroscopic theory the anisotropy energy is represented by an equivalent expansion in direction cosines of the magnetization vector (e.g. see Prinz 1992) or approximately by effective anisotropy fields (e.g. see De Jongh and Miedema 1974).

Although we have assumed for simplicity in many of the calculations that the arrangement of *magnetic* ions is cubic, it is important to note that the overall symmetry of the system may be non-cubic due, for example, to

the presence of non-magnetic ions in a magnetic compound. Also, as mentioned earlier, the lowered symmetry at a surface and/or interface may allow terms in the anisotropy expansion which do not occur in the bulk.

Magnetocrystalline effects are only one source of anisotropy. Another significant one for thin films arises from the anisotropic dipole-dipole interaction which (among other things) leads to the so-called shape anisotropy. We may include this static anisotropy in the spin Hamiltonian in the form of an effective (demagnetizing) field acting in addition to the applied field H_0 (e.g. see Lévy 1981, Prinz 1992). The exchange coupling may also be anisotropic as in the case of the Hamiltonian

$$\sum_{ij} \mathbf{J}^{D}_{ij} \cdot \mathbf{S}_i \times \mathbf{S}_j \qquad (1.2.2)$$

(see Dzialoshinski 1958, Moriya 1960) which is nonuniaxial. This exchange interaction is important in materials such as $FeBO_3$, $CoCO_3$ and several rare-earth orthoferrites. The methods of the present study may be straightforwardly applied to this Hamiltonian, as described in Appendix I.

1.3 Model of an Anisotropic Ferromagnetic Thin Film

The Hamiltonian (1.2.1) is written in a general form that allows for different exchange and anisotropy constants at every site within the magnet and for exchange interactions to exist between every pair of spins. This situation is overly complicated and some simplifications

are needed in order to make the problem solvable. The resulting model is realistic and legitimate comparisons with real systems can be made.

The first such simplification is achieved by insisting that the x and y dimensions of the sample be effectively infinite so that translational invariance in the xy plane may be assumed. This condition is easily satisfied, as the films will be considered to have thicknesses on the order of 10 layers (a few nm) or more while their x and y dimensions will be macroscopically large (e.g. 1 mm or more). We may therefore assume that all magnetic sites in a given layer are equivalent and that a single value of each constant (e.g. D_n and F_n where n = 1,2..,N is the layer index) will suffice to describe the anisotropy at each.

We further assume that the exchange and anisotropy parameters may be modified, compared with the bulk values, only at the surfaces (layers 1 and N), since this is where the wavefunctions are most appreciably perturbed. We therefore assign values of D_s and F_s (or $D_{s'}$ and $F_{s'}$) to spins in layer 1 (or N) and D and F for layers in the bulk. The factors which affect the presence or degree of anisotropy result from the crystal field which may be perturbed at the surface as mentioned above. Specifically we assume that

$$D_i = \begin{cases} D_s & \text{if i is in layer 1} \\ D_{s'} & \text{if i is in layer N} \\ D & \text{otherwise} \end{cases}$$

$$F_i = \begin{cases} F_s & \text{if i is in layer 1} \\ F_{s'} & \text{if i is in layer N} \\ F & \text{otherwise.} \end{cases} \qquad (1.3.1)$$

This modification somewhat limits the applicability of the results and a

prescription for changing this condition (e.g. to assume perturbed values on the layers adjacent to the surfaces as well) is given in Appendix I. Furthermore, throughout the study we have assumed a single species of magnetic ion in a given film but the methods may be extended to consider ferrimagnets (in which the sublattices contain oppositely oriented spins of different species) in much the same way that antiferromagnets are dealt with in Chapter 5.

Another simplification concerns the exchange interaction which is, as noted earlier, short-ranged. For simplicity we assume coupling between nearest neighbours only, although next-nearest neighbour pairs could be considered as shown in Appendix I. By analogy with the anisotropy constants we will consider that only those pairs on a surface have their exchange parameter modified from the bulk value. We will therefore consider that if *both* spins are located in layer 1 (or N) the exchange constant will be J_s (or $J_{s'}$) and otherwise the value will be J. Specifically

$$J_{ij} = \begin{cases} J_s & \text{if i and j are both in layer 1} \\ J_{s'} & \text{if i and j are both in layer N.} \\ J & \text{otherwise} \end{cases} \qquad (1.3.2)$$

The simple cubic film is depicted in figure 1.1.

The calculations are carried out for several special cases of the above model. We classify these cases according to whether the nonuniaxial term is non-zero for every site in the film (*case A*) or non-zero for sites on the surfaces only (*case B*). The latter case therefore describes the situation in the Fe films mentioned above.

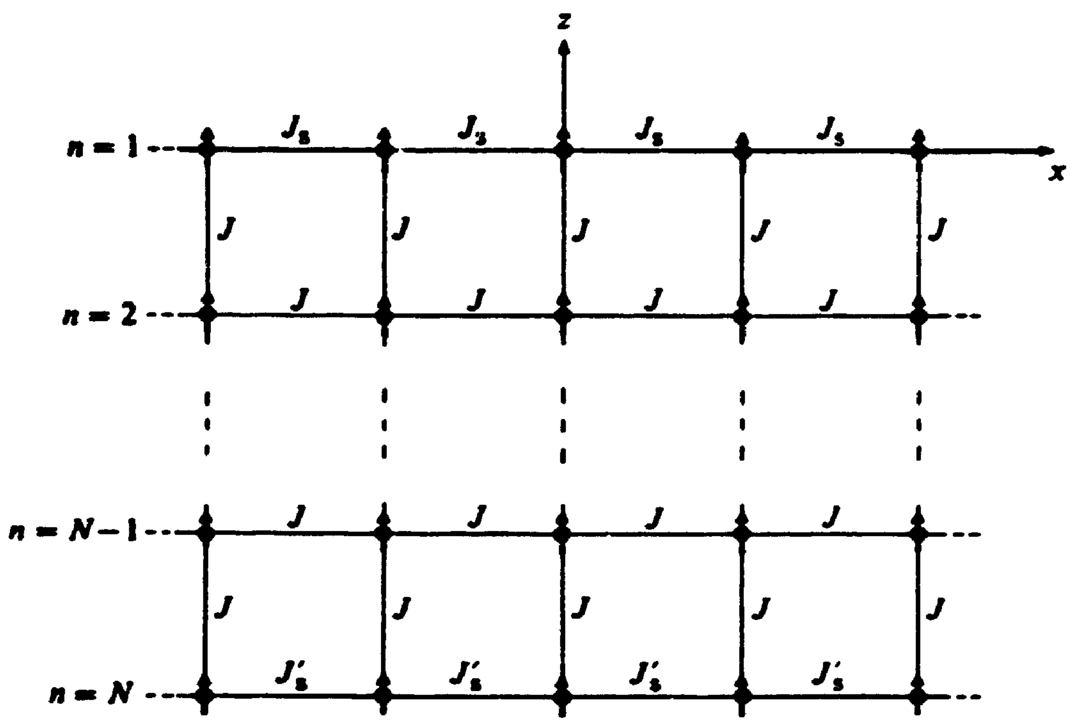

Figure 1.1 Model of the sc (001) ferromagnetic film showing nearest-neighbour exchange constants.

1.4 Spin Waves

A Heisenberg ferromagnet in the absence of single-ion anisotropy (described by (1.2.1) with $J_i > 0$ and $\mathcal{H}_A = 0$) has a ground state in which all spins are in the state where $S^z = S$ so that the net spin alignment is along the z direction. For ferromagnets with $\mathcal{H}_A \neq 0$, the problem of determining the exact ground state becomes more complicated, particularly if the nonuniaxial component is large. Here we assume that $D_i > F_i > 0$ and that the net spin alignment is along the z axis. The spin alignment in antiferromagnets is discussed in Chapter 5.

The magnetization of the ferromagnet is proportional to the thermal and spatial average of the z component of spin, $\langle S^z \rangle$. At temperatures above absolute zero this quantity decreases from its saturation value of S as thermal effects compete with ordering effects. There is a phase transition to a paramagnetic state (at a temperature known as the Curie temperature T_c for ferromagnets) where long-range magnetic order, in the absence of an applied field, vanishes as illustrated in figure 1.2.

The molecular field theory of Weiss (1907) was the first theory of ferromagnetism to predict spontaneous magnetization and the existence of the phase transition. Molecular field theory assumes the spins are coupled through a Zeeman-like term to an effective field proportional to the magnetization itself. With the development of the Heisenberg exchange Hamiltonian (Heisenberg 1928) came an explanation for the origin and magnitude of the effective field. Molecular field theory remains a useful means of modelling static properties at any temperature

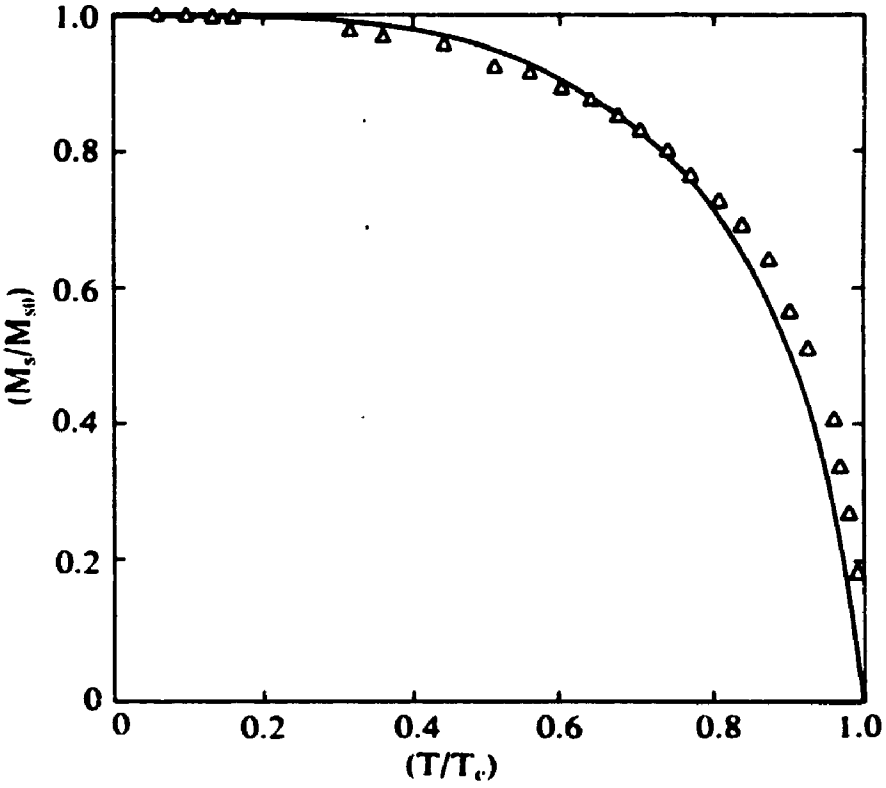

Figure 1.2 Temperature dependence of the spontaneous magnetization M_s (relative to the saturation value at absolute zero M_{so}) for a ferromagnet. Triangles represent experimental data for metallic Ni with T_c = 631 K (after Blakemore 1985).

in many different magnetic systems including antiferromagnets and ferrimagnets (e.g. see Callaway 1991, Smart 1966). The Heisenberg theory of exchange led to the development of spin wave theory, initially proposed by Bloch (1930). Unlike molecular field theory, spin wave theory includes dynamic effects and correctly accounts for the observed $T^{3/2}$ dependence of the magnetization at low temperatures in ferromagnets (e.g. see Phillips and Rosenberg 1966, Keffer 1966).

According to the spin wave theory, the low-lying eigenstates of the Heisenberg Hamiltonian are wave-like excitations associated with the transverse components of spin (S^x and S^y) and involve a *collective* deviation from the ground state. A single quantum of spin deviation can be shared among the spins at a lower energy cost than if a single spin deviated by the same amount. The spin waves are quantized with the term *magnon* being used for a quantum in analogy with the use of the term *phonon* for quantized lattice vibrations. In a useful semi-classical description (Heller and Kramers 1934, Phillips and Rosenberg 1966) the spins are considered to precess about their z axes as illustrated in figure 1.3. The x and y components of spin are governed by travelling wave functions of frequency ω and wavevector $\mathbf{k}$ hence, hence the name *spin wave*. The quantum mechanical picture is of correlations between the transverse components of spin at different sites. The interpretation of spin waves in antiferromagnets is discussed in Chapter 5. The existence of spin waves has long been accepted on the basis of experimental results (e.g. see Keffer 1966, Phillips and Rosenberg 1966, Puszkarski 1970, Cottam and Lockwood 1986, Borovik-Romanov and Sinha 1988, Cottam 1994).

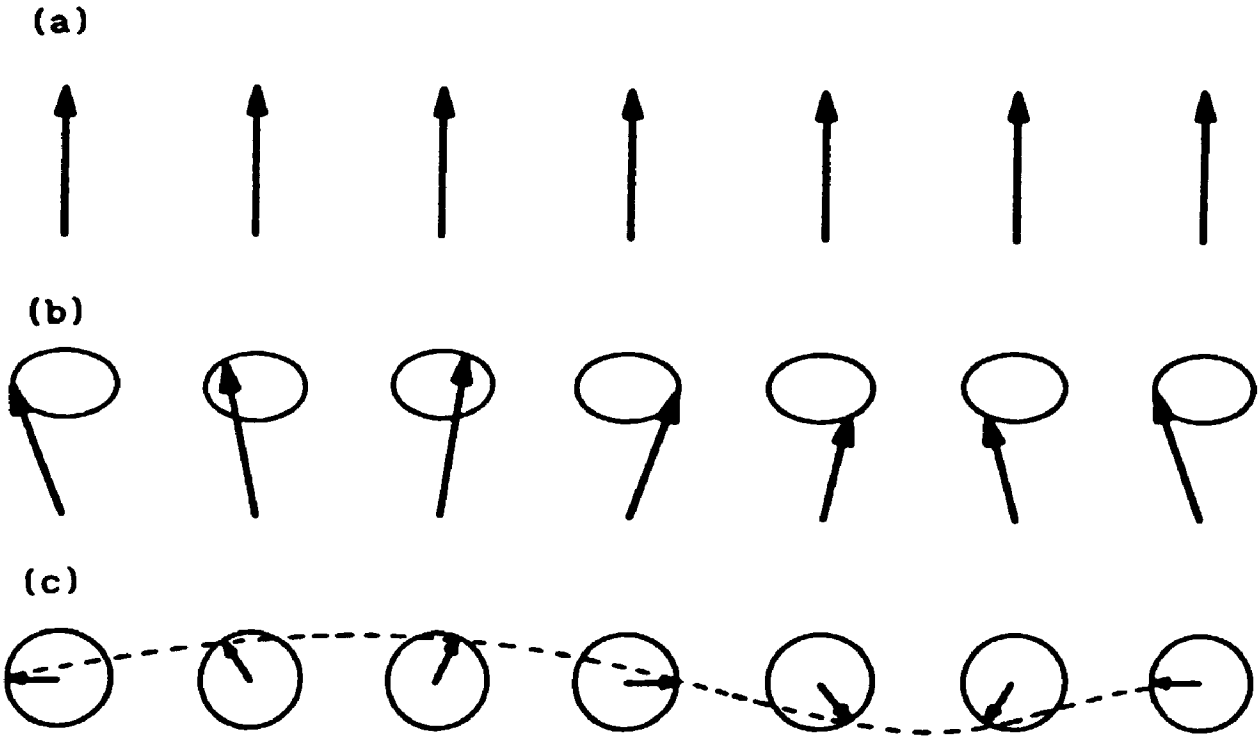

Figure 1.3 Semi-classical depiction of a spin wave. The ground state is represented in (a). In (b) a perspective view and in (c) a top view of spin precession are shown.

1.4.1 Spin Waves in Infinite Ferromagnets

Spin waves are not exact normal modes for the system and in general the interactions among them must be considered (e.g. see Phillips and Rosenberg 1966). We will, however, be restricting our attention to those temperatures, well below T_c, where the magnetic state may be approximated as a superposition of non-interacting (linear) spin waves. In this limit the energy eigenvalues for the bulk (i.e. effectively infinite) isotropic Heisenberg ferromagnet are found to be (e.g. see Phillips and Rosenberg 1966, Kittel 1987)

$$E = E_0 + \sum_{\mathbf{k}} n_{\mathbf{k}}\, \omega(\mathbf{k}) \qquad (1.4.1)$$

where E_0 is a constant, $n_{\mathbf{k}}$ is the number of spin waves of wavevector $\mathbf{k}$ and $\omega(\mathbf{k})$ is the energy of such a spin-wave in units such that $\hbar = 1$. The dependence of the energy on the wavevector, $\omega(\mathbf{k})$, is the *dispersion relation*. The determination of such relations for anisotropic magnetic thin films was a major goal of this project. For the isotropic bulk magnet with spin S, and applied field H_0 we have

$$\omega(\mathbf{k}) = g\mu_B H_0 + S[J(0) - J(\mathbf{k})] \qquad (1.4.2)$$

where

$$J(\mathbf{k}) = 2[\cos(k_x a_0) + \cos(k_y a_0) + \cos(k_z a_0)] \qquad (1.4.3)$$

for a simple cubic ferromagnet of lattice parameter a_0. We see that as $|\mathbf{k}|$ increases the energy increases monotonically from the value $g\mu_B H_0$ at the centre of the Brillouin zone (where $|\mathbf{k}| = 0$) and for small k is approximately quadratic. There is a single branch to the dispersion relation, illustrated in figure 1.4. The different bulk spin-wave spectrum for antiferromagnets is discussed in Chapter 5.

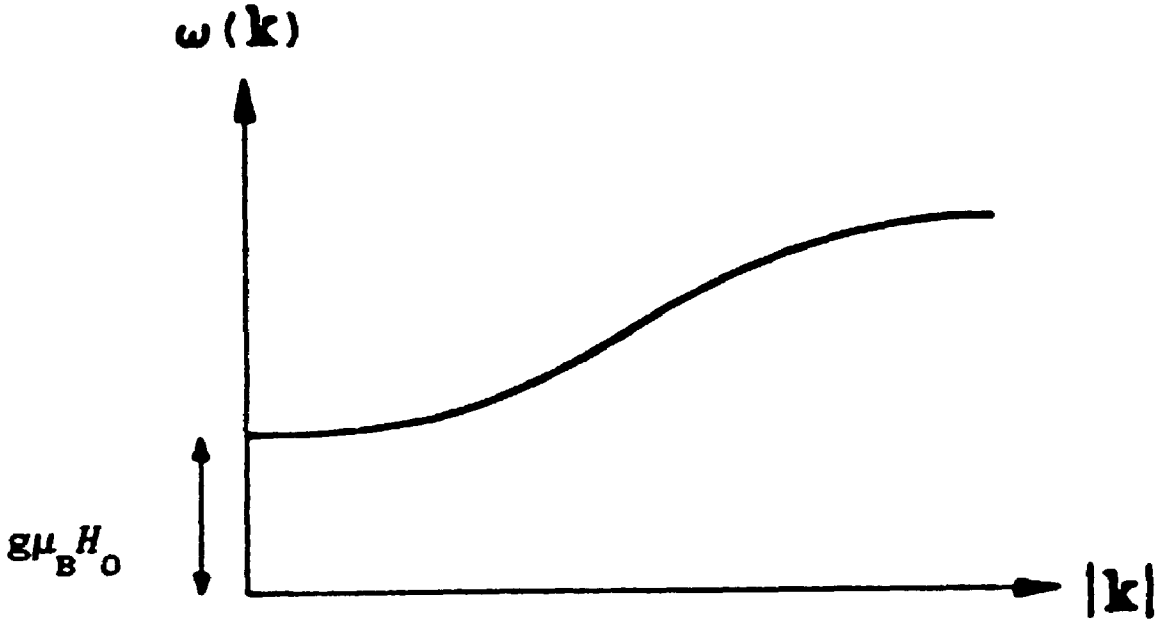

Figure 1.4 Schematic depiction of the ferromagnetic dispersion relation for infinite systems.

1.4.2 Spin Waves in Thin Films

In semi-infinite or thin film systems there may arise spin waves that are localized near the surface(s) in addition to the usual bulk modes (e.g see Wolfram and DeWames 1972, Cottam and Tilley 1989). In these *surface* spin waves the transverse spin components have a decaying (usually exponential) dependence on the distance in the direction normal to the surface (z) characterized by a reciprocal attenuation length λ_s and a travelling-wave-like variation in the the xy plane characterized by a wavevector $\mathbf{k}_{\parallel} = (k_x, k_y)$. For very thin films the exponential tails of the modes associated with each surface may in fact overlap leading to an alteration of the surface mode characteristics. As film thickness decreases the surface contributions to properties such as specific heat and susceptibility become relatively more important.

Simple symmetry arguments based on Bloch's Theorem can be used to show how the localized modes occur as well as the more usual non-localized modes (see e.g. Cottam and Tilley 1989). Briefly, in infinite media, the full three-dimensional (3-D) translational symmetry leads to the spin-dependent part of the wavefunctions being periodic. The position dependence can be described by $\exp(i\mathbf{k}\cdot\mathbf{r})$ where $\mathbf{k}$ is a 3-D wavevector. In contrast, in a semi-infinite or thin film system there is translational symmetry in the xy plane only and the wavefunctions are found to have position dependence of the form $\exp(i\mathbf{k}_{\parallel}\cdot\mathbf{r}_{\parallel})u(z)$ where $\mathbf{k}_{\parallel}$ is an above-mentioned 2-D wavevector. This is the 2-D analogue of Bloch's theorem. Depending on the boundary conditions the function u(z) is often found to have solutions of the form $\exp(\pm\lambda_s z)$ where λ_s is real.

Solutions of the form $u(z) = \exp(ik_z z)$ are also admitted and lead to the usual non-localized excitations. We note that the solution $\exp(\lambda_s z)$, corresponding to a mode which grows exponentially in amplitude with distance, is prohibited in a semi-infinite medium but may occur in a thin film.

In the case where the film is of finite thickness boundary conditions at each surface must be accommodated. In particular the allowed values of k_z are restricted and thus the bulk modes in a thin film are quantized and are in fact standing wave modes of the system as we show later. In addition, bulk spin waves are generally found to have modified amplitudes in the vicinity of a surface. In ferromagnetic films the total number of surface and quantized bulk spin-wave branches is equal to the number of layers, N.

1.5 Theoretical Methods

The principal calculational methods used in this thesis are introduced in this section. They are the operator equation-of-motion method and the Green function equation-of-motion method. Of the two the Green function method, while more useful and more comprehensive, is more difficult to apply. The operator method is therefore utilized first, in Chapter 2. The results of the operator method are contained within those of the Green-function method so that the dispersion relations of Chapters 2 and 3 provide a means of checking the later Green function calculations. The operator method also serves as an example of an alternative theoretical approach to finding dispersion relations which is seen in the literature. In addition, much of the matrix formalism

necessary for the Green function analysis can be developed first for the operator method. The Green function method yields spectral functions and therefore both static properties (such as magnetization) and dynamic properties can be calculated as well as the dispersion relations. The application of the Green function method to the ferromagnetic thin films is the subject of Chapter 4.

Alternative techniques, which will not be used here, include the diagrammatic perturbation method for calculating the Green functions (see e.g. Parry 1973, Rickayzen 1980). This technique cannot be applied directly to spin operators and therefore a transformation, such as the drone-fermion representation (see e.g. Parry 1973), must be used. The results of this method are equivalent to those of the equation-of-motion method in the linear approximation (e.g. see Cottam 1976 for an application to the semi-infinite isotropic ferromagnet). It has the advantage of permitting, in a more methodical way, the extension to higher order terms in the Hamiltonian, (i.e. to consider interactions between the spin waves). However, unless these interactions are the subject of the study the equation-of-motion approach has the advantage of relative simplicty.

In much of the literature on spin waves (see e.g. Cottam and Slavin 1994) a semi-classical macroscopic (or continuum) approach is used which works well for long wavelength modes which are typically those most easily detected experimentally. The microscopic methods used here, however, have the advantage of applying throughout the entire Brillouin zone.

Although we have presented the Hamiltonian in terms of spin operators we will be using boson creation and annihilation operators throughout the thesis. The transformation from spin operators to the boson operators following the method of Holstein and Primakoff (1940) is presented in Chapter 2.

1.5.1 The Operator Equation-of Motion Method

The operator equation-of-motion method is based on the standard quantum mechanical result for any operator A within the Heisenberg representation (e.g. see Cohen-Tannoudji 1977)

$$\frac{d}{dt} A = i[\mathcal{H}, A] \qquad (1.5.1)$$

wherein the operators are assumed to be time-dependent while the wavefunctions are not. Here the square brackets denote a commutator and we are using units where $\hbar = 1$. In principle, we can find a differential equation for any one of our site- and time-labelled boson operators. We then Fourier transform from the time representation to a frequency representation. The resulting equation may contain the boson operators for neighbouring sites which are also described by an equation of the form (1.5.1). We may exploit the symmetry in the xy plane to Fourier transform from site labels to a representation involving the in-plane wavevector $\mathbf{k}_{\parallel}$. We find a set of coupled equations involving boson operators, labelled by the layer index n, which are coupled to those of the adjacent layers, n+1 and n-1. Ultimately the operator equations may be rewritten in the form of a homogeneous matrix equation. The condition for the existence of a solution then generally requires

that the determinant be equal to zero. This existence condition can be used to find a relationship between the spin-wave energies (or frequencies) and wavevectors (hence yielding the dispersion relation) as shown in later chapters.

1.5.2 The Green Function Equation-of-Motion Method

We here outline the derivation of the corresponding Green function equation-of-motion by first defining double-time Green functions in terms of correlation functions between operators according to Zubarev (1960). We then describe the relationship between correlation functions and spectral intensities contained in the fluctuation-dissipation theorem and demonstrate how the Green functions can be used to find both. The static and dynamic properties of the system can be determined once the correlation functions are known as will be seen in Chapter 4. What follows is a brief summary of the major points of the Green function theory and the equation-of-motion method. For more details the reader is referred to Zubarev (1960), Parry (1973), or Rickayzen (1980).

The *retarded* commutator Green function for arbitrary operators A and B is defined as

$$\langle\langle A(t);B(t')\rangle\rangle = -i\theta(t - t')\langle[A(t),B(t')]\rangle \qquad (1.5.2)$$

where $\theta(t)$ is the unit step function

$$\theta(t) \equiv \begin{cases} 1 & t > 0 \\ 0 & t < 0. \end{cases} \qquad (1.5.3)$$

Also, $[A(t),B(t')]$ is the commutator for the operators in the Heisenberg representation and $\langle..\rangle$ denotes a thermal average with respect to the Hamiltonian of the system. It is possible to define other similar Green

functions, namely the *advanced* and *causal* Green functions. However, we will not be using these here. The equation of motion is found by differentiating the Green function with respect to time:

$$\frac{d}{dt}\langle\langle A(t);B(t')\rangle\rangle = -i\frac{d}{dt}\theta(t-t')\langle[A(t),B(t')]\rangle + \langle\langle\frac{d}{dt}A(t);B(t')\rangle\rangle. \quad (1.5.4)$$

Using (1.5.3) we can write

$$\frac{d}{dt}\theta(t-t') = \delta(t-t'). \quad (1.5.5)$$

From the above, together with (1.5.1) we find

$$\frac{d}{dt}\langle\langle A(t);B(t')\rangle\rangle = -i\delta(t-t')\langle[A(t),B(t')]\rangle + i\langle\langle[C(t)];B(t')\rangle\rangle \quad (1.5.6)$$

where $C = [\mathcal{H},A]$ and a new Green function has been introduced. The equation of motion for this new Green function is found in the same way, and so on. If the result is not a closed set of coupled equations a decoupling scheme is needed although this is not the case in this particular study. The set of coupled equations is solved in a manner analogous to that described above for operators, except that here we have to solve an inhomogeneous (rather than homogeneous) set of equations.

The definition of the Green function contains the correlation functions $\langle A(t)B(t')\rangle$ and $\langle B(t')A(t)\rangle$. The corresponding *spectral intensities* (or *spectral functions*), $\xi(\omega)$ and $\xi'(\omega)$, are defined as follows

$$\langle B(t')A(t)\rangle = \int_{-\infty} \xi(\omega)\exp[-i\omega(t-t')]d\omega$$

$$\langle A(t)B(t')\rangle = \int_{-\infty}^{\infty} \xi'(\omega)\exp[-i\omega(t-t')]d\omega. \qquad (1.5.7)$$

It may be shown that (Zubarev 1960)

$$\xi'(\omega) = \xi(\omega)\exp[\beta\omega] \qquad (1.5.8)$$

where $\beta = 1/k_B T$, k_B is the Boltzmann constant and T the temperature. This result allows us to calculate both correlation functions from a single spectral intensity.

The Green functions have Fourier transforms

$$G(\omega) = \frac{1}{2\pi}\int_{-\infty}^{\infty} G(t-t')\exp[i\omega t]dt \qquad (1.5.9)$$

where the notation $G(t-t') = \langle\langle A(t);B(t')\rangle\rangle$ has been introduced. The Green function and the spectral function are related by the *fluctuation-dissipation theorem* (Zubarev 1960)

$$\xi(\omega) = \frac{-2}{\exp(\beta\omega) - 1}\,\mathrm{Im}\, G(\omega + i\varepsilon) \qquad (1.5.10)$$

where ε is a real, positive and infinitesimal quantity. The Green functions $G(\omega)$ that we find will have poles related to the spin-wave frequencies. In simpler cases (such as isotropic or uniaxial ferromagnets) the Green-function denominators can be written in the explicit form $(\omega - \omega^0)$ where ω^0 is a spin-wave frequency. In such a case we can make the analytic continuation $\omega \to \omega + i\varepsilon$ and make use of (1.5.10) to find the spectral functions and hence the correlation functions via (1.5.7) and (1.5.8). The imaginary parts of $G(\omega + i\varepsilon)$ are extracted using the operator identity (see e.g. Parry 1973)

$$\left(\frac{1}{x + i\varepsilon}\right) = P\left(\frac{1}{x}\right) - i\pi\delta(x) \qquad (1.5.11)$$

where P signifies the principal value in an integration over any real

variable x. In the more complicated cases which are the subject of this thesis the analysis is slightly less direct, as explained in Chapter 4.

In the study of spin waves the operators A and B are generally spin operators (e.g. S^+, S^- and S^z) or the corresponding boson operators related to them by e.g. the Holstein-Primakoff (1940) transformation. Thermodynamic quantities such as magnetization, magnetic susceptibility and specific heat can all be calculated from correlation functions involving these operators as can cross-sections for light scattering and absorption strengths for magnetic resonance as described in Chapter 4.

1.6 Experimental Methods for Studying Spin Waves

In this section we briefly review some experimental methods which are relevant to this thesis. Among the methods currently available for studying spin waves in thin films, the most useful are inelastic light scattering and spin wave resonance.

The inelastic scattering of light by spin waves is the subject of a book (Cottam and Lockwood 1986) which deals with a number of different types of magnetic systems including thin films. Several detailed reviews (e.g. Demokritov and Tsymbal 1994 and Dutcher 1994) deal with recent results for the case of thin magnetic films. Raman scattering and Brillouin light scattering (BLS) are principally distinguished by the means of detecting the scattered light e.g. a grating spectrometer for Raman scattering experiments or a Fabry-Perot interferometer for BLS. From the standpoint of theory, however they are the same.

In brief, incident light may be scattered with a change in energy due to the creation or annihilation of a spin wave (or spin waves). The wavevector of the spin wave is closely related to the wavevectors associated with visible light so that $|\mathbf{k}| \cong 10^5$ cm^{-1}. Light scattering experiments therefore primarily study spin waves near the centre of the Brillouin zone. Depending on the actual light source and the scattering geometry it is generally possible to detect dipole-dominated modes, dipole-exchange modes or exchange-dominated modes. The mechanism is summarized as follows. Thermally excited magnetic fluctuations (spin waves) in the scattering material give rise to modulations in the electric susceptibilty through which the electric field vector of the incident photon interacts with the target medium and is scattered. Cottam and Lockwood (1986) show how the scattering cross section is constructed from correlation functions involving elements of the susceptibilty tensor. These elements can be in turn represented by expansions in powers of spin operators with coefficents known as magneto-optical coupling constants. In Chapter 4 we will show how this calculation can be performed using spin correlation functions derived from our Green function results. Conservation of energy and momentum allow the deduction of the energy and wavevector of the spin wave involved in the scattering. In addition to the dispersion relations the light scattering spectra are a source of information about spin-wave lifetimes, the type of magneto-optic coupling, surface anisotropy, etc. This type of information may have some relevance for the development of magneto-optic recording media (e.g. see Falicov *et al* 1990).

In spin wave resonance (SWR) a spin wave is excited by the resonant absorption of energy from a transverse oscillating rf field. The spin waves can either be surface modes with $k_{\parallel} = 0$ or standing bulk modes. This latter case is therefore also referred to as standing spin wave resonance or SSWR. In the case of symmetric films only those standing modes which are symmetric with respect to the film centre are excited by the spatially uniform rf field. In practice only acoustic (i.e. low frequency) surface modes are excited. The thin film SWR experiment is generally performed with a static applied field perpendicular to the oscillating field. The oscillating field frequency ω_0 is fixed while the static field is varied and resonant absorption occurs when ω_0 matches the frequency of a spin wave mode. In this way the dispersion relation is determined. The resonant absorption strength can be calculated from an appropriate set of spin correlation functions (e.g. see Moul and Cottam 1983). Other information available from the SWR spectrum is similar to that for the light scattering spectrum. SWR, first predicted by Kittel (1958), is reviewed by Puszkarski (1979). Dutcher (1994) reviews recent results for thin films.

The interaction of neutron spins with atomic spins provides a powerful means of studying magnetic structure through elastic scattering, and spin wave dispersion, chiefly in bulk materials, through inelastic scattering. For the study of *surface* spin waves, neutron scattering has not, however, been as useful since in most materials neutrons penetrate deeply and therefore scattering experiments are not particularly surface sensitive. In contrast, in light scattering experiments it is often the case that the target material is opaque (e.g. metallic) and therefore

the incident light interacts preferentially with excitations in the vicinity of the surface, or it may be possible to choose a wavelength of incident light for which the material is optically absorptive. The development of neutron scattering techniques with enhanced surface sensitivity includes work with grazing incidence and the use of multilayers as targets so that the scattering volume contains a number of surfaces (or interfaces) (e.g. see Felcher 1985). Advances have chiefly been in the important area of magnetic structure measurements (i.e. surface magnetism) whereas progress in the study of surface dynamics, such as scattering from surface spin waves, seems to be more elusive. The range of de Broglie wavelengths of thermal neutrons generally allows the study of bulk spin wave dispersion throughout the Brillouin zone. Therefore it is possible that the adaptation to surface spin waves could extend knowledge gained using the techniques mentioned above (BLS, SWR) which are restricted to the vicinity of the zone centre. The extensive literature on neutron scattering includes the standard works by Marshall and Lovesey (1971) and Lovesey (1984). Recent progress, of particular relevance to surface studies is documented in, for example, the Proceedings of the Conference on Neutrons and X-rays in Magnetism (1993).

Other experimental techniques relevant to this project include those whereby anisotropies, particularly surface anisotropies, are explored. These include torsion magnetometry (e.g. see Gradmann 1986), Mössbauer spectroscopy (e.g. see Gradmann *et al* 1986), surface magneto-optic Kerr effect (SMOKE) (e.g. see Bader 1992) and ferromagnetic resonance (FMR), which is similar to SWR except that the uniform ($\mathbf{k} = 0$) mode is excited

(e.g. see Prinz *et al* 1982). These authors make reference to the results for Fe (110) films. The review article by Falicov *et al* (1990) discusses a variety of techniques for the characterization and fabrication of magnetic thin films.

CHAPTER 2

OPERATOR METHOD FOR FERROMAGNETIC THIN FILMS

In this chapter the operator equation-of-motion method is used to study spin waves in anisotropic ferromagnetic thin films. As mentioned in Section 1.3, the formalism is different in detail for some special cases identified among these systems, namely we shall refer to case A (where the nonuniaxial anisotropy parameter is non-zero throughout the film although it may take different values at the surfaces) and case B (where it is non-zero at the surfaces only). The operator equation-of-motion method is described first for a general situation and continued for cases A and B separately. Case A is further subdivided according to film symmetry and the relative strength of the surface and bulk nonuniaxial parameters while case B is subdivided according to whether or not both surfaces are nonuniaxial. The formal results for the spin-wave dispersion relations are obtained as a series of polynomials. The numerical techniques used to derive spin-wave frequencies from these polynomials are discussed in Chapter 3 where we also present a number of representative examples of dispersion relations. The Green-function method is presented in Chapter 4 for the same cases. As a preliminary step the Holstein-Primakoff transformation from spin operat to boson operators is described.

2.1 The Holstein-Primakoff Transformation

The spin Hamiltonian for the most general case was discussed in detail in Section 1.2. It contains two parts $\mathcal{H} = \mathcal{H}_H + \mathcal{H}_A$, where $\mathcal{H}_H$ is the

usual Heisenberg Hamiltonian containing exchange and Zeeman terms and $\mathcal{H}_A$ describes the anisotropy (see (1.2.1)).

Following the method of Holstein and Primakoff (1940) we transform to boson operators in order to make use of the standard many-body theory methods established for such operators which do not apply directly to spin operators. The spin operators S^x and S^y are first written in terms of S^+ and S^- as follows (e.g. see Cohen-Tannoudji *et al*, 1977):

$$S^{\pm} = S^x \pm iS^y. \tag{2.1.1}$$

Then the operators S_j^+, S_j^- and S_j^z for site j are written as

$$\begin{aligned} S_j^+ &= (2S)^{1/2}\left(1 - b_j^\dagger b_j / (2S)\right)^{1/2} b_j \\ S_j^- &= (2S)^{1/2}\, b_j^\dagger \left(1 - b_j^\dagger b_j / (2S)\right)^{1/2} \\ S_j^z &= S - b_j^\dagger b_j \end{aligned} \tag{2.1.2}$$

where $b_j^\dagger$ and b_j are the usual boson creation and annihilation operators obeying the following commutation relations (e.g. see Cohen-Tannoudji *et al* 1977):

$$[b_i, b_j^\dagger] = \delta_{ij}, \quad [b_i, b_j] = [b_i^\dagger, b_j^\dagger] = 0. \tag{2.1.3}$$

We make the *near-saturation approximation* which holds at low temperatures ($T \ll T_c$) where $\langle S_i^z \rangle \approx S$. Treating $b_j^\dagger b_j / S$ as a small quantity we can expand as follows:

$$\begin{aligned} S_j^+ &= (2S)^{1/2}\left(1 - b_j^\dagger b_j / (4S) + \ldots\right) b_j \\ S_j^- &= (2S)^{1/2}\, b_j^\dagger \left(1 - b_j^\dagger b_j / (4S) + \ldots\right) \\ S_j^z &= S - b_j^\dagger b_j. \end{aligned} \tag{2.1.4}$$

Performing the transformation on (1.2.1) we eventually find (apart from constant terms)

$$\mathcal{H}_H \cong -\sum_{ij} J_{ij}(b_i^\dagger b_j - b_i^\dagger b_i) + g\mu_B H_0 \sum_i b_i^\dagger b_i \qquad (2.1.5)$$

and

$$\mathcal{H}_A \cong 2S\eta \sum_i D_i b_i^\dagger b_i - S\eta' \sum_i F_i (b_i b_i + b_i^\dagger b_i^\dagger) \qquad (2.1.6)$$

where the symbols $\eta = 1 - \frac{1}{2S}$ and $\eta' = \eta^{1/2}$ have been introduced (see Appendix II). For S = 1/2 these constants vanish and therefore $\mathcal{H}_A$ has no effect, as expected. Terms of quartic or higher order in the operators are neglected so that the interactions between spin waves, which may play an important role at higher temperatures, are thereby ignored. This is the "linear spin-wave approximation". As seen above this approximation is valid provided that $\langle S^z \rangle$ does not differ significantly from its saturation value. This condition is met over a fairly wide range of temperatures due to the relatively slow variation of $\langle S^z \rangle$ with T at low temperatures (see figure 1.1).

We note that if the equation-of-motion method is used for the spin raising and lowering operators S^+ and S^- (rather than the boson operators defined above) then the linearizing approximation takes a different form (e.g. it involves the so-called Random Phase Approximation), but it leads to the same results for $T \ll T_c$.

2.2 General Formalism

The boson operators obey the following equations of motion (see (1.5.1)):

$$i \frac{d}{dt} b_j = [b_j, \mathcal{H}]$$

$$i\frac{d}{dt}b_j^\dagger = [b_j^\dagger, \mathcal{H}]. \qquad (2.2.1)$$

Evaluating the commutators leads to:

$$i\frac{d}{dt}b_j = g\mu_B H_0 b_j + 2S\eta D_j b_j - 2S\eta' F_j b_j^\dagger - S\sum_{ij} J_{ij}(b_i - b_j)$$

$$i\frac{d}{dt}b_j^\dagger = -g\mu_B H_0 b_j^\dagger - 2S\eta D_j b_j^\dagger + 2S\eta' F_j b_j + S\sum_{ij} J_{ij}(b_i^\dagger - b_j^\dagger). \qquad (2.2.2)$$

The coupling of the operators b_j and $b_j^\dagger$ through the nonuniaxial term leads to some of the distinctive physical features of the nonuniaxial case, e.g. elliptical spin precession, as well as a greater degree of mathematical complication relative to the uniaxial case.

In order to solve the coupled differential equations (2.2.2) we Fourier transform from the time representation to the frequency representation as follows:

$$b_j(t) = \int_{-\infty}^{\infty} b_j(\omega)e^{-i\omega t}d\omega$$

$$b_j^\dagger(t) = \int_{-\infty}^{\infty} b_j^\dagger(\omega)e^{-i\omega t}d\omega \qquad (2.2.3)$$

and (2.2.2) becomes:

$$\left[\omega - g\mu_B H_0 - 2D_j S\eta - S\sum_i J_{ij}\right]b_j(\omega) + S\sum_i J_{ij}b_i(\omega) = -2F_j S\eta' b_j^\dagger(\omega)$$

$$\left[\omega + g\mu_B H_0 + 2D_j S\eta + S\sum_i J_{ij}\right]b_j^\dagger(\omega) - S\sum_i J_{ij}b_i^\dagger(\omega) = 2F_j S\eta' b_j(\omega). \qquad (2.2.4)$$

According to the general model established in Section 1.3 each of the N sites in a particular layer is equivalent. The resulting translational symmetry in the xy plane allows the following 2-D Fourier transform to the wavevector representation:

$$b_i(\omega) = N^{-1/2}\sum_{\mathbf{k}_\parallel} b_n(\mathbf{k}_\parallel, \omega)\exp(-i\mathbf{k}_\parallel\cdot\mathbf{r}_i)$$

$$b_i^\dagger(\omega) = N^{-1/2} \sum_{\mathbf{k}_\parallel} b_n^\dagger(\mathbf{k}_\parallel,\omega)\, \exp(i\mathbf{k}_\parallel \cdot \mathbf{r}_i) \qquad (2.2.5)$$

where n is the layer index for site i and $\mathbf{k}_\parallel = (k_x, k_y)$ is the wavevector parallel to the xy plane. The spin waves will propagate in the direction defined by $\mathbf{k}_\parallel$ and can be either the localized surface type or the non-localized bulk type, according to the dependence on n (and therefore z) as described in Chapter 1.

We use (1.3.1) and (1.3.2) to assign values to the anisotropy and exchange parameters according to the layer number. The following two sets of N finite-difference equations result (for n = 1,2,..,N):

$$\left[\omega - g\mu_B H_0 - 2D_n S\eta - Su_n(0) - Sv_n(0) - Sv_{n-1}(0) + Su_n(\mathbf{k}_\parallel)\right] b_n(-\mathbf{k}_\parallel,\omega)$$
$$+ Sv_{n-1}(\mathbf{k}_\parallel) b_{n-1}(-\mathbf{k}_\parallel,\omega) + Sv_n(\mathbf{k}_\parallel) b_{n+1}(-\mathbf{k}_\parallel,\omega) = -2F_n S\eta' b_n^\dagger(-\mathbf{k}_\parallel,\omega) \qquad (2.2.6)$$

$$\left[\omega + g\mu_B H_0 + 2D_n S\eta + Su_n(0) + Sv_n(0) + Sv_{n-1}(0) - Su_n(\mathbf{k}_\parallel)\right] b_n^\dagger(\mathbf{k}_\parallel,\omega)$$
$$- Sv_{n-1}(\mathbf{k}_\parallel) b_{n-1}^\dagger(\mathbf{k}_\parallel,\omega) - Sv_n(\mathbf{k}_\parallel) b_{n+1}^\dagger(\mathbf{k}_\parallel,\omega) = 2F_n S\eta' b_n(-\mathbf{k}_\parallel,\omega). \qquad (2.2.7)$$

Here we have introduced the sums

$$u_n(\mathbf{k}_\parallel) = \sum_{\delta_1} J_{ij} \exp[i\mathbf{k}_\parallel \cdot \delta_1]$$
$$v_n(\mathbf{k}_\parallel) = \sum_{\delta_2} J_{ij} \exp[i\mathbf{k}_\parallel \cdot \delta_2] \qquad (2.2.8)$$

where δ_1 and δ_2 are vectors connecting any site i in layer n with its neighbours in layers n and n+1 respectively. Assuming, as described in Chapter 1, that J_{ij} is non-zero for nearest neighbours only and described by (1.3.2), we write for the sc (001) film:

$$u_n(k_\parallel) = \begin{cases} J_s\gamma(k_\parallel) & n = 1 \\ J\gamma(k_\parallel) & n = 2,3,..N-1 \\ J_s,\gamma(k_\parallel) & n = N \end{cases}$$

$$v_n(k_\parallel) = \begin{cases} J & n = 1,2,..N-1 \\ 0 & \text{otherwise} \end{cases} \qquad (2.2.9)$$

with

$$\gamma(k_\parallel) = \sum_i \exp[ik_\parallel \cdot (r_i - r_j)] \qquad (2.2.10)$$

where the sum is over those nearest neighbours of site j which lie in the same plane. For the sc systems (of lattice parameter a_0) assumed here we have

$$\gamma(k_\parallel) = 2\cos(k_x a_0) + 2\cos(k_y a_0). \qquad (2.2.11)$$

For other lattice types and surface orientations the evaluation of the exchange sums is discussed in Appendix I.

Equations (2.2.6) and (2.2.7) may be written more compactly in matrix form as follows:

$$(-\Omega\underline{I} + \underline{A})\underline{b} = \underline{f}\ \underline{b}^\dagger$$

$$(\Omega\underline{I} + \underline{A})\underline{b}^\dagger = \underline{f}\ \underline{b} \qquad (2.2.12)$$

where $\underline{b}^\dagger$ and $\underline{b}$ are 1×N matrices whose elements are the boson operators $b_n^\dagger(k_\parallel,\omega)$ and $b_n(-k_\parallel,\omega)$ defined as in (2.2.5), $\underline{I}$ is the N×N identity matrix, and $\underline{f}$ and $\underline{A}$ are the following N×N matrices:

$$\underline{f} = \begin{bmatrix} f_s & 0 & 0... & & & \\ 0 & f & 0... & & & \\ 0 & 0 & f... & & & \\ \vdots & \vdots & \vdots & \vdots & \vdots & \vdots \\ & & ...f & 0 & 0 & \\ & & ...0 & f & 0 & \\ & & ...0 & 0 & f_{s'} & \end{bmatrix} \qquad (2.2.13)$$

$$\underline{A} = \begin{bmatrix} a_s & -1 & 0 & 0 & \dots & & & \\ -1 & a & -1 & 0 & \dots & & & \\ 0 & -1 & a & -1 & \dots & & & \\ \vdots & \vdots & \vdots & \vdots & & \vdots & \vdots & \vdots \\ & & & & \dots & a & -1 & 0 \\ & & & & \dots & -1 & a & -1 \\ & & & & \dots & 0 & -1 & a_{s'} \end{bmatrix}. \qquad (2.2.14)$$

The following dimensionless quantities have been defined for the sc lattice using (1.3.1)

$$\Omega = \omega \,/\, (SJ)$$

$$a_s = [g\mu_B H_0 + 2D_s S\eta + S(4J_s + J) - SJ_s\gamma(\mathbf{k}_\parallel)] \,/\, (SJ)$$

$$a = [g\mu_B H_0 + 2DS\eta + S(6J) - SJ\gamma(\mathbf{k}_\parallel)] \,/\, (SJ)$$

$$a_{s'} = [g\mu_B H_0 + 2D_{s'} S\eta + S(4J_{s'} + J) - SJ_{s'}\gamma(\mathbf{k}_\parallel)] \,/\, (SJ)$$

$$f_s = 2F_s S\eta' \,/\, (SJ)$$

$$f = 2FS\eta' \,/\, (SJ)$$

$$f_{s'} = 2F_{s'} S\eta' \,/\, (SJ). \qquad (2.2.15)$$

The tridiagonal matrix $\underline{A}$ may be rewritten as (DeWames and Wolfram 1969, Cottam 1976)

$$\underline{A} = \underline{A}_0 + \underline{\Delta} \qquad (2.2.16)$$

where

$$\underline{A}_0 = \begin{bmatrix} a & -1 & 0 & 0 & \dots & & & \\ -1 & a & -1 & 0 & \dots & & & \\ 0 & -1 & a & -1 & \dots & & & \\ \vdots & \vdots & \vdots & \vdots & & \vdots & \vdots & \vdots \\ & & & & \dots & a & -1 & 0 \\ & & & & \dots & -1 & a & -1 \\ & & & & \dots & 0 & -1 & a \end{bmatrix} \qquad (2.2.17)$$

$$\underline{\Delta} = \begin{bmatrix} \Delta_s & 0 \dots & & \\ 0 & 0 \dots & & \\ \vdots & \vdots & \vdots & \vdots \\ & & \dots 0 & 0 \\ & & \dots 0 & \Delta_{s'} \end{bmatrix} \qquad (2.2.18)$$

with $\Delta_s \equiv a_s - a$ and $\Delta_{s'} \equiv a_{s'} - a$. Note that we have effectively separated the bulk and surface properties into the matrices $\underline{A}_0$ and $\underline{\Delta}$ respectively. The inverse of a finite-dimensional tridiagonal matrix such as $\underline{A}_0$ is known (e.g. see Cottam and Kontos 1980) to have elements

$$(\underline{A}_0^{-1})_{ij} = \frac{x^{i+j} - x^{|i-j|} + x^{2N+2-(i+j)} - x^{2N+2-|i-j|}}{(1 - x^{2N+2})(x - x^{-1})} \qquad (2.2.19)$$

where x is a complex variable such that $|x| \leq 1$ and $x + x^{-1} = a$. This property of the inverse is used frequently in the calculations described in the remainder of this thesis.

The nature of the matrix $\underline{f}$ appearing in (2.2.12) determines how the matrix equations are to be solved. As mentioned earlier two special cases for $\underline{f}$ arise depending on whether the anisotropy i. nonuniaxial throughout the film (case A) or just on the surface(s) (case B). These cases present different problems for solving the matrix equations and for eventual numerical extraction of dispersion relations. Each of these situations is treated in a separate section.

2.3. Case A : The Anisotropy is Nonuniaxial Throughout The Film

In this instance the matrix $\underline{f}$ may be written as $f\underline{\nu}$ where $\underline{\nu}$ is an *invertible* matrix which differs from the unit matrix only in the 1,1 and N,N elements which are f_s/f and $f_{s'}/f$ respectively:

$$\underline{\nu} = \begin{bmatrix} f_s/f & 0 & 0\ldots & & & \\ 0 & 1 & 0\ldots & & & \\ 0 & 0 & 1\ldots & & & \\ \vdots & \vdots & \vdots & \vdots & \vdots & \vdots \\ & & \ldots & 0 & 0 & \\ & & \ldots 0 & 1 & 0 & \\ & & \ldots 0 & 0 & f_s,/f & \end{bmatrix}. \qquad (2.3.1)$$

For convenience, the present case may be further subdivided. In case *A.1* we consider the nonuniaxial parameter F to have the same value everywhere, and we see that $\underline{\nu}$ reduces to the unit matrix. In case *A.2* we have $F_s \neq F \neq F_s$, $(\neq 0)$ in general and no such simplification occurs. In either situation $\underline{\nu}$ is an invertible matrix and (2.2.12) is solved analytically as shown below.

2.3.1 Case A.1: The Nonuniaxial Parameter F is the Same Throughout the Film

In the present case where $F_s = F = F_s$, (or $f_s = f = f_s$,), $\underline{\nu}$ is simply the unit matrix, and the matrix equations (2.2.12) become

$$(-\Omega\underline{I} + \underline{A}_0 + \underline{\Delta})\underline{b} = f\underline{b}^\dagger$$
$$(\Omega\underline{I} + \underline{A}_0 + \underline{\Delta})\underline{b}^\dagger = f\underline{b}. \qquad (2.3.2)$$

These lead to

$$[(\Omega\underline{I} + \underline{A}_0 + \underline{\Delta})\ (-\Omega\underline{I} + \underline{A}_0 + \underline{\Delta}) - f^2\underline{I}]\ \underline{b} = 0$$
$$[(-\Omega\underline{I} + \underline{A}_0 + \underline{\Delta})\ (\Omega\underline{I} + \underline{A}_0 + \underline{\Delta}) - f^2\underline{I}]\ \underline{b}^\dagger = 0 \qquad (2.3.3)$$

or

$$(\underline{A}_1 + \underline{\Delta})\ (\underline{A}_2 + \underline{\Delta})\ \underline{b} = 0$$
$$(\underline{A}_2 + \underline{\Delta})\ (\underline{A}_1 + \underline{\Delta})\ \underline{b}^\dagger = 0. \qquad (2.3.4)$$

Here we have defined $\underline{A}_1$ and $\underline{A}_2$ as follows:

$$\underline{A}_1 = \underline{A}_0 - \sqrt{\Omega^2 + f^2}\ \underline{I}$$
$$\underline{A}_2 = \underline{A}_0 + \sqrt{\Omega^2 + f^2}\ \underline{I}. \qquad (2.3.5)$$

The matrices $\underline{A}_1$ and $\underline{A}_2$ are tridiagonal with inverses therefore given by (2.2.19) in terms of the complex variables x_1 and x_2 respectively (analogous to the complex x in (2.2.19)). These variables therefore have the following definitions:

$$x_1 + x_1^{-1} = a - \sqrt{\Omega^2 + f^2}$$
$$x_2 + x_2^{-1} = a + \sqrt{\Omega^2 + f^2} \qquad (2.3.6)$$

with $|x_1| \leq 1$ and $|x_2| \leq 1$.

From (2.3.4) we can see that non-trivial solutions exist (for both $\underline{b}$ and $\underline{b}^{\dagger}$) if either of the conditions

$$\det\ (\underline{I} + \underline{A}_1^{-1}\underline{\Delta}) = 0$$
$$\det\ (\underline{I} + \underline{A}_2^{-1}\underline{\Delta}) = 0 \qquad (2.3.7)$$

are satisfied. We can write the first of these conditions in terms of x_1 (as shown in detail below). The zeroes of this function (a polynomial of order ~ N) are related to the set of spin-wave frequencies $\{\Omega^S\}$ by the definitions in (2.3.6). The roots must be found numerically, however, in all but the most simple cases. Finding the roots and the corresponding spin-wave frequencies is the subject of Chapter 3. It will be shown that the second determinantal condition (which leads to a polynomial in x_2) is redundant in that it does not give rise to any new physical modes.

Although the nonuniaxial parameter is assumed at present to have the same value throughout the material it is possible that the other constants (D_i and J_{ij}) do not. We consider separately the cases in which the film surfaces are symmetric and asymmetric with respect to these parameters.

In the symmetric case, where $D_s = D_{s'}$ and $J_s = J_{s'}$, the matrix $\underline{\Delta}$ has identical 1,1 and N,N elements: $\Delta_s = a_s - a$. We consider at present the $\det(I + \underline{A}_1^{-1}\underline{\Delta}) = 0$ condition. The matrix $\underline{Q} \equiv \underline{A}_1^{-1}$ has the following general symmetry properties (as can be seen from (2.2.19)):

$$Q_{11} = Q_{NN}, \quad Q_{ij} = Q_{ji}, \quad Q_{iN} = Q_{(N-i+1)1} \quad \text{etc.}$$

Using these properties the matrix $(\underline{I} + \underline{Q\Delta}) \equiv \underline{P}$ can be written in partitioned form as:

$$\underline{P} = \begin{bmatrix} P_1 & \vdots & 0 & \vdots & P_3 \\ \cdots & & \cdots & & \cdots \\ \underline{P}_2 & \vdots & \underline{I} & \vdots & \underline{P}_5 \\ \cdots & & \cdots & & \cdots \\ P_3 & \vdots & 0 & \vdots & P_1 \end{bmatrix} \tag{2.3.8}$$

where $P_1 = Q_{11}\Delta_s + 1$, $P_3 = Q_{1N}\Delta_s$, and $\underline{P}_2$ and $\underline{P}_5$ are $1\times(N-2)$ column matrices. The determinant of $\underline{P}$ can be written as follows:

$$\begin{aligned} \det \underline{P} &= P_1^2 - P_3^2 \\ &= (Q_{11}\Delta_s + 1 - Q_{1N}\Delta_s)\,(Q_{11}\Delta_s + 1 + Q_{1N}\Delta_s). \end{aligned} \tag{2.3.9}$$

The spin-wave frequencies are related to the roots of these expressions. The right-hand side of (2.3.9) can be written in terms of x_1 using (2.2.19) as $y_1^{A1}(x_1)y_2^{A1}(x_1)/(1 - x_1^{2N+2})$. We define the functions

$$\begin{aligned} y_1^{A1}(x_1) &= g(x_1)\Delta_s + r(x_1) \\ y_2^{A1}(x_1) &= h(x_1)\Delta_s + s(x_1) \end{aligned} \tag{2.3.10}$$

where

$$\begin{aligned} g(x_1) &= x_1 - x_1^N \\ h(x_1) &= x_1 + x_1^N \\ r(x_1) &= 1 - x_1^{N+1} \\ s(x_1) &= 1 + x_1^{N+1}. \end{aligned} \tag{2.3.11}$$

Identical expression in terms of x_2 arise from the factor $(\underline{I} + \underline{A}_2^{-1}\underline{\Delta})$.

In Chapter 3 these equations will be used to extract the surface and bulk spin-wave frequencies.

To demonstrate that our results are consistent with those of some earlier studies we examine some special cases at this point. In the limit of thick films, where N is very large and therefore $x_1^N \to 0$, each of the functions y_1^{A1} and y_2^{A1} above has roots where $x_1 = -1/\Delta_s$ which, along with (2.3.6), is the result found previously for semi-infinite systems having the same nonuniaxial parameter throughout (Gopalan and Cottam 1990). The thick-film limit may be thought of as a film in which the surfaces are far enough apart to be isolated from one another. We expect that each surface would then resemble the single surface of a "semi-infinite" system. The criteria for this limit are discussed in Chapter 3.

We note also that the expressions (2.3.10) and (2.3.11) are formally the same as those derived for the uniaxial thin film (Cottam and Kontos 1980). However here we have defined x_1 and x_2 differently so that they involve a nonuniaxial parameter f (2.3.6). In Chapter 3 we will show that the nonuniaxial dispersion relations are shifted (downwards) in frequency relative to those for uniaxial films. For the spin-wave frequencies we recover the uniaxial thin-film result by simply setting f equal to zero in (2.3.6). The uniaxial limit is discussed in more detail in Chapters 3 and 4.

Semi-infinite uniaxial or isotropic systems have been treated by several authors (e.g. see review by Wolfram and DeWames 1972). In the formalism

employed here the spin-wave solution can be expressed as $x_1 = -1/\Delta_s$ (see e.g. Cottam 1976) with Δ_s depending on the specific assumptions made regarding uniaxial anisotropy (if any) and exchange. Our solution, as noted above, is distinguished by the inclusion of f in the definition of x_1. By taking the limit that $N \to \infty$ and setting f equal to zero in (2.3.6) we recover the results of these earlier studies.

A more general case is that in which the films are not symmetric with repect to their surface parameters and the matrices $\underline{P}$ and $\underline{\Delta}$ do not have the symmetry properties mentioned above. This situation may occur if, for example, the film is prepared with an overlayer (if any) and substrate of different species. Generalizing (2.3.8), we have

$$\underline{P} = \begin{bmatrix} P_1 & \vdots & 0 & \vdots & P_6 \\ \cdots & & \cdots & & \cdots \\ \underline{P}_2 & \vdots & \underline{I} & \vdots & \underline{P}_5 \\ \cdots & & \cdots & & \cdots \\ P_3 & \vdots & 0 & \vdots & P_4 \end{bmatrix}. \qquad (2.3.12)$$

It follows that

$$\det \underline{P} = P_1P_4 - P_3P_6$$
$$= (Q_{11}\Delta_s + 1)\,(Q_{11}\Delta_{s'} + 1) - (Q_{1N}\Delta_s)\,(Q_{1N}\Delta_{s'}). \qquad (2.3.13)$$

The numerator of this expression can be written as

$$y^{A1a}(x_1) = g(x_1)h(x_1)\Delta_s\Delta_{s'} + q(x_1)(\Delta_s + \Delta_{s'}) + r(x_1)s(x_1) \qquad (2.3.14)$$

where

$$q(x_1) = x_1 - x_1^{2N+1} \qquad (2.3.15)$$

and $g(x_1)$, $h(x_1)$, $r(x_1)$ and $s(x_1)$ are defined as in (2.3.11). The superscript refers to the asymmetric case of model A.1.

The determination of spin-wave frequencies from (2.3.14) is also discussed in Chapter 3 with examples of numerical results for various

values of the exchange and anisotropy parameters provided. We note that if the surfaces are symmetric then $\Delta_s = \Delta_{s'}$, and (2.3.14) factorizes to give the functions in (2.3.10). These results for the more general asymmetric case therefore incorporate those of the special symmetric case, as expected. In the limit that $N \to \infty$ we find that (2.3.14) reduces to $(x_1\Delta_s + 1)(x_1\Delta_{s'} + 1)$. Each of these factors corresponds to the semi-infinite result for a different surface, as expected.

2.3.2 Case A.2: The Nonuniaxial Parameter is Modified on the Surfaces

In this more general case the surface nonuniaxial parameters F_s and $F_{s'}$ may have different values than the bulk value F (which is still non-zero). We write the matrix $\underline{f}$ defined in (2.2.13) as $f\underline{\nu}$ where $\underline{\nu}$ is given by (2.3.1), and (2.2.12) becomes:

$$(-\Omega\underline{I} + \underline{A})\underline{b} = f\underline{\nu}\underline{b}^{\dagger}$$
$$(\Omega\underline{1} + \underline{A})\underline{b}^{\dagger} = f\underline{\nu}\underline{b}. \qquad (2.3.16)$$

We use the invertibility of $\underline{\nu}$ to find

$$\left[(\Omega\underline{I} + \underline{A})\underline{\nu}^{-1}(-\Omega\underline{I} + \underline{A}) - f^2\underline{\nu}\right]\underline{b} = 0$$
$$\left[(-\Omega\underline{I} + \underline{A})\underline{\nu}^{-1}(\Omega\underline{I} + \underline{A}) - f^2\underline{\nu}\right]\underline{b}^{\dagger} = 0. \qquad (2.3.17)$$

In order to simplify these expressions we rewrite the diagonal matrix $\underline{\nu}$ as $\underline{\nu} = \underline{I} + \underline{\theta}$ and the diagonal matrix $\underline{\nu}^{-1}$ as $\underline{\nu}^{-1} = \underline{I} + \underline{\upsilon}$ where $\underline{\theta}$ and $\underline{\upsilon}$ are non-zero only in their 1,1 and N,N elements. Using (2.2.16) and the above definitions we can rewrite (2.3.17) as

$$\left[(\Omega\underline{I} + \underline{A}_0 + \underline{\Delta})(\underline{I} + \underline{\upsilon})(-\Omega\underline{I} + \underline{A}_0 + \underline{\Delta}) - f^2(\underline{I} + \underline{\theta})\right]\underline{b} = 0$$
$$\left[(-\Omega\underline{I} + \underline{A}_0 + \underline{\Delta})(\underline{I} + \underline{\upsilon})(\Omega\underline{I} + \underline{A}_0 + \underline{\Delta}) - f^2(\underline{I} + \underline{\theta})\right]\underline{b}^{\dagger} = 0 \qquad (2.3.18)$$

or

$$\left[\underline{A}_0^2 - (\Omega^2 + f^2)\underline{I} + \underline{\Lambda}^+\right]\underline{b} = 0$$

$$\left[\underline{A}_0^2 - (\Omega^2 + f^2)\underline{I} + \underline{\Lambda}^-\right]\underline{b}^\dagger = 0 \qquad (2.3.19)$$

where $\underline{A}_0$ and $\underline{\Delta}$ are defined as in (2.2.17) and (2.2.18), and

$$\underline{\Lambda}^\pm = \underline{A}_0\underline{\Delta} + \underline{\Delta}\underline{A}_0 + \underline{\Delta}^2 - \Omega^2\underline{v} - f^2\underline{\vartheta} \pm \Omega\underline{v}\underline{A}_0 \pm \Omega\underline{A}_0\underline{v}$$
$$\pm \Omega\underline{v}\underline{\Delta} \mp \Omega\underline{\Delta}\underline{v} + \underline{A}_0\underline{v}\underline{\Delta} - \underline{\Delta}\underline{v}\underline{A}_0 + \underline{\Delta}\underline{v}\underline{\Delta} + \underline{A}_0\underline{v}\underline{A}_0. \qquad (2.3.20)$$

The N×N matrices $\underline{\Lambda}^\pm$ have only a few non-zero elements:

$$\Lambda^\pm_{11} = (a + \Delta)^2 \nu_s^{-1} - a^2 - \Omega^2(\nu_s^{-1} - 1) - f^2(\nu_s - 1)$$
$$\Lambda^\pm_{12} = \pm\Omega(\nu_s^{-1} - 1) + a - (a + \Delta)\nu_s^{-1}$$
$$\Lambda^\pm_{21} = \mp\Omega(\nu_s^{-1} - 1) + a - (a + \Delta)\nu_s^{-1}$$
$$\Lambda^\pm_{22} = \nu_s^{-1} - 1$$
$$\Lambda^\pm_{N-1,N-1} = \nu_{s'}^{-1} - 1$$
$$\Lambda^\pm_{N-1,N} = \mp\Omega(\nu_{s'}^{-1} - 1) + a - (a + \Delta)\nu_{s'}^{-1}$$
$$\Lambda^\pm_{N,N-1} = \pm\Omega(\nu_{s'}^{-1} - 1) + a - (a + \Delta)\nu_{s'}^{-1}$$
$$\Lambda^\pm_{N,N} = (a + \Delta)^2 \nu_{s'}^{-1} - a^2 - \Omega^2(\nu_{s'}^{-1} - 1) - f^2(\nu_{s'} - 1) \qquad (2.3.21)$$

where we denote $\nu_s \equiv f_s/f$ and $\nu_{s'} \equiv f_{s'}/f$.

Defining $\underline{A}_1$ and $\underline{A}_2$ as in (2.3.5) we can rewrite (2.3.19) as

$$[\underline{A}_1\underline{A}_2 + \underline{\Lambda}^+]\underline{b} = 0$$

$$[\underline{A}_1\underline{A}_2 + \underline{\Lambda}^-]\underline{b}^\dagger = 0 \qquad (2.3.22)$$

which implies

$$[\underline{I} + \underline{A}_2^{-1}\underline{A}_1^{-1}\underline{\Lambda}^+]\underline{b} = 0.$$

$$[\underline{I} + \underline{A}_2^{-1}\underline{A}_1^{-1}\underline{\Lambda}^-]\underline{b}^\dagger = 0. \qquad (2.3.23)$$

For operator $\underline{b}$ the condition for a non-trivial solution to exist is $\det[\underline{I} + \underline{A}_1^{-1}\underline{A}_2^{-1}\underline{\Lambda}^+] = 0$. This condition can be used to find the spin-wave frequencies. The matrix $[\underline{I} + \underline{A}_1^{-1}\underline{A}_2^{-1}\underline{\Lambda}^+] \equiv \underline{M}$ may be written in

partitioned form as

$$\underline{M} = \begin{bmatrix} \underline{M}_1 & \vdots & 0 & \vdots & \underline{M}_6 \\ \cdots & & \cdots & & \cdots \\ \underline{M}_2 & \vdots & \underline{I} & \vdots & \underline{P}_5 \\ \cdots & & \cdots & & \cdots \\ \underline{M}_3 & \vdots & 0 & \vdots & \underline{M}_4 \end{bmatrix} \tag{2.3.24}$$

where $\underline{M}_1$, $\underline{M}_3$, $\underline{M}_4$ and $\underline{M}_6$ are 2×2 matrices and therefore the determinant of $\underline{M}$ is given by

$$\det \underline{M} = \begin{vmatrix} \underline{M}_1 & \vdots & \underline{M}_6 \\ \cdots & & \cdots \\ \underline{M}_3 & \vdots & \underline{M}_4 \end{vmatrix} \tag{2.3.25}$$

which will have more terms than det $\underline{P}$ defined above. In addition we note that this determinant will be expressed in terms of both x_1 and x_2, and so this expression is more complicated than that found in case A.1. The procedures for extracting numerical results, together with examples, are discussed in Chapter 3. We note at this point that if $F_s = F_{s'} = F$ then $\underline{\Lambda}^{\pm}$ is greatly simplified and we recover the results for case A.1, as expected.

2.4 Case B: The Anisotropy is Nonuniaxial on the Surfaces Only

Two cases which are of interest arise here, that in which the nonuniaxial term is non-zero on both surfaces and that in which it is non-zero on one surface only. These cases, called *B.1* and *B.2* respectively, are the subjects of Sections 2.4.1 and 2.4.2. In either case the bulk nonuniaxial parameter F is zero and the matrix $\underline{f}$, defined in (2.2.13), is not invertible.

2.4.1 Case B.1: The Nonuniaxial Parameter is Non-zero on Both Surfaces

We assume, for simplicity, that the nonuniaxial parameter has the same value on each surface (i.e. $F_s = F_{s'}$) to write $\underline{f} = f_s \underline{\nu}$ where:

$$\underline{\nu} = \begin{bmatrix} 1 & 0 & 0\ldots & & & \\ 0 & 0 & 0\ldots & & & \\ 0 & 0 & 0\ldots & & & \\ \vdots & \vdots & \vdots & \vdots & \vdots & \vdots \\ & & \ldots & 0 & 0 & \\ & & \ldots 0 & 0 & 0 & \\ & & \ldots 0 & 0 & 1 & \end{bmatrix}. \qquad (2.4.1)$$

The coupled matrix equations (2.2.12) are written as

$$(-\Omega\underline{I} + \underline{A}_0 + \underline{\Delta})\ \underline{b} = f_s\underline{\nu b}^\dagger$$

$$(\Omega\underline{I} + \underline{A}_0 + \underline{\Delta})\ \underline{b}^\dagger = f_s\underline{\nu b} \qquad (2.4.2)$$

or

$$(\underline{A}_1 + \underline{\Delta})\ \underline{b} = f_s\underline{\nu b}^\dagger$$

$$(\underline{A}_2 + \underline{\Delta})\ \underline{b}^\dagger = f_s\underline{\nu b}. \qquad (2.4.3)$$

Here we have used (2.2.16) and have modified the definitions of $\underline{A}_1$ and $\underline{A}_2$ in (2.3.6) to become

$$\underline{A}_1 = \underline{A}_0 - \Omega\underline{I}$$

$$\underline{A}_2 = \underline{A}_0 + \Omega\underline{I}. \qquad (2.4.4)$$

The matrices $\underline{A}_1$ and $\underline{A}_2$ are tridiagonal and can be inverted as described before in (2.2.19) so that now we define

$$x_1 + x_1^{-1} = a - \Omega$$

$$x_2 + x_2^{-1} = a + \Omega \qquad (2.4.5)$$

with $|x_1| \leq 1$ and $|x_2| \leq 1$ as before.

We straightforwardly solve (2.4.3) finding

$$\left[\underline{I} - f_s^2(\underline{I} + \underline{A}_1^{-1}\underline{\Delta})^{-1}\underline{A}_1^{-1}\underline{\nu}(\underline{I} + \underline{A}_2^{-1}\underline{\Delta})^{-1}\underline{A}_2^{-1}\underline{\nu}\right]\underline{b} = 0.$$

$$\left[\underline{I} - f_s^2(\underline{I} + \underline{A}_2^{-1}\underline{\Delta})^{-1}\underline{A}_2^{-1}\underline{\nu}(\underline{I} + \underline{A}_1^{-1}\underline{\Delta})^{-1}\underline{A}_1^{-1}\underline{\nu}\right]\underline{b}^\dagger = 0. \qquad (2.4.6)$$

As usual we must find the zeroes of the determinants of these matrices in order to evaluate the spin-wave frequencies. We first introduce simpler notation where $\underline{A}_1^{-1} \equiv \underline{Q}$, $\underline{A}_2^{-1} \equiv \underline{S}$, $(\underline{I} + \underline{Q\Delta}) \equiv \underline{P}$ and $(\underline{I} + \underline{S\Delta}) \equiv \underline{R}$.

Writing $\underline{P}$ in block form as in (2.3.12) it then follows that

$$\underline{P}^{-1} = \begin{bmatrix} X_1 & : & 0 & : & X_6 \\ \cdots & & \cdots & & \cdots \\ \underline{X}_2 & : & \underline{I} & : & \underline{X}_5 \\ \cdots & & \cdots & & \cdots \\ X_3 & : & 0 & : & X_4 \end{bmatrix} \tag{2.4.7}$$

where (e.g. see Cottam and Kontos 1980):

$$\begin{aligned} X_1 &= -(P_4^{-1}P_3 - P_6^{-1}P_1)^{-1}P_6^{-1} \\ \underline{X}_2 &= -\underline{P}_5\underline{P}_6^{-1} + \underline{P}_5(\underline{P}_5^{-1}\underline{P}_2 - P_6^{-1}P_1)(P_4^{-1}P_3 - P_6^{-1}P_1)^{-1}P_6^{-1} \\ X_3 &= P_6^{-1} + P_6^{-1}P_1(P_4^{-1}P_3 - P_6^{-1}P_1)^{-1}P_6^{-1} \\ X_4 &= -P_6^{-1}P_1(P_4^{-1}P_3 - P_6^{-1}P_1)^{-1}P_4^{-1} \\ \underline{X}_5 &= -\underline{P}_5(\underline{P}_5^{-1}\underline{P}_2 - P_6^{-1}P_1)(P_4^{-1}P_3 - P_6^{-1}P_1)^{-1}P_4^{-1} \\ X_6 &= (P_4^{-1}P_3 - P_6^{-1}P_1)^{-1}P_4^{-1}. \end{aligned} \tag{2.4.8}$$

Similar expressions exist for the matrix $\underline{R}^{-1}$. If, for the sake of simplicity, we assume that the surfaces are identical in their D_S and J_S parameters, so that $\Delta_S = \Delta_{S'}$, then we can make use of the corresponding symmetry properties described above to write $X_4 = X_1$ and $X_6 = X_3$. Considering the case of $\underline{b}$ at present, we can write $\underline{P}^{-1}\underline{Q\nu}\underline{R}^{-1}\underline{S\nu} \equiv \underline{T}$ where

$$\underline{T} = \begin{bmatrix} T_1 & : & 0 & : & T_3 \\ \cdots & & \cdots & & \cdots \\ \underline{T}_2 & : & 0 & : & \underline{T}_5 \\ \cdots & & \cdots & & \cdots \\ T_3 & : & 0 & : & T_1 \end{bmatrix} \tag{2.4.9}$$

with the result that

$$\det[\underline{I} - f_S^2\underline{T}] = (1 - f_S^2T_1 - f_S^2T_3)(1 - f_S^2T_1 + f_S^2T_3). \tag{2.4.10}$$

The existence condition for a non-trivial solution will be related to the zeroes of (2.4.10). Explicitly the numerators of these expressions can be written as

$$\begin{aligned} y_1^{B1}(x_1,x_2) &= [g(x_1)\Delta_S + r(x_1)][g(x_2)\Delta_S + r(x_2)] - f_S^2\, g(x_1)g(x_2) \\ y_2^{B1}(x_1,x_2) &= [h(x_1)\Delta_S + s(x_1)][h(x_2)\Delta_S + s(x_2)] - f_S^2\, h(x_1)h(x_2) \end{aligned} \tag{2.4.11}$$

where $g(x)$, $h(x)$, $r(x)$, and $s(x)$ are defined as in (2.3.11). We note that in this case the solutions depend directly on the nonuniaxial parameter f_s while in case A.1 the dependence was via the definitions of x_1 and x_2. Furthermore, here the expressions (2.4.11) do not reduce to separate, equivalent conditions on x_1 and x_2. Identical expressions result from considering the condition on $\underline{b}^{\dagger}$. The extraction of spin-wave frequencies is discussed in Chapter 3.

At this point we note that in the thick-film limit where $N \to \infty$ the functions y_1^{B1} and y_2^{B1} each reduce to

$$y_1^{B1} = y_2^{B1} = (x_1\Delta_s + 1)(x_2\Delta_s + 1) - f_s^2 x_1 x_2. \qquad (2.4.12)$$

Upon defining a new complex variable $\alpha \equiv x_1 x_2$, where $|\alpha| \leq 1$, and using (2.4.5) to write

$$x_1 + x_1^{-1} + x_2 + x_2^{-1} = 2a \qquad (2.4.13)$$

(2.4.12) becomes

$$y_1^{B1} = y_2^{B1} = \alpha^2(\Delta_s^2 - f_s^2) + \alpha(\Delta_s^2 - f_s^2) + 2a\alpha\Delta_s + 1 + \alpha. \qquad (2.4.14)$$

This is the same expression found previously (Gopalan and Cottam 1990) for a semi-infinite system where the anisotropy is nonuniaxial on the surface but not in the bulk.

If, on the other hand we let $f_s = 0$ in (2.4.11) we recover the uniaxial, finite-thickness result (Cottam and Kontos 1980) in which the solutions for $\underline{b}$ are then determined by (2.3.10). The roots of the corresponding expressions in terms of x_2 are associated with $\underline{b}^{\dagger}$. In the uniaxial, thick-film limit (2.4.12) becomes

$$y_1^{B1} = y_2^{B1} = (x_1\Delta_s + 1)(x_2\Delta_s + 1). \qquad (2.4.15)$$

The solutions $x_1 = -1/\Delta_s$ and $x_2 = -1/\Delta_s$ are then associated with $\underline{b}$ and

$\underline{b}^{\dagger}$ respectively in a semi-infinite uniaxial (or isotropic) system. The uniaxial limit is discussed in more detail in Chapters 3 and 4.

2.4.2 Case B.2: The Anisotropy is Nonuniaxial on One Surface Only

In the second variation of case B, where the anisotropy is nonuniaxial at one surface only, $\underline{\nu}$ is

$$\underline{\nu} = \begin{bmatrix} 1 & 0 & 0 & \cdots & & & \\ 0 & 0 & 0 & \cdots & & & \\ 0 & 0 & 0 & \cdots & & & \\ \vdots & \vdots & \vdots & & \vdots & \vdots & \vdots \\ & & & \cdots & 0 & 0 & \\ & & & \cdots 0 & 0 & 0 & \\ & & & \cdots 0 & 0 & 0 & \end{bmatrix} \tag{2.4.16}$$

For convenience the surfaces are assumed to be symmetric with respect to exchange and other parameters. The matrix $\underline{T}$ defined in (2.4.9) becomes

$$\underline{T} = \begin{bmatrix} T_1 & \vdots & 0 & \vdots & 0 \\ \cdots & & \cdots & & \cdots \\ \underline{T}_2 & \vdots & 0 & \vdots & 0 \\ \cdots & & \cdots & & \cdots \\ T_3 & \vdots & 0 & \vdots & 0 \end{bmatrix} \tag{2.4.17}$$

with

$$\det[\underline{I} - f_s^2\underline{T}] = 1 - f_s^2 T_1. \tag{2.4.18}$$

We write the numerator of this factor as

$$\begin{aligned} y^{B2}(x_1,x_2) = {} & [g(x_1)\Delta_s + r(x_1)][h(x_1)\Delta_s + s(x_1)] \\ & \times [g(x_2)\Delta_s + r(x_2)][h(x_2)\Delta_s + s(x_1)] \\ & - f_s^2[g(x_1)h(x_1)\Delta_s + q(x_1)][g(x_2)h(x_2)\Delta_s + q(x_2)] \end{aligned} \tag{2.4.19}$$

where $g(x)$, $h(x)$, $r(x)$ and $s(x)$ are defined as in (2.3.11) and $q(x)$ is defined in (2.3.15). The uniaxial limit ($f_s \to 0$) is the same as that for case B.1. In the thick-film limit y^{B2} can be factorized to

$$(x_1\Delta_s + 1)(x_2\Delta_s + 1)[(x_1\Delta_s + 1)(x_2\Delta_s + 1) - f_s^2 x_1 x_2] \tag{2.4.20}$$

The first two factors arise in the uniaxial semi-infinite case and are therefore related to the surface (n = N) where $f_s = 0$. The second factor is found in the semi-infinite limit for case B.1 and is therefore associated with the surface (n = 1) where $f_s \neq 0$. The strategy for finding numerical results from (2.4.19) is similar to that used for (2.4.11) as discussed, with numerical examples, in Chapter 3.

2.5 Discussion

We have treated a number of variations of our general model wherein the exchange, uniaxial and nonuniaxial anisotropy parameters may be modified at the surfaces of a finite-thickness film. We have considered both symmetric and asymmetric films and systems wherein the anisotropy is nonuniaxial for every site and those in which this type of anisotropy arises only at the surface(s). We have shown that in the limit that N is large we recover the previous results for semi-infinite systems and that, if N is finite but the nonuniaxial parameter is zero then we recover the results for uniaxial films. In all cases but one (case A.2) we have found conditions for the existence of spin-wave solutions expressed in terms of polynomials in the complex variables x_1 and/or x_2. These expressions (labelled y^m or y_1^m and y_2^m, where the superscript m identifies the particular special case, e.g. A.1, etc.) are found in (2.3.10), (2.3.14), (2.4.11) and (2.4.19). The extraction of explicit dispersion relations, including numerical examples, from these formal expressions is the subject of Chapter 3. Also in Chapter 3 a different procedure is devised for the analysis of case A.2 where the formal result is given by (2.3.25).

CHAPTER 3

DISPERSION RELATIONS FOR FERROMAGNETIC THIN FILMS

The operator equation-of-motion method has been used to find a set of existence conditions for spin waves for several variations of our general model, as described in Chapter 2. For cases A.1, B.1 and B.2 (as defined earlier) these conditions involve finding the zeroes of a set of functions summarized in (2.3.10), (2.3.14), (2.4.11) and (2.4.19) while for case A.2 the result is given formally by (2.3.25). In the former cases the functions are polynomials (in the complex variables x_1 and/or x_2) which contain surface and bulk parameters describing the exchange, anisotropy, applied field, and the wavevector $\mathbf{k}_{\parallel}$. The roots of these polynomials can be related to the spin-wave frequencies (in terms of the dimensionless quantity $\Omega \equiv \omega/(SJ)$) by the definition of the variables x_1 and x_2. The dispersion relations, which describe the dependence of spin-wave frequency (or energy) on the in-plane wavevector $\mathbf{k}_{\parallel}$, are thereby extracted.

In the much simpler case of semi-infinite uniaxial systems we have $x_1 = -1/\Delta_s$ for the surface spin-wave mode (Cottam 1976) and so explicit solutions exist. In our more complicated expressions the surface and quantized bulk dispersion relations must be determined numerically or graphically, except in some limiting cases. The distinction between (localized) surface and (non-localized) bulk modes has been discussed in Chapter 1. In Sections 3.1 and 3.2 we describe the procedure for determining the dispersion relation for cases A and B respectively. We

discuss the number of surface modes which occur under various conditions and present some numerical results for surface and bulk modes.

3.1 Case A: The Anisotropy is Nonuniaxial Throughout the Film

The condition for the existence of spin-wave solutions is different for cases A.1 (where the nonuniaxial parameter is the same throughout the film) and A.2 (where it is modified on the surfaces). In case A.1 we obtain identical polynomial expressions in terms of either x_1 or x_2, (see 2.3.10). Such a simplification is not possible for case A.2 (see (2.3.25)) which will therefore be treated separately.

3.1.1 Case A.1: The Nonuniaxial Parameter is the Same Throughout the Film

The nonuniaxial parameter is assumed to be non-zero throughout the film and, in addition, to have the same value everywhere. The surfaces may be symmetric or asymmetric with respect to exchange and uniaxial anisotropy parameters. In this case we are able to factor the determinant into separate and identical expressions for x_1 and x_2. As shown below we need only consider one such factor to find the entire set of spin-wave frequencies. We consider only x_1 here.

We recall that x_1 is a complex variable with $|x_1| \leq 1$. Surface modes correspond to those values of x_1 which are real and inside the unit circle ($-1 < x_1 < 1$) while bulk modes correspond to those values which are on the unit circle ($|x_1| = 1$) (see also Appendix III). For surface modes we can write $x_1 = \exp(\phi)$ where $\phi = -\lambda_s a_0$ (for $0 < x_1 < 1$) or $\phi = i\pi - \lambda_s a_0$ (for $-1 < x_1 < 0$) corresponding to *optic* and *acoustic* modes

respectively. For optic modes the frequency is greater than that of the bulk modes (of the same $k_{\parallel}$) while for acoustic modes it is less. The precession of spins on adjacent layers is in phase in the case of acoustic modes while it is out of phase in the case of optic modes (figure 3.1). For bulk modes we can write $x_1 = \exp(ik_z a_0)$ where k_z is a real wave-vector component with $k_z a_0 \in [0,\pi]$. The attenuation length of a surface mode in the semi-infinite limit, $L \equiv 1/\lambda_s$, can be found by noting that

$$|x_1| = \exp(-\lambda_s a_0) \qquad (3.1.1)$$

so that

$$L/a_0 = -1/\ln(|x_1|). \qquad (3.1.2)$$

In the present case of finite-thickness films this quantity can provide a measure of the attenuation length in films in which the overlap between the surface modes is not too pronounced.

We consider in turn the cases of symmetric films and asymmetric films. Some numerical results for both cases are presented in Section 3.1.2.

The existence condition for a solution (representing either a bulk or a surface mode) in the symmetric case is (2.3.10). When x_1 is real, corresponding to surface modes, the two terms in (2.3.10) may each be solved using standard numerical methods, limiting the variable x_1 to the interval (-1,1) of physical interest. The technique that we have employed is equivalent to the graphical one depicted in figure 3.2. Zeroes are identified by looking for changes in sign of the function on the interval of interest. The frequencies $\{\Omega^S\}$ can then be calculated from the solutions for x_1 as follows. We recall that x_1 is defined as

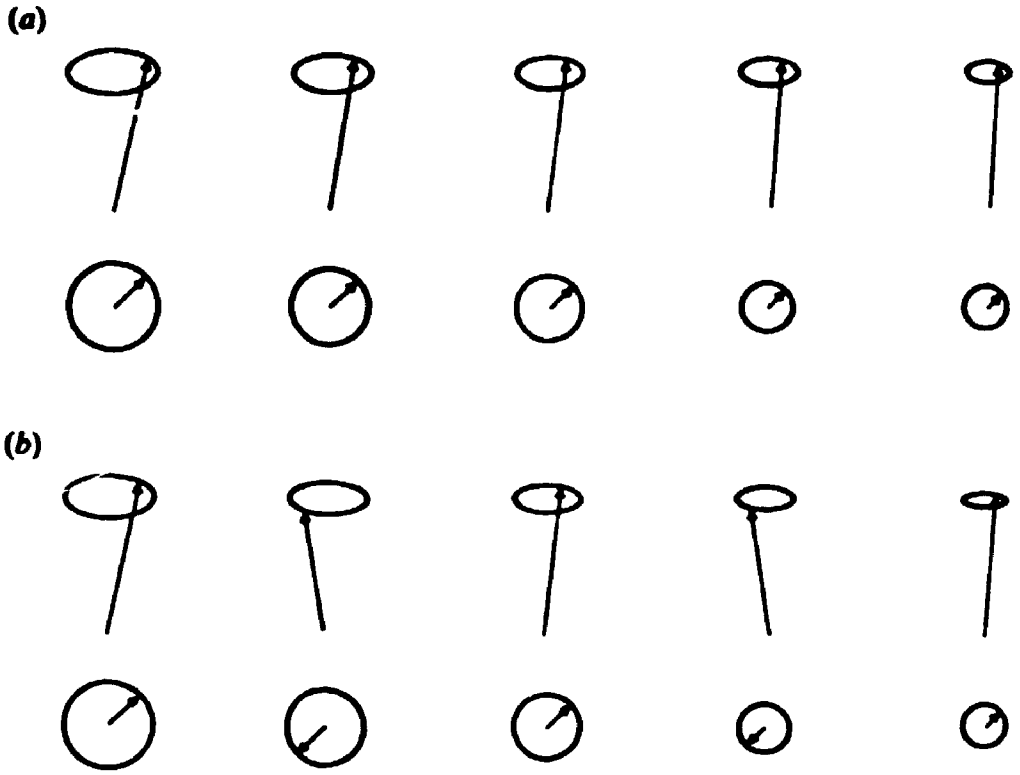

Figure 3.1 Semi-classical representation of surface spin waves showing the spin precession and decreasing amplitude in adjacent layers for acoustic (a) and optic (b) modes.

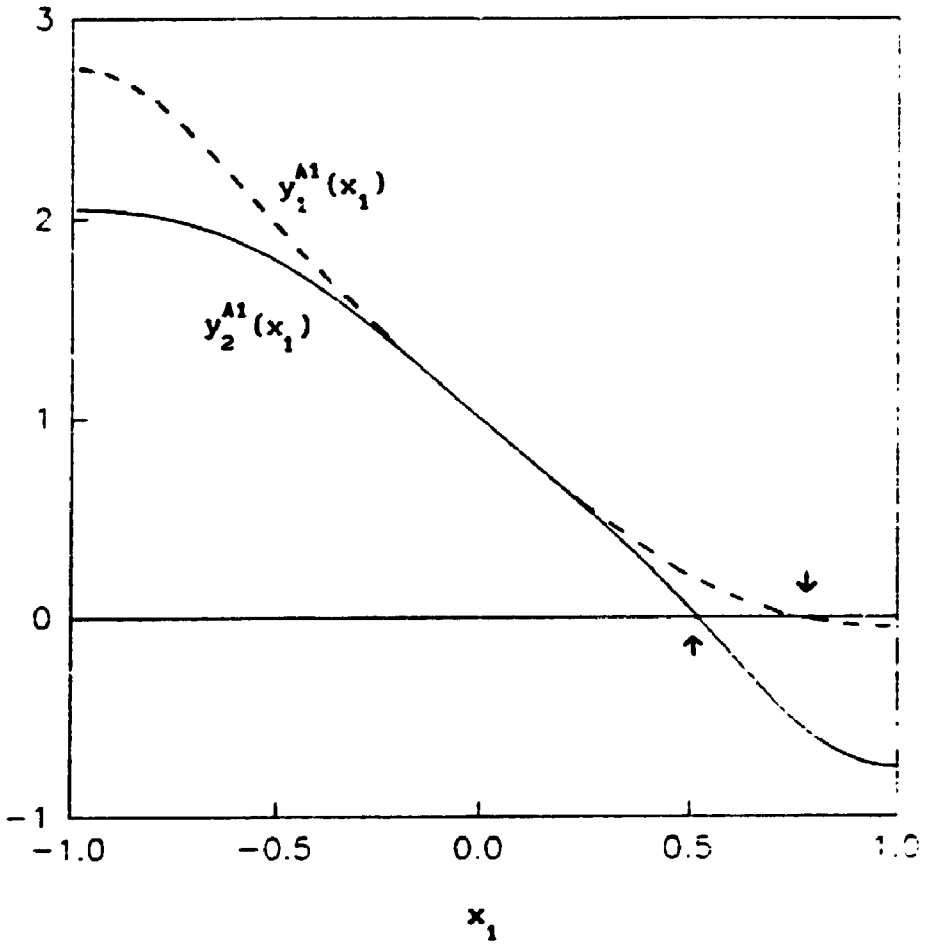

Figure 3.2 Schematic illustration of the graphical method of locating the roots of $y_1^{A1}(x_1)$ and $y_2^{A1}(x_1)$, defined in (2.3.10), on the interval $-1 < x < 1$ for case A.1. The roots are indicated by arrows. Here we have chosen $N = 3$ and $\Delta_s = -1.75$.

in (2.3.6) so that the surface-mode frequency is

$$\Omega^S = \pm [(x_1 + x_1^{-1} - a)^2 - f^2]^{1/2}. \qquad (3.1.3)$$

We note that both positive- and negative-frequency solutions are derived from each root. We will discuss the significance of this occurrence, not seen in the theory for uniaxial systems, with reference to the Green function results in Chapter 4. Expressions identical to (2.3.10) and (3.1.3) exist for x_2 and therefore either variable may be used to find the entire set of surface modes.

Depending on the values of Δ_S and N we find that zero, one or two positive-frequency surface modes exist. Surface modes may only occur if $|\Delta_S| > 1$ which is the condition for finding a solution of (2.3.10) which satisfies $|x_1| < 1$. The parameter Δ_S may be written as

$$\Delta_S = 2\eta[D_S - D]/J + [4 - \gamma(\mathbf{k}_\parallel)][J_S - J]/J - 1 \qquad (3.1.4)$$

using (2.2.15). If $D_S = D$ and $J_S = J$ then we have the limiting case of $\Delta_S = -1$ corresponding to $x_1 = \pm 1$ (which define the boundaries of the bulk-mode region). Previous studies on the sc (001) system have shown that if the exchange couples nearest neighbours only then the existence of surface modes depends on the perturbation of exchange and/or uniaxial parameters at the surface(s) (e.g. see Filipov 1967, Wallis *et al* 1967, Dobrzynski and Mills 1969, DeWames and Wolfram 1969, Wolfram and DeWames 1972). Kittel (1958) introduced the idea of surface pinning and established that the existence of a localized mode is contingent upon surface conditions. In the context of spin wave resonance Puszkarski (1979) reviews the number of surface modes possible under various conditions of surface pinning. Using a similar formalism as in the

present project (but for uniaxial systems) Cottam and Kontos (1980) conclude that one surface mode occurs if $1 < |\Delta_s| < (1 + \delta)$, two if $|\Delta_s| > (1 + \delta)$ and zero otherwise, where the parameter $\delta \equiv 2 / (N - 1)$. These simple conclusions do not, however, extend to cases A.2, B.1 and B.2 below.

The bulk modes are identified by evaluating (2.3.9) using $x_1 = \exp(i\theta)$ with $\theta = k_z a_0$ and using standard identities for complex exponentials. We find

$$y_1^{A1}(\theta) = g(\theta)\Delta_s + r(\theta)$$
$$y_2^{A1}(\theta) = h(\theta)\Delta_s + s(\theta) \qquad (3.1.5)$$

where

$$g(\theta) = \sin\left(\frac{N - 1}{2}\theta\right)$$
$$h(\theta) = \cos\left(\frac{N - 1}{2}\theta\right)$$
$$r(\theta) = \sin\left(\frac{N + 1}{2}\theta\right)$$
$$s(\theta) = \cos\left(\frac{N + 1}{2}\theta\right). \qquad (3.1.6)$$

The numerical technique is analogous to that used for the surface modes except that now the appropriate interval is $\theta \in [0, \pi]$. The bulk-mode frequencies are

$$\Omega_B = \pm\sqrt{(2\cos\theta - a)^2 - f^2}\ . \qquad (3.1.7)$$

Again we derive both positive- and negative-frequency modes from each root. Expression (3.1.7) is formally identical to the bulk dispersion relation in the cases of effectively infinite or semi-infinite samples (where $\theta = k_z a_0$ is unrestricted and the bulk modes form a continuum). In contrast, here a discrete set of values of k_z is obtained, corresponding to "quantization" of the bulk modes in a film. The values

of $k_z a_0 = 0$ and $k_z a_0 = \pi$, corresponding to the Brillouin zone centre and boundary respectively, provide lower and upper bounds for the bulk-mode frequencies for a given $\mathbf{k}_{\parallel}$.

In the case of an asymmetric film the spin-wave frequencies are related to the zeroes of (2.3.14). The surface-mode frequencies are then determined as for the symmetric films discussed above. For bulk modes we evaluate (2.3.13) using $x_1 = \exp(i\theta)$ to find

$$y^{A1a}(\theta) = g(\theta)h(\theta)\Delta_s\Delta_{s'} + q(\theta)(\Delta_s + \Delta_{s'}) + r(\theta)s(\theta) \qquad (3.1.8)$$

with $g(\theta)$, $h(\theta)$, $r(\theta)$ and $s(\theta)$ as in (3.1.6) and

$$q(\theta) = \sin(N\theta). \qquad (3.1.9)$$

The same method is used to find the roots of these equations as in the case of symmetric films.

3.1.2 Numerical Results for Case A.1

The principal numerical results are dispersion relations. Figures 3.3 through 3.8 show plots of frequency (in terms of the dimensionless quantity $\Omega \equiv \omega/SJ$) as a function of wavevector $|\mathbf{k}_{\parallel}a_0|$ for various choices of exchange and anisotropy parameters. As noted above both the bulk and surface spin-wave spectra are symmetric about $\Omega = 0$, therefore we have chosen to show only the positive-frequency branches.

The general features of the dispersion relations in ultrathin films are illustrated by figure 3.3 where we have chosen the spin quantum number S = 1, $D/J = 1.5$, $g\mu_B H_0/(SJ) = 0.3$, and $\mathbf{k}_{\parallel}$ is in the [100] direction, as in all subsequent figures in this chapter. The number of modes is seen to equal the number of layers, three in this case. For various values

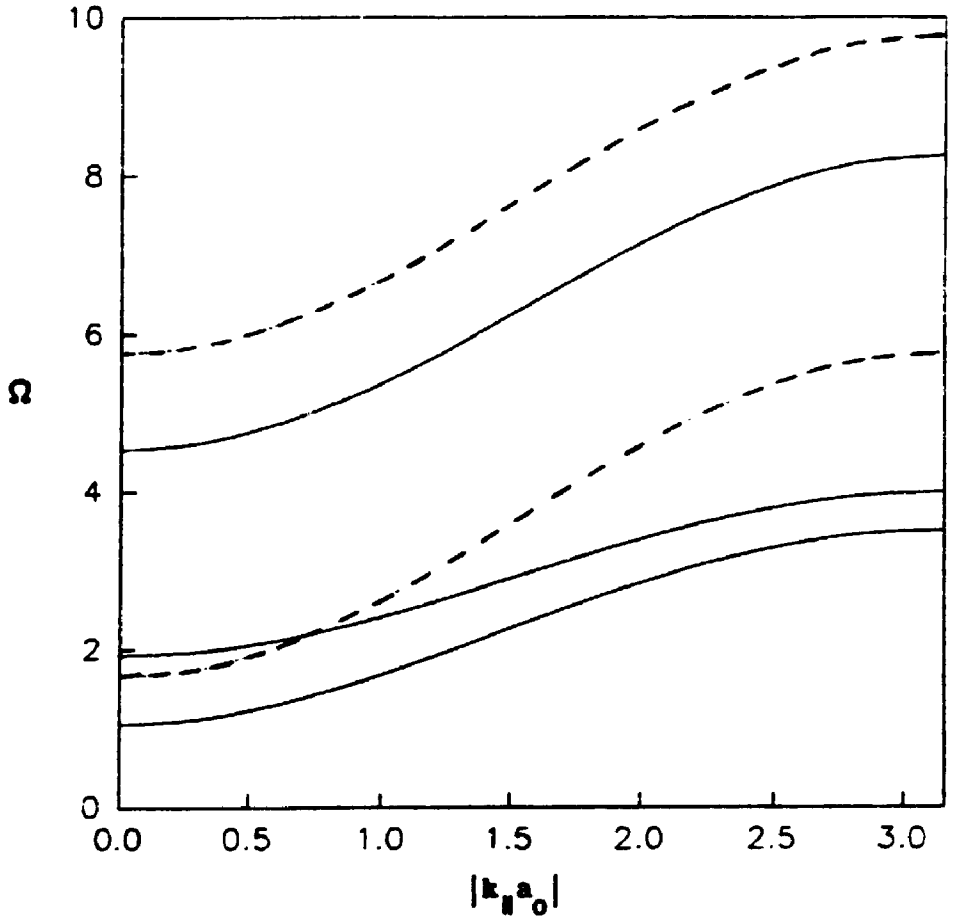

Figure 3.3 The spin-wave frequencies (in units of SJ) plotted against $|k_{\parallel}a_o|$ for a symmetric case A.1 ferromagnetic film. Here we have chosen $N = 3$, $J_s/J = J_{s'}/J = 0.5$, $D_s/D = D_{s'}/D = 0.5$, and $F/J = F_s/J = F_{s'}/J = 0.5$.

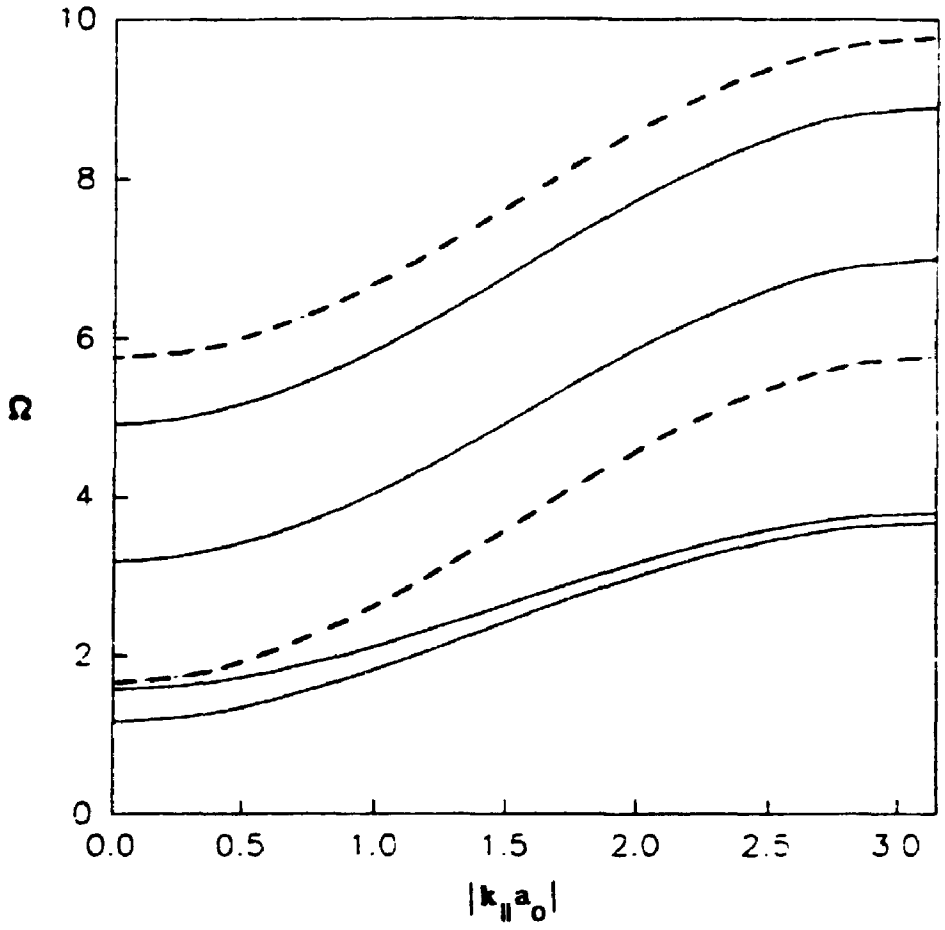

Figure 3.4 The spin-wave frequencies (in units of SJ) plotted against $|k_{\parallel}a_0|$ for a symmetric case A.1 ferromagnetic film. Here we have chosen N = 4, and all other parameters as in figure 3.3.

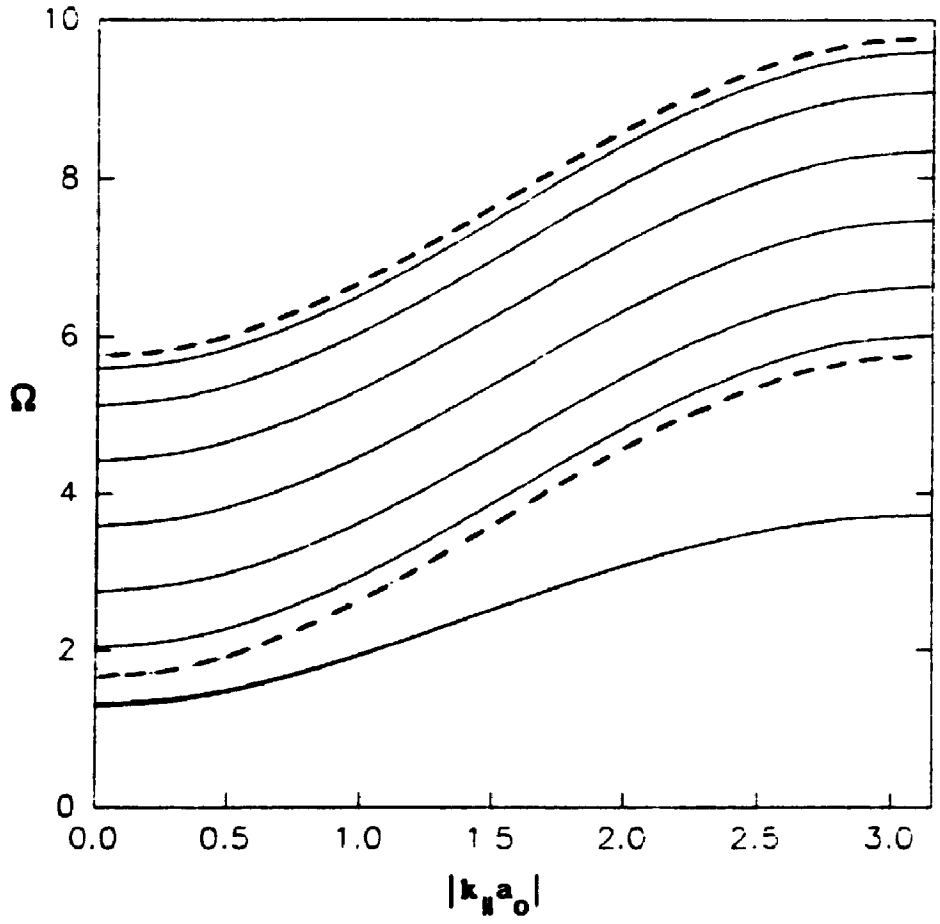

Figure 3.5 The spin-wave frequencies (in units of SJ) plotted against $|k_{\parallel}a_0|$ for a symmetric case A.1 ferromagnetic film. Here we have chosen N = 8 and all other parameters as in figure 3.3.

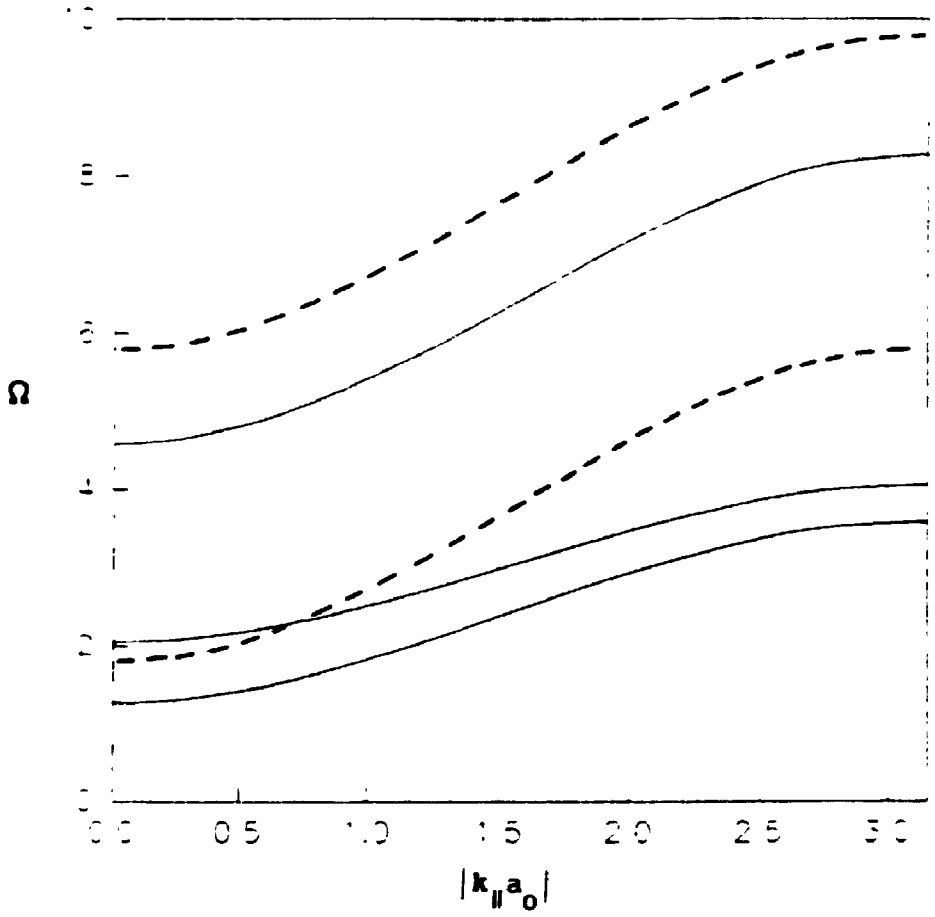

Figure 3.6 The spin-wave frequencies (in units of SJ) plotted against $|k_{\parallel}a_0|$ for a uniaxial symmetric ferromagnetic film. Here we have chosen $N = 3$, $F = F_s = F_{s'} = 0$, and all other parameters as in figure 3.3.

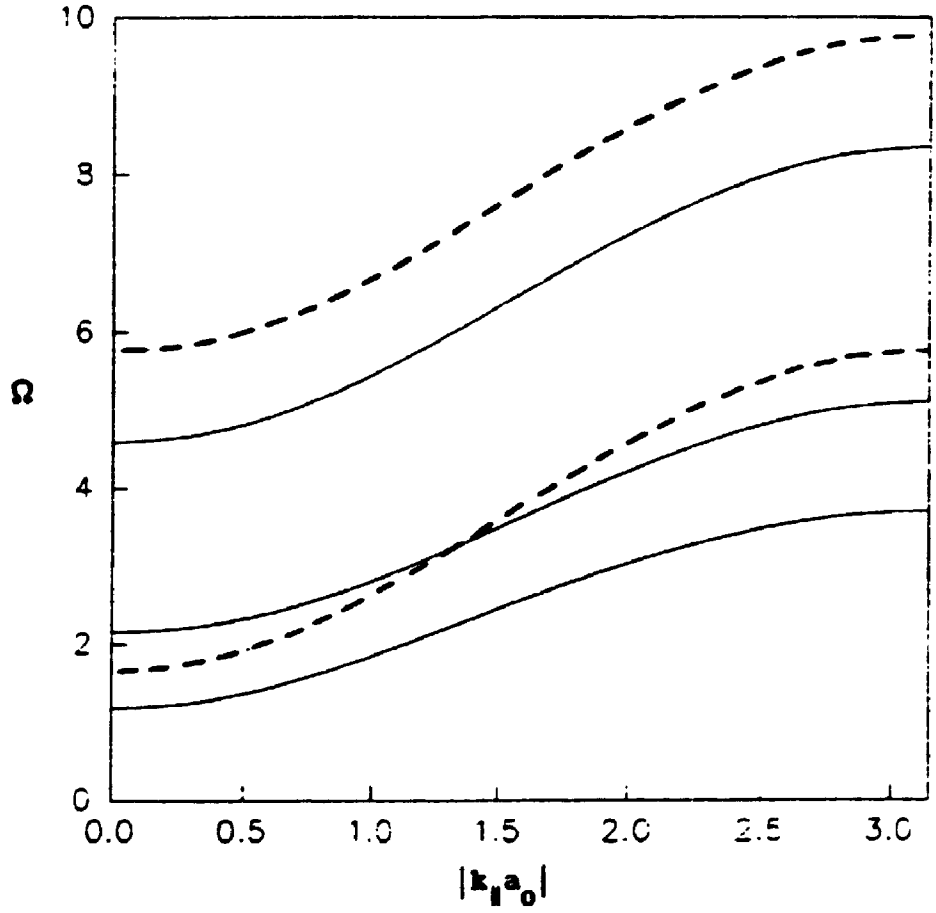

Figure 3.7 The spin-wave frequencies (in units of SJ) plotted against $|k_{\parallel}a_0|$ for an asymmetric case A.1 ferromagnetic film. Here we have chosen N = 3, $J_s/J = 0.5$, $J_{s'}/J = 0.75$, $D_s/D = 0.5$, $D_{s'}/D = 0.75$, and $F/J = F_s/J = F_{s'}/J = 0.5$.

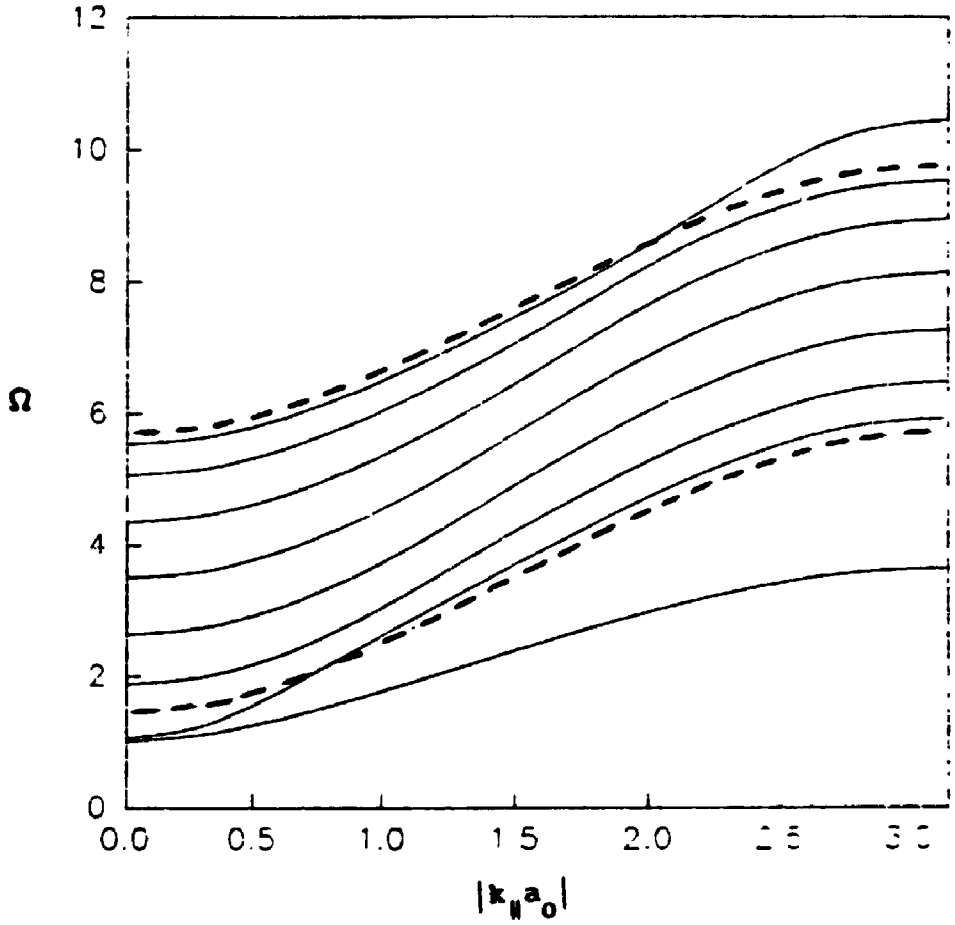

Figure 3.8 The spin-wave frequencies (in units of SJ) plotted against $|k_{\parallel}a_0|$ for an asymmetric case A.1 ferromagnetic film. Here we have chosen N = 8, $J_s/J = 0.5$, $J_{s'}/J = 2.0$, $D_s/D = 1.5$, $D_{s'}/D = 0.5$, and $F/J = F_s/J = F_{s'}/J = 0.75$.

of $|k_{\parallel}a_0|$ there are one or two surface modes. These modes are acoustic, appearing below the bulk region, which is bounded by dotted lines. Other examples showing acoustic surface modes are given in figures 3.4 through 3.7. By contrast, in figure 3.8 an optic mode appears above the bulk-mode region for large values of $|k_{\parallel}a_0|$. The appearance of a truncated optic mode is related to the surface exchange parameter J_s, exceeding the bulk value J by analogy with the case of uniaxial ferromagnets (e.g. see Wolfram and DeWames 1972). The frequency of each mode increases as $|k_{\parallel}a_0|$ increases (or the wavelength decreases). All of these plots are distinguished from those of the semi-infinite case by the possible presence of two surface modes and the finite number of bulk modes. The attenuation length L, calculated using (3.1.2), for the surface modes of figure 3.8 is plotted (in units where $a_0 = 1$) against $|k_{\parallel}a_0|$ in figure 3.9. Where a surface mode frequency approaches the bulk mode region we find $L \to \infty$. The bulk modes, being non-localized, may be considered to have an unlimited penetration depth. The surface modes farther away in frequency from the bulk region have shorter attenuation lengths.

As noted above the total number of modes is equal to the number of layers, N. As the film thickness increases so does the number of bulk modes, the greater number of layers permitting more values of k_z. Eventually the discrete nature of the spectrum is obscured as the frequencies merge into a continuum. In the case of symmetric films the frequencies of the two surface modes are very nearly degenerate when the film is relatively thick (N = 8, figure 3.5) and split when the film is relatively thin (N = 3, figure 3.3). In simple terms this splitting may

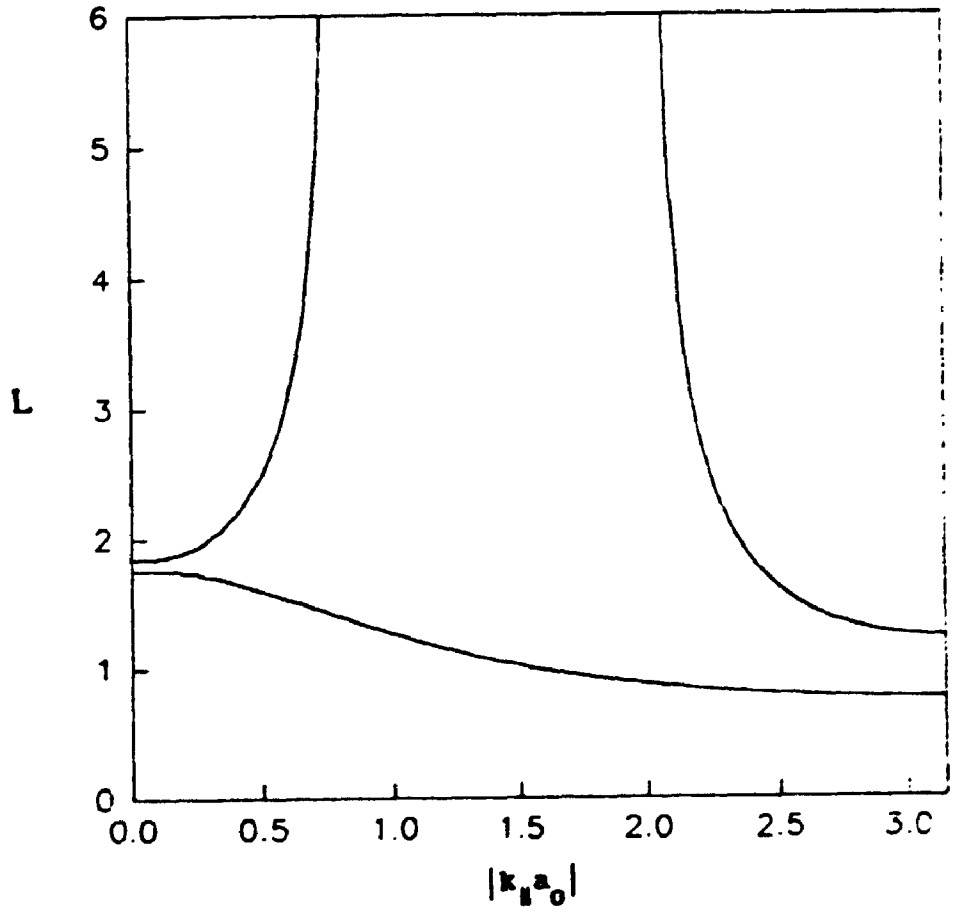

Figure 3.9 The surface spin-wave attenuation length L (in units of a_0) plotted against $|k_{\parallel}a_0|$ for an asymmetric case A.1 film. All parameters are chosen as in figure 3.7.

viewed as a consequence of overlap between the exponential tails of the respective modes. This feature is also illustrated in figures 3.10 (a) and (b) which depict the surface spin-wave frequency variation with film thickness (at $k_{\parallel} = 0$) for a symmetric film and an asymmetric film respectively. It is seen that as the number of layers increases the frequencies approach the values obtained from the semi-infinite result where $x_1 = -1/\Delta_s$.

Spin wave dispersion in asymmetric films is illustrated by figures 3.7 and 3.8. In figure 3.7 we note that the surface modes are more dissimilar than in figure 3.3. In figure 3.8, as noted above, for various values of $|k_{\parallel}a_0|$ there are two acoustic surface modes, one acoustic mode, or one acoustic and one optic mode. For semi-infinite systems a surface having $J_s < J$ will give rise to an acoustic mode while a surface having $J_s > J$ will give rise to a mode which is acoustic for long wavelengths but optic for short wavelengths (e.g. see Wolfram and DeWames 1972). Here we have one surface with each of these characteristics.

Some of the effects of including the nonuniaxial term in the Hamiltonian can be seen by comparing figur ' and 3.6 for three-layer nonuniaxial and uniaxial films respectively. The two plots are qualitatively similar. The frequencies are lower in the nonuniaxial case, most noticeably for the long-wavelength acoustic surface modes near the centre of the Brillouin zone. In these excitations the neighbouring spins are nearly parallel and the nonuniaxial anisotropy energy may be large relative to the exchange energy. The higher energy bulk modes are

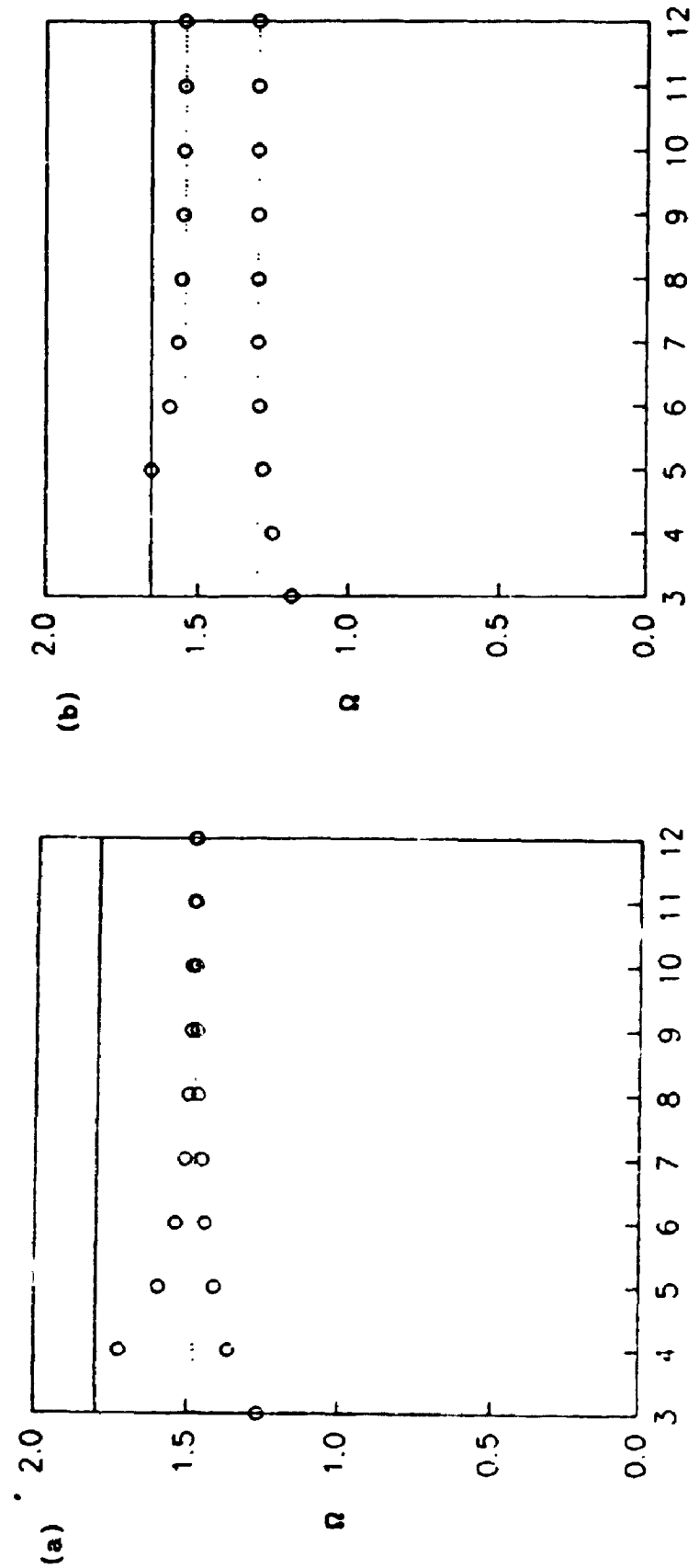

Figure 3.10 The surface spin-wave frequencies (in units of SJ) at $k_{\parallel} = 0$ plotted against film thickness N (in units of a_o) for a symmetric case A.1 film. For (a) and (b) all parameters are as in figures 3.3 and 3.6 respectively. The dotted lines represent semi-infinite solutions. The solid horizontal line represents the lower bound of the bulk-mode region.

less affected, as are the shorter wavelength surface modes away from the zone centre.

The lowering of spin-wave energies in the presence of nonuniaxial anisotropy has some further implications. It is possible that for some value of F the energy of the lowest-lying excitation may be reduced to zero, as illustrated in figures 3.11 (a) and (b). This occurrence signifies an instability and indicates at the ground state involves spin alignment in some different direction than along the positive z-axis. In such a situation we may adapt our calculations by relabelling this new direction as the new z-axis. If, however, we are interested in perpendicular magnetization in the presence of large nonuniaxial anisotropy we may simply introduce a larger applied field to align the spins along the z axis. Alternatively, the film thickness may be varied since figure 3.11 shows that for larger N ground-state ordering along the z-axis may be assumed over a wider range of values of the nonuniaxial parameter. We also note that the number of surface modes is unaffected by F, it is determined solely by the criteria described in Chapter 2.

3.1.3 Case A.2: the Nonuniaxial Parameter is Perturbed on the Surfaces

In this case the existence condition for the modes is given formally by (2.3.25), a complicated function which contains both x_1 and x_2. One possible method for extracting numerical results from the expression for $\underline{b}$ is to calculate numerically the matrix elements of $\underline{A}_1^{-1}$, $\underline{A}_2^{-1}$, $\underline{\Lambda}^+$ and the determinant of $\underline{M} = [\underline{I} + \underline{A}_1^{-1}\underline{A}_2^{-1}\underline{\Lambda}^+]$ for a series of values of x_1 on the interval appropriate for either surface or bulk modes. The variable

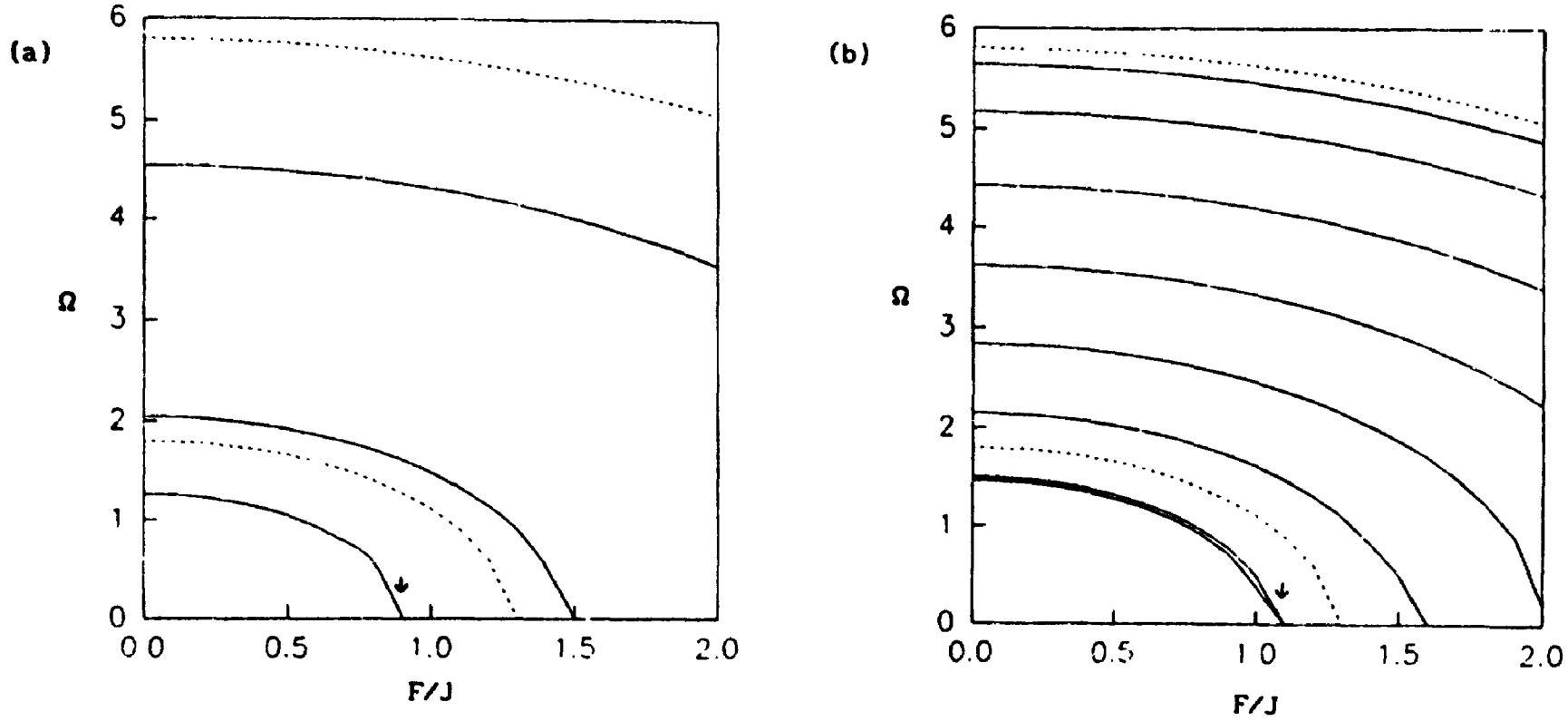

Figure 3.11 The spin-wave frequencies (in units of SJ) at $k_{\parallel} = 0$ plotted against the nonuniaxial parameter F (in units of SJ) for case A.1. For (a) N = 3 and for (b) N = 8. All other parameters are as in figure 3.3. The dotted lines mark the boundaries of the bulk-mode region.

x_2 may be considered to be a function of x_1 according to (2.4.13). The determinant as a function of x_1 is therefore known and solutions for x_1 (and hence the spin-wave energies) may be found as in case A.1. The condition on $\underline{b}^\dagger$ yields an identical spin-wave spectrum, as expected on physical grounds.

For surface modes x_1 and x_2 are each real and satisfy $|x_1|<1$ and $|x_2|<1$ (see Appendix III). For surface modes (2.4.13) leads to

$$x_2 = \frac{-(x_1 + x_1^{-1} - 2a) \pm [(x_1 + x_1^{-1} - 2a)^2 - 4]^{1/2}}{2} \qquad (3.1.10)$$

where only those values of x_2 which satisfy the localization condition $|x_2|<1$ are considered. For bulk modes x_1 is complex and x_2 is real or vice versa (see Appendix III). If x_1 is considered to be complex so that $x_1 = \exp(i\theta)$ then we find x_2 using

$$x_2 = -(\cos\theta - a) \pm [(\cos\theta - a)^2 - 1]^{1/2}. \qquad (3.1.11)$$

We have not produced numerical results for the bulk spin-wave frequencies in this case because of the considerable complexity. The results are unlikely to differ much from those of case A.1. Instead we concentrate on the more interesting case of the surface spin waves, since these are likely to be more sensitive to the surface anisotropy.

A representative plot of the surface spin-wave dispersion for a four-layer symmetric ($F_s = F_{s'}$) film appears in figure 3.12 which is seen to be qualitatively similar to that in which the nonuniaxial parameter is unperturbed at the surface (e.g. see figure 3.4 for N = 4). For the particular case of a symmetric film in which the exchange and uniaxial parameters are unperturbed at the surface (figure 3.13) a

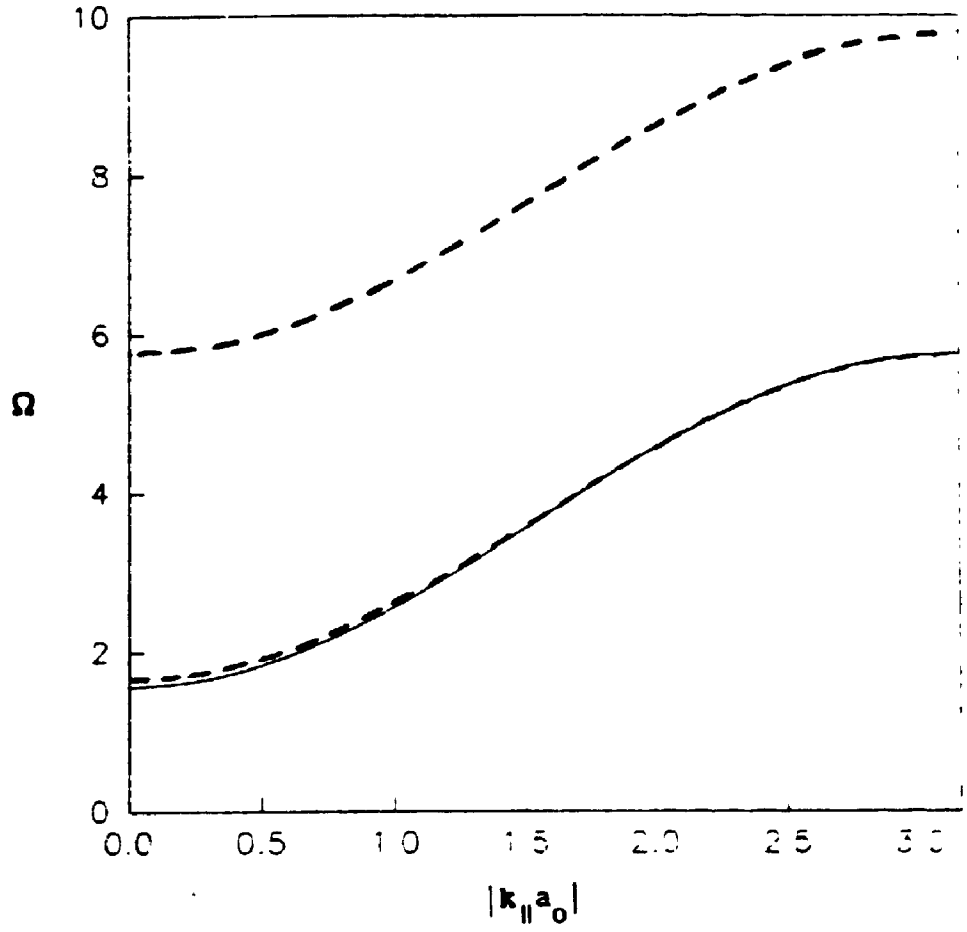

Figure 3.12 The surface spin-wave frequencies (in units of SJ) plotted against $|k_{\parallel}a_0|$ for a symmetric ferromagnetic case A.2 film. Here we have chosen N = 4, F/J = 1.0, $F_s/J = F_{s'}/J$ = 1.5, and all other parameters as in figure 3.3.

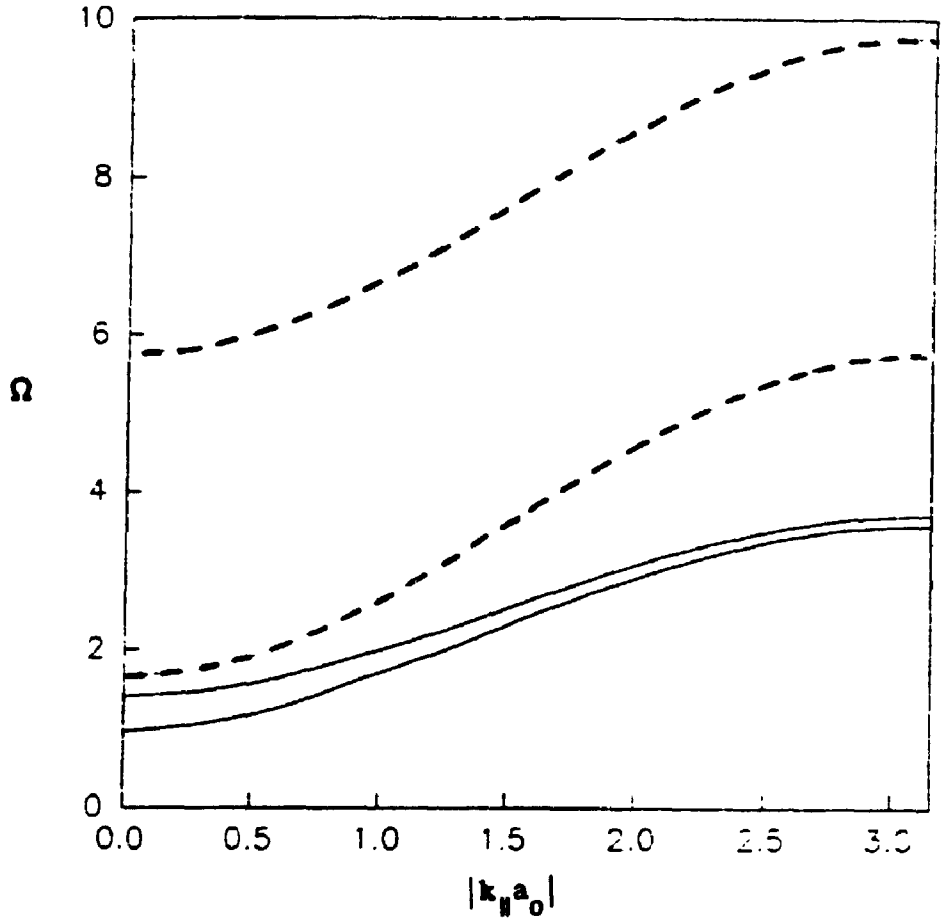

Figure 3.13 The surface spin-wave frequencies (in units of SJ) plotted against $|k_{\parallel}a_0|$ for a symmetric ferromagnetic case A.2 film. Here we have chosen N = 8, $J_s = J = J_{s'}$, $D_s = D = D_{s'}$, $F/J = 1.0$, and $F_s/J = F_{s'}/J = 1.5$.

weakly-localized surface mode occurs which is seen to be become nearly degenerate with the lower edge of the bulk region as the wavelength decreases and the anisotropy energy becomes relatively less important than that due to exchange. From the numerical study of (2.3.25) we conclude that $F_s > F$ seems to be a sufficient condition for the appearance of a surface mode. This conclusion is consistent with the following analysis of the case B systems.

3.2 Case B: The Anisotropy is Nonuniaxial on the Surfaces Only

Physically this situation may be considered to be an extreme case of the surface nonuniaxial parameter differing from the bulk value. We assume for convenience that the surfaces are symmetric with respect to the parameters D_s and J_s. The condition for existence of a solution for the spin waves was found to be (2.4.11) for case B.1 or (2.4.19) for case B.2. These expressions may not be factored into separate conditions on x_1 and x_2 and therefore the numerical solution is relatively more complicated than for case A.1. There are, however, several possible strategies here. As in case A.2 we may exploit the relationship between x_1 and x_2 to consider, for example, x_2 as a function of x_1 and then look for zeroes on the interval $-1<|x_1|<1$. For surface modes we sample x_1 on the interval $(-1,1)$ and use (3.1.9) to find the corresponding value of x_2 which is real and satisfies the additional localization condition $|x_2|\leq 1$. The functions y_1^{B1} and y_2^{B2} may have two roots, one related to $+\Omega$ the other to $-\Omega$, or they may have no roots. Therefore for both $\underline{b}$ and $\underline{b}^\dagger$ we again find a spin-wave spectrum that is symmetric about $\Omega = 0$. For bulk modes we consider x_1 to be complex so that $x_1 = \exp(i\theta)$. We sample θ on the interval $(0,\pi)$ and use (3.1.11) to find the corresponding real

value of x_2. Numerical results achieved by this method for cases B.1 and B.2 are presented below.

An alternative method is an extension of that applied by Gopalan and Cottam (1990) to the semi-infinite case. As shown in Chapter 2 in the discussion of the thick-film limit of case B.1, the expressions can be rewritten in terms of a new complex variable $\alpha \equiv x_1 x_2$ using (2.4.13) so that $x_1 + x_2 = 2a\alpha/(1 + \alpha)$. This technique is not as straightforwardly applicable here as our equations contain terms such as $x_1^N + x_2^N$ which must first be expressed in terms of x_1x_2 and $x_1 + x_2$ and then in terms of α. This is relatively easily achieved for specific values of N (see Appendix III) provided that they are not too large (e.g. less than about 10). The surface modes are then readily extracted by considering the interval $-1 < \alpha < 1$. However, the bulk modes present an additional complication because, as mentioned above one of the variables x_1 and x_2 is real and the other is complex and therefore α is complex and is only restricted to be on or within the unit circle. There is no simple way to sample this region looking for zeroes of our equations and therefore our method described above is preferred for bulk modes.

3.2.1 Case B.1: The Nonuniaxial Parameter is the Same on Both Surfaces

In this case the nonuniaxial parameter is zero in the bulk and has the value F_s on each surface. The appropriate expression for finding the surface spin-wave frequencies is (2.4.11) while for bulk modes we have

$$y_1^{B1} = [g(\theta)\Delta_s + r(\theta)][g(x_2)\Delta_s + r(x_2)] - f_s^2\, g(\theta)g(x_2)$$

$$y_2^{B1} = [h(\theta)\Delta_s + s(\theta)][h(x_2)\Delta_s + s(x_2)] - f_s^2\, h(\theta)h(x_2) \qquad (3.2.1)$$

with $g(\theta)$, $h(\theta)$, $r(\theta)$ and $s(\theta)$ as in (3.1.5).

Dispersion relations are presented in figures 3.14 and 3.15. Qualitatively they differ little from those of case A.1. In figure 3.14 it is seen that the long-wavelength surface modes have frequencies slightly higher than those in figure 3.4 for a case A.1 film. In the present case the anisotropy is nonuniaxial for only a small fraction of the spins and therefore the behaviour resembles that of a uniaxial material more than in case A.1. In figure 3.14 the surface modes are nearly degenerate, reflecting the film thickness and symmetry.

In figure 3.15 we see that there are two surface modes throughout the Brillouin zone in contrast to figure 3.3 for a case A.1 film. The variation of the number of surface modes and their frequencies with F_s is depicted in figure 3.16 where it is also seen that the bulk modes are relatively unaffected by the surface nonuniaxial anisotropy. Comparing figures 3.16 (a) and (b) with figures 3.11 (a) and (b) for case A.1 we see that in the present case of surface nonuniaxial anisotropy only, the assumption of ground state ordering along the positive z-axis is more easily justified. We also note that in case A.1 the number of surface modes is not affected by the nonuniaxial parameter whereas here, for the three-layer film, we may find one or two zone-centre acoustic surface modes, depending on the value of F_s. We see that in the present case the existence of a localized solution for $|\Delta_s| = 1$ is not ruled out in (2.4.11). However, unlike the earlier case (A.1), this expression does

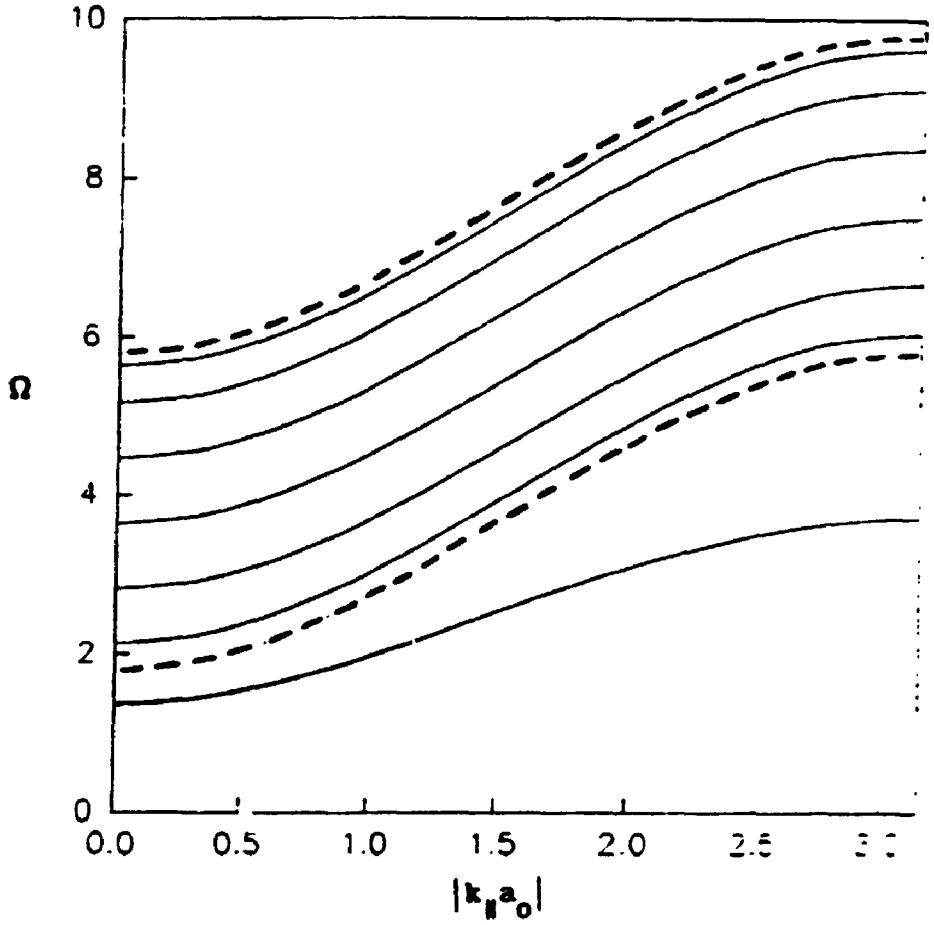

Figure 3.14 The spin-wave frequencies (in units of SJ) plotted against $|k_{\parallel}a_o|$ for a symmetric ferromagnetic case B.1 film. Here we have chosen $N = 8$, $J_s/J = J_{s'}/J = 0.5$, $D_s/D = D_{s'}/D = 0.5$, $F/J = 0$, and $F_s/J = F_{s'}/J = 0.5$.

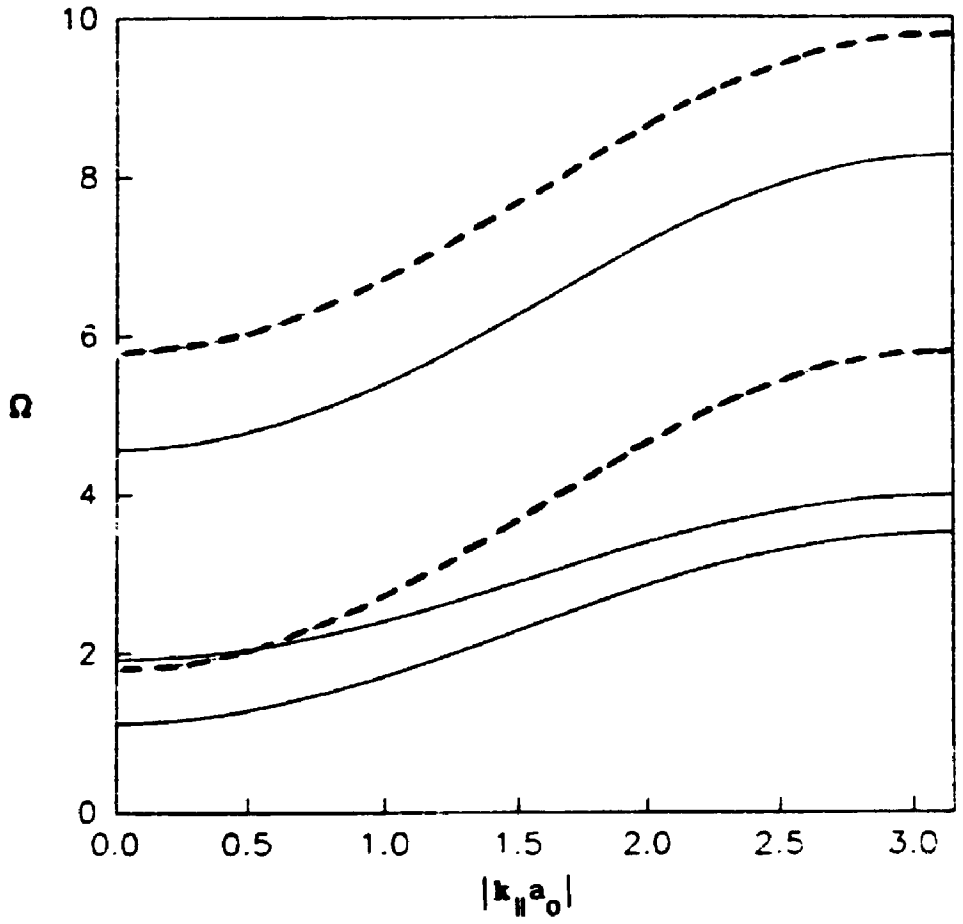

Figure 3.15 The spin-wave frequencies (in units of SJ) plotted against $|k_{\parallel}a_0|$ for a symmetric ferromagnetic case B.1 film. Here we have chosen N = 3 and all other parameters as in figure 3.14.

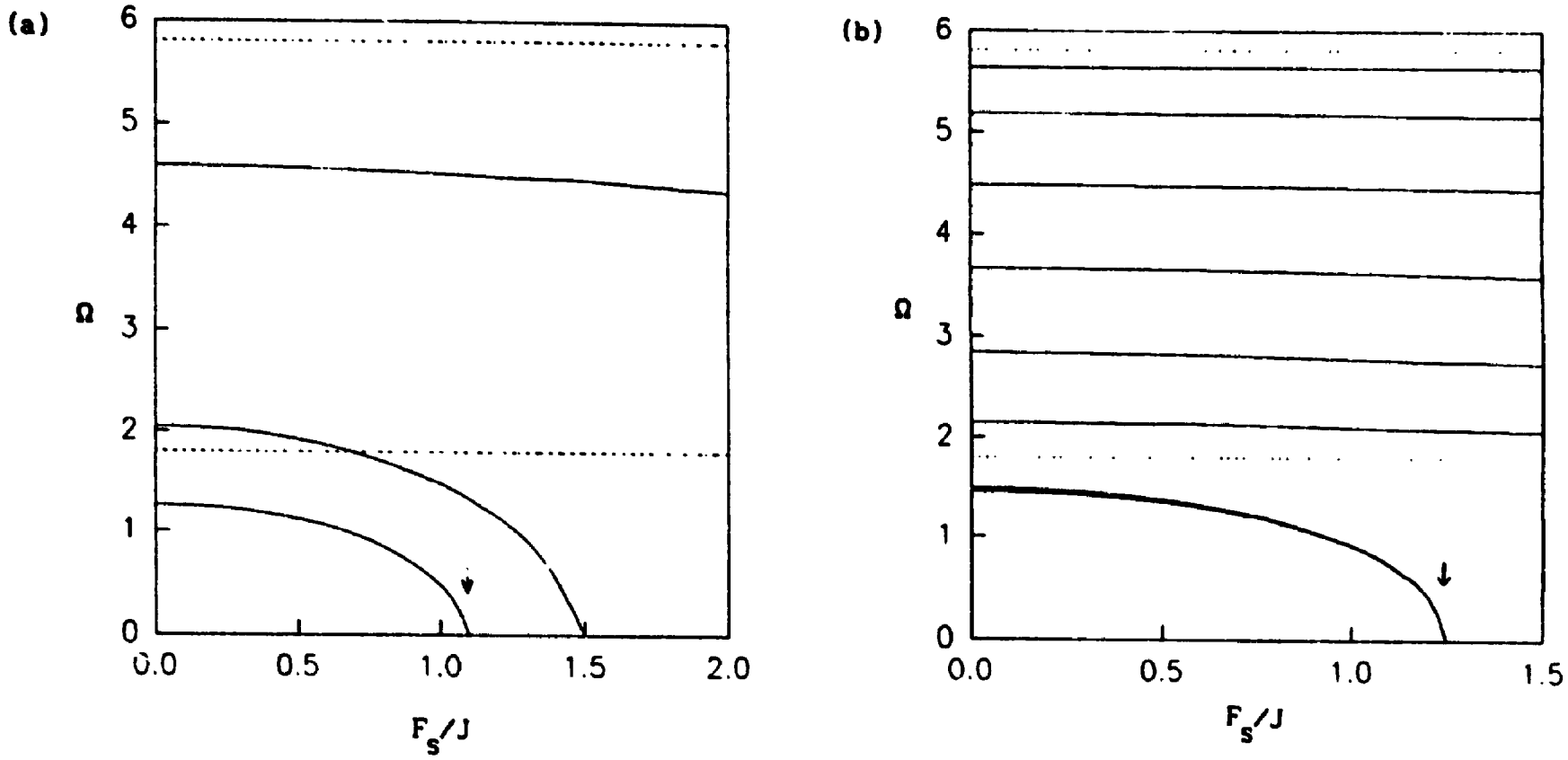

Figure 3.16 The spin-wave frequencies (in units of SJ) at $k_{\parallel} = 0$ plotted against the surface nonuniaxial parameter F_S (in units of SJ) for case B.1. For (a) N = 3 and for (b) N = 8. All other parameters are as in figure 3.3. The dotted lines mark the boundaries of the bulk-mode region.

not lead straightforwardly to more general predictions concerning the number of surface modes. From the numerical studies it seems that surface nonuniaxial anisotropy is a sufficient condition for the existence of a surface mode as was noted in the discussion of case A.2 (see figure 3.13). Such a mode appears in figure 3.17 where the exchange and uniaxial parameters are unperturbed at the surface.

3.2.2 Case B.2: The Nonuniaxial Parameter is Non-zero on one Surface Only

In this case the anisotropy is nonuniaxal on one surface and uniaxial on the other as well as in the bulk. The surfaces are taken to be symmetric with respect to the uniaxial and exchange parameters, D_s and J_s. The expression which must be solved to find surface modes is (2.4.19) while for bulk modes we must find the roots of

$$\begin{aligned} y^{B2}(\theta,x_2) = {} & [g(\theta)\Delta_s + r(\theta)][h(\theta)\Delta_s + s(\theta)] \\ & \times [g(x_2)\Delta_s + r(x_2)][h(x_2)\Delta_s + s(x_2)] \\ & - f_s^2[g(\theta)h(\theta)\Delta_s + q(\theta)][g(x_2)h(x_2)\Delta_s + q(x_2)] \end{aligned} \qquad (3.2.2)$$

with all functions as defined above.

Some representative dispersion relations are shown in figures 3.18 and 3.19. In contrast to the corresponding case B.1 plots here the film is asymmetric and therefore the surface-mode frequencies are dissimilar even for large N. Figure 3.20 shows the variation of spin-wave frequency with F_s. It is seen that one surface mode is influenced by F_s while all other modes are relatively unaffected. In figure 3.20 (a) the number of surface excitations is seen to depend on F_s, as in cases A.2 and B.1.

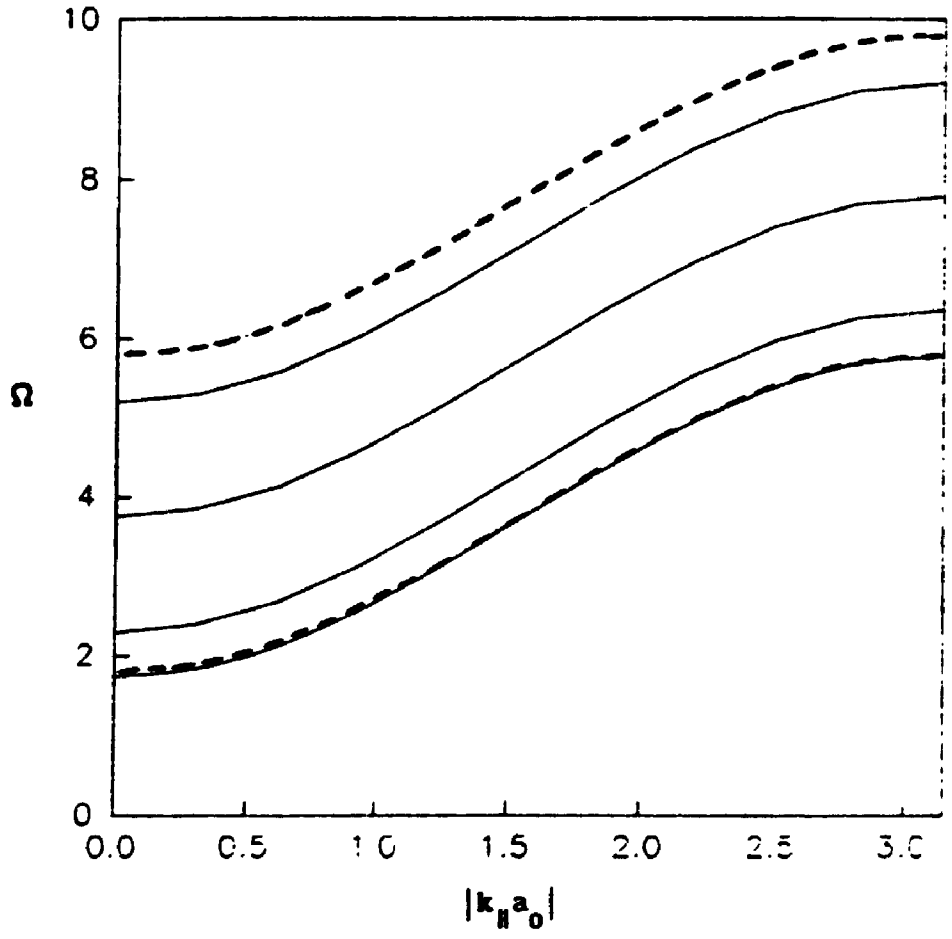

Figure 3.17 The spin-wave frequencies (in units of SJ) plotted against $|k_{\parallel}a_0|$ for a symmetric ferromagnetic case B.1 film. Here we have chosen N = 4, $J_s = J_{s'} = J$, $D_s = D_{s'} = D$, $F/J = 0$ and $F_s/J = F_{s'}/J = 0.5$.

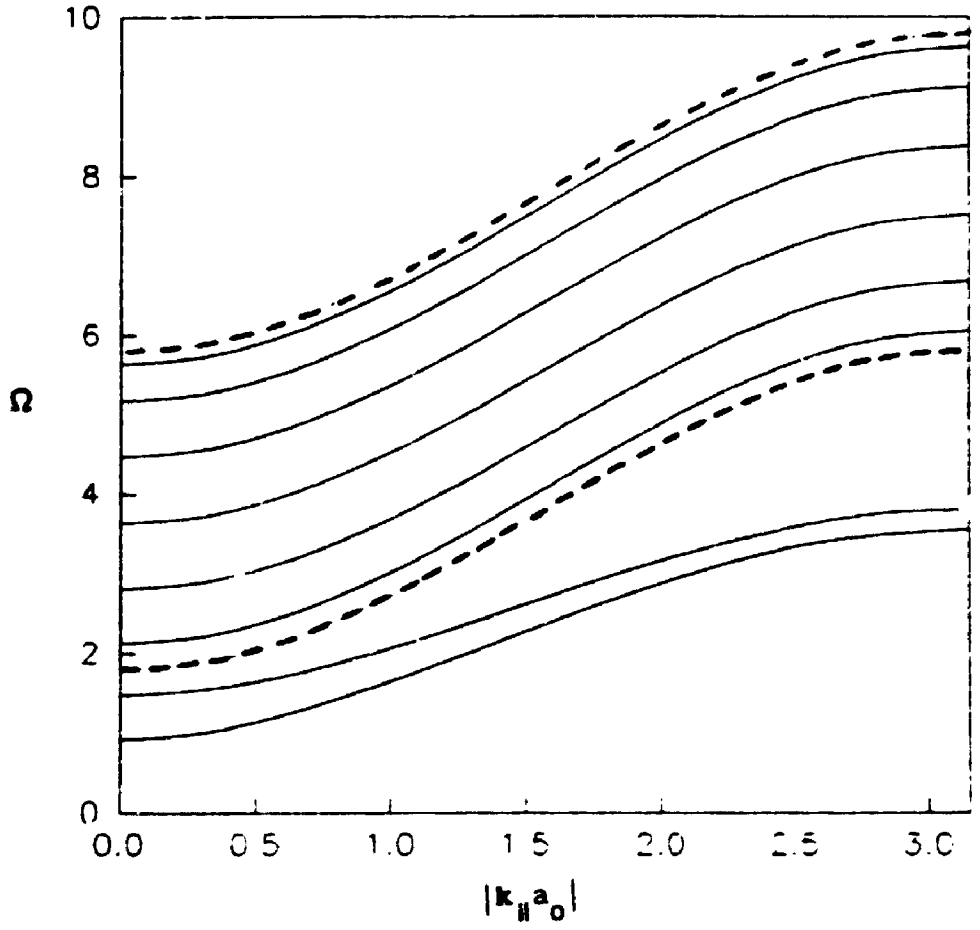

Figure 3.18 The spin-wave frequencies (in units of SJ) plotted against $|k_{\parallel}a_0|$ for an asymmetric ferromagnetic case B.2 film. Here we have chosen N = 8, F_s/J = 1.0, $F_{s'}/J$ = F/J = 0, and all other parameters as in figure 3.3.

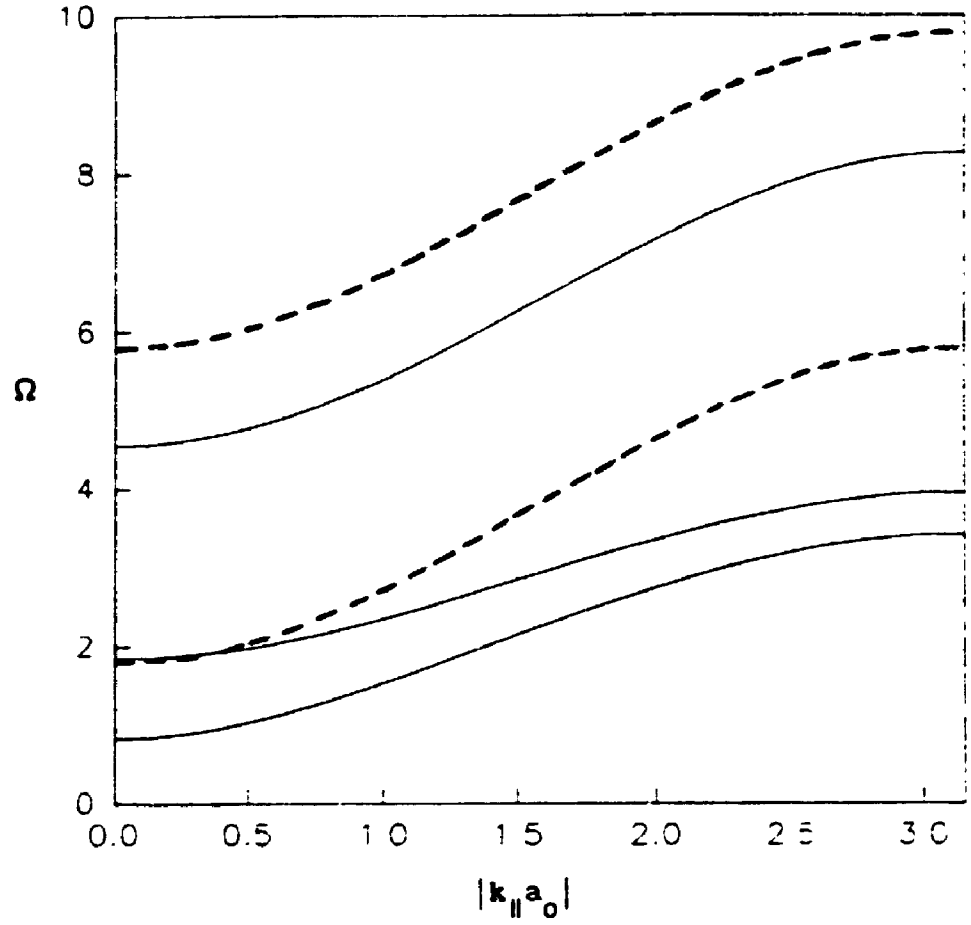

Figure 3.19 The spin-wave frequencies (in units of SJ) plotted against $|k_{\parallel}a_0|$ for an asymmetric ferromagnetic case B.2 film. Here we have chosen N = 3 and all other parameters as in figure 3.18.

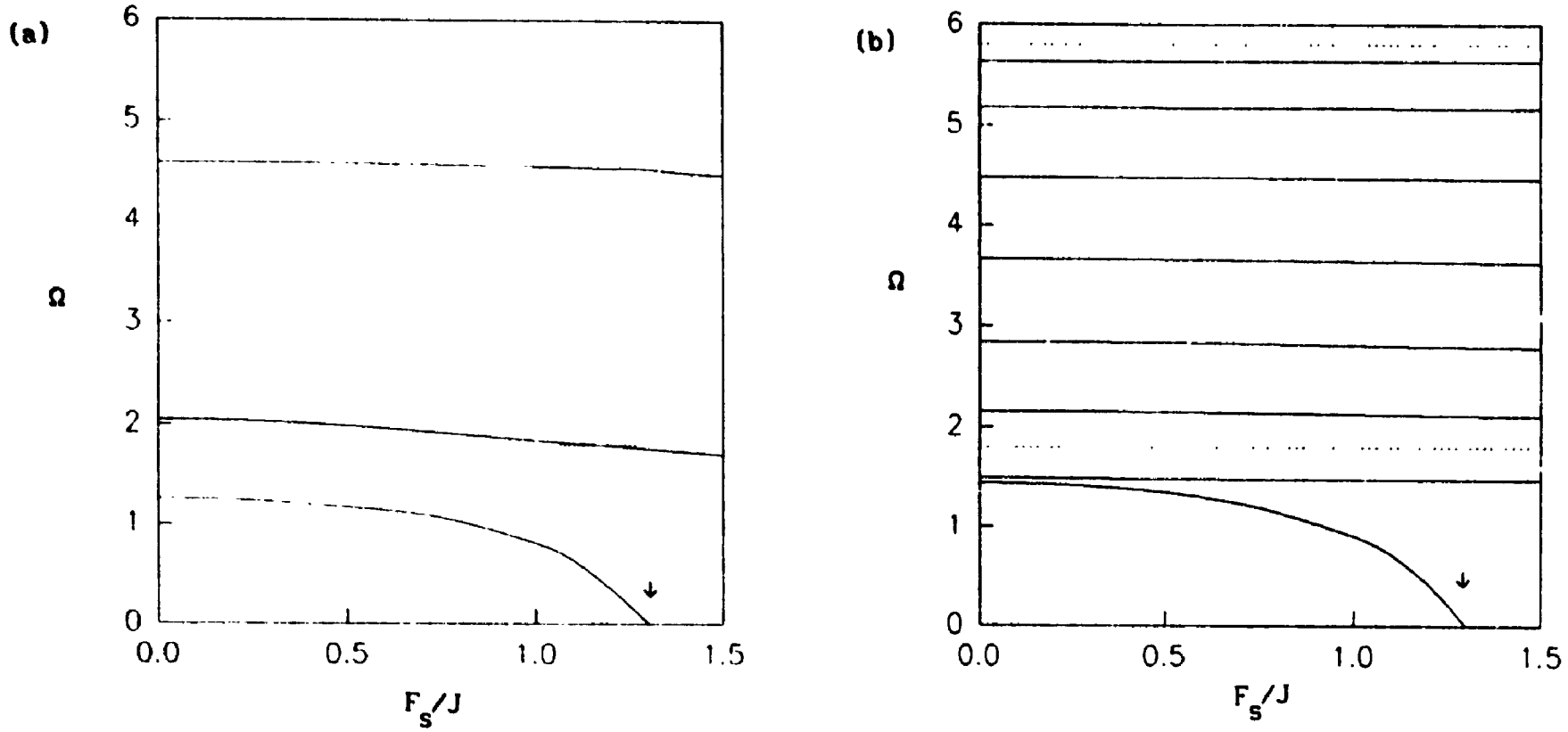

Figure 3.20 The spin-wave frequencies (in units of SJ) at $k_{\parallel} = 0$ plotted against the surface nonuniaxial parameter F_s (in units of SJ) for case B.2. For (a) N = 3 and for (b) N = 8. All other parameters are as in figure 3.18. The dotted lines mark the boundaries of the bulk region.

3.3 Discussion

Numerical dispersion relations have been generated in all of the cases we have studied. These include films in which the anisotropy is uniformly nonuniaxial and where it has nonuniaxial parameters perturbed at the surface(s) relative to the bulk value, which is possibly zero. We have examined the variation of surface and bulk spin-wave frequency with anisotropy constants and film thickness thoughout the Brillouin zone. The results of our numerical calculations are all well understood on physical grounds. Our results are in accord with previous studies on uniaxial films and nonuniaxial semi-infinite systems as limiting cases of our general theory.

The major conclusions are summarised as follows. For the nonuniaxial films each of the coupled operators $\underline{b}$ and $\underline{b}^{\dagger}$ leads to spin-wave dispersion relations which are symmetric about $\Omega = 0$. The spin-wave frequencies (energies) decrease as the nonuniaxial parameter increases, most noticeably in the region where $|\mathbf{k}_{\parallel} a_0|$ is small. The greatest effect is seen in films where all sites have $F_i \neq 0$. In all cases there is a spin-wave instability for sufficiently large nonuniaxial anisotropy, indicated by the frequency of a mode becoming zero. The number of surface modes is determined by the surface features. In particular, for cases in which no surface mode would occur for uniaxial films (e.g. $|\Delta_s| = 1$) the condition that F_s and/or $F_{s'} > F$ (including when $F = 0$) is sufficient for the existence of such a mode. Where $F_s \neq F$ then the number of surface modes in general depends on F_s (and/or $F_{s'}$). The intensities associated with the spin waves will be examined in Chapter 4 using a Green function analysis.

CHAPTER 4

GREEN FUNCTION METHOD FOR FERROMAGNETIC THIN FILMS

In this chapter we study spin waves in anisotropic ferromagnetic thin films using the Green function equation-of-motion method. We have already determined the dispersion relations for spin waves in some special cases of these films in Chapters 2 and 3 using the operator equation-of-motion method. The Green functions allow us to also calculate the spectral intensities associated with the spin waves. These intensities represent the relative weighting attached to the various possible spin-wave modes in a calculation of an experimentally observable quantity.

In Section 4.1 we present the general formalism of the equation-of-motion approach and determine the spin Green functions in the special cases defined earlier. The similarity between the Green function and operator methods allows us to refer frequently to equations appearing in Chapters 2 and 3 and we will verify that the Green function method leads to the same dispersion relations found there. Here we concentrate on films in which the anisotropy is uniformly nonuniaxial throughout (case A.1), or is nonuniaxial on the surface(s) (cases B.1 and B.2). For most real films that have some degree of nonuniaxial anisotropy the major features can be understood with reference to one of these three models. We have therefore not included any discussion of the most general, but also mathematically most complicated situation,

namely case A.2. Comparisons of our results with those of earlier studies on uniaxial and semi-infinite systems are made when possible.

Once we have determined the Green functions for our systems we may proceed with the calculation of the spectral intensities as described in detail for special case A.1 in Section 4.2 where we also present more briefly the results for cases B.1. and B.2. From the intensities we can derive spin correlation functions as shown in Section 4.3 where we use equal-time correlation functions to evaluate some static magnetic properties. In particular we present numerical results for the amplitude and ellipticity of the spin precession in each layer of the film. We also discuss the evaluation of the static magnetization. In Section 4.4 we describe how spin correlation functions can be used in other applications e.g. to calculate the cross-section for light scattering. We recall that in Section 1.5 we presented general information on Green functions and the equation-of-motion method, and these results will be referred to frequently here.

4.1 General Formalism

As in the case of the operator equation-of-motion approach we work with the boson operators b and $b^\dagger$ related to the spin operators S^+, S^- and S^z by the Holstein-Primakoff (1940) representation. Because spin waves are excitations associated with the transverse components of spin we are interested in correlation functions such as $\langle b_i(t)b_j^\dagger(t')\rangle$ and $\langle b_i^\dagger(t)b_j(t')\rangle$. We therefore introduce the corresponding commutator Green function $\langle\langle b_i(t);b_j^\dagger(t')\rangle\rangle$ which, according to (1.5.6), obeys the

following equation of motion:

$$\frac{d}{dt}\langle\langle b_i(t);b_j^\dagger(t')\rangle\rangle = -i\delta(t-t')\langle[b_i,b_j^\dagger]\rangle + i\langle\langle C(t);b_j^\dagger(t')\rangle\rangle \quad (4.1.1)$$

where $C = [\mathcal{H},b_i]$. From (2.1.3) we see that $[b_i,b_j^\dagger] = \delta_{ij}$. The commutator $[\mathcal{H},b_i]$ may be evaluated using the linearized Hamiltonian in the form (2.1.5) and (2.1.6). We find

$$[\mathcal{H},b_i] = [-g\mu_B H_0 - 2D_i S\eta - S\sum_m J_{im}]b_i + S\sum_m J_{im}b_m + 2S\eta' F_i b_i^\dagger \quad (4.1.2)$$

where η and all other variables are defined as in Chapter 2. The equation of motion can therefore be written as

$$\frac{d}{dt}\langle\langle b_i(t);b_j^\dagger(t')\rangle\rangle = i\delta(t-t')\delta_{ij}$$

$$+ i[-g\mu_B H_0 - 2D_i S\eta - S\sum_m J_{im}]\langle\langle b_i(t);b_j^\dagger(t')\rangle\rangle$$

$$+ i\sum_m J_{mi}\langle\langle b_m(t);b_j^\dagger(t')\rangle\rangle + i2S\eta' F_i\langle\langle b_i^\dagger(t);b_j^\dagger(t')\rangle\rangle. \quad (4.1.3)$$

We see that the Green function $\langle\langle b_i(t);b_j^\dagger(t')\rangle\rangle$ is coupled to the Green function $\langle\langle b_i^\dagger(t);b_j^\dagger(t')\rangle\rangle$ through the nonuniaxial term. According to (1.5.6) the new function has the following equation of motion:

$$\frac{d}{dt}\langle\langle b_i^\dagger(t);b_j^\dagger(t')\rangle\rangle = i\,[g\mu_B H_0 + 2D_i S\eta + S\sum_m J_{im}]\langle\langle b_i^\dagger(t);b_j^\dagger(t')\rangle\rangle$$

$$- i\sum_m J_{mi}\langle\langle b_m^\dagger(t);b_j^\dagger(t')\rangle\rangle - i2S\eta' F_i\langle\langle b_i(t);b_j^\dagger(t')\rangle\rangle. \quad (4.1.4)$$

In order to solve the coupled differential equations (4.1.3) and (4.1.4), which form a closed set, we perform the frequency Fourier transform of $\langle\langle b_i(t);b_j^\dagger(t')\rangle\rangle$ and $\langle\langle b_i^\dagger(t);b_j^\dagger(t')\rangle\rangle$ to $G_{ij}(\omega)$ and $G'_{ij}(\omega)$ respectively, as defined in (1.5.7), and also make use of the integral representation

$$\delta(t-t') = \frac{1}{2\pi}\int_{-\infty}^{\infty}\exp[-i\omega(t-t')]d\omega. \quad (4.1.5)$$

The coupled equations (4.1.3) and '4.1.4) become

$$[-\omega + g\mu_B H_0 + 2D_i S\eta + S\sum_m J_{im}]G_{ij}(\omega) - S\sum_m J_{im}G_{mj}(\omega)$$
$$= \frac{1}{2\pi}\delta_{ij} + 2F_i S\eta' G'_{ij}(\omega) \qquad (4.1.6)$$

$$[\omega + g\mu_B H_0 + 2D_i S\eta + S\sum_m J_{im}]G'_{ij}(\omega) - S\sum_m J_{im}G'_{mj}(\omega)$$
$$= 2F_i S\eta' G_{ij}(\omega). \qquad (4.1.7)$$

As in Chapter 2 we use the translational invariance in the xy plane to perform a further Fourier transform from site labels to the in-plane wavevector representation defining

$$G_{ij}(\omega) = \frac{1}{N}\sum_{\mathbf{k}_\parallel} \exp[i\mathbf{k}_\parallel\cdot(\mathbf{r}_i - \mathbf{r}_j)]\; G_{nn'}(\mathbf{k}_\parallel,\omega)$$
$$G'_{ij}(\omega) = \frac{1}{N}\sum_{\mathbf{k}_\parallel} \exp[i\mathbf{k}_\parallel\cdot(\mathbf{r}_i - \mathbf{r}_j)]\; G'_{nn'}(\mathbf{k}_\parallel,\omega) \qquad (4.1.8)$$

where n and n' are the layer indices of sites i and j respectively and $\mathbf{k}_\parallel$ is the 2-d wavevector defined in Chapter 1. From (4.1.6) we find the following set of coupled equations for $G_{nn'}$ and $G'_{nn'}$:

$$\left[\omega + g\mu_B H_0 + 2D_n S\eta + Su_n(0) + Sv_n(0) + Sv_{n-1}(0)\right]G_{nn'} - Su_n(\mathbf{k}_\parallel)G_{nn'}$$
$$- Sv_{n-1}(\mathbf{k}_\parallel)G_{n-1n'} - Sv_n(\mathbf{k}_\parallel)G_{n+1n'} = \frac{1}{2\pi}\delta_{nn'} + 2F_n S\eta' G'_{nn'} \qquad (4.1.9)$$

$$\left[-\omega + g\mu_B H_0 + 2D_n S\eta + Su_n(0) + Sv_n(0) + Sv_{n-1}(0)\right]G'_{nn'} - Su_n(\mathbf{k}_\parallel)G'_{nn'}$$
$$- Sv_{n-1}(\mathbf{k}_\parallel)G'_{n-1n'} - Sv_n(\mathbf{k}_\parallel)G'_{n+1n'} = 2F_n S\eta' G_{nn'} \qquad (4.1.10)$$

where th summations $u_n(\mathbf{k}_\parallel)$ and $v_n(\mathbf{k}_\parallel)$ are defined in (2.2.8) and we have abbreviated $G_{nn'}(\mathbf{k}_\parallel,\omega)$ as $G_{nn'}$. We introduce **G** and **G'** as N×N matrices whose elements are the Green functions $G_{nn'}$ and $G'_{nn'}$ respectively and write the above coupled equations as

$$(-\Omega\underline{I} + \underline{A})G = \mu\underline{I} + \underline{f}G'$$

$$(\Omega\underline{I} + \underline{A})G' = \underline{f}G. \qquad (4.1.11)$$

Here Ω and the matrices $\underline{f}$ and $\underline{A}$ are defined as in (2.2.13), (2.2.14) and (2.2.15). The constant $\mu \equiv 1/(2\pi SJ)$. We note that (4.1.11) and (2.2.12) are similar except for the inclusion of an inhomogeneous term in the present case. As in the operator equation-of-motion method the manner in which (4.1.11) is solved depends on the way in which the matrix $\underline{f}$ is defined for the various special cases.

4.1.1 Green Functions for Case A.1

We recall that in this case the nonuniaxial parameter has the same value for every site in the film i.e. $F_s = F = F_{s'}$. As in Section 2.3.1 we use this fact to write the matrix $\underline{f}$ as $f\underline{I}$. Using (2.2.16), (2.2.17), (2.2.18), and (2.3.5) we formally solve (4.1.11) as follows:

$$G = \mu(\underline{I} + \underline{A}_1^{-1}\underline{\Delta})^{-1}\underline{A}_1^{-1}(\underline{I} + \underline{A}_2^{-1}\underline{\Delta})^{-1}\underline{A}_2^{-1}(\Omega\underline{I} + \underline{A})$$

$$G' = \mu f(\underline{I} + \underline{A}_1^{-1}\underline{\Delta})^{-1}\underline{A}_1^{-1}(\underline{I} + \underline{A}_2^{-1}\underline{\Delta})^{-1}\underline{A}_2^{-1} \qquad (4.1.12)$$

which we can rewrite as

$$G = \frac{\mu\ \mathrm{adj}(\underline{I} + \underline{A}_1^{-1}\underline{\Delta})\underline{A}_1^{-1}\mathrm{adj}(\underline{I} + \underline{A}_2^{-1}\underline{\Delta})\underline{A}_2^{-1}(\Omega\underline{I} + \underline{A})}{\det(\underline{I} + \underline{A}_1^{-1}\underline{\Delta})\ \det(\underline{I} + \underline{A}_2^{-1}\underline{\Delta})}$$

$$G' = \frac{\mu f\ \mathrm{adj}(\underline{I} + \underline{A}_1^{-1}\underline{\Delta})\underline{A}_1^{-1}\mathrm{adj}(\underline{I} + \underline{A}_2^{-1}\underline{\Delta})\underline{A}_2^{-1}}{\det(\underline{I} + \underline{A}_1^{-1}\underline{\Delta})\ \det(\underline{I} + \underline{A}_2^{-1}\underline{\Delta})}. \qquad (4.1.13)$$

The Green functions have poles which represent the frequencies of the spin waves where $\det(\underline{I} + \underline{A}_1^{-1}\underline{\Delta})$ and/or $\det(\underline{I} + \underline{A}_2^{-1}\underline{\Delta}) = 0$. We have therefore recovered the same result for these frequencies as derived in Section 2.3.1 using the operator equation-of-motion method. We observe that in the present nonuniaxial case the spin waves are represented in

the Green functions by poles on both the positive and negative real axes in the frequency plane. This mathematical feature of the Green functions will be seen to have some implications in the calculation of physical properties. To recover the Green function results of the uniaxial case we set f = 0 in the definitions of x_1 and x_2 and find that $(\Omega\underline{I} + \underline{A}) = (\underline{A}_2 + \underline{\Delta})$. Therefore (4.1.13) becomes

$$\mathbf{G} = \frac{\mu\ \mathrm{adj}(\underline{I} + \underline{A}_1^{-1}\underline{\Delta})\underline{A}_1^{-1}}{\det(\underline{I} + \underline{A}_1^{-1}\underline{\Delta})}$$

$$\mathbf{G}' = 0 \qquad (4.1.14)$$

as expected (Cottam and Kontos 1980). A comparison of (4.1.14) and (4.1.13) shows that the present nonuniaxial case is considerably more complicated.

Using the results for $\det(\underline{I} + \underline{A}_1^{-1}\underline{\Delta})$ derived in Chapter 2 (e.g. (2.3.10)) we may rewrite the Green function matrix **G** in terms of x_1 and x_2 as follows:

$$\mathbf{G} = \frac{\mu\ \underline{W}^{A1}(x_1,\Omega)\ v^{A1}(x_1)}{y^{A1}(x_1)} \qquad (4.1.15)$$

where

$$\underline{W}^{A1} \equiv \mathrm{adj}(\underline{I} + \underline{A}_1^{-1}\underline{\Delta})\underline{A}_1^{-1}\mathrm{adj}(\underline{I} + \underline{A}_2^{-1}\underline{\Delta})\underline{A}_2^{-1}(\Omega\underline{I} + \underline{A}). \qquad (4.1.16)$$

For films which are symmetric with respect to surface exchange and anisotropy constants, we have

$$y^{A1}(x_1) = [g(x_1)\Delta_S + r(x_1)][h(x_1)\Delta_S + s(x_1)]$$
$$\times\ [g(x_2)\Delta_S + r(x_2)][h(x_2)\Delta_S + s(x_2)]$$
$$v^{A1}(x_1) = r(x_1)s(x_1)r(x_2)s(x_2). \qquad (4.1.17)$$

Here g(x), h(x), r(x) and s(x) are defined in (2.3.11). For the set of quantized bulk modes x_1 is complex and we have written it as x_1 =

$\exp(i\theta)$ as discussed in Chapter 2. It is therefore more appropriate to express the results in terms of θ as

$$y^{A1}(\theta) = [g(\theta)\Delta_s + r(\theta)][h(\theta)\Delta_s + s(\theta)] \times [g(x_2)\Delta_s + r(x_2)][h(x_2)\Delta_s + s(x_2)]$$
$$v^{A1}(\theta) = r(\theta)s(\theta)r(x_2)s(x_2). \qquad (4.1.18)$$

with $g(\theta)$, $h(\theta)$, $r(\theta)$ and $s(\theta)$ defined as in (3.1.4).

In the case of asymmetric A.1 films we have formally the same expression for G as (4.1.15) but we use (2.3.14) to write

$$y^{A1a}(x_1) = [g(x_1)h(x_1)\Delta_s\Delta_{s'} + q(x_1)(\Delta_s + \Delta_{s'}) + r(x_1)s(x_1)] \times [g(x_2)h(x_2)\Delta_s\Delta_{s'} + q(x_2)(\Delta_s + \Delta_{s'}) + r(x_2)s(x_2)]$$
$$v^{A1a} = r(x_1)s(x_1)r(x_2)s(x_2) \qquad (4.1.19)$$

where $g(x)$ etc. are defined in (2.3.11) and (2.3.15). For the set of quantized bulk modes we write (4.1.19) in the form

$$y^{A1a}(\theta) = [g(\theta)h(\theta)\Delta_s\Delta_{s'} + q(\theta)(\Delta_s + \Delta_{s'}) + r(\theta)s(\theta)] \times [g(x_2)h(x_2)\Delta_s\Delta_{s'} + q(x_2)(\Delta_s + \Delta_{s'}) + r(x_2)s(x_2)]$$
$$v^{A1a}(\theta) = r(\theta)s(\theta)r(x_2)s(x_2). \qquad (4.1.20)$$

4.1.3 Green Functions for Case B

In this section we solve (4.1.11) for films in which the nonuniaxial parameter may be non-zero on both surfaces (case B.1) or only one surface (case B.2) and write the results in terms of x_1 and x_2.

The case B.1 films have a nonuniaxial parameter which is non-zero on both surfaces and zero in the bulk. As in Chapter 2, we further assume, for convenience, that that the films are symmetric with respect to all

surface parameters F_s, D_s and J_s. We again write $\underline{f}$ as $f_s\underline{\nu}$ with $\underline{\nu}$ as in (2.4.1). From (4.1.11) we find the formal solutions

$$\underline{G} = \mu\left[\underline{I} - f_s^2(\underline{I} + \underline{A}_1^{-1}\underline{\Delta})^{-1}\underline{A}_1^{-1}\underline{\nu}(\underline{I} + \underline{A}_2^{-1}\underline{\Delta})^{-1}\underline{A}_2^{-1}\underline{\nu}\right]^{-1}(\underline{I} + \underline{A}_1^{-1}\underline{\Delta})^{-1}\underline{A}_1^{-1}$$

$$\underline{G}' = \mu f_s\left[\underline{I} - f_s^2(\underline{I} + \underline{A}_1^{-1}\underline{\Delta})^{-1}\underline{A}_1^{-1}\underline{\nu}(\underline{I} + \underline{A}_2^{-1}\underline{\Delta})^{-1}\underline{A}_2^{-1}\underline{\nu}\right]^{-1}$$
$$\times (\underline{I} + \underline{A}_1^{-1}\underline{\Delta})^{-1}\underline{A}_1^{-1}(\underline{I} + \underline{A}_2^{-1}\underline{\Delta})^{-1}\underline{A}_2^{-1} \qquad (4.1.21)$$

where $\underline{A}_1$ and $\underline{A}_2$ are defined as in (2.4.4). We rewrite (4.1.21) as

$$\underline{G} = \frac{\mu\ \mathrm{adj}[\underline{I} - f_s^2(\underline{I} + \underline{A}_1^{-1}\underline{\Delta})^{-1}\underline{A}_1^{-1}\underline{\nu}(\underline{I} + \underline{A}_2^{-1}\underline{\Delta})^{-1}\underline{A}_2^{-1}\underline{\nu}]\ \mathrm{adj}(\underline{I} + \underline{A}_1^{-1}\underline{\Delta})\underline{A}_1^{-1}}{\det[\underline{I} - f_s^2(\underline{I} + \underline{A}_1^{-1}\underline{\Delta})^{-1}\underline{A}_1^{-1}\underline{\nu}(\underline{I} + \underline{A}_2^{-1}\underline{\Delta})^{-1}\underline{A}_2^{-1}\underline{\nu}]\ \ \det(\underline{I} + \underline{A}_1^{-1}\underline{\Delta})}$$

$$\underline{G}' = \frac{\mu f_s\ \mathrm{adj}[\underline{I} - f_s^2(\underline{I} + \underline{A}_1^{-1}\underline{\Delta})^{-1}\underline{A}_1^{-1}\underline{\nu}(\underline{I} + \underline{A}_2^{-1}\underline{\Delta})^{-1}\underline{A}_2^{-1}\underline{\nu}]}{\det[\underline{I} - f_s^2(\underline{I} + \underline{A}_1^{-1}\underline{\Delta})^{-1}\underline{A}_1^{-1}\underline{\nu}(\underline{I} + \underline{A}_2^{-1}\underline{\Delta})^{-1}\underline{A}_2^{-1}\underline{\nu}]}$$
$$\times \frac{\mathrm{adj}(\underline{I} + \underline{A}_1^{-1}\underline{\Delta})\underline{A}_1^{-1}\mathrm{adj}(\underline{I} + \underline{A}_2^{-1}\underline{\Delta})\underline{A}_2^{-1}}{\det(\underline{I} + \underline{A}_1^{-1}\underline{\Delta})\ \ \det(\underline{I} + \underline{A}_2^{-1}\underline{\Delta})} \qquad (4.1.22)$$

As in case A.1 we simplify the expression for $\underline{G}$ using the results for the determinants derived in Chapter 2. We write

$$\underline{G} = \frac{\mu\ \underline{W}^{B1}\ v^{B1}(x_1)}{y^{B1}(x_1)} \qquad (4.1.23)$$

where

$$\underline{W}^{B1} \equiv \mathrm{adj}\left[\underline{I} - f_s^2(\underline{I} + \underline{A}_1^{-1}\underline{\Delta})^{-1}\underline{A}_1^{-1}\underline{\nu}(\underline{I} + \underline{A}_2^{-1}\underline{\Delta})^{-1}\underline{A}_2^{-1}\underline{\nu}\right]$$
$$\times\ \mathrm{adj}(\underline{I} + \underline{A}_1^{-1}\underline{\Delta})\underline{A}_1^{-1} \qquad (4.1.24)$$

and

$$y^{B1}(x_1,x_2) = \left[[g(x_1)\Delta_s + r(x_1)][g(x_2)\Delta_s + r(x_2)] - f_s^2 g(x_1)g(x_2)\right]$$
$$\times \left[[h(x_1)\Delta_s + s(x_1)][h(x_2)\Delta_s + s(x_2)] - f_s^2 h(x_1)h(x_2)\right]$$
$$v^{B1}(x_1,x_2) = [g(x_2)\Delta_s + r(x_2)][h(x_2)\Delta_s + s(x_2)]r(x_1)s(x_1). \qquad (4.1.25)$$

The functions $g(x)$, $h(x)$, $r(x)$, and $s(x)$ are defined in (2.3.11). The

Green function poles corresponding to the zeroes of $y^{B1}(x_1,x_2)$ represent the spin-wave frequencies which have already been discussed in Chapters 2 and 3. For the set of quantized bulk modes we have $x_1 = \exp(i\theta)$ and x_2 real and we use

$$y^{B1}(\theta,x_2) = \left[[g(\theta)\Delta_s + r(\theta)][g(x_2)\Delta_s + r(x_2)] - f_s^2 g(\theta)g(x_2)\right] \times \left[[h(\theta)\Delta_s + s(\theta)][h(x_2)\Delta_s + s(x_2)] - f_s^2 h(\theta)h(x_2)\right]$$

$$v^{B1}(\theta,x_2) = [g(x_2)\Delta_s + r(x_2)][h(x_2)\Delta_s + s(x_2)]r(\theta)s(\theta) \qquad (4.1.26)$$

where $g(\theta)$, $h(\theta)$, $r(\theta)$ and $s(\theta)$ are given in (3.1.6).

We note that if $f_s = 0$ in (4.1.24) and (4.1.25) then we find only the expected poles at $[g(x_1)\Delta_s + r(x_1)] = 0$ and $[h(x_1)\Delta_s + s(x_1)] = 0$. We have also $G' = 0$ and the uniaxial result, formally given by (4.1.14), is thereby recovered.

The case B.2 films have a nonuniaxial parameter which is non-zero on one surface and zero everywhere else. We consider, as in Chapter 2 that the surfaces are otherwise symmetric. In this case we write the matrix $\underline{f}$ appearing in (4.1.11) as $f_s\underline{\nu}$ with $\underline{\nu}$ now defined as in (2.4.16). We solve (4.1.11) to find the same formal expressions as in (4.1.21) and (4.1.22). However we write the denominator of the Green function in terms of x_1 and x_2 using (2.4.19) and (2.3.10) as

$$y^{B2}(x_1,x_2) = [g(x_1)\Delta_s + r(x_1)][g(x_2)\Delta_s + r(x_2)] \times [h(x_1)\Delta_s + s(x_1)][h(x_2)\Delta_s + s(x_2)] - f_s^2[g(x_1)h(x_1)\Delta_s + q(x_1)][g(x_2)h(x_2)\Delta_s + q(x_2)]$$

$$v^{B2}(x_1,x_2) = [g(x_2)\Delta_s + r(x_2)][h(x_2)\Delta_s + s(x_2)]r(x_1)s(x_1) \qquad (4.1.27)$$

where $g(x)$, $h(x)$, $r(x)$ and $s(x)$ are defined in (2.3.11) and $q(x)$ is

defined in (2.3.15). For the set of quantized bulk modes we use

$$y^{B2}(\theta,x_2) = [g(\theta)\Delta_s + r(\theta)][g(x_2)\Delta_s + r(x_2)]$$
$$\times [h(\theta)\Delta_s + s(\theta)][h(x_2)\Delta_s + s(x_2)]$$
$$- f_s^2[g(\theta)h(\theta)\Delta_s + q(\theta)][g(x_2)h(x_2)\Delta_s + q(x_2)]$$
$$v^{B2}(\theta,x_2) = [g(x_2)\Delta_s + r(x_2)][h(x_2)\Delta_s + s(x_2)]r(\theta)s(\theta). \qquad (4.1.28)$$

Again we see that in the limit that $f_s = 0$, then $G' = 0$ while G has the expected poles at $[g(x_1)\Delta_s + r(x_1)] = 0$ and/or $[h(x_1)\Delta_s + s(x_1)] = 0$.

We now have expressions for the spin Green functions in each of the cases of interest from which to derive spectral intensities.

4.2 Spectral Intensities

As we have mentioned the Green functions are a rich source of information concerning the spin-wave states beyond simply delivering the dispersion relations. In the linear spin-wave approximation the state of the system is described as a superposition of thermally excited spin waves. The Green functions allow us to examine the role played by these excitations both in determining equilibrium properties and the response of the system to an external stimulus such as the photons or neutrons etc. in a scattering experiment, or the RF field in SWR. The first step in modelling these types of physical behaviour is calculating the spectral intensities.

The general procedure for determining the spectral intensities has been discussed in Section 1.5 and can be outlined as follows. We know the denominator of G to be a function of Ω through the Ω-dependent variables

x_1 and x_2 appearing there. We make the analytic continuation of Ω to the complex value $\Omega + i\varepsilon$ (where ε is a real, positive, infinitesimal quantity) and then extract the imaginary parts of G. Due to the translational symmetry parallel to the surfaces we continue to use a representation in terms of the in-plane wave-vector $\mathbf{k}_{\|}$, and for the perpendicular direction we choose to examine elements of G where $n = n'$. This will eventually allow us to evaluate equal-site correlation functions. The fluctuation-dissipation theorem (1.5.10) is used to to find $\xi_n(\mathbf{k}_{\|},\Omega)$, which represents the spectral intensity in layer n, from the diagonal Green function $G_{nn}(\mathbf{k}_{\|},\Omega)$ (where we use the dimensionless frequency Ω). We present the calculation in detail for special case A.1. The analogous case B results are quoted later.

An immediate difficulty is that, unlike some earlier cases to which the equation-of-motion method has been applied (e.g. the semi-infinite film in Gopalan and Cottam 1990), here the variable Ω does not appear explicitly in our matrix Green function denominator. We must therefore consider the effect of the analytic continuation on x_1 and x_2 and then on the function $y^{A1}(x_1,x_2)$ appearing in (4.1.15). Therefore there are several intervening steps required before we can extract the imaginary parts of $G_{nn}(\mathbf{k}_{\|},\Omega+i\varepsilon)$. We exploit the relationship between x_1 and x_2 described in Chapters 2 and 3 to consider x_2 to be a function of x_1. Therefore y^{A1} is a function of x_1 alone which is in turn a function of Ω. For illustration we will first consider the case of films which are symmetric with respect to surface exchange and anisotropy constants.

This case is treated in detail and provides a model for the calculations relating to the other cases.

In order to determine the effect of the substitution $\Omega \rightarrow \Omega + i\varepsilon$ on the denominator function y (where for simplicity we have dropped the superscript label) we make the approximations

$$x_1(\Omega + i\varepsilon) \cong x_1(\Omega) + x_1'(\Omega)i\varepsilon. \tag{4.2.1}$$

and

$$y[x_1(\Omega) + x_1'(\Omega)i\varepsilon] \cong y(x_1) + y'(x_1)x_1'(\Omega)i\varepsilon. \tag{4.2.2}$$

For (4.1.15) we then have

$$G = \frac{\mu \underline{W} v(x_1)}{[\psi(x_1) + i\varepsilon]y'(x_1)x_1'(\Omega)}. \tag{4.2.3}$$

where

$$\psi(x_1) = \frac{y(x_1)}{y'(x_1)x_1'(\Omega)}. \tag{4.2.4}$$

The effect of the approximations (4.2.1) and (4.2.2) is negligible in the limit $\varepsilon \rightarrow 0$. In the special case of a semi-infinite system (Gopalan and Cottam 1990) the Green function denominator can be written explicitly in the form $(\Omega - \Omega^S)(\Omega + \Omega^S)$ and extraction of the imaginary part of the Green function follows immediately upon the analytic continuation. The result is the same as that of our general approach outlined above.

The matrix Green function in (4.2.3) is now in a form from which we can easily extract the imaginary part of $G_{nn}(\mathbf{k}_{\|}, \Omega + i\varepsilon)$ (denoted below simply as G_{nn}) using (1.5.11). For layer n (when $1 \leq n \leq N$) we find:

$$\mathrm{Im}\ G_{nn} = \frac{-\mu\pi\ W_{nn} v(x_1)\delta[\psi(x_1)]}{y'(x_1)x_1'(\Omega)}. \qquad (4.2.5)$$

We use a standard identity (e.g. see Parry 1973) to write

$$\delta[\psi(x_1)] = \sum_s \frac{\delta[x_1(\Omega) - x_1^s]}{|\psi'(x_1^s)|} \qquad (4.2.6)$$

where the sum is over the roots of $\psi(x_1)$. These roots constitute the set of discrete spin-wave modes, here labelled s. In the present case (A) the roots of $x_1(\Omega) - x_1^s$ occur in pairs (denoted as $+\Omega^s$ and $-\Omega^s$) due to the dependence of x_1 on Ω^2 in (2.3.6). We can therefore again use the identity to write

$$\delta[x_1(\Omega) - x_1^s] = \sum_s \frac{\delta(\Omega - \Omega^s)}{|x_1'(+\Omega^s)|} + \frac{\delta(\Omega + \Omega^s)}{|x_1'(-\Omega^s)|}. \qquad (4.2.7)$$

We can now rewrite (4.2.5) as

$$\mathrm{Im}(G_{nn}) = \frac{-\mu\pi\ W_{nn} v(x_1)}{y'(x_1)x_1'(\Omega)} \sum_s \frac{1}{|\psi'(x_1^s)|}\left[\frac{\delta(\Omega - \Omega^s)}{|x'(\Omega_1^s)|} + \frac{\delta(\Omega + \Omega^s)}{|x'(-\Omega_1^s)|}\right]. \qquad (4.2.8)$$

By examining the functions $\psi(x_1)$, $\psi'(x_1)$ and $x_1'(\Omega)$ we can simplify this expression. First we note that when x_1 is real (e.g. for surface modes) the definition in (2.3.6) leads to the following derivative:

$$x_1'(\Omega) = \frac{\Omega}{2(\Omega^2 + f^2)^{1/2}}\left[1 \pm \frac{a + (\Omega^2 + f^2)^{1/2}}{[a + (\Omega^2 + f^2)^{1/2}]^2 - 4)^{1/2}}\right] \qquad (4.2.9)$$

and therefore $x_1'(\Omega) = -x_1'(-\Omega)$, a relation which also applies in the case of bulk modes, when $x_1 = \exp(i\theta)$. In addition we have, according to (4.2.4),

$$\psi'(x_1^s) = \frac{y'(x_1^s)}{y'(x_1^s)x_1'(\Omega^s)} - \frac{y(x_1^s)y''(x_1^s)}{[y'(x_1^s)x_1'(\Omega^s)]^2}. \qquad (4.2.10)$$

Since x_1^s represents a root of $y(x_1)$, we find

$$|\psi'(x_1^S)| = \frac{1}{|x_1'(\Omega^S)|}. \qquad (4.2.11)$$

The imaginary part of the Green function G_{nn} may therefore be written more simply as

$$\mathrm{Im}(G_{nn}) = \frac{-\mu\pi\, W_{nn} v(x_1)}{y'(x_1)x_1'(\Omega)} \sum_S [\delta(\Omega - \Omega^S) + \delta(\Omega + \Omega^S)] \qquad (4.2.12)$$

Finally, we can use (1.5.10) to find the spectral intensity in layer n for the spin wave modes at wavevector $\mathbf{k}_\parallel$. At any given temperature we write this quantity in terms of the dimensionless frequency $\Omega \equiv \omega/SJ$ using $\beta\omega = \alpha\Omega$ where $\alpha \equiv \beta SJ \gg 1$ for the low temperature regime $T \ll T_c$. We obtain

$$\xi_n(\mathbf{k}_\parallel,\Omega) = \frac{2\pi\mu\, W_{nn} v(x_1)}{[\exp(\alpha\Omega) - 1]y'(x_1)x_1'(\Omega)} \sum_S [\delta(\Omega - \Omega^S) + \delta(\Omega + \Omega^S)]. \qquad (4.2.13)$$

We note that the poles in the Green function at $-\Omega^S$ and $+\Omega^S$ have each contributed a δ-function component in the intensity.

A similar procedure applied to G′ leads to the spectral intensity $\xi_n'(\mathbf{k}_\parallel,\Omega)$. Using (1.5.7) and (1.5.8) we can find the correlation functions $\langle b_n(t)b_n^\dagger(t')\rangle_{\mathbf{k}_\parallel}$ and $\langle b_n^\dagger(t')b_n(t)\rangle_{\mathbf{k}_\parallel}$ from (4.2.13). We can find the correlation function $\langle b_n^\dagger(t)b_n^\dagger(t')\rangle_{\mathbf{k}_\parallel}$ from $\xi_n'(\mathbf{k}_\parallel,\Omega)$ and, similarly, $\langle b_n(t)b_n(t')\rangle_{\mathbf{k}_\parallel}$. As we have mentioned these correlation functions provide a link between the microscopic theory and experimentally observable quantities. We first give the corresponding case B spectral intensity results and then demonstrate the use of the correlation functions mentioned above in the calculation of some thermodynamic properties.

In case B, as in case A, we find that both positive- and negative-frequency branches of the spin-wave spectrum contribute to the spectral intensities for G and G'. However, unlike case A.1, here the degenerate modes are not related to the same value of x_1. This leads to minor changes in the calculation of the spectral functions, e.g. the derivative of x_1 is now

$$x_1'(\Omega) = \frac{1}{2}\left[1 \pm \frac{a + \Omega}{[a + \Omega]^2 - 4)^{1/2}}\right] \qquad (4.2.14)$$

Otherwise the development follows closely that for case A.1 and the results are

$$\xi_n(k_{\parallel}, \Omega) = \frac{2\pi\mu\, W_{nn} v(x_1)}{[\exp(\alpha\Omega) - 1]y'(x_1)x_1'(\Omega)} \sum_s \delta(\Omega - \Omega^s) \qquad (4.2.15)$$

with the definitions of the various matrix elements and derivatives appropriate to either case B.1 or B.2. In this case the sum over s must be taken over all positive- and negative-frequency spin-wave solutions.

4.3 Spin-Wave Correlation Functions and Static Magnetic Properties

The spectral intensities determined in Section 4.2 can now be used to find the correlation functions which relate to the particular Green function. The correlation functions, as in the case of the dispersion relations, must be evaluated numerically. Equal-time correlation functions ($t = t'$) can be used to calculate properties such as the mean-squared amplitude of spin precession and its degree of ellipticity. The significance of these quantitities is seen in the discussion of the related figures. To facilitate comparisons the numerical results for

cases A.1, B.1 and B.2 are presented together in Section 4.3.2. Also contributions to the static magnetization may be obtained as discussed in Section 4.3.3.

4.3.1 Equal-Time Correlation Functions and Spin-Wave Amplitudes

The mean-squared amplitude of spin precession in layer n and at wave-vector $\mathbf{k}_{\parallel}$ may be written in terms of the boson operators as follows:

$$\langle (S_n^x)^2 + (S_n^y)^2 \rangle_{\mathbf{k}_{\parallel}} \cong S[\langle b_n^{\dagger} b_n \rangle_{\mathbf{k}_{\parallel}} + \langle b_n b_n^{\dagger} \rangle_{\mathbf{k}_{\parallel}}] \qquad (4.3.1)$$

using (2.1.2) and (2.1.1). We denote this thermally-averaged quantity as $A_n^{+}(\mathbf{k}_{\parallel})$ below. The ellipticity of the spin precession in layer n and at wave-vector $\mathbf{k}_{\parallel}$ can be expressed in terms of the quantity defined as

$$\langle (S_n^x)^2 - (S_n^y)^2 \rangle_{\mathbf{k}_{\parallel}} \cong S[\langle b_n b_n \rangle_{\mathbf{k}_{\parallel}} + \langle b_n^{\dagger} b_n^{\dagger} \rangle_{\mathbf{k}_{\parallel}}]. \qquad (4.3.2)$$

denoted by $A_n^{-}(\mathbf{k}_{\parallel})$ below. In uniaxial (or isotropic) systems with magnetization along the z axis there is no distinction between the x and y components of spin and the thermally averaged quantity in (4.3.2) will be identically equal to zero. Non-zero ellipticity is therefore characteristic of nonuniaxial anisotropy.

We consider first the case A.1 films. In order to find equal-time correlation functions from the spectral intensity in (4.2.13) we use (1.5.7) and (1.5.8) and set $t = t'$. We note that this quantity is independent of t since these correlation functions in general depend on $t - t'$ (as seen in (1.5.7)). Specifically, in terms of the dimensionless frequency Ω we have

$$\langle b_n b_n^\dagger \rangle_{k_\parallel} = \frac{1}{SJ} \int_{-\infty}^{+\infty} \xi_n(k_\parallel, \Omega) \exp(\alpha\Omega)\, d\Omega \qquad (4.3.3)$$

The integral is easily evaluated due to the δ-functions in $\xi_n(k_\parallel, \Omega)$. We find

$$\langle b_n b_n^\dagger \rangle_{k_\parallel} = \sum_S \frac{v(x_1^S)}{y'(x_1^S)x_1'(\Omega^S)} \left[\frac{W_{nn}(x_1^S, x_2^S, \Omega^S) \exp(\alpha\Omega^S)}{[\exp(\alpha\Omega^S) - 1]} - \frac{W_{nn}(x_1^S, x_2^S, -\Omega^S) \exp(-\alpha\Omega^S)}{[\exp(-\alpha\Omega^S) - 1]} \right] \qquad (4.3.4)$$

We use (1.5.7) to derive $\langle b_n^\dagger b_n \rangle_{k_\parallel}$ from (4.2.13) and substitute it, along with (4.3.4), into (4.3.1). We find

$$A_n^+(k_\parallel) = S \sum_S \frac{v(x_1^S)}{y'(x_1^S)x_1'(\Omega^S)} \coth\left[\frac{\alpha\Omega^S}{2}\right] \left[W_{nn}(x_1^S, x_2^S, \Omega^S) + W_{nn}(x_1^S, x_2^S, -\Omega^S) \right]. \qquad (4.3.5)$$

The correlation functions $\langle b_n^\dagger b_n^\dagger \rangle_{k_\parallel}$ and $\langle b_n b_n \rangle_{k_\parallel}$ can similarly be derived. For example, from the matrix Green function G′ in (4.1.13) we find

$$\langle b_n^\dagger b_n^\dagger \rangle_{k_\parallel} = f \sum_S \frac{Z_{nn}(x_1^S, x_2^S, \Omega^S) v(x_1^S)}{y'(x_1^S)x'(\Omega^S)} [(\exp(\alpha\Omega^S)-1)^{-1} - (\exp(-\alpha\Omega^S)-1)^{-1}] \qquad (4.3.6)$$

where Z_{nn} is a diagonal element of $[\mathrm{adj}(\underline{I} + \underline{A}_1^{-1}\underline{\Delta})\underline{A}_1^{-1}\mathrm{adj}(\underline{I} + \underline{A}_2^{-1}\underline{\Delta})\underline{A}_2^{-1}]$. To obtain a measure of the ellipticity we have

$$A_n^-(k_\parallel) = 2fS \sum_S \frac{v(x_1^S)Z_{nn}(x_1^S, x_2^S)}{y'(x_1^S)x_1'(\Omega^S)} \coth\left[\frac{\alpha\Omega^S}{2}\right] \qquad (4.3.7)$$

where we have noted that, unlike $\underline{W}$, the quantity $\underline{Z}$ depends on Ω only through x_1 and x_2. It is evident that this quantity vanishes in the

limit that $f \to 0$ where the spin precession is (i.e. semi-classical terms) circular.

A similar procedure is used for the case B films. Instead of (4.3.4) we eventually find

$$\langle b_n b_n^\dagger \rangle_{\mathbf{k}_\parallel} = \sum_s \frac{W_{nn}(x_1^s, x_2^s, \Omega^s)\ v(x_1^s)\ \exp(\alpha\Omega^s)}{[\exp(\alpha\Omega^s) - 1]y_1'(x_1^s)x'(\Omega^s)} \qquad (4.3.8)$$

where the sum over s incorporates all positive- and negative-frequency bulk and surface modes of wavevector $\mathbf{k}_\parallel$. We derive the correlation function $\langle b_n^\dagger b_n \rangle_{\mathbf{k}_\parallel}$ from G also. The functions $\langle b_n^\dagger b_n^\dagger \rangle_{\mathbf{k}_\parallel}$ and $\langle b_n b_n \rangle_{\mathbf{k}_\parallel}$ are found similarly. Here we obtain

$$A_n^+(\mathbf{k}_\parallel) = S \sum_s \frac{v(x_1^s)W_{nn}(x_1^s, x_2^s)}{y'(x_1^s)x'(\Omega^s)} \coth\left[\frac{\alpha\Omega^s}{2}\right]$$

$$A_n^-(\mathbf{k}_\parallel) = f_s\, S \sum_s \frac{v(x_1^s)Z_{nn}(x_1^s, x_2^s)}{y'(x_1^s)x'(\Omega^s)} \coth\left[\frac{\alpha\Omega^s}{2}\right]. \qquad (4.3.9)$$

Again the ellipticity-dependent quantity is seen to vanish as $f_s \to 0$.

4.3.2 Numerical Results

In this section we present numerical results for the layer-dependent mean-squared amplitudes $A_n^+(\mathbf{k}_\parallel)$ and $A_n^-(\mathbf{k}_\parallel)$ in cases A.1, B.1 and B.2. The expressions in (4.3.5) and (4.3.7) for case A.1 or (4.3.9) for cases B.1 and B.2 are evaluated for the set of appropriate spin-wave frequencies determined using the methods of Chapters 2 and 3. Appropriate expressions for the derivatives $y'(x_1)$ and $x_1'(\Omega)$ are easily obtained for both the surface and quantized bulk modes. We have chosen

to plot the contributions of the set of surface modes and the set of bulk modes separately. A few figures show the relative contributions due to the Green function poles at $-\Omega^S$ and $+\Omega^S$. The significance of the non-zero contributions at $-\Omega^S$ will be seen in the discussion of the static magnetization below. In all figures the temperature is such that $k_B T/SJ = 0.1$.

For symmetric case A.1 films, numerical examples of $A_n^+(k_\parallel)$ and $A_n^-(k_\parallel)$ at $|k_\parallel a_0| = 0$ appear in figures 4.1 (a) and 4.2 (a) for the films with dispersion relations depicted in figures 3.3 and 3.5 respectively. The surface mode amplitude (represented by closed circles) is seen to decay with distance from either surface. In figure 4.2 (a) for an eight-layer film this quantity is reduced to almost zero in the middle of the slab. By contrast, the contributions of the bulk modes (open circles) are seen to be comparable across the entire film thickness, having a maximum in the film centre in these examples. Figures 4.1 (b) and 4.2 (b) contain plots of ellipticity as a function of layer number for surface modes (closed squares) and quantized bulk modes (open squares). As discussed earlier, this quantity vanishes in the limit that $f \to 0$. Figure 4.3 shows the relative contributions at positive and negative frequencies to $A_n^+(k_\parallel)$ of one of the $k_\parallel = 0$ surface modes in figure 3.3. The contribution at $-\Omega^S$ is smaller than that at $+\Omega^S$ and can be shown numerically to tend to zero in the uniaxial limit, as expected.

For asymmetric case A.1 films representative plots of $A_n^+(k_\parallel)$ and $A_n^-(k_\parallel)$ versus layer number for $|k_\parallel a_0| = \pi$ appear in figures 4.4 (a) and (b)

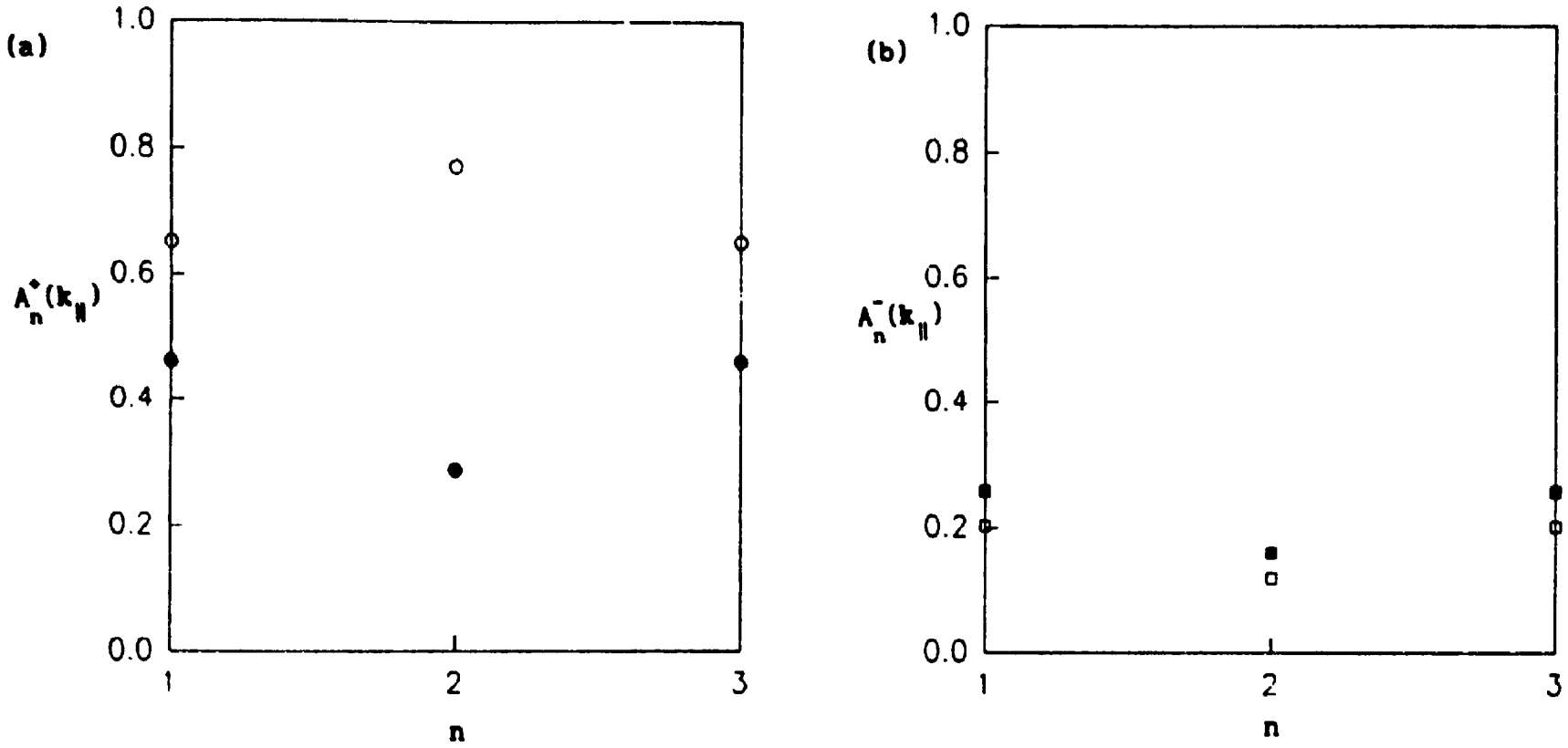

Figure 4.1 $A_n^+(k_\parallel)$ (a) and $A_n^-(k_\parallel)$ (b) at $k_\parallel = 0$ plotted against layer index n for a symmetric case A.1 film with the dispersion relation of figure 3.3. Contributions of surface modes are represented by closed circles (a) or squares (b), those of the set of quantized bulk modes by open circles (a) or squares (b).

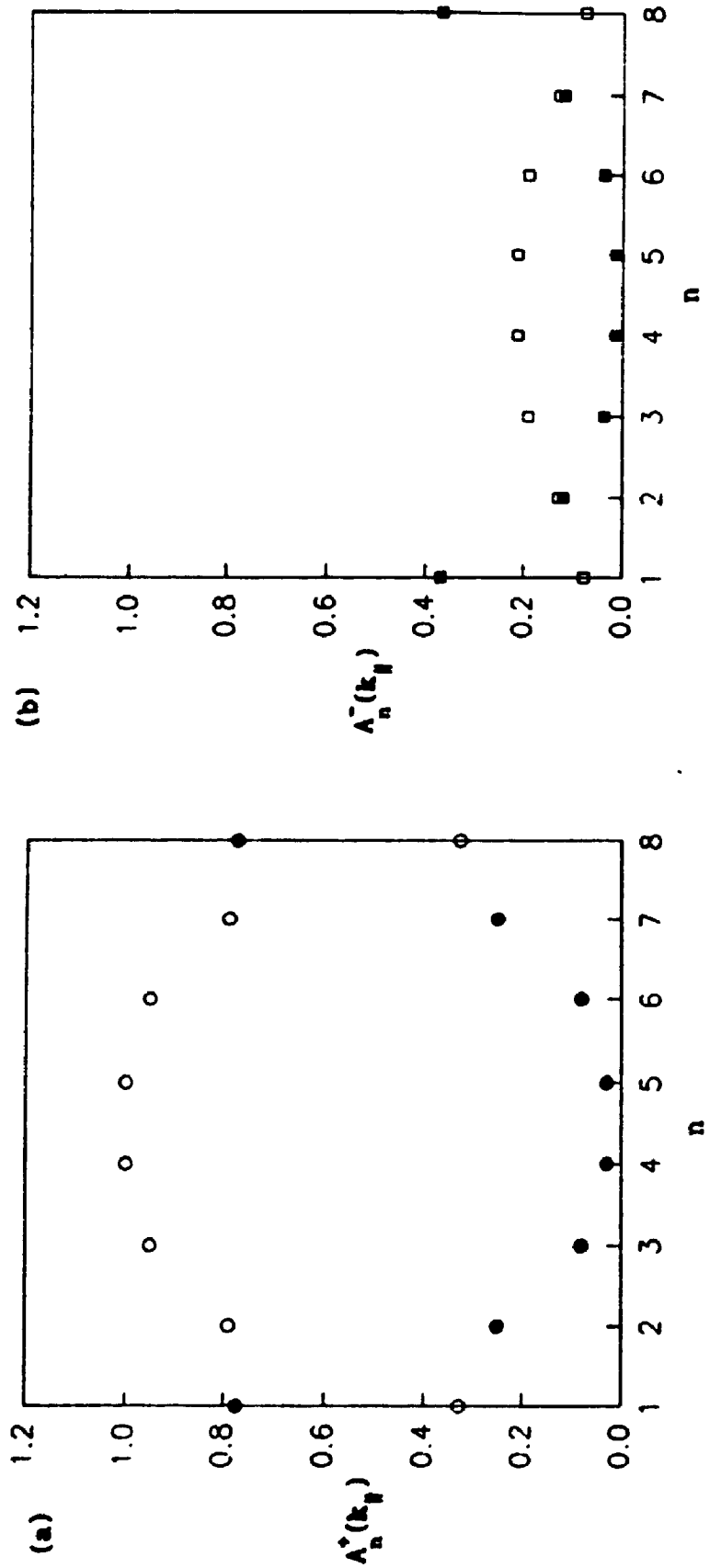

Figure 4.2 $A_n^+(k_\parallel)$ (a) and $A_n^-(k_\parallel)$ (b) at $k_\parallel = 0$ plotted against layer index n for a symmetric case A.1 film with the dispersion relation of figure 3.5; symbols defined as in figure 4.1.

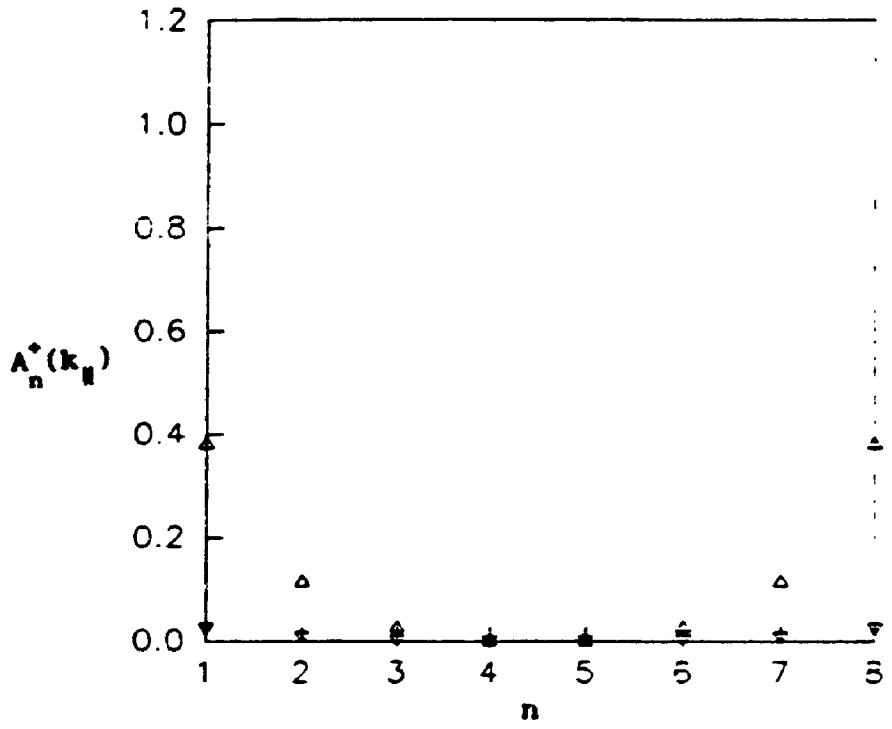

Figure 4.3 Contributions to $A_n^+(k_\parallel)$ (at $k_\parallel = 0$) of an acoustic surface mode at positive (upright triangles) and negative (inverted triangles) frequencies . All parameters as in figure 4.2.

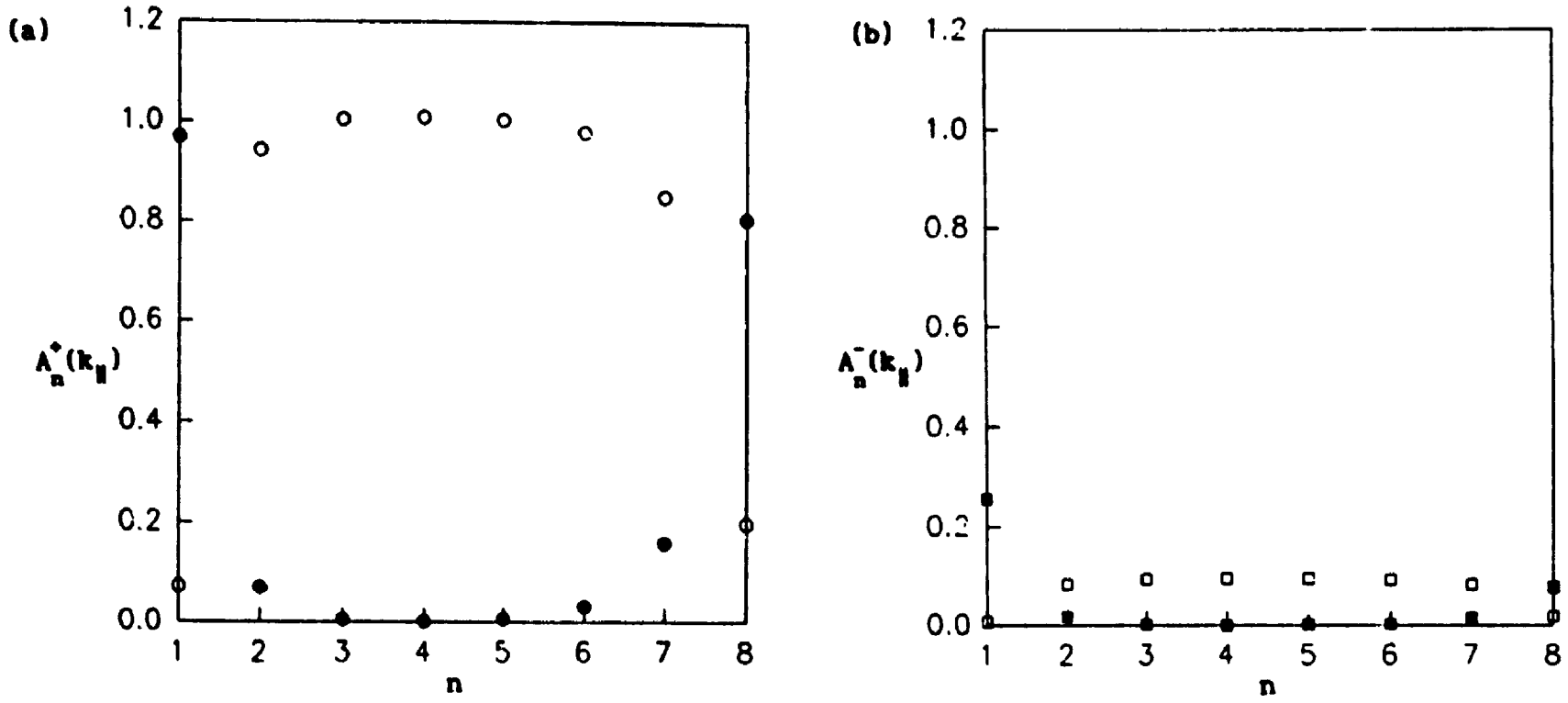

Figure 4.4 $A_n^+(k_\parallel)$ (a) and $A_n^-(k_\parallel)$ (b) at $|k_\parallel a_0| = \pi$ (in the [100] direction) plotted against layer index n for an asymmetric case A.1 film with the dispersion relation of figure 3.8. Symbols defined as in figure 4.1.

respectively for a film with the dispersion relation of figure 3.8. The asymmetry of these plots reflects that of the film. In the dispersion relation plot in figure 3.8 the surface mode which is acoustic for all $|k_{\parallel}a_o|$ is mainly associated with the n = 1 surface and its behaviour resembles those in figures 3.5 and 4.2 (a). In comparing figure 4.4 (a) with 4.2 (a) we see that amplitude decays more rapidly near the zone edge than at the zone centre. In figure 4.4 (b) we see that the ellipticity for both surface and bulk modes is less pronounced here than in figure 4.2 (b), because the higher energy zone-centre modes are relatively less influenced by the nonuniaxial anisotropy. This is particularly true in the vicinity of the n = N surface where the optic mode is mainly localized.

For case B.1 a representative plot of $A_n^+(k_{\parallel})$ at $k_{\parallel}$ = 0 for surface and quantized bulk modes as a function of layer number is provided in figure 4.5 (a). For the most part the features are the same as for the symmetric films in case A.1. The ellipticity is seen to decay more rapidly than in figure 4.2 (b), reflecting the fact that here only the surface spins have nonuniaxial anisotropy.

Finally, for case B.2, examples of numerical results for $A_n^+(k_{\parallel})$ and $A_n^-(k_{\parallel})$ appear in figures 4.6 (a) and (b) respectively. The asymmetry of the film is evident in the asymmetry of the plots. In particular the ellipticity is seen to be zero on the n = N surface and non-zero on the other (n = 1). Figures 4.7 (a) and (b) depict the contributions to $A_n^+(k_{\parallel})$ of the lower and higher energy surface modes respectively. In

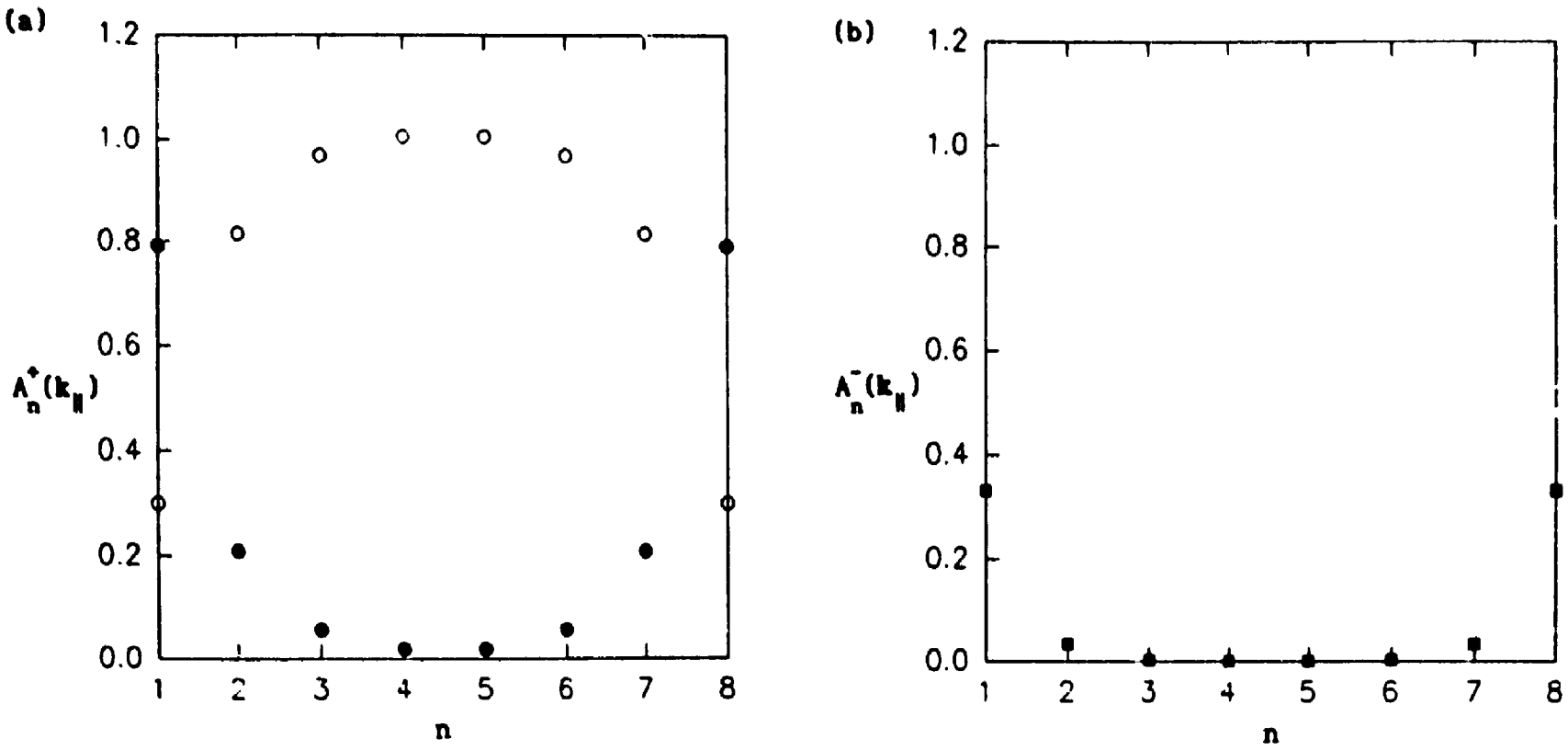

Figure 4.5 $A_n^+(k_\parallel)$ (a) and $A_n^-(k_\parallel)$ (b) at $k_\parallel = 0$ plotted against layer index n for a symmetric case B.1 film with the dispersion relation of figure 3.14; in (b) contributions of surface modes only.

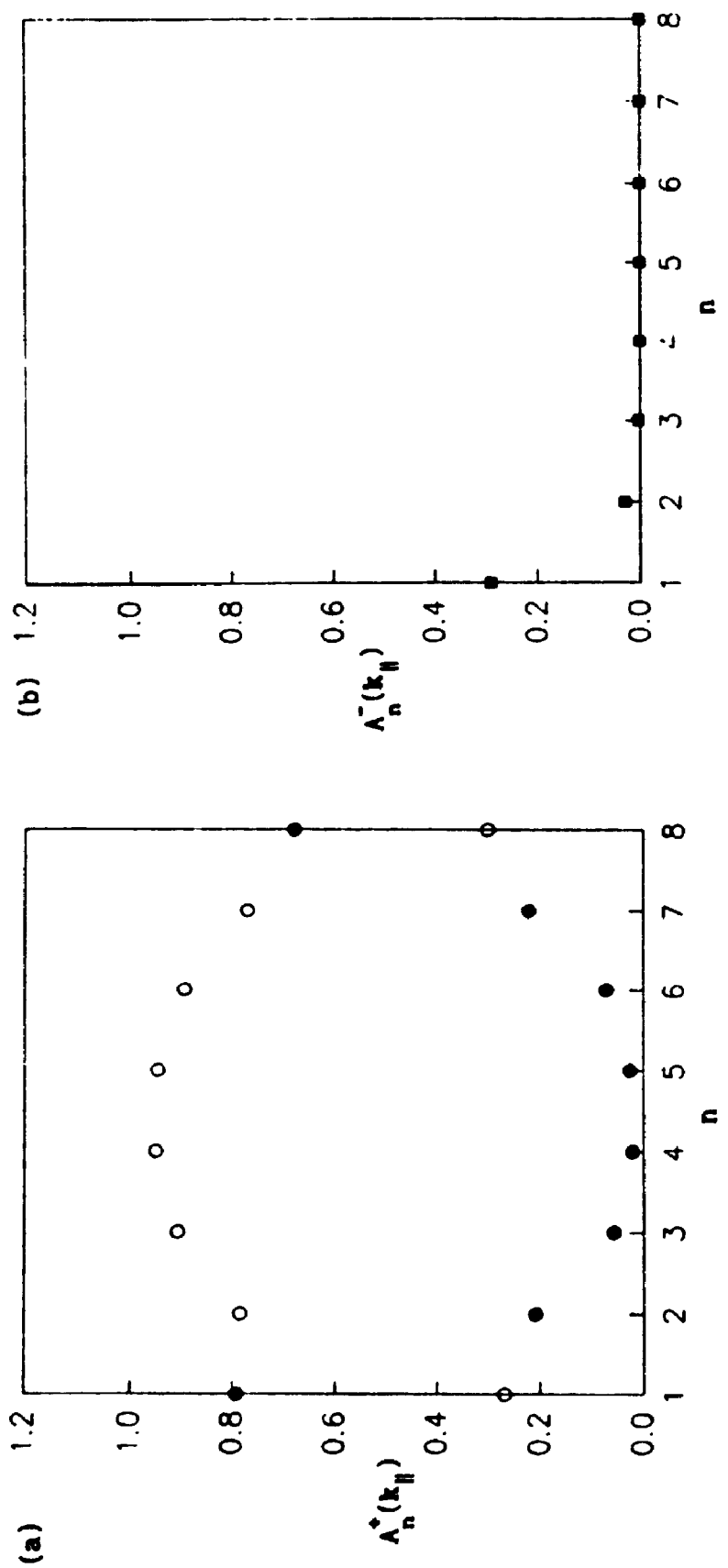

Figure 4.6 $A_n^+(k_\parallel)$ (a) and $A_n^-(k_\parallel)$ (b) at $k_\parallel$ = 0 plotted against layer index n for an asymmetric case B.2 film with the dispersion relation of figure 3.12, in (b) contributions of surface modes only.

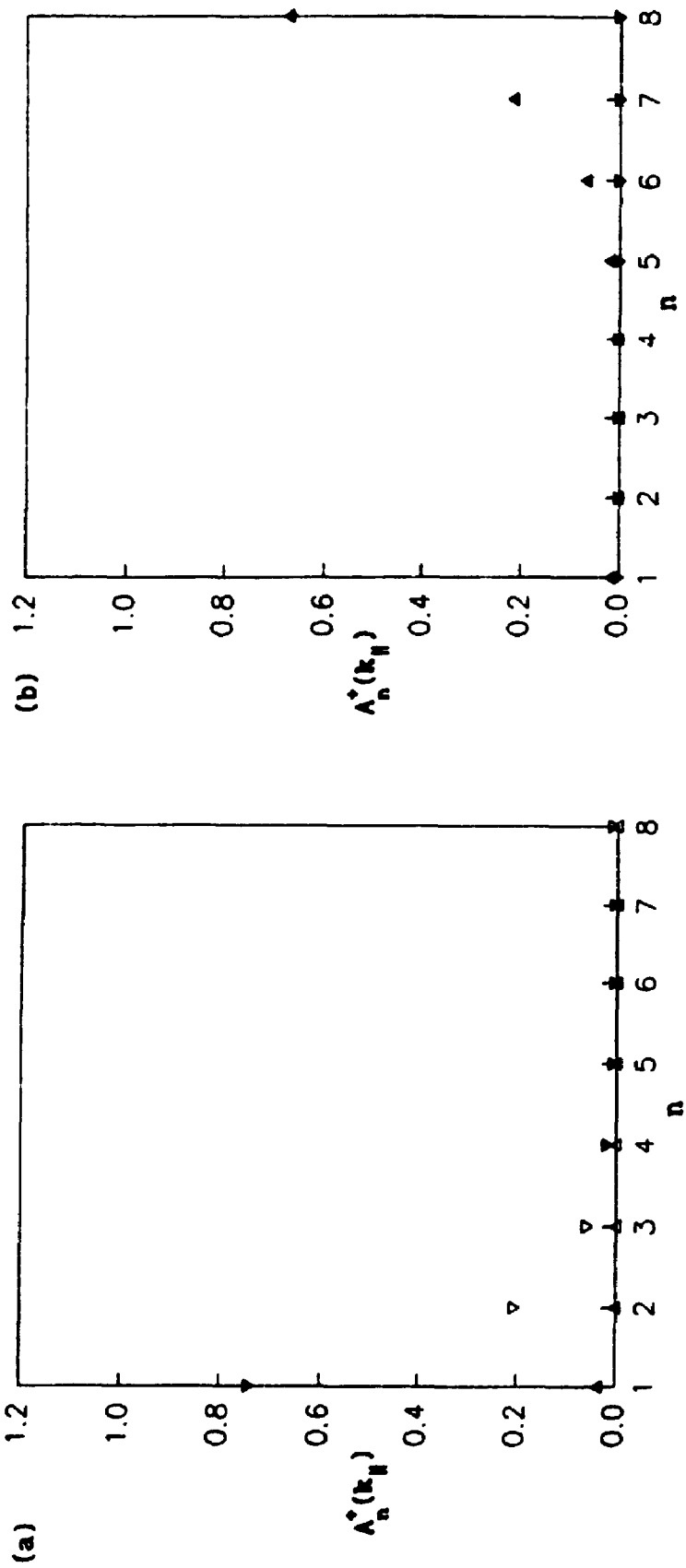

Figure 4.7 Contributions to $A_n^*(k_\parallel)$ at $k_\parallel = 0$ at positive (upright triangles) and negative (inverted triangles) of the lower (a) and higher (b) energy surface modes. All parameters as in figure 4.6.

figure 4.7 (a) it is seen that for the mode which is localized near the nonuniaxial (n = 1) surface, there are non-zero contributions due to both $-\Omega^S$ (inverted triangles) and $+\Omega^S$ (upright triangles) whereas in figure 4.7 (b) it is seen that for the mode localized near the uniaxial (n = N) surface there is non-zero intensity due to $+\Omega^S$ only.

4.3.3 The Static Magnetization

Other thermodynamic quantities, such as the static magnetization and the specific heat, can be determined using the equal-time correlation functions above. The static magnetization, proportional to $\langle S^z \rangle$, may be non-uniform in a thin film, particularly in the vicinity of a surface. We are therefore interested in calculating $\langle S_n^z \rangle$ or deviation of this quantity from the maximum value S. The average spin deviation in layer n as

$$\Delta S_n = S - \langle S_n^z \rangle. \qquad (4.\ 10)$$

Using (2.1.4), and exploiting the in-layer translational invariance we can write this in terms of the boson operators for site i (in layer n) as

$$\Delta S_n = \langle b_i^\dagger(t) b_i(t) \rangle \qquad (4.3.11)$$

which is, according to (4.1.8), simply

$$\Delta S_n = \frac{1}{N} \sum_{\mathbf{k}_\parallel} \langle b_n^\dagger b_n \rangle_{\mathbf{k}_\parallel}. \qquad (4.3.12)$$

The correlation functions in (4.3.12) can be calculated for any $\mathbf{k}_\parallel$ in the manner described above. Specifically, we use (1.5.8) to write

$$\Delta S_n = \frac{SJ}{N} \sum_{\mathbf{k}_\parallel} \int_{-\infty}^{+\infty} \xi_n(\mathbf{k}_\parallel, \Omega)\, d\Omega \qquad (4.3.13)$$

where $\xi_n(\mathbf{k}_\parallel,\Omega)$ is given by (4.2.13) for case A.1 or (4.2.15) for cases B.1 and B.2. The integral over Ω is accomplished easily using properties of the δ-functions in $\xi_n(\mathbf{k}_\parallel,\Omega)$ at $\{\pm\Omega^S\}$. The thermal factors associated with $\{+\Omega^S\}$ are of the form $[\exp(-\alpha|\Omega^S|) - 1]^{-1}$ which vanish in the limit that $T \to 0$ (or $\alpha \to \infty$). In contrast, for $\{-\Omega^S\}$, the thermal factors $[\exp(-\alpha|\Omega^S|) - 1]^{-1} \to -1$ in the limit that $T \to 0$ so that for a nonuniaxial system ΔS_n is non-zero even at $T = 0$ (e.g. see Mills 1989). This is analogous to the zero-point magnetization in bulk antiferromagnets (e.g. see Kittel 1987) where the frequency spectrum also has positive and negative branches. We recall that the ground state of the Hamiltonian in (1.2.1) with $F \neq 0$ is only approximately the same as that found in uniaxial ferromagnets (where $F = 0$) and the zero-temperature deviation from perfect order is therefore expected. We observe that the appearance of Green function poles at both positive and negative frequencies has some (indirect) physical meaning.

Due to the macroscopically large x and y dimensions of the film the allowed values of $\mathbf{k}_\parallel$ effectively constitute a continuum and we may therefore write the sum over the 2-D Brillouin zone as

$$\Delta S_n \cong \frac{a_0^2}{4\pi^2} \int \langle b_n^\dagger b_n \rangle_{\mathbf{k}_\parallel} d^2\mathbf{k}_\parallel \qquad (4.3.14)$$

or

$$\Delta S_n \cong \frac{1}{\pi^2} \int_0^\pi \int_0^\pi \langle b_n^\dagger b_n \rangle_{\mathbf{k}_\parallel} d(k_x a_0) d(k_y a_0) \qquad (4.3.15)$$

where we have used the four-fold symmetry of the Brillouin zone to

restrict our attention to the first quadrant. The integral in (4.3.15) is evaluated numerically as follows. We divide the 2-D Brillouin zone into n_0^2 square elements, each labelled k, and consider the finite sum

$$\Delta S_n \cong \frac{1}{\pi^2} \sum_k \left(\frac{\pi}{n_0} \right)^2 B_{nk} \qquad (4.3.16)$$

where the value of $\langle b_n^\dagger b_n \rangle_{k_\parallel}$ for each element k is denoted by B_{nk}. The value of n_0 required for reasonable accuracy depends on factors such as the temperature etc. Here we found that for $n_0 = 10$ the results converged well.

The surface mode contributions to ΔS_n are plotted against n in figure 4.8 for T = 0. The results for F/J = 0.5 are represented by open circles while the smaller values corresponding to F/J = 0.4 are represented by open squares. At T = 0, in the limit that $F \to 0$ we find that $\Delta S_n \to 0$. The bulk modes will have some contribution to ΔS_n; however we are chiefly interested in the variation with distance from the surface, which we expect to be largely dictated by the surface mode contributions. Numerically the temperature-dependent part of ΔS_n is dominated by the acoustic surface modes near the zone-centre as these have the lowest energy.

4.4 Other Applications of the Green Function Results

In this section we outline how the spin Green functions can be used to find the differential cross-section for inelastic light scattering from spin-waves, following Cottam and Lockwood (1986) and Moul and Cottam (1983). More briefly we discuss some other applications such as spin

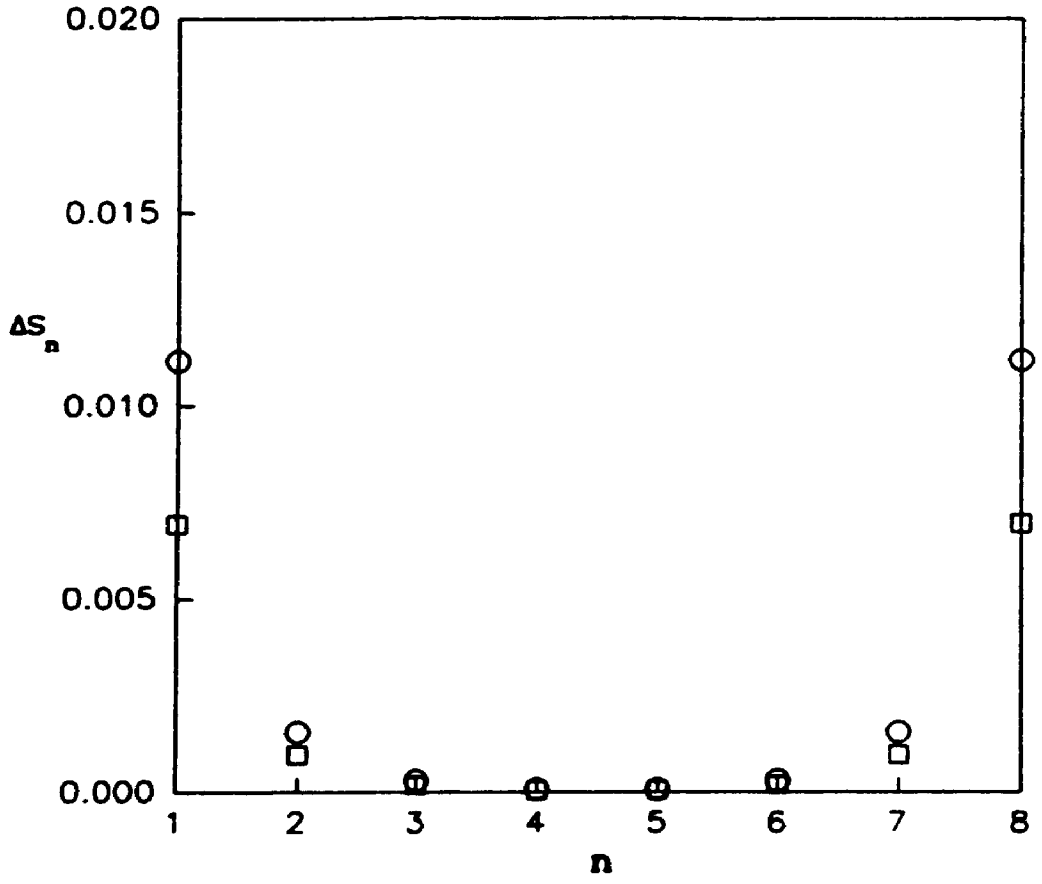

Figure 4.8 The surface spin wave contribution to the average spin deviation ΔS_n (in units of S) plotted against layer index n for a symmetric case A.1 film with the dispersion relation of figure 3.5. Here n_o = 10 and T ≈ 0, F/J = 0.5 (circles) and F/J = 0.4 (squares).

wave resonance.

We assume that incident (I) light of frequency ω_I is scattered by creating or destroying a spin wave of frequency ω. The scattered (S) light beam has frequency $\omega_S = \omega_I - \omega$, by conservation of energy. In addition to the peak due to elastic scattering ($\omega = 0$) the light scattering spectrum will generally have sets of peaks due to Stokes ($\omega > 0$) and anti-Stokes scattering ($\omega < 0$). The wavevectors of the incident and scattered light are denoted by $\mathbf{k}_I$ and $\mathbf{k}_S$, respectively, while that of the spin-wave is $\mathbf{k} = (\mathbf{k}_{\parallel}, \kappa_z)$. The component κ_z is real for bulk modes or complex (usually purely imaginary) for surface modes. For films we have conservation of momentum in the direction parallel to the surface and therefore $\mathbf{k}_{S,\parallel} = \mathbf{k}_{I,\parallel} - \mathbf{k}_{\parallel}$.

We assume a typical thin-film scattering geometry wherein the incident and scattered light beams (which enter and leave the same surface) are at angles θ_I and θ_S, respectively, to the z axis and may be in different vertical planes. The components of the polarization $\mathbf{P}$ of the target material at position $\mathbf{r}$ and time t may be written as

$$P^{\mu}(\mathbf{r}, t) = \varepsilon_0 \sum_{\nu} \chi^{\mu\nu}(\mathbf{r}, t) E_I^{\nu}(\mathbf{r}, t) \qquad (4.4.1)$$

where ε_0 is the permittivity of free space, χ is the susceptibilty tensor and $\mathbf{E}_I$ is the electric field vector of the incident light. The electric field vector of the resultant scattered light, $\mathbf{E}_S$, may be written in terms of the polarization $\mathbf{P}$ using Maxwell's equations. We define the differential cross-section for scattering into the elementary solid angle $d\Omega$ with frequency between ω_S and $\omega_S + d\omega_S$ as

$$\frac{d^2\sigma}{d\Omega d\omega_s} = \frac{\omega_I}{\omega_s}\frac{\bar{I}_s}{\bar{I}_I} \qquad (4.4.2)$$

where $\bar{I}_s$ and $\bar{I}_I$ are the cycle-averaged intensities of the scattered and incident light beams respectively, which are proportional to the square of the electric field vectors. Eventually we may write the cross-section in terms of Green functions following the procedure of Camley *et al* (1981) and Moul and Cottam (1983). A convenient form of the expression is

$$\frac{d^2\sigma}{d\Omega d\omega_s} = [1 - \exp(-\beta\omega)]^{-1}\ \mathrm{Im}\left[\sum_{n,n'}\exp(-iB^{*}na_0)\exp(iBn'a_0)\right.$$

$$\left.\times\sum_{\nu,\mu,\nu',\mu'}F(\nu,\mu,\nu',\mu')\ \langle\langle(\chi_n^{\mu\nu})^{*};\chi_{n'}^{\mu'\nu'}\rangle\rangle_{\mathbf{k}_{\|}}\right]. \qquad (4.4.3)$$

Here n and n′ refer to summations over the layer indices of the film and ν, μ, ν', and μ' are Cartesian indices. The exponential factors arise due to the variation of light intensity as a function of depth into the film, where B is a complex wavevector (with Im B > 0) describing the light propagation in the absorptive medium. The function F depends on the magneto-optical coupling, the scattering geometry, and optical transmission coefficents. The cross-section contains Green functions involving the components of the susceptibilty tensor χ, where a 2D Fourier transform to wavevector $\mathbf{k}_{\|}$ has been made (as before) and the position in the film is indicated by the layer index. As mentioned in Chapter 1 spin waves lead to periodic modulations in the susceptibility and thereby affect the polarization of the target material and hence the scattered light. The susceptibilty components can be expressed, in a phenomenological manner, as an expansion in terms of powers of the spin

operators S^x, S^y and S^z with appropriate magneto-optical coefficents. Linear magneto-optic coupling leads to terms in S^x and S^y while quadratic magneto-optic coupling leads to terms proportional to $S^xS^z + S^zS^x$ and $S^yS^z + S^zS^y$. Equivalently these components may be written as an expansion in terms of S^+, S^- and S^z and hence the boson operators b and $b^\dagger$ we have been using, with appropriately modified coefficients. For systems with nonuniaxial anisotropy it follows that (e.g. see Cottam and Latiff-Awang 1977 for the infinite case) the required Green functions are those that we have already calculated, e.g. $G_{nn'}(\mathbf{k}_\parallel,\omega) = \langle\langle b_n; b_{n'}^\dagger \rangle\rangle_{\mathbf{k}_\parallel,\omega}$, $G'_{nn'}(\mathbf{k}_\parallel,\omega) = \langle\langle b_n^\dagger; b_{n'}^\dagger \rangle\rangle_{\mathbf{k}_\parallel,\omega}$ etc.

In the case of 180° backscattering ($\theta_I = -\theta_S \equiv \theta$), assuming polarization of the incident and scattered light to be $\mathbf{e}_I = (\cos\theta, 0, \sin\theta)$ and $\mathbf{e}_S = (0, 1, 0)$, we may write the cross-section as follows:

$$\frac{d^2\sigma}{d\Omega d\omega_S} = -\frac{\bar{A}\omega_I\omega_S^3\cos^2\theta\sin^2\theta}{8\pi^2c^4}\,[1 - \exp(-\beta\omega)]^{-1}\,|f^z g^{yy}|$$

$$\times \mathrm{Im}\left[\sum_{n,n'}\exp(-iB^*na_0)\exp(iBn'a_0)\left\{M_1\langle\langle b_n; b_{n'}\rangle\rangle_{\mathbf{k}_\parallel,\omega}\right.\right.$$

$$\left.\left. + M_2\langle\langle b_n; b_{n'}^\dagger\rangle\rangle_{\mathbf{k}_\parallel,\omega} + M_3\langle\langle b_n^\dagger; b_{n'}\rangle\rangle_{\mathbf{k}_\parallel,\omega} + M_4\langle\langle b_n^\dagger; b_{n'}^\dagger\rangle\rangle_{\mathbf{k}_\parallel,\omega}\right\}\right] \quad (4.4.4)$$

where $\bar{A}$ is the area of the film surface through which the scattered beam emerges, and f and g are coefficients for the transmission of the incident beam and scattered beams, respectively, through the upper surface of the film. The coefficients of the Green functions are

$$M_1 = |K|^2 + 2iSG^*K - 2iSGK^* + 4S^2|G|^2$$

$$M_2 = |K|^2 + 2iSG^*K + 2iSGK^* - 4S^2|G|^2$$

$$M_3 = |K|^2 - 2iSG^*K - 2iSGK^* - 4S^2|G|^2$$
$$M_4 = |K|^2 - 2iSG^*K + 2iSGK^* + 4S^2|G|^2 \qquad (4.4.5)$$

where K and G are the linear and quadratic magneto-optic coupling constants respectively. Similar expressions may be derived for other geometries and polarizations. We have described earlier how to find the imaginary part of the Green functions. The quantity in (4.4.5) may be evaluated numerically for the set of spin-wave frequencies determined by the methods of Chapter 2 and 3.

We can also use the spin Green functions we have derived to calculate the absorption strength for spin wave resonance. As mentioned in Chapter 1, spin wave modes can be excited by a transverse oscillating field provided there is a frequency match between the spin wave and the applied RF field. We follow Moul and Cottam (1983) and assume a field $H_i^{RF}\exp(-i\omega t)$ applied along the y axis. The energy associated with the interaction between H_i^{RF} and the spins is

$$W \propto - g\mu_B \sum_i H_i^{RF} \cdot S_i \qquad (4.4.6)$$

where the sum is over all sites. The SWR absorption strength $A(\omega)$ at frequency ω is given by

$$A(\omega) \propto \frac{\omega}{2\pi} \text{ Im } \langle\langle W^*; W \rangle\rangle_\omega \qquad (4.4.7)$$

where we can use (4.4.7) to write these Green functions in terms of spin operators. We write the spatially dependent part of the RF field as

$$H_i^{RF} = h_i^0 \hat{u}_y \exp(i\mathbf{Q}_\parallel \cdot \rho_i)\exp(iQna_0) \qquad (4.4.8)$$

where $\hat{u}_y$ is the unit vector in the y direction, $\mathbf{Q}_\parallel$ and Q are wavevector components, and $\rho = (x_i, y_i)$. We can eventually write

$$A(\omega) \propto -\omega \ \mathrm{Im} \sum_{n,n'} \exp[-i(Q^{*}na_0 - Qn'a_0)] \Big[\langle\langle b_n ; b_{n'}^{\dagger} \rangle\rangle_{k_{\parallel},\omega} - \langle\langle b_n ; b_{n'}^{\dagger} \rangle\rangle_{k_{\parallel},\omega} - \langle\langle b_n^{\dagger} ; b_{n'} \rangle\rangle_{k_{\parallel},\omega} + \langle\langle b_n^{\dagger} ; b_{n'}^{\dagger} \rangle\rangle_{k_{\parallel},\omega} \Big] \qquad (4.4.10)$$

which represents a generalization to nonuniaxial systems of the results of Moul and Cottam (1983) for uniaxial systems. The imaginary parts of these Green functions and hence the absorption strength contain a series of δ-functions at surface and bulk spin-wave frequencies. If the RF field is applied along the x axis an expression similar to (4.4.10) results. However, in a nonuniaxial material the x and y directions are (by definition) not equivalent and therefore the absorption strengths will be slightly different (involving a combination of the same Green functions but with different weighting factors).

For other experiments involving dynamical processes, e.g. inelastic neutron scattering, the appropriate cross-sections may be similarly calculated using our basic spin Green functions.

4.5 Discussion

In this chapter we have derived spin Green functions for the anisotropic ferromagnetic films and verified that the resulting spin-wave dispersion relations are the same as those derived in Chapters 2 and 3 using the operator method. We have compared our results with previous calculations on semi-infinite and/or uniaxial systems and conclude that our study represents a generalization of earlier work. We have derived the spectral intensities, describing our strategy for dealing with the

difficulties posed by the complicated Green-function denominators. The use of correlation functions extracted from the intensities to calculate thermodynamic properties has been described and illustrative numerical examples provided. We have also shown how our Green functions could be used to find the light-scattering cross-section and SWR absorption strength.

The numerical examples of the mean-squared amplitude and ellipticity have been discussed and the distinctive features of the nonuniaxial systems identified, notably the elliptical spin precession. We have seen that the correct calculation of magnetic properties involves Green function poles at both positive and negative frequencies for each spin wave mode. Uniaxial (or isotropic) systems, in contrast, have circular spin precession and the physical description is achieved using Green functions where each spin wave mode is associated with a pole at positive frequency only. Such systems have been seen to be a special case of our more general one. The figures can also be used to illustrate features of spin waves which are common to nonuniaxial and uniaxial (or isotropic) systems e.g. the localization of surface modes. If the film thickness is large compared with the attenuation length of the surface modes then we see that the film resembles a system in which two surfaces are effectively isolated from one another. At this point we recover the results of previous studies on "semi-infinite" systems. In the case of systems with uniform nonuniaxial anisotropy (A.1) we have calculated the static magnetization on each layer in the film and illustrated the zero-temperature spin deviation.

CHAPTER 5

GREEN FUNCTION METHOD FOR SEMI-INFINITE ANTIFERROMAGNETS

The second major object of this thesis is the study of spin waves in antiferromagnetic films with nonuniaxial single-ion anisotropy. As mentioned in Chapter 1, antiferromagnetic ordering involves oppositely oriented spins occupying different *sublattices* in the material with the result that the Green function formalism is somewhat modified here. The main focus of this thesis is on single-ion anisotropy effects which, as we explain below, are particularly significant in antiferromagnetic materials. In addition, antiferromagnets are generally insulators and therefore well described by the Heisenberg local moment model that we employ. Spin waves in antiferromagnets have been extensively studied by means of light scattering experiments, mainly in bulk samples (e.g. see Cottam and Lockwood 1986). Our Green function results may be used to calculate the appropriate cross sections for thin films, as was shown in Chapter 4.

Spin waves in semi-infinite systems with uniaxial single-ion anisotropy have been thoroughly studied theoretically. Wolfram and DeWames (1972) review spin-wave frequencies while Cottam (1978) provides a microscopic Green-function treatment. The uniaxial thin fi m case has been studied using Green functions for S = 1/2 by Diep (1991). Nonuniaxial single-ion anisotropy occurs in antiferromagnets such as NiO and K_2FeF_4. We extend previous studies on infinite (or bulk) systems (e.g. see Cottam and Latiff-Awang 1979 (a), Balucani *et al* 1980 (b)) to

semi-infinite systems in the present chapter and in Chapter 6 generalize the results to thin films. In general, as in the case of ferromagnets, we consider several different models for the relative surface and bulk nonuniaxial parameters. However here we emphasize the case of surface nonuniaxial anisotropy (while the bulk is uniaxial) since the theory is more tractable.

Section 5.1 contains general background material for the antiferromagnetic systems which also pertains to Chapter 6. The full spin Hamiltonian is presented in Section 5.1 along with a brief discussion of spin waves in antiferromagnets. We concentrate on the body-centred tetragonal (bct) lattice, seen in such antiferromagnets as MnF_2 and the nonuniaxial system NiF_2. A description of the particular assumptions we have made appears in Section 5.1.3. The Holstein-Primakoff transformation for the two-sublattice antiferromagnet is presented in Section 5.2. In Section 5.3 the equation-of-motion method is used to find coupled Green functions for the semi-infinite systems which are then solved for particular special cases in Sections 5.4 and 5.5. Examples of numerical results for dispersion relations are included. As well, the mean-squared amplitude of spin precession for surface modes is calculated as in Chapter 4 and numerical examples are used to illustrate some of the features of spin waves in antiferromagnets.

Much of the theoretical approach will be similar to that employed in previous chapters and we include fewer details here, referring to

earlier equations whenever possible. The sublattice structure makes it somewhat more difficult to find the Green functions explicitly here than in the ferromagnetic case. However once these functions have been determined then the extraction of dispersion relations, intensities, and correlation functions etc., is straightforward. No discussion of the operator equation-of-motion method is found here since we go directly to the Green-function formalism.

5.1 Basic Theory for Anisotropic Heisenberg Antiferromagnets

The Heisenberg exchange Hamiltonian $\mathcal{H}_{ex} = -J_{ij}\mathbf{S}_i \cdot \mathbf{S}_j$ for a pair of spins i and j can be used with $J_{ij} > 0$ to describe ferromagnets and with $J_{ij} < 0$ to describe antiferromagnets. The interaction leads to the parallel spin alignment seen in ferromagnets and the antiparallel alignment seen in antiferromagnets. As mentioned above, an antiferromagnet can usually be described as being composed of two interpenetrating sublattices ("spin-up" and "spin-down") which contain spins of opposite orientation so that the nearest neighbours of a spin on one sublattice typically lie on the other sublattice. In the absence of an applied magnetic field the net magnetization is zero. The net magnetization of each sublattice is non-zero for temperatures below the Néel temperature (T_N) at which long-range order vanishes. Other types of antiferromagnet, such as those involving more than two sublattices or those involving frustration of the antiparallel alignment due tc geometric limitations will not be considered here.

Experimental means of studying spin waves in antiferromagnets are essentially the same as those mentioned in Section 1.6 for ferromagnets and discussed in detail in the references given there. In the present case the excitation of spin waves by a transverse oscillating field is called antiferromagnetic resonance (AFMR) for the $\mathbf{k} = 0$ mode and surface antiferromagnetic resonance (SAFMR) for the surface $\mathbf{k}_{\parallel} = 0$ mode.

5.1.1 Antiferromagnetic Hamiltonian with Single-ion Anisotropy

The general form of the spin Hamiltonian used here is $\mathcal{H} = \mathcal{H}_H + \mathcal{H}_A$ where

$$\mathcal{H}_H = \sum_{ij} J_{ij}\, \mathbf{S}_i \cdot \mathbf{S}_j - g\mu_B H_0 \sum_i S_i^z - g\mu_B H_0 \sum_j S_j^z$$

$$\mathcal{H}_A = -\sum_i D_i (S_i^z)^2 - \sum_j D_j (S_j^z)^2 - \sum_i F_i [(S_i^x)^2 - (S_i^y)^2]$$

$$- \sum_j F_j [(S_j^x)^2 - (S_j^y)^2]. \qquad (5.1.1)$$

The indices i and j refer to sites on the spin-up and spin-down sublattices respectively. The first term in $\mathcal{H}_H$ describes the exchange interaction which, as noted earlier, promotes antiparallel alignment of neighbouring spins. Note that we have chosen the sign before the exchange term so that the exchange constant J_{ij} is considered to be positive. We also assume it to be non-zero only for nearest-neighbour spin pairs on opposite sublattices for the bct lattices we consider here.

The Zeeman terms in $\mathcal{H}_A$ contain an applied field H_0 along the positive z axis which provides a direction for spin quantization. The applied field has different energy implications for the spin-up and spin-down sublattices. The effect of this asymmetry on spin waves is discussed

below. In a large applied field the Zeeman terms will dominate and there is a transition to the so-called spin-flop phase (e.g. see Wagner 1972, Keffer 1966) in which the spins are oriented approximately perpendicular to the applied field, with spins on opposite sublattices still in different directions. Figure 5.1 depicts the H_0-T phase diagram for a typical antiferromagnet. The single-ion anisotropy plays an important role in determining the critical field H_{SF} for this transition, which has no ferromagnetic analogue. In general our calculations apply in the antiferromagnetic phase.

The anisotropy Hamiltonian $\mathcal{H}_A$ contains terms identical to those which occur in the ferromagnetic Hamiltonian in (1.2.1). The uniaxial anisotropy serves to stabilize antiferromagnetic ordering along the positive and negative z axis, particularly in the antiferromagnetic phase. This anisotropy is frequently represented phenomenologically in the literature by an effective anisotropy field which has the same magnitude but opposite direction on each sublattice. We have used the more accurate single-ion form in $\mathcal{H}_A$. As in the ferromagnetic case very large nonuniaxial anisotropy can lead to a spin-wave instability and an alteration in the net spin alignment. We have again restr' 'ed our attention to values of F_i for which the assumption of colinear ordering along the z axis is valid.

5.1.2 Spin Waves in Antiferromagnets

In contrast to the ferromagetic case, the ground state of the Heisenberg antiferromagnet is not known exactly. The Néel state, in which spins on

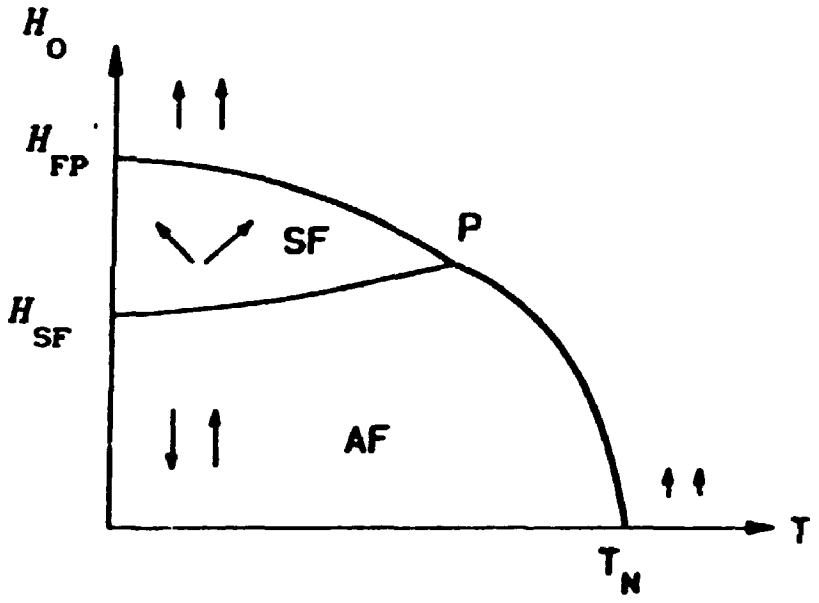

Figure 5.1 Schematic H_o vs. T phase diagram for an antiferromagnet showing the antiferromagnetic phase (AF), the spin-flop phase (SF), the paramagnetic phase (P), and the critical fields for phase transitions.

one sublattice have $S^z = S$ and spins on the other have $S^z = -S$, is the classical state of lowest energy, but it is not an eigenstate of $\mathcal{H}_H$. However, for cases such as we are considering here it serves as an approximate ground state upon which theoretical descriptions of spin waves may be based (e.g. see Wagner 1972, Mattis 1988, Keffer 1966). The deviations from the Néel state at T = 0 can be estimated in a manner similar to our calculation of ΔS_n in Chapter 4.

Spin waves in bulk antiferromagnets are discussed in standard solid state texts (e.g. see Kittel 1987) and magnetism texts (see e.g. Mattis 1988, Wagner 1972). Detailed reviews are found in Keffer (1966) and Philips and Rosenberg (1966). The bulk antiferromagnetic dispersion relation differs from that of bulk ferromagnets in the following ways. In the case of uniaxial antiferromagnets there are generally two branches, one of positive frequency and one or negative frequency. The branches are non-degenerate in magnitude in an applied field and, in semi-classical terms, involve precession in opposite directions. In contrast, a full physical description of the spin-wave frequencies in uniaxial bulk ferromagnets is contained in a single branch. In addition, in the isotropic limit the long-wavelength antiferromagnetic spin waves vary approximately with $|\mathbf{k}|$ instead of $|\mathbf{k}|^2$ as in the ferromagnetic case. Also, the antiferromagnetic spectrum features a gap at $\mathbf{k} = 0$ determined by both exchange and anisotropy factors (and the applied field) while in ferromagnets the gap is independent of exchange. In semi-classical terms (e.g. see Keffer *et al* 1953), a spin wave involves different precessional amplitudes on each sublattice, as shown

in figure 5.2. The positive-frequency (in our notation) spin waves have greater precessional amplitude on the spin-up sublattice while the negative-frequency modes have greater precessional amplitude on the spin-down sublattice. In the absence of an applied field the two modes are symmetric.

An applied field, if included, serves to raise the energy of the positive-frequency modes and lower that of the negative-frequency modes. This introduces the possibility of the energy of the lowest-lying negative-frequency spin-wave being reduced to zero, an occurrence which indicates an instability and marks the onset of the spin-flop transition mentioned above.

In a semi-infinite or finite-thickness antiferromagnet there can be both localized (surface) and non-localized (bulk) spin waves. In a thin film the bulk modes are again quantized. The theory of surface spin waves in antiferromagnets is reviewed in detail in Wolfram and DeWames (1972) and Cottam and Lockwood (1986). As in the ferromagnetic case the number and nature of the localized modes may depend on surface characteristics such as the ratio of surface and bulk exchange constants. In addition, in antiferromagnets the relationship of the surface to the sublattice structure is of importance. For example, in the absence of an applied field, bulk bct systems have two equivalent sublattices. A (001) surface, however, (see figure 5.3) contains spins of only one sublattice and removes the equivalence. As a result there may be two surface modes (one each of positive- and negative-frequency) which are *non-degenerate.*

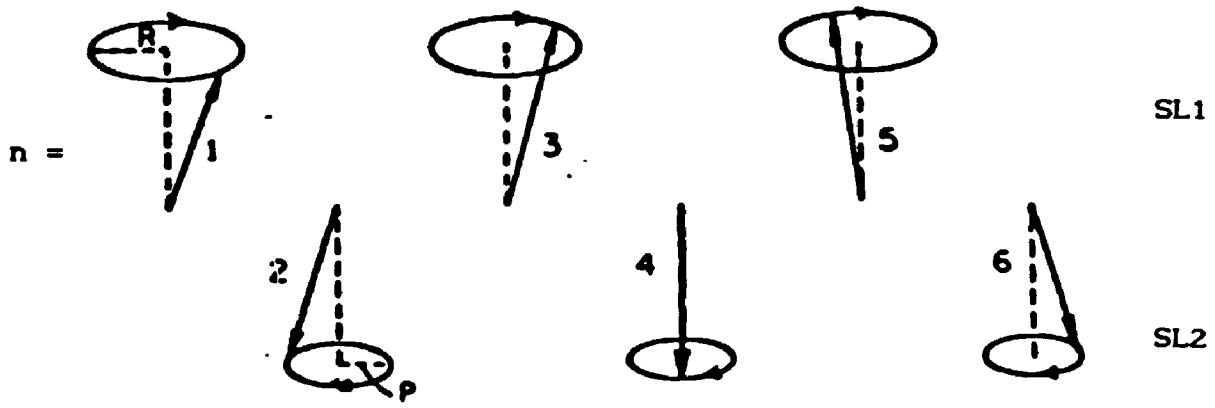

Figure 5.2 Semi-classical depiction of antiferromagnetic spin waves showing the different precession circles on the two sublattices (after Keffer *et al* 1953).

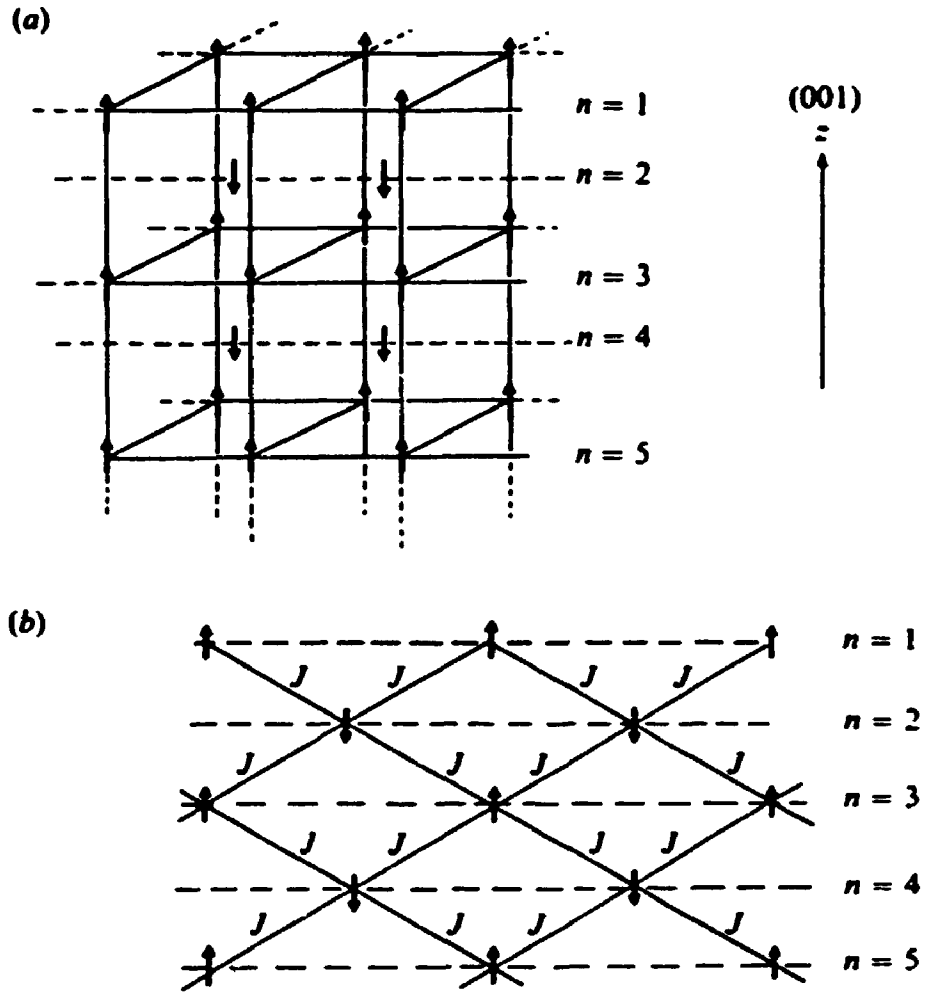

Figure 5.3 Antiferromagnetic ordering in a semi-infinite body-centred tetragonal (bct) (001) system showing the spin-up and spin-down sublattices. In (a) a persepctive view, in (b) a side view showing nearest-neighbour exchange constants.

In contrast, for an sc antiferromagnet the (001) surface contains spins of both sublattices so that the equivalence is not removed and the surface modes are degenerate. .

5.1.3 Model of an Anisotropic Antiferromagnet

We have chosen to study in detail the above-mentioned bct lattice with a (001) surface. As well as being non-degenerate, the surface modes may be well separated from the bulk region in the small $\mathbf{k}_{\parallel}$ regime in contrast to the sc (001) case (see e.g. Wolfram and DeWames 1972). In addition, in each layer in the bct (001) system all spins belong to the same sublattice and have nearest neighbours located on the adjacent layer (and other sublattice). This will simplify the theoretical formalism.

As in the case of ferromagnetic systems, the particular model we have studied involves some simplifications in the choice of exchange and anisotropy parameters. For the semi-infinite systems (with the surface layer labelled n = 1) we take

$$J_{ij} = \begin{cases} J_S & \text{if i OR j is in layer 1} \\ J & \text{otherwise} \end{cases}$$

$$D_i = \begin{cases} D_S & \text{if i is in layer 1} \\ D & \text{otherwise} \end{cases}$$

$$F_i = \begin{cases} F_S & \text{if i is in layer 1} \\ F & \text{otherwise.} \end{cases} \qquad (5.1.2)$$

As for the ferromagnets the principal special cases will be that in which $F_S = F$ (case A) and that in which $F_S \neq 0$ but $F = 0$ (case B). The

antiferromagnetic films which are the subject of Chapter 6 are also bct (001) with similar assumptions made concerning the exchange and anisotropy parameters.

5.2 The Holstein-Primakoff Transformation

The Holstein-Primakoff transformation from spin operators to boson creation and annihilation operators is carried out in the case of antiferromagnets in a similar manner as for ferromagnets (see Section 2.1) except that here we must accommodate different spin orientations on the two sublattices. We refer to the spin-up and spin-down sublattices as SL1 and SL2 respectively. For SL1 we introduce the boson operators b and $b^\dagger$ as before and the transformation is given by (2.1.2). For spins on SL2 we introduce another set of boson operators, a and a , and the transformation is

$$S_j^+ = (2S)^{1/2} a_j^\dagger \left(1 - a_j^\dagger a_j/(2S)\right)^{1/2}$$

$$S_j^- = (2S)^{1/2} \left(1 - a_j^\dagger a_j/(2S)\right)^{1/2} a_j$$

$$S_j^Z = -S + a_j^\dagger a_j . \qquad (5.2.1)$$

This transformation for SL2 spins is defined so that (in contrast to the SL1 situation) the creation operator leads to deviations from the $S^Z = -S$ state. We again make the near-saturation approximation which holds for $T \ll T_N$ and the two parts of the Hamiltonian are transformed to

$$\mathcal{H}_H \cong S \sum_{ij} J_{ij} [b_i a_j + b_i^\dagger a_j^\dagger + b_i^\dagger b_i + a_j^\dagger a_j] + g\mu_B H_0 \sum_i b_i^\dagger b_i - g\mu_B H_0 \sum_j a_j^\dagger a_j$$

$$\mathcal{H}_A \cong 2S\eta \sum_i D_i b_i^\dagger b_i + 2S\eta \sum_j D_j a_j^\dagger a_j - \sum_i F_i S\eta' [b_i^\dagger b_i^\dagger + b_i b_i] - \sum_j F_j S\eta' [a_j^\dagger a_j^\dagger + a_j a_j] \qquad (5.2.2)$$

where the constants η and η' are introduced in Section 2.1 and again all constant and higher order terms are neglected. We note that (5.2.2) contains terms like $b_i a_j$ and $b_i^\dagger a_j^\dagger$ which couple sites on different sublattices through the exchange interaction.

5.3 Coupled Green Functions for Semi-infinite Antiferromagnets

As in the ferromagnetic case we anticipate some applications for Green functions involving spins located in the same layer. We find, therefore, that here we need a different set of Green functions for each sublattice. We consider first spins on SL1 where the Green function of primary interest is $\langle\langle b_i(t); b_k^\dagger(t')\rangle\rangle \equiv G_{ik}^{(1)}(t,t')$ (the superscript denotes SL1). We use (1.5.6) and the Hamiltonian as written in (5.2.2) to find the equation of motion for $G_{ik}^{(1)}$. As in the earlier ferromagnetic case, additional Green functions are introduced to form a closed set. In this case they are $\langle\langle b_i^\dagger(t); b_k^\dagger(t')\rangle\rangle \equiv G'^{(1)}_{ik}(t,t')$, $\langle\langle a_j^\dagger(t); b_k^\dagger(t')\rangle\rangle \equiv \mathcal{G}^{(1)}_{jk}(t,t')$ and $\langle\langle a_j(t); b_k^\dagger(t')\rangle\rangle \equiv \mathcal{G}'^{(1)}_{jk}(t,t')$. Following the same prccedures as in Section 4.1 we find

$$[\omega - Sv_n(0) - Sv_{n-1}(0) - g\mu_B H_0 - 2D_n S\eta] G^{(1)}_{nn'} = \frac{1}{2\pi}\delta_{nn'} + Sv_{n-1}(\mathbf{k}_\parallel)\mathcal{G}^{(1)}_{n-1n'} + Sv_n(\mathbf{k}_\parallel)\mathcal{G}^{(1)}_{n+1n'} - 2S\eta' F_n G'^{(1)}_{nn'} \qquad n = 1,3,5.. \qquad (5.3.1)$$

$$[\omega + Sv_n(0) + Sv_{n-1}(0) + g\mu_B H_0 + 2D_n S\eta] G'^{(1)}_{nn'} = - Sv_{n-1}(\mathbf{k}_\parallel)\mathcal{G}'^{(1)}_{n-1n'} - Sv_n(\mathbf{k}_\parallel)\mathcal{G}'^{(1)}_{n+1n'} + 2S\eta' F_n G^{(1)}_{nn'} \qquad n = 1,3,5.. \qquad (5.3.2)$$

$$[\omega + Sv_m(0) + Sv_{m-1}(0) - g\mu_B H_0 + 2D_m S\eta]\mathcal{G}^{(1)}_{mn'} = - Sv_{m-1}(k_\parallel)G^{(1)}_{m-1n'} - Sv_m(k_\parallel)G^{(1)}_{m+1n'} + 2S\eta' F_m \mathcal{G}'^{(1)}_{mn'} \qquad m = 2,4,6.. \qquad (5.3.3)$$

$$[\omega - Sv_m(0) - Sv_{m-1}(0) + g\mu_B H_0 - 2D_m S\eta]\mathcal{G}'^{(1)}_{mn'} = Sv_{m-1}(k_\parallel)G'^{(1)}_{m-1n'} + Sv_m(k_\parallel)G'^{(1)}_{m+1n'} - 2S\eta' F_m \mathcal{G}^{(1)}_{mn'} \qquad m = 2,4,6.. \qquad (5.3.4)$$

Here $G^{(1)}_{ik}(\omega)$ is related to $G^{(1)}_{ik}(t,t')$ by a frequency Fourier transform as in (1.5.9). $G^{(1)}_{ik}(\omega)$ is in turn related by a wavevector Fourier transform as in (4.1.8) to $G^{(1)}_{nn'}(k_\parallel,\omega)$ (which we have abbreviated as $G^{(1)}_{nn'}$). Similar transforms have been defined for the other three coupled Green functions. The summations $v_n(k_\parallel)$ are defined as in Chapter 2 (see (2.2.8)). Here we have

$$v_n(k_\parallel) = \begin{cases} J_s\gamma(k_\parallel) & \text{if } n = 1 \\ J\gamma(k_\parallel) & \text{otherwise} \end{cases} \qquad (5.3.5)$$

with, for a bct lattice,

$$\gamma(k_\parallel) = 4\cos\left(\tfrac{1}{2}k_x a_0\right)\cos\left(\tfrac{1}{2}k_y a_0\right). \qquad (5.3.6)$$

We note that there is no summation corresponding to $u_n(k_\parallel)$ in (2.2.8) as here the spins have no nearest neighbours in the same layer.

For SL2 the coupled equations analogous to (5.3.1) through (5.3.4) are

$$[\omega + Sv_n(0) + Sv_{n-1}(0) - g\mu_B H_0 + 2D_n S\eta]G^{(2)}_{nn'} = \frac{1}{2\pi}\delta_{nn'} - Sv_{n-1}(k_\parallel)\mathcal{G}^{(2)}_{n-1n'} - Sv_n(k_\parallel)\mathcal{G}^{(2)}_{n+1n'} + 2S\eta' F_n G'^{(2)}_{nn'} \qquad (5.3.7)$$

$$[\omega - Sv_n(0) - Sv_{n-1}(0) + g\mu_B H_0 - 2D_n S\eta]G'^{(2)}_{nn'} = Sv_{n-1}(k_\parallel)\mathcal{G}'^{(2)}_{n-1n'} + Sv_n(k_\parallel)\mathcal{G}'^{(2)}_{n+1n'} - 2S\eta' F_n G^{(2)}_{nn'} \qquad (5.3.8)$$

$$[\omega - Sv_n(0) - Sv_{n-1}(0) - g\mu_B H_0 - 2D_n S\eta]\mathcal{G}'^{(2)}_{nn'} = Sv_{n-1}(k_\parallel)G^{(2)}_{n-1n'} + Sv_n(k_\parallel)G^{(2)}_{n+1n'} - 2S\eta' F_n \mathcal{G}'^{(2)}_{1n'} \quad (5.3.9)$$

$$[\omega + Sv_n(0) + Sv_{n-1}(0) + g\mu_B H_0 + 2D_n S\eta]\mathcal{G}'^{(2)}_{nn'} = - Sv_{n-1}(k_\parallel)G'^{(2)}_{n-1n'} - Sv_n(k_\parallel)G'^{(2)}_{n+1n'} + 2S\eta' F_n \mathcal{G}^{(2)}_{1n'} \quad (5.3.10)$$

where we now employ superscript (2) and define $\langle\langle a_i^\dagger(t); a_j(t')\rangle\rangle \equiv G^{(2)}_{ij}(t,t')$, $\langle\langle a_i(t); a_j(t')\rangle\rangle \equiv G'^{(2)}_{ij}(t,t')$, $\langle\langle b_i(t); a_j(t')\rangle\rangle \equiv \mathcal{G}^{(2)}_{ij}(t,t')$, and $\langle\langle b_i^\dagger(t); a_j(t')\rangle\rangle \equiv \mathcal{G}'^{(2)}_{ij}(t,t')$.

We note that here, due to the sublattice structure, we have two systems of four coupled equations each while in Chapter 4 for the ferromagnets we had a single system of two coupled equations. In that case we wrote the equations in matrix form immediately. Here we take a slightly different approach. We first make assumptions concerning the values of the nonuniaxial constants. As mentioned above, we consider examples of the special cases A and B corresponding to the anisotropy being nonuniaxial throughout the system and only on the surface respectively. For each of these models the sets of coupled equations are simplified somewhat and we proceed to eliminate the Green functions $\mathcal{G}$ and $\mathcal{G}'$ from the equations for G and G'. We write the resulting equations for G and G' in matrix form and solve in a manner analogous to that used in Chapter 4. Section 5.4 deals with case A while case B is presented in Section 5.5. In addition, for convenience, we shall consider that the applied field $H_0 = 0$ in the following calculations.

5.4 Case A: The Anisotropy is Nonuniaxial Throughout The System

For simplicity we now take F_i, D_i and J_{ij} to have the bulk values (F, D and J) everywhere including the vicinity of the surface. Considering SL1 we use (5.3.1) through (5.3.4) and eliminate $\mathcal{G}^{(1)}$ and $\mathcal{G}'^{(1)}$ from the equations for $G^{(1)}$ and $G'^{(1)}$ to find

$$(\underline{A}_0 + \delta_A^{(1)}\underline{\nu})\mathbf{G}^{(1)} = \sigma\underline{I} + \delta_B^{(1)}(\underline{B}_0 + \underline{\nu})\mathbf{G}'^{(1)}$$
$$(\underline{A}_0 + \delta_C^{(1)}\underline{\nu})\mathbf{G}'^{(1)} = \delta_D^{(1)}(\underline{B}_0 + \underline{\nu})\mathbf{G}^{(1)} \qquad (5.4.1)$$

where $\mathbf{G}^{(1)}$ and $\mathbf{G}'^{(1)}$ are $\infty\times\infty$ matrices whose elements are the Green functions $G^{(1)}_{nn'}$ and $G'^{(1)}_{nn'}$ respectively. Also we have

$$\underline{A}_0 = \begin{bmatrix} a & -1 & 0 & 0\ldots \\ -1 & a & -1 & 0\ldots \\ 0 & -1 & a & -1\ldots \\ \vdots & \vdots & \vdots & \vdots \end{bmatrix} \qquad (5.4.2)$$

$$\underline{\nu} = \begin{bmatrix} 1 & 0 & 0 & 0\ldots \\ 0 & 0 & 0 & 0\ldots \\ 0 & 0 & 0 & 0\ldots \\ \vdots & \vdots & \vdots & \vdots \end{bmatrix} \qquad (5.4.3)$$

with $\underline{B}_0$ having the same tridiagonal form as $\underline{A}_0$ but with diagonal elements b. The parameters are

$$a = -\frac{[(\Omega + d + 8)(\Omega - d - 8) + f^2]}{\gamma^2(k_{\parallel})} - 2$$

$$b = \frac{[(\Omega + d + 8)(\Omega - d - 8) + f^2]}{\gamma^2(k_{\parallel})} - 2 \qquad (5.4.4)$$

$$\delta_A^{(1)} = \frac{-4[(\Omega + d + 8)(\Omega - d - 8) + f^2]}{\gamma^2(k_{\parallel})(\Omega - d - 8)} + 1$$

$$\delta_C^{(1)} = \frac{4[(\Omega + d + 8)(\Omega - d - 8) + f^2]}{\gamma^2(k_{\parallel})(\Omega + d + 8)} + 1$$

$$\delta_B^{(1)} = \frac{f}{(\Omega - d - 8)}$$

$$\delta_D^{(1)} = \frac{-f}{(\Omega + d + 8)}$$

$$\sigma = \frac{-[(\Omega + d + 8)(\Omega - d - 8) + f^2]}{\gamma^2(k_{\|})(2\pi SJ)(\Omega - d - 8)} \qquad (5.4.5)$$

with f and Ω defined as in (2.2.15) and $d \equiv 2D\eta/J$.

Rearranging (5.4.1) we find

$$\underline{G}^{(1)} = \sigma[\underline{I} - \delta_B^{(1)}\delta_D^{(1)}\underline{P}^{(1)-1}\underline{QBR}^{(1)-1}\underline{QB}]^{-1}\underline{P}^{(1)-1}\underline{Q}$$

$$\underline{G'}^{(1)} = \sigma\,\delta_D^{(1)}[\underline{I} - \delta_B^{(1)}\delta_D^{(1)}\underline{R}^{(1)-1}\underline{QBP}^{(1)-1}\underline{QB}]^{-1}\underline{R}^{(1)-1}\underline{QBP}^{(1)-1}\underline{Q} \qquad (5.4.6)$$

or

$$\underline{G}^{(1)} = \frac{\sigma\ \mathrm{adj}[\underline{I} - \delta_B^{(1)}\delta_D^{(1)}\underline{P}^{(1)-1}\underline{QBR}^{(1)-1}\underline{QB}]\ \mathrm{adj}\underline{P}^{(1)}\ \underline{Q}}{\det[\underline{I} - \delta_B^{(1)}\delta_D^{(1)}\underline{P}^{(1)-1}\underline{QBR}^{(1)-1}\underline{QB}]\ \det\underline{P}^{(1)}}$$

$$\underline{G'}^{(1)} = \frac{\sigma\ \delta_D^{(1)}\mathrm{adj}[\underline{I} - \delta_B^{(1)}\delta_D^{(1)}\underline{R}^{(1)-1}\underline{QBP}^{-1}\underline{QB}]\ \mathrm{adj}\underline{R}^{(1)}\ \underline{Q}\ \underline{B}\ \mathrm{adj}\underline{P}^{(1)}\ \underline{Q}}{\det[\underline{I} - \delta_B^{(1)}\delta_D^{(1)}\underline{R}^{(1)-1}\underline{QBP}^{(1)-1}\underline{QB}]\ \det\underline{R}^{(1)}\ \det\underline{P}^{(1)}} \qquad (5.4.7)$$

where $\underline{B} = (\underline{B}_0 + \underline{\nu})$. Other matrices are

$$\underline{P}^{(1)} = (\underline{I} + \delta_A^{(1)}\underline{Q\nu})$$

$$\underline{R}^{(1)} = (\underline{I} + \delta_C^{(1)}\underline{Q\nu})$$

$$\underline{Q} = \underline{A}_0^{-1}. \qquad (5.4.8)$$

The elements of $\underline{Q}$ are given by (Wax 1954, DeWames and Wolfram 1969)

$$\underline{Q}_{pq} = \frac{x^{p+q} - x^{|p-|}}{x - x^{-1}} \qquad (5.4.9)$$

which is the large N limit of the expression used to invert tridiagonal matrices in Chapter 2. Here x is a complex variable satisfying $|x| \leq 1$ and

$$x + x^{-1} = a. \qquad (5.4.10)$$

$\underline{P}^{(1)}$ can be written in partitioned form as

$$\underline{P}^{(1)} = \begin{bmatrix} P_1^{(1)} & \vdots & \underline{0} \\ \cdots & \cdots & \cdots \\ \underline{P}_2^{(1)} & \vdots & \underline{I} \end{bmatrix} \qquad (5.4.11)$$

It follows that

$$\underline{P}^{(1)-1} = \begin{bmatrix} X_1^{(1)} & \vdots & \underline{0} \\ \cdots & \cdots & \cdots \\ \underline{X}_2^{(1)} & \vdots & \underline{I} \end{bmatrix} \qquad (5.4.12)$$

where

$$X_1^{(1)} = 1 \; / \; P_1^{(1)}$$
$$\underline{X}_2^{(1)} = -\underline{P}_2^{(1)} \; / \; P_1^{(1)}. \qquad (5.4.13)$$

Similar expressions apply in the case of $\underline{R}^{(1)}$.

The zeroes of $\det[\underline{I} - \delta_B^{(1)}\delta_D^{(1)}\underline{P}^{(1)-1}\underline{QBR}^{(1)-1}\underline{QB}]$ can in principle be used to find the spin-wave frequencies using standard numerical techniques. However, this function is very complicated and, for this reason no numerical examples of dispersion relations are given in this case. We note that in the limit that F = 0 then $\delta_B^{(1)} = 0$ and $\delta_D^{(1)} = 0$ and we find the formal uniaxial result (Cottam 1978)

$$G^{(1)} = \frac{\sigma \; \mathrm{adj}\underline{P}^{(1)} \; \underline{Q}}{1 + \delta_A^{(1)} x}.$$
$$G'^{(1)} = 0 \qquad (5.4.14)$$

This result is also discussed with reference to case B below.

5.5 Case B: The Anisotropy is Nonuniaxial on the Surface Only

Here the nonuniaxial parameter has the value F_S for spins on the surface and is zero otherwise. Other parameters are taken to be as in (5.1.2). This case proves to be considerably simpler than case A above and we

readily find numerical results. We first solve explicitly (5.3.1) through (5.3.4) for SL1 and (5.3.7) through (5.3.10) for SL2. In Section 5.5.2 we present the dispersion relation results and in Section 5.5.3 the spectral-intensity results.

5.5.1 Green Function Results

We first calculate the correlation functions associated with SL1 using (5.3.1) through (5.3.4) with the above-mentioned modification in nonuniaxial parameters. We again eliminate $\mathcal{G}^{(1)}_{nn'}$ and $\mathcal{G}'^{(1)}_{nn'}$ from the equations for $G^{(1)}_{nn'}$ and $G'^{(1)}_{nn'}$. Writing the result in matrix form we have

$$\begin{aligned}(\underline{A}_0 + \delta_A^{(1)}\underline{\nu})\mathbf{G}^{(1)} &= \sigma\underline{I} + \delta_B^{(1)}\underline{\nu}\,\mathbf{G}'^{(1)} \\ (\underline{A}_0 + \delta_C^{(1)}\underline{\nu})\mathbf{G}'^{(1)} &= \delta_D^{(1)}\underline{\nu}\,\mathbf{G}^{(1)}\end{aligned} \tag{5.5.1}$$

where the matrices $\underline{A}_0$ and $\underline{\nu}$ are defined as in (5.4.2) and (5.4.3). The parameters are redefined as

$$\begin{aligned}a &= -[(\Omega - d - 8)(\Omega + d + 8) + 2\gamma^2(\mathbf{k}_\parallel)]/[\gamma^2(\mathbf{k}_\parallel)] \\ \delta_A^{(1)} &= 2 - J_s/J + (\Omega - d - 8)(\Omega + d + 8)/[\gamma^2(\mathbf{k}_\parallel)] \\ &\quad - (\Omega - 4J_s/J - d_s)(\Omega + 4J_s/J + 4 + d_s)/[\gamma^2(\mathbf{k}_\parallel)J_s/J] \\ \delta_C^{(1)} &= 2 - J_s/J + (\Omega + d + 8)(\Omega - d - 8)/[\gamma^2(\mathbf{k}_\parallel)] \\ &\quad - (\Omega + 4J_s/J + d_s)(\Omega - 4J_s/J - 4 - d_s)/[\gamma^2(\mathbf{k}_\parallel)J_s/J] \\ \delta_B^{(1)} &= f_s(\Omega + d + 8)/[\gamma^2(\mathbf{k}_\parallel)] \\ \delta_D^{(1)} &= -f_s(\Omega - d - 8)/[\gamma^2(\mathbf{k}_\parallel)] \\ \sigma &= -(\Omega + d + 8)/[2\pi SJ\gamma^2(\mathbf{k}_\parallel)]\end{aligned} \tag{5.5.2}$$

where f_s is defined in (2.2.15) and $d_s \equiv 2D_s\eta/J$. We note, in particular that the parameters $\delta_A^{(1)}$ and $\delta_C^{(1)}$ are analogous to the Δ's used in earlier chapters as they reflect the perturbation at the surface of the coordination number and the exchange and uniaxial parameters.

Rearranging (5.5.1) we find

$$G^{(1)} = \sigma[\underline{I} - \delta_B^{(1)}\delta_D^{(1)}\underline{P}^{(1)-1}\underline{Q\nu R}^{(1)-1}\underline{Q\nu}]^{-1}\underline{P}^{(1)-1}\underline{Q}$$

$$G'^{(1)} = \sigma\,\delta_D^{(1)}[\underline{I} - \delta_B^{(1)}\delta_D^{(1)}\underline{R}^{(1)-1}\underline{Q\nu P}^{(1)-1}\underline{Q\nu}]^{-1}\underline{R}^{(1)-1}\underline{Q\nu P}^{(1)-1}\underline{Q} \qquad (5.5.3)$$

where all matrix definitions in Section 5.4 apply. We rewrite (5.5.3) as

$$G^{(1)} = \frac{\sigma\ \mathrm{adj}[\underline{I} - \delta_B^{(1)}\delta_D^{(1)}\underline{P}^{(1)-1}\underline{Q\nu R}^{(1)-1}\underline{Q\nu}]\ \mathrm{adj}\underline{P}^{(1)}\ \underline{Q}}{\det[I - \delta_B^{(1)}\delta_D^{(1)}\underline{P}^{(1)-1}\underline{Q\nu R}^{(1)-1}\underline{Q\nu}]\ \det\ \underline{P}^{(1)}}$$

$$G'^{(1)} = \frac{\sigma\ \delta_D^{(1)}\mathrm{adj}[\underline{I} - \delta_B^{(1)}\delta_D^{(1)}\underline{R}^{(1)-1}\underline{Q\nu P}^{(1)-1}\underline{Q\nu}]\ \mathrm{adj}\underline{R}^{(1)}\ \underline{Q}\ \underline{\nu}\ \mathrm{adj}\underline{P}^{(1)}\ \underline{Q}}{\det[\underline{I} - \delta_B^{(1)}\delta_D^{(1)}\underline{R}^{(1)-1}\underline{Q\nu P}^{(1)-1}\underline{Q\nu}]\ \det\underline{R}^{(1)}\ \det\underline{P}^{(1)}}. \qquad (5.5.4)$$

We use (5.4.8) through (5.4.13) to write $G^{(1)}$ as

$$G^{(1)} = \frac{\sigma\ \mathrm{adj}[\underline{I} - \delta_B^{(1)}\delta_D^{(1)}\underline{P}^{(1)-1}\underline{Q\nu R}^{(1)-1}\underline{Q\nu}]\ \mathrm{adj}\underline{P}^{(1)}\underline{Q}\ (1 + \delta_C^{(1)}x)}{(1 + \delta_A^{(1)}x)(1 + \delta_C^{(1)}x) - \delta_B^{(1)}\delta_D^{(1)}x^2}. \qquad (5.5.5)$$

The zeroes of

$$y^{(1)}(x,\Omega) \equiv (1 + \delta_A^{(1)}x)(1 + \delta_C^{(1)}x) - \delta_B^{(1)}\delta_D^{(1)}x^2 \qquad (5.5.6)$$

are therefore all we need consider to obtain the spin-wave frequencies.

The Green functions referring to SL2 can similarly be found from equations (5.3.7) through (5.3.10). The analogous result to (5.5.5) is

$$G^{(2)} = \frac{\mu\ \mathrm{adj}[\underline{I} - \delta_B^{(2)}\delta_D^{(2)}\underline{P}^{(2)-1}\underline{Q\nu R}^{(2)-1}\underline{Q\nu}]\ \mathrm{adj}\underline{P}^{(2)}\underline{Q}\ (1 + \delta_C^{(2)}x)}{(1 + \delta_A^{(2)}x)(1 + \delta_C^{(2)}x) - \delta_B^{(2)}\delta_D^{(2)}x^2} \qquad (5.5.7)$$

in which all matrices have the same form as those defined above but with

the following parameters:

$$\delta_A^{(2)} = 1 - \frac{J_s^2}{J^2}\left[\frac{(\Omega + d_s + 4J_s/J)(\Omega - d - 8)}{[\Omega + d_s + 4J_s/J)(\Omega - d_s - 4J_s/J) + f_s^2]}\right] + \left[1 - \frac{J_s}{J}\right]\frac{4(\Omega - d - 8)}{\gamma^2(k_\parallel)}$$

$$\delta_C^{(2)} = 1 - \frac{J_s^2}{J^2}\left[\frac{(\Omega - d_s - 4J_s/J)(\Omega + d + 8)}{[\Omega + d_s + 4J_s/J)(\Omega - d_s - 4J_s/J) + f_s^2]}\right] - \left[1 - \frac{J_s}{J}\right]\frac{4(\Omega + d + 8)}{\gamma^2(k_\parallel)}$$

$$\delta_B^{(2)} = f_s\frac{J_s^2}{J^2}\left[\frac{(\Omega - d - 8)}{[\Omega + d_s + 4J_s/J)(\Omega - d_s - 4J_s/J) + f_s^2]}\right]$$

$$\delta_D^{(2)} = -f_s\frac{J_s^2}{J^2}\left[\frac{(\Omega + d + 8)}{[\Omega + d_s + 4J_s/J)(\Omega - d_s - 4J_s/J) + f_s^2]}\right]$$

$$\mu = (\Omega - d - 8)/[2\pi SJ\gamma^2(k_\parallel)]. \qquad (5.5.8)$$

We define $y^{(2)}(x,\Omega) \equiv (1 + \delta_A^{(2)}x)(1 + \delta_C^{(2)}x) - \delta_B^{(2)}\delta_D^{(2)}x^2$.

At this point it is useful to consider the uniaxial limit. We see that if $F_s = 0$ then $\delta_B^{(1)} = 0$ and $\delta_D^{(1)} = 0$ and we find the expected uniaxial Green function result (Cottam 1978) given in (5.4.14). Poles will occur at $x = -1/\delta_A^{(1)}$ (the condition $x = -1/\delta_A^{(2)}$ leads to the same set of frequencies). In cases where $D_s \neq D$ and/or $J_s \neq J$ two non-degenerate surface modes may be found. For the simple case where $J_s = J$ and $D_s = D$ we find an analytic expression for the spin-wave frequencies yielding a *single* surface branch which (in our notation) is positive in frequency.

In the present case F_s is non-zero, however, and if $D_s = D$ and $J_s = J$ and we find that the surface spin waves are represented by poles at both positive and negative frequencies. Each pole gives rise to a δ-function component in the spectral intensity, however the contributions of each are unequal as can be seen by considering (5.5.5) for the SL1 Green function matrix $\mathbf{G}^{(1)}$. If F_s is small but non-zero then the root of $y^{(1)}$ associated with $+\Omega^S$ is very near the root of $(1 + \delta_A^{(1)}x)$ while that associated with $-\Omega^S$ is near the root of $(1 + \delta_C^{(1)}x)$. The latter will have a vanishingly small spectral function due to the presence of this same factor in the Green-function numerator in (5.5.5). This is illustrated numerically with mean-squared amplitude results below.

5.5.2 Numerical Dispersion Relation Results

Although the denominators of $\mathbf{G}^{(1)}$ and $\mathbf{G}^{(2)}$ are different analytic functions it can be shown numerically that $y^{(1)}$ and $y^{(2)}$ have the same roots (for Ω) as illustrated by figure 5.4. For simpler cases, such as the uniaxial limit, this can easily be demonstrated analytically. We can therefore use either of these functions to determine the dispersion relations. This equivalence is expected because spin waves are excitations of the whole system and not just of one sublattice.

The procedure for numerically evaluating the dispersion relations using the function $y^{(1)}(x)$ differs slightly from that used in Chapter 3. Here the parameters $\delta_A^{(1)}$, $\delta_C^{(1)}$, etc., all depend on Ω (as does x through a) whereas in Chapter 3 all comparable parameters such as Δ etc. were independent of Ω. The variables x, $\delta_A^{(1)}$, etc., are all evaluated for a

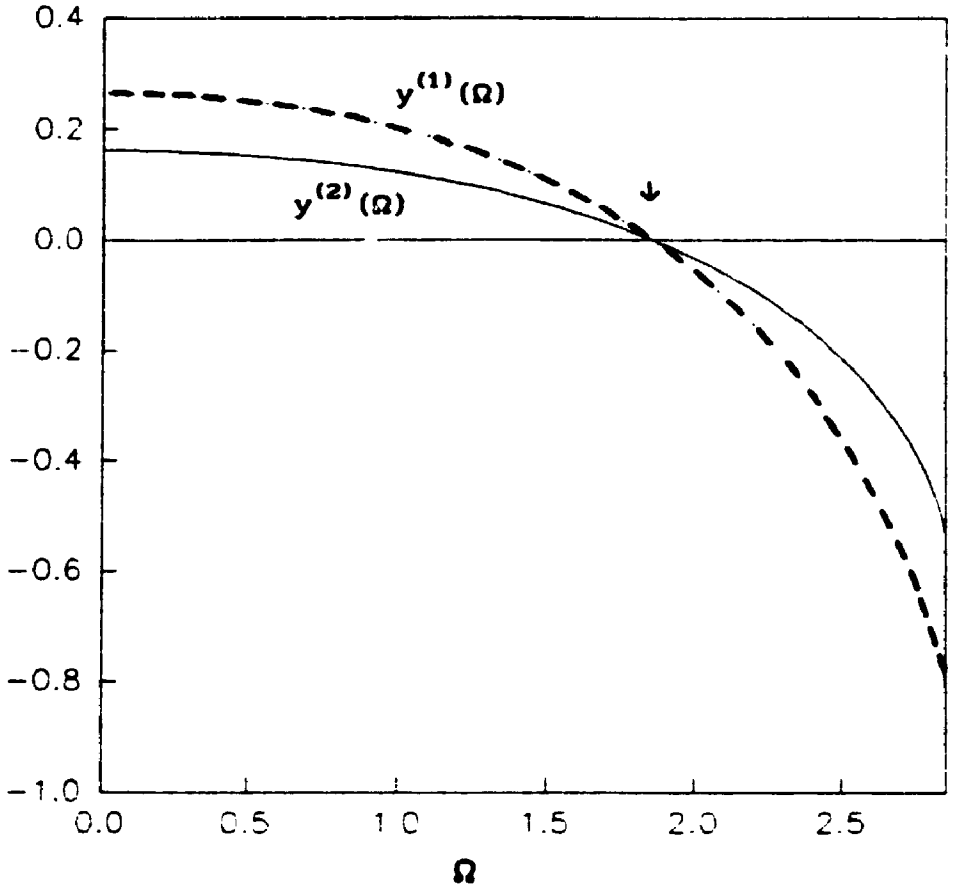

Figure 5.4 Examples of functions $y^{(1)}(\Omega)$ and $y^{(2)}(\Omega)$ plotted against Ω. Equivalent roots are indicated by arrows.

series of values of Ω on an interval in which the localization condition for surface modes is satisfied and are then used to calculate and identify the roots of $y^{(1)}(\Omega)$.

In addition to the surface modes a *continuum* of bulk modes is found. The limits of the continuum are determined by $x = \pm 1$ which implies through (5.5.2) that $a = \pm 2$. The upper and lower limits (Ω_U and Ω_L respectively) at any value of $\mathbf{k}_{\|}$ are given by

$$\Omega_U = \pm(d + 8)$$
$$\Omega_L = \pm[(d + 8)^2 - 4\gamma^2(\mathbf{k}_{\|})]^{1/2} \qquad (5.5.9)$$

and are used to determine the intervals in which a surface mode might occur e.g. an acoustic mode has $0 < \Omega_S < \Omega_L$. That the upper limit is nondispersive is a clear difference from the ferromagnetic case.

Some representative numerical dispersion relation results for the special case in which $J_S = J$ and $D_S = D$ appear in figures 5.5 and 5.6 for $F_S/J = 0.5$ and $F_S = 0$ respectively. In these figures we have chosen $S = 1$, $\mathbf{k}_{\|}$ in the [100] direction, and $D/J = 0.5$. The shaded area represents the continuum of bulk modes. As noted above, in this case for $F_S \neq 0$ we find a spin-wave frequency spectrum which is symmetric about $\Omega = 0$. As $F_S \to 0$ the frequencies of the acoustic surface modes approach the uniaxial value given by $x = -1/\delta_A$. As anticipated by the above discussion, for $F_S = 0$ the Green function will have a pole at $+\Omega^S$ only. For a surface on SL2 (i.e. the surface spins oriented along the negative z axis) the single pole would occur at $-\Omega^S$.

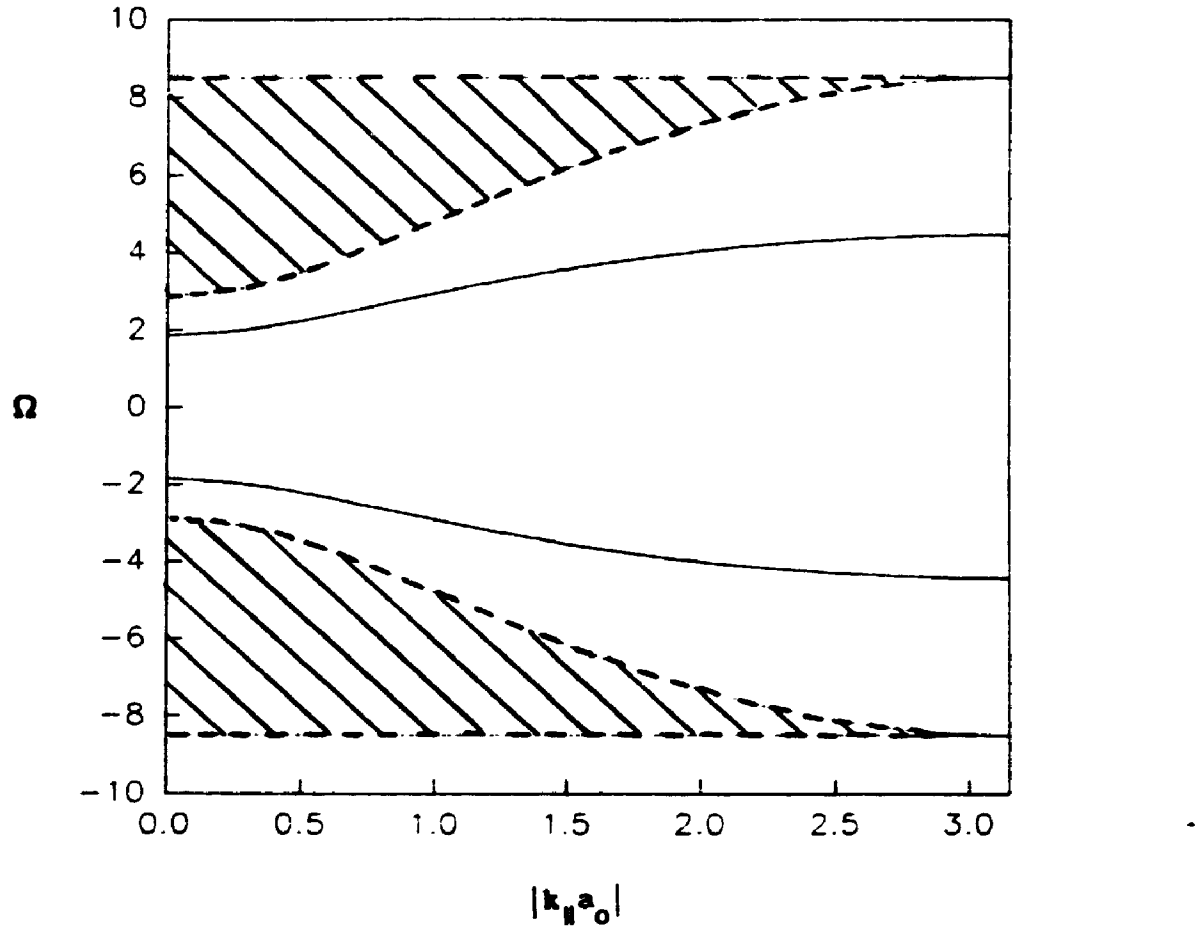

Figure 5.5 The spin-wave frequencies (in units of SJ) plotted against $|k_{\parallel}a_0|$ for a semi-infinite case B antiferromagnet. Here we have chosen $F_s/J = 0.5$ and $F/J = 0$. Shaded region represents the bulk mode continuum.

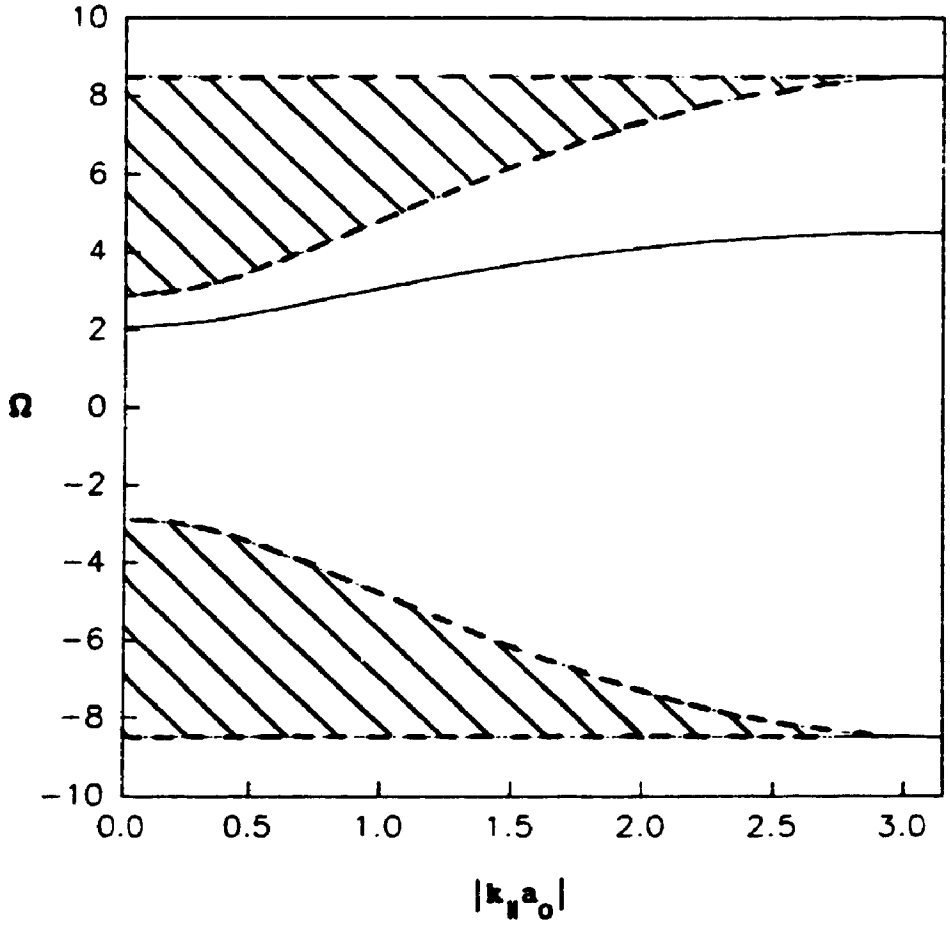

Figure 5.6 The spin-wave frequencies (in units of SJ) plotted against $|k_{\parallel}a_0|$ for a semi-infinite uniaxial antiferromagnet. Here we have chosen $F_s/J = F/J = 0$.

5.5.3 Numerical Amplitude Results

The Green functions will be used here to calculate the mean-squared amplitude of spin precession on successive layers as in Chapter 4. For SL1 (e.g. layers 1,3,5..) we use the Green functions in $\mathbf{G}^{(1)}$ while for SL2 (e.g. layers 2,4,6..) we use $\mathbf{G}^{(2)}$. As in the ferromagnetic case $\mathbf{G}'^{(1)}$ and $\mathbf{G}'^{(2)}$ can be used to find a measure of the ellipticity of precession.

Following a similar procedure as that shown in detail in Chapter 4, we can calculate the component of the mean-squared amplitude $A_n^+(\mathbf{k}_\parallel)$ (defined in (4.3.1)) due to the surface modes at any value of $\mathbf{k}_\parallel$. We eventually find

$$A_n^+(\mathbf{k}_\parallel) = -S \sum_S \frac{\sigma(\Omega^S) W_{nn}^{(1)}(\Omega^S)(1 + \delta_c^{(1)} x^S)}{y^{(1)'}(\Omega^S)} \coth\left[\frac{\alpha\Omega^S}{2}\right] \quad n = 1,3,5..$$

$$A_n^+(\mathbf{k}_\parallel) = -S \sum_S \frac{\mu(\Omega^S) W_{nn}^{(2)}(\Omega^S)(1 + \delta_c^{(2)} x^S)}{y^{(2)'}(\Omega^S)} \coth\left[\frac{\alpha\Omega^S}{2}\right] \quad n = 2,4,6.. \qquad (5.5.10)$$

where $y^{(1)'}(\Omega)$ and $y^{(2)'}(\Omega)$ are derivatives with respect to Ω and $W_{nn}^{(1)}$ and $W_{nn}^{(2)}$ are diagonal elements of the matrices in the numerators of $\mathbf{G}^{(1)}$ and $\mathbf{G}^{(2)}$ respectively. The temperature-dependent variable α is defined in Section 4.3. The summations in (5.5.10) include both positive- and negative-frequency spin-wave modes.

Some representative plots of $A_n^+(\mathbf{k}_\parallel)$ versus n are found in figures 5.7 ($F_S/J = 0.5$) and 5.8 ($F_S = 0$). These plots illustrate the decaying amplitude of the surface modes with distance into the crystal. Unlike

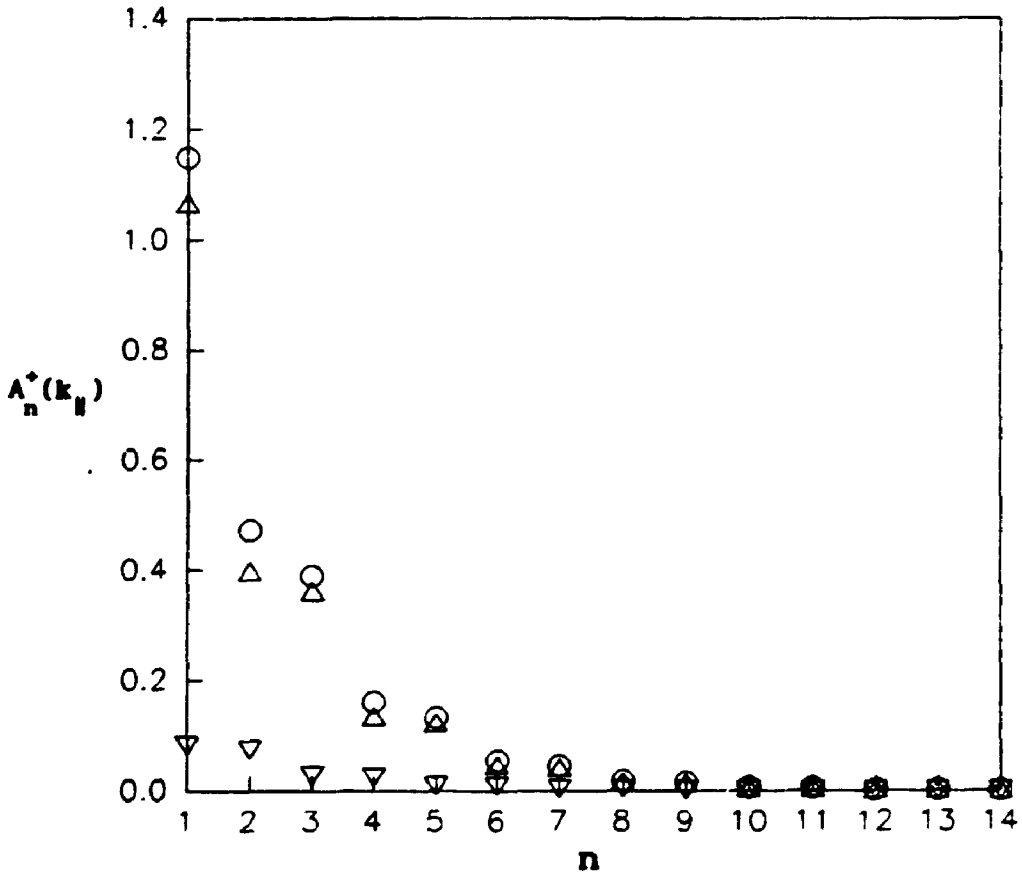

Figure 5.7 $A_n^+(k_\parallel)$ for surface modes plotted against the layer index n for a semi-infinite case B antiferromagnet. Here we have chosen F_s/J = 0.5, F/J = 0 and $|k_\parallel a_0|$ = 0. Symbols explained in accompanying text.

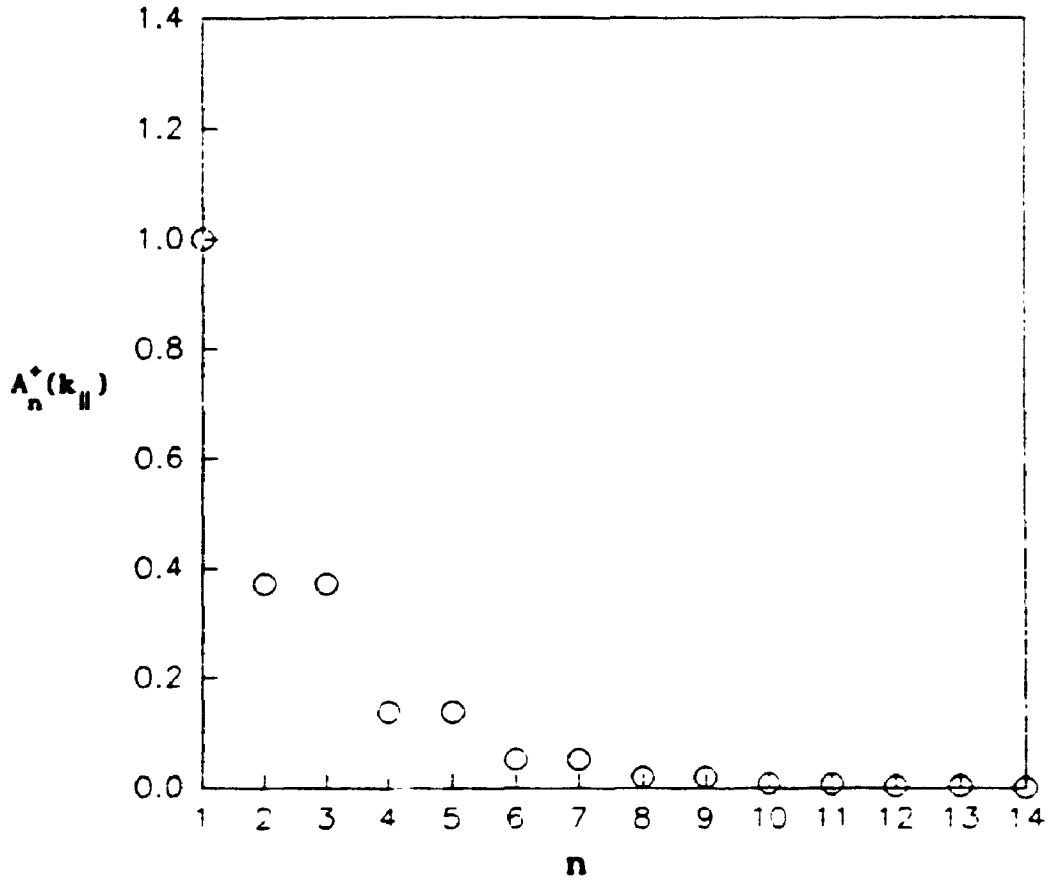

Figure 5.8 $A_n^+(k_\parallel)$ for surface modes plotted against the layer index n for a semi-infinite uniaxial antiferromagnet. Here we have chosen $F_s/J = 0$ and $|k_\parallel a_o| = 0$.

the ferromagnetic case, however, this decay is not purely exponential in antiferromagnets due to the sublattice structure. In figure 5.9 we plot the natural logarithm of the amplitudes from figure 5.8 as a function of layer number. The plots pertaining to the two sublattices each have the same slope and therefore a single decay length characterizes the mode. The positive-frequency mode has greater precessional amplitude on SL1 than on SL2. The converse is true for the negative-frequency mode. This general feature of antiferromgnetic spin waves is mentioned in Section 5.1. In addition we see that when $F_s = 0$ the contribution from the negative mode vanishes which is the expected result discussed above.

An indicator of the ellipticity of precession is the quantity $A_n^-(k_\parallel)$ defined in (4.3.2). Formally we write

$$A_n^-(k_\parallel) = -S \sum_S \frac{\sigma(\Omega^S)\delta_D^{(1)} Z_{nn}^{(1)}(\Omega^S)}{y^{(1),}(\Omega^S)} \coth\left[\frac{\alpha\Omega^S}{2}\right] \quad n = 1,3,5..$$

$$A_n^-(k_\parallel) = -S \sum_S \frac{\mu(\Omega^S)\delta_D^{(2)} Z_{nn}^{(2)}(\Omega^S)}{y^{(2),}(\Omega^S)} \coth\left[\frac{\alpha\Omega^S}{2}\right] \quad n = 2,4,6.. \qquad (5.5.11)$$

where $Z_{nn}^{(1)}$ and $Z_{nn}^{(2)}$ are the diagonal elements of the numerator matrices in $G'^{(1)}$ and $G'^{(2)}$ respectively. No numerical results are presented here although it is clear that this quantity will be non-zero in general for $f_s \neq 0$.

5.6 Discussion

In this chapter we have generalized previous calculations on spin waves in semi-infinite antiferromagnets to include the effects of nonuniaxial

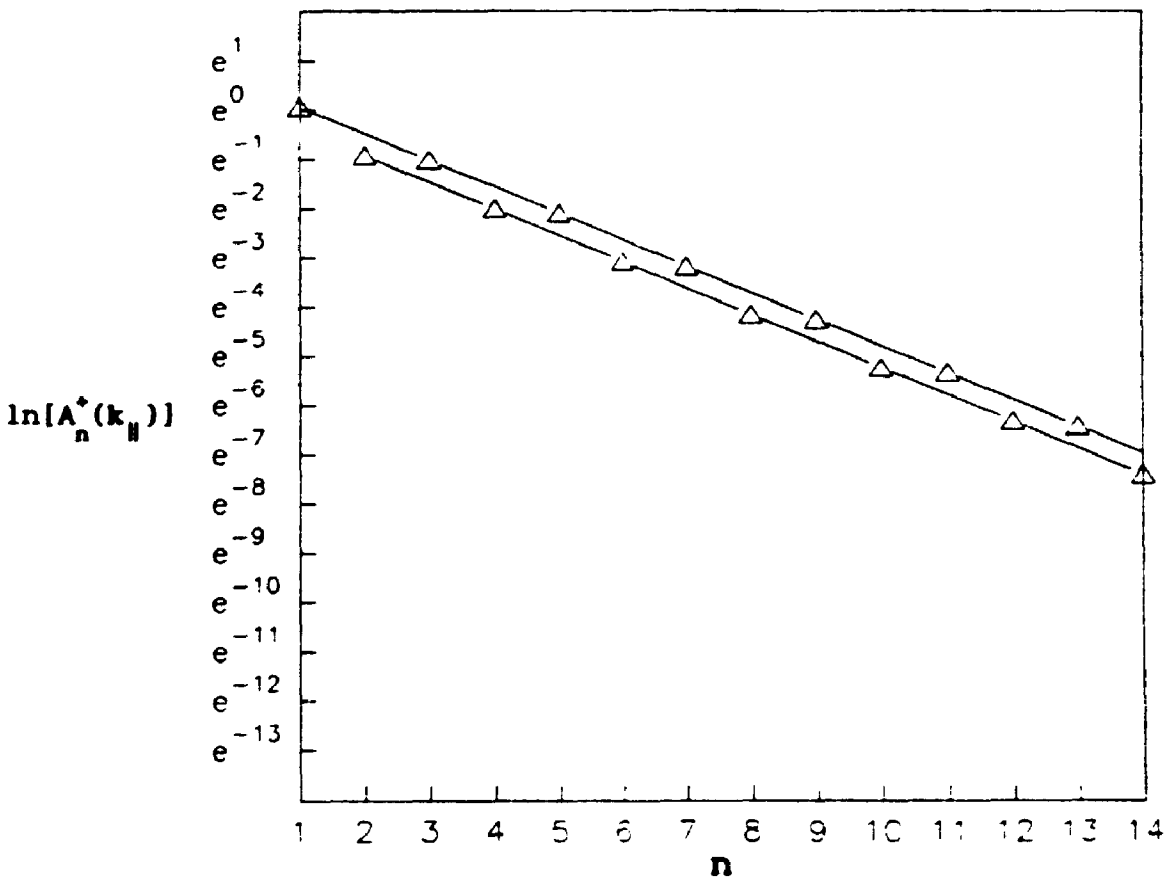

Figure 5.9 The natural logarithm of $A_n^+(k_{\parallel})$ plotted against layer index n for the surface modes in figure 5.7.

anisotropy. We have found that the spin waves are characterized by elliptical precession (in semi-classical terms). We have generated numerical results for dispersion relations and mean-squared amplitudes of precession in a special case where the anisotropy is nonuniaxial on the surface only. In the case where the applied field is zero and the exchange and uniaxial parameters are unperturbed in the vicinity of the surface we have seen that the spectrum involves a single surface mode with a frequency quantitatively different from that found in a uniaxial system. The results of this chapter will provide a basis for comparison, in the limit of large thickness, with the results of Chapter 6.

Other choices of crystal lattice and surface orientation can be accommodated but not as straightforwardly as in the ferromagnetic case. An example is the sc (001) system in which each layer will contain spins of both sublattices. As a result a different set of Green functions is required and there will be a substantially different set of coupled equations than those which apply to the bct (001) system ((5.3.1) through (5.3.4) and (5.3.7) through (5.3.10)). In contrast the change of lattice type in ferromagnets involves, in many cases, a simple substitution for the exchange summations $v_n(\mathbf{k}_\parallel)$ and $u_n(\mathbf{k}_\parallel)$.

CHAPTER 6

GREEN FUNCTION METHOD FOR ANTIFERROMAGNETIC THIN FILMS

In this chapter we describe the application of the Green function equation-of-motion method to the more general case of antiferromagnetic films with N layers. The Hamiltonian and theoretical procedure are the same as those used for the semi-infinite systems in Chapter 5. In addition to the surface modes, the frequencies of the *quantized* bulk modes will also be studied. We simplify by assuming that the applied field $H_0 = 0$ and also that the intersublattice exchange and uniaxial parameters are unperturbed in the vicinity of the surfaces i.e.

$$\begin{aligned} J_{ij} &= J \qquad \text{for all (nearest neighbour) } i,j \\ D_i &= D \qquad \text{for all } i. \end{aligned} \tag{6.0.1}$$

Furthermore, we deal only with case B in which the anisotropy is uniaxial in the bulk and nonuniaxial on the surface(s)

$$F_i = \begin{cases} F_s & \text{if } i \text{ is in layer 1} \\ F_{s'} & \text{if } i \text{ is in layer N} \\ 0 & \text{otherwise} \end{cases} \tag{6.0.2}$$

In particular we will consider separately case B.1 in which $F_s = F_{s'}$ and case B.2 in which $F_s \neq 0$, $F_{s'} = 0$. We may also classify the films according to whether N is odd or even. In the first case both surfaces are associated with the *same* sublattice while in the second each surface is associated with a *different* sublattice. The different symmetry properties of these cases have consequences for the spin-wave spectra. We note that each sublattice must have at least three layers in order for the matrix algebra to be appropriate and therefore the lower limit on N is six or seven layers. Spin waves in thinner films may be studied

as special cases using the same equations of motion but have not been considered explicitly here.

Films where N is odd are the subject of Section 6.1 while the corresponding discussion of films where N is even is contained in Section 6.2. In each case we generalize equations (5.1.3) through (5.1.4) then solve for the Green functions and find expressions for the dispersion relations. Spectral intensities are calculated in the same manner as in Chapters 4 and 5 and we quote only the final results here. In Section 6.3 we present numerical results for dispersion relations and the mean-squared amplitude of spin precession $A_n^+(\mathbf{k}_\parallel)$ for each of the special cases. As mentioned in Chapter 5, the Green functions relating to either sublattice may be used to find the dispersion relations. Therefore, we include only the formalism for SL1 here, and for simplicity we omit the superscripts (1) and (2) of Chapter 5.

6.1 Films with an Odd Total Number of Layers

For films where N is odd, both surfaces belong to SL1. Following the same procedures as in Chapter 5 and using (6.0.1) and (6.0.2) we find equations analogous to (5.1.3) through (5.1.4). They are

$$[\omega - Sv_B(0) - 2DS\eta]G_{1n'} = \frac{1}{2\pi}\delta_{1n'} + Sv_B(\mathbf{k}_\parallel)\mathcal{G}_{2n'} - 2S\eta' F_S G'_{1n'}, \qquad (n = 1)$$

$$[\omega - 2Sv_B(0) - 2DS\eta]G_{nn'} = \frac{1}{2\pi}\delta_{nn'} + Sv_B(\mathbf{k}_\parallel)\mathcal{G}_{n-1n'} + Sv_B(\mathbf{k}_\parallel)\mathcal{G}_{n+1n'}, \qquad (n = 3,5,..N-2)$$

$$[\omega - Sv_B(0) - 2DS\eta]G_{Nn'} = \frac{1}{2\pi}\delta_{Nn'} + Sv_B(\mathbf{k}_\parallel)\mathcal{G}_{N-1n'} - 2S\eta' F_S G'_{Nn'}, \qquad (n = N) \qquad (6.1.1)$$

$$[\omega + 2Sv_B(0) + 2DS\eta]\mathcal{G}_{nn'} = - Sv_B(k_\parallel)G_{n-1n'} - Sv_B(k_\parallel)G_{n+1n'}$$
$$(n = 2,4,..N-1) \qquad (6.1.2)$$

$$[\omega + Sv_B(0) + 2DS\eta]G'_{1n'} = - Sv_B(k_\parallel)\mathcal{G}'_{2n'} + 2S\eta' F_S G_{1n'}$$
$$(n = 1)$$
$$[\omega + 2Sv_B(0) + 2DS\eta]G'_{nn'} = - Sv_B(k_\parallel)\mathcal{G}'_{n-1n'} - Sv_B(k_\parallel)\mathcal{G}'_{n+1n'}$$
$$(n = 3,5,..N-2)$$
$$[\omega + Sv_B(0) + 2DS\eta]G'_{Nn'} = - Sv_B(k_\parallel)\mathcal{G}'_{N-1n'} + 2S\eta' F_S, G_{Nn'}$$
$$(n = N) \qquad (6.1.3)$$

$$[\omega - 2Sv_B(0) - 2DS\eta]\mathcal{G}'_{nn'} = + Sv_B(k_\parallel)G'_{n-1n'} + Sv_B(k_\parallel)G'_{n+1n'}$$
$$(n = 2,4,..N-1) \qquad (6.1.4)$$

where the Green functions are the same as those defined in Chapter 5 for SL1 (omitting the superscript (1) for convenience). Eliminating $\mathcal{G}$ and $\mathcal{G}'$ from the equations for G and G' we find

$$(\underline{A}_0 + \underline{\delta}_A)\mathbf{G} = \sigma\underline{I} + \underline{\delta}_B\mathbf{G}'$$
$$(\underline{A}_0 + \underline{\delta}_C)\mathbf{G}' = \underline{\delta}_D\mathbf{G}. \qquad (6.1.5)$$

These coupled matrix equations are analogous to the Chapter 5 result for case B semi-infinite systems (5.5.1). The number of layers in SL1 is now M ≡ (N+1)/2 and therefore we have M×M matrices here. $\underline{A}_0$ has the tridiagonal form of (2.2.17). The matrix $\underline{\delta}_A$ is given by

$$\underline{\delta}_A = \begin{bmatrix} \delta_A & 0.. & & \\ 0 & 0.. & & \\ \vdots & \vdots & . & . \\ & & ..0 & 0 \\ . & . & ..0 & \delta'_A \end{bmatrix} \qquad (6.1.6)$$

and $\underline{\delta}_B$, $\underline{\delta}_C$ and $\underline{\delta}_D$ have this same form. We can formally solve the

coupled matrix equations in (6.1.5) to write

$$G = \frac{\sigma\ \mathrm{adj}[\underline{I} - \underline{P}^{-1}\underline{Q}\underline{\delta}_B\underline{R}^{-1}\underline{Q}\underline{\delta}_D]\ \mathrm{adj}\underline{P}\ \underline{Q}}{\det[\underline{I} - \underline{P}^{-1}\underline{Q}\underline{\delta}_B\underline{R}^{-1}\underline{Q}\underline{\delta}_D]\ \det\underline{P}}$$

$$G' = \frac{\sigma\ \mathrm{adj}[\underline{I} - \underline{R}^{-1}\underline{Q}\underline{\delta}_D\underline{P}^{-1}\underline{Q}\underline{\delta}_B]\ \mathrm{adj}\underline{R}\ \underline{Q}\ \underline{\delta}_D\mathrm{adj}\underline{P}\ \underline{Q}}{\det[\underline{I} - \underline{R}^{-1}\underline{Q}\underline{\delta}_D\underline{P}^{-1}\underline{Q}\underline{\delta}_B]\ \det\underline{R}\ \det\underline{P}}. \qquad (6.1.7)$$

Here we have $\underline{Q} \equiv \underline{A}_0^{-1}$, $\underline{P} \equiv (\underline{I} + \underline{A}_0^{-1}\underline{\delta}_A)$, and $\underline{R} \equiv (\underline{I} + \underline{A}_0^{-1}\underline{\delta}_C)$. The elements of $\underline{Q}$ are calculated in the same way as for the ferromagnetic films, using (2.2.19) with the complex variable x defined as in (5.4.10) and substituting M for N. When N is odd and the surfaces are identical with respect to all exchange and anisotropy parameters we find that $\delta_A = \delta_{A'}$ and $\delta_C = \delta_{C'}$, so that we may write $\underline{\delta}_A = \delta_A\underline{\nu}$ and $\underline{\delta}_C = \delta_C\underline{\nu}$ where $\underline{\nu}$ is defined as in (2.4.1). The matrix $\underline{P} = (\underline{I} + \delta_A\underline{A}_0^{-1}\underline{\nu})$ therefore has the same symmetry as in (2.3.8) and its inverse, $\underline{P}^{-1}$, is given by (2.4.7) and (2.4.8). Similar expressions apply to $\underline{R}$. Some parameters are given by

$$\delta_A = 1 - 4(\Omega + d + 8)/[\gamma^2(k_\parallel)]$$

$$\delta_C = 1 + 4(\Omega - d - 8)/[\gamma^2(k_\parallel)]. \qquad (6.1.8)$$

Also we find

$$a = -[(\Omega - d - 8)(\Omega + d + 8) + 2\gamma^2(k_\parallel)]/[\gamma^2(k_\parallel)]$$

$$\sigma = -(\Omega + d + 8)/[2\pi SJ\gamma^2(k_\parallel)]. \qquad (6.1.9)$$

Here quantities such as d and $\gamma(k_\parallel)$ have the same definitions as in Chapter 5. We now proceed with cases B.1 and B.2 separately.

6.1.1 Case B.1: The Nonuniaxial Parameter has the Same Value on Both Surfaces

In this section we consider films where N is odd and $F_s = F_{s'}$. In this

case we find that $\delta_B = \delta_{B'}$ and $\delta_D = \delta_{D'}$, and we can therefore write $\underline{\delta}_B = \delta_B \underline{\nu}$ and $\underline{\delta}_D = \delta_D \underline{\nu}$. We have

$$\delta_B = f_S(\Omega + d + 8)/[\gamma^2(k_{\|})]$$
$$\delta_D = -f_S(\Omega - d - 8)/[\gamma^2(k_{\|})]. \qquad (6.1.10)$$

We note that the parameters δ_A, δ_B, etc. for this case are those defined in (5.5.2) for case B semi-infinite systems with the simplifications of (6.0.1) and (6.0.2). We can write (6.1.7) as

$$G = \frac{\sigma \text{ adj}[\underline{I} - \delta_B\delta_D\underline{P}^{-1}\underline{Q\nu R}^{-1}\underline{Q\nu}] \text{ adj}\underline{P}\ \underline{Q}}{\det[\underline{I} - \delta_B\delta_D\underline{P}^{-1}\underline{Q\nu R}^{-1}\underline{Q\nu}] \det \underline{P}}$$

$$G' = \frac{\sigma\ \delta_D \text{adj}[\underline{I} - \delta_B\delta_D\underline{R}^{-1}\underline{Q\nu P}^{-1}\underline{Q\nu}] \text{ adj}\underline{R}\ \underline{Q}\ \underline{\nu}\ \text{adj}\underline{P}\ \underline{Q}}{\det[\underline{I} - \delta_B\delta_D\underline{R}^{-1}\underline{Q\nu P}^{-1}\underline{Q\nu}] \det \underline{R} \det \underline{P}}. \qquad (6.1.11)$$

We rewrite G as

$$G = \frac{\sigma \text{ adj}[\underline{I} - \delta_B\delta_D\underline{P}^{-1}\underline{Q\nu R}^{-1}\underline{Q\nu}] \text{ adj}\underline{P}\ \underline{Q}\ v(x)}{y_1(x)y_2(x)} \qquad (6.1.12)$$

where

$$y_1(x) = [r(x) + \delta_A g(x)][r(x) + \delta_C g(x)] - \delta_B\delta_D g^2(x)$$
$$y_2(x) = [s(x) + \delta_A h(x)][s(x) + \delta_C h(x)] - \delta_B\delta_D h^2(x)$$
$$v(x) = [r(x) + \delta_C g(x)][s(x) + \delta_C h(x)]r(x)s(x) \qquad (6.1.13)$$

The functions r(x), s(x), g(x) and h(x) are defined as in (2.3.11) with M instead of N. We see that the spin-wave frequencies are related to the zeroes of $y_1(x)$ and $y_2(x)$. A similar result can be found for SL2 but is not written here explicitly.

In addition to the surface modes (corresponding to x real with $-1 < x < 1$) there will be a set of quantized bulk modes. As in the case of ferromagnetic films the bulk mode frequencies are related to those

zeroes of the functions y_1 and y_2 for which $x = \exp(i\theta)$ with θ real and satisfying $0 < \theta < \pi$. We rewrite these functions in terms of θ as in Chapter 3. We consider θ to be a function of Ω according to (5.4.10) which implies that $2\cos(\theta) = a(\Omega)$. In order to find numerical results we look for roots of $y_1(\Omega)$ and $y_2(\Omega)$ on the interval (Ω_L, Ω_U) where Ω_L and Ω_U are the lower and upper boundaries, respectively, of the bulk mode region. These are determined as in (5.5.9). Numerical dispersion relation results for both surface and quantized bulk spin waves appear in Section 6.3.

At this point we consider some limiting cases of our formal results. For the thick-film limit we take $M \to \infty$ and find

$$y_1(x) = y_2(x) = (1 + \delta_A x)(1 + \delta_C x) - \delta_B \delta_D x^2 \qquad (6.1.14)$$

The result of Section 5.5 is therefore recovered, as expected. For finite M we take the uniaxial limit ($F_S = 0$) and obtain

$$G = \frac{\sigma \, \mathrm{adj}\underline{P} \, \underline{Q} \, r(x)s(x)}{[r(x) + \delta_A g(x)][s(x) + \delta_A h(x)]}$$

$$G' = 0 \qquad (6.1.15)$$

where the denominator of G leads to two surface branches, each with positive frequency. Taking $M \to \infty$ and $F_S \to 0$ simultaneously we find that

$$G = \frac{\sigma \, \mathrm{adj}\underline{P} \, \underline{Q}}{[1 + \delta_A x]^2}$$

$$G' = 0 \qquad (6.1.16)$$

which is the expected result for a uniaxial system with well-separated surfaces both associated with the same sublattice and identical in other respects (Cottam 1978).

6.1.2 Case B.2: The Nonuniaxial Parameter is Non-zero on one Surface Only

In the present case we take the anisotropy to be nonuniaxial on layer 1 only. We modify (6.1.1) through (6.1.4) by removing the terms involving F_S which appear in the equations for $G_{Nn'}$ and $G'_{Nn'}$. Following the usual procedure we find the same formal expressions, (6.1.5) and (6.1.7), for the Green functions as in case B.1. However here $\delta_{B'} = \delta_{D'} = 0$ and we can write $\underline{\delta}_B = \delta_B \underline{\nu}'$ and $\underline{\delta}_D = \delta_D \underline{\nu}'$ where $\underline{\nu}'$ is an MxM matrix whose sole non-zero element is $\nu'_{11} = 1$. We can therefore write, instead of (6.1.11),

$$G = \frac{\sigma \, \mathrm{adj}[\underline{I} - \delta_B \delta_D \underline{P}^{-1} \underline{Q} \underline{\nu}' \underline{R}^{-1} \underline{Q} \underline{\nu}'] \, \mathrm{adj}\underline{P} \; \underline{Q}}{\det[I - \delta_B \delta_D \underline{P}^{-1} \underline{Q} \underline{\nu}' \underline{R}^{-1} \underline{Q} \underline{\nu}'] \, \det \underline{P}}$$

$$G' = \frac{\sigma \, \delta_D \mathrm{adj}[\underline{I} - \delta_B \delta_D \underline{R}^{-1} \underline{Q} \underline{\nu}' \underline{P}^{-1} \underline{Q} \underline{\nu}'] \, \mathrm{adj}\underline{R} \; \underline{Q} \; \underline{\nu}' \mathrm{adj}\underline{P} \; \underline{Q}}{\det[I - \delta_B \delta_D \underline{R}^{-1} \underline{Q} \underline{\nu}' \underline{P}^{-1} \underline{Q} \underline{\nu}'] \, \det \underline{R} \, \det \underline{P}}. \qquad (6.1.17)$$

We rewrite G as

$$G = \frac{\sigma \, \mathrm{adj}[\underline{I} - \delta_B \delta_D \underline{P}^{-1} \underline{Q} \underline{\nu}' \underline{R}^{-1} \underline{Q} \underline{\nu}'] \, \mathrm{adj}\underline{P} \; \underline{Q} \; v(x)}{y(x)} \qquad (6.1.18)$$

with

$$y(x) = [r(x) + \delta_A g(x)][s(x) + \delta_A h(x)][r(x) + \delta_C g(x)][s(x) + \delta_C h(x)]$$
$$- \delta_B \delta_D [q(x) + \delta_A g(x)h(x)][q(x) + \delta_C g(x)h(x)] \qquad (6.1.19)$$

and v(x) as defined in (6.1.13). Again we use (2.3.11) (with M instead of N) for r(x), s(x), g(x) and h(x) and (2.3.15) for q(x). Numerical results for spin-wave frequencies determined from these expressions appear in Section 6.3.

In the uniaxial limit ($F_S = 0$ and $\delta_B = \delta_D = 0$) we find the same result as for the case B.1 films, (6.1.15). Alternatively, taking $M \to \infty$ in (6.1.18) we find

$$G = \frac{\sigma \, \mathrm{adj}[\underline{I} - \delta b \delta d \underline{P}^{-1} \underline{Q} \nu \underline{R}^{-1} \underline{Q} \nu] \, \mathrm{adj} \underline{P} \, \underline{Q} \, (1 + \delta_C x)}{[(1 + \delta_A x)(1 + \delta_C x) - \delta_B \delta_D x^2](1 + \delta_A x)} \qquad (6.1.20)$$

so that the denominator has poles relating to both the semi-infinite nonuniaxial solution (5.5.6) and the semi-infinite uniaxial solution (5.4.14). This is to be expected since here the films have one surface of each type. The uniaxial limit for thick films is clearly (6.1.16) as in case B.1.

6.2 Films with an Even Number of Layers

When N is even the films have one surface (layer 1) associated with SL1 and one surface (layer N) associated with SL2. The symmetry between the two sublattices is not broken as it is in the case of films where N is odd, but the two surfaces are no longer equivalent. The number of layers in each sublattice is M = N/2. Instead of (6.1.1) through (6.1.4) we now have

$$[\omega - Sv_B(0) - 2DS\eta]G_{1n'} = \frac{1}{2\pi}\delta_{1n'} + Sv_B(k_\parallel)\mathcal{G}_{2n'} - 2S\eta' F_S G'_{1n'} \qquad (n = 1)$$

$$[\omega - 2Sv_B(0) - 2DS\eta]G_{nn'} = \frac{1}{2\pi}\delta_{nn'} + Sv_B(k_\parallel)\mathcal{G}_{n-1n'} + Sv_B(k_\parallel)\mathcal{G}_{n+1n'} \qquad (n = 3,5,..N-1) \qquad (6.2.1)$$

$$[\omega + 2Sv_B(0) + 2DS\eta]\mathcal{G}_{nn'} = - Sv_B(k_\parallel)G_{n-1n'} - Sv_B(k_\parallel)G_{n+1n'} \qquad (n = 2,4,..N-2)$$

$$[\omega + Sv_B(0) + 2DS\eta]\mathcal{G}_{Nn'} = - Sv_B(k_\parallel)G_{N-1n'} + 2S\eta' F_S,\mathcal{G}'_{Nn'}$$
$$(n = N) \qquad (6.2.2)$$

$$[\omega + Sv_B(0) + 2DS\eta]G'_{1n'} = - Sv_B(k_\parallel)\mathcal{G}'_{2n'} + 2S\eta' F_S G_{1n'}$$
$$(n = 1)$$
$$[\omega + 2Sv_B(0) + 2DS\eta]G'_{nn'} = - Sv_B(k_\parallel)\mathcal{G}'_{n-1n'} - Sv_B(k_\parallel)\mathcal{G}'_{n+1n'}$$
$$(n = 3,5,..N-1) \qquad (6.2.3)$$

$$[\omega - 2Sv_B(0) - 2DS\eta]\mathcal{G}'_{nn'} = Sv_B(k_\parallel)G'_{n-1n'} + Sv_B(k_\parallel)G'_{n+1n'}$$
$$(n = 2,4,..N-2)$$
$$[\omega - 2Sv_B(0) - 2DS\eta]\mathcal{G}'_{Nn'} = Sv_B(k_\parallel)G'_{N-1n'} - 2S\eta' F_S,\mathcal{G}_{Nn'}.$$
$$(n = N) \qquad (6.2.4)$$

We eliminate $\mathcal{G}$ and $\mathcal{G}'$ from the equations for G and G' and find formally the same expressions for the Green functions as in the case of N odd, (6.1.5) and (6.1.7). In this case when the surfaces have the same exchange and anisotropy constants we still find that $\delta_A \neq \delta_{A'}$ and $\delta_C \neq \delta_{C'}$. Therefore the matrices $\underline{P}$ and $\underline{R}$ (defined formally as above) have the symmetry of (2.3.12) and inverses given by (2.4.8). We now proceed with cases B.1 and B.2 separately.

6.2.1 Case B.1: The Nonuniaxial Parameter has the Same Value on Both Surfaces

In this case we have $F_S = F_{S'}$, however we still find that $\delta_B \neq \delta_{B'}$ and $\delta_D \neq \delta_{D'}$ because they refer to different sublattices. The parameters appearing in the Green functions (given formally by (6.1.7)) are

$$\delta_A = 1 - \frac{4(\Omega + d + 8)}{\gamma^2(k_\parallel)}$$

$$\delta_{A'} = 1 - \frac{(\Omega - d - 4)(\Omega + d + 8)}{(\Omega - d - 4)(\Omega + d + 4) + f_s^2}$$

$$\delta_C = 1 + \frac{4(\Omega - d - 8)}{\gamma^2(k_{\|})}$$

$$\delta_{C'} = 1 - \frac{(\Omega + d + 4)(\Omega - d - 8)}{(\Omega - d - 4)(\Omega + d + 4) + f_s^2}$$

$$\delta_B = f_s \frac{(\Omega + d + 8)}{\gamma^2(k_{\|})}$$

$$\delta_{B'} = -f_s \frac{(\Omega + d + 8)}{(\Omega - d - 4)(\Omega + d + 4) + f_s^2}$$

$$\delta_D = -f_s \frac{(\Omega - d - 8)}{\gamma^2(k_{\|})}$$

$$\delta_{D'} = f_s \frac{(\Omega - d - 8)}{(\Omega - d - 4)(\Omega + d + 4) + f_s^2} \qquad (6.2.5)$$

with a and σ defined as in (6.1.9). We may write G as

$$G = \frac{\sigma \, \mathrm{adj}[\underline{I} - \underline{P}^{-1}\underline{Q}\underline{\delta}_B\underline{R}^{-1}\underline{Q}\underline{\delta}_D] \, \mathrm{adj}\underline{P} \, \underline{Q} \, v(x)}{y(x)}. \qquad (6.2.6)$$

The function y(x) appearing here is considerably more complicated than in its counterparts in earlier cases (e.g. (6.1.19)) but may be written explicitly as

$$y(x) = w_1(x)w_2(x) - w_3(x)w_4(x) \qquad (6.2.7)$$

with

$$\begin{aligned} w_1(x) = &\Big[r^2(x)s^2(x)[r(x)s(x) + (\delta_A + \delta_{A'})q(x) + \delta_A\delta_{A'}g(x)h(x)] \\ &\times [r(x)s(x) + (\delta_C + \delta_{C'})q(x) + \delta_C\delta_{C'}g(x)h(x)]\Big] \\ &-\delta_D\Big[[q(x)r(x)s(x) + \delta_A q^2(x) - \delta_{A'}p^2(x)] \\ &\times [q(x)r(x)s(x) + \delta_C q^2(x) - \delta_{C'}p^2(x)]\Big] \\ &-\delta_B\delta_D\Big[[p(x)r(x)s(x) + (\delta_A - \delta_{A'})p(x)q(x)] \\ &\times [q(x)r(x)s(x) + \delta_C q^2(x) - \delta_C p(x)q(x)]\Big] \end{aligned}$$

$$
\begin{aligned}
w_2(x) = &\Big[r^2(x)s^2(x)[r(x)s(x) + (\delta_A + \delta_A')q(x) + \delta_A\delta_A' g(x)h(x)] \\
&\times [r(x)s(x) + (\delta_C + \delta_C')q(x) + \delta_C\delta_C' g(x)h(x)]\Big] \\
&- \delta_B\delta_D'\Big[[q(x)r(x)s(x) + \delta_A' q^2(x) - \delta_A p(x)q(x)] \\
&\times [p(x)r(x)s(x) + (\delta_C - \delta_C')p(x)q(x)]\Big] \\
&- \delta_B'\delta_D\Big[[q(x)r(x)s(x) + \delta_A' q^2(x) - \delta_A p^2(x)] \\
&\times [q(x)r(x)s(x) + \delta_C' q^2(x) - \delta_C p^2(x)]\Big]
\end{aligned}
$$

$$
\begin{aligned}
w_3(x) = \delta_B\delta_D\Big[&[q(x)r(x)s(x) + \delta_A' q^2(x) - \delta_A p(x)q(x)] \\
&\times [q(x)r(x)s(x) + \delta_C q^2(x) - \delta_C' p^2(x)]\Big] \\
&+ \delta_B'\delta_D\Big[[q(x)r(x)s(x) + \delta_A' q^2(x) - \delta_A p^2(x)] \\
&\times [q(x)r(x)s(x) + \delta_C' q^2(x) - \delta_C p(x)q(x)]\Big]
\end{aligned}
$$

$$
\begin{aligned}
w_4(x) = \delta_B\delta_D'\Big[&[q(x)r(x)s(x) + \delta_A q^2(x) - \delta_A' p^2(x)] \\
&\times [p(x)r(x)s(x) + (\delta_C - \delta_C')p(x)q(x)]\Big] \\
&+ \delta_B'\delta_D\Big[[p(x)r(x)s(x) + (\delta_A - \delta_A')p(x)q(x)] \\
&\times [q(x)r(x)s(x) + \delta_C' q^2(x) - \delta_C p^2(x)]\Big]
\end{aligned}
\qquad (6.2.8)
$$

with

$$
p(x) = x^M - x^{M+2}. \qquad (6.2.9)
$$

We also have

$$
\begin{aligned}
v(x) = r(x)s(x)&\Big[r(x)s(x) + (\delta_A + \delta_A')q(x) + \delta_A\delta_A' g(x)h(x)\Big] \\
&\times \Big[r(x)s(x) + (\delta_C + \delta_C')q(x) + \delta_C\delta_C' g(x)h(x)\Big]^2
\end{aligned}
\qquad (6.2.10)
$$

Numerical results of spin-wave frequencies determined from these expressions appear in Section 6.3.

In the uniaxial limit δ_B, δ_B', δ_D and δ_D' are each zero and we can write

$$
G = \frac{\sigma \ \mathrm{adj}\underline{P}\ \underline{Q}\ r(x)s(x)}{r(x)s(x) + (\delta_A + \delta_A')q(x) + \delta_A\delta_A' g(x)h(x)} \ ,
$$

$$
G' = 0. \qquad (6.2.11)
$$

In contrast to case B.1 for films with N odd, here the denominator has roots leading to one positive-frequency branch associated with layer 1 (SL1) and one negative-frequency branch associated with layer N (SL2). The frequencies are non-degenerate in magnitude. In the limit that $M \to \infty$ but $F_S \neq 0$ then (6.2.6) can be rewritten using

$$y(x) = [(1 + \delta_A,x)(1 + \delta_C,x) - \delta_B\delta_D x^2]\,[(1 + \delta_A,x)(1 + \delta_C x) - \delta_B,\delta_D,x^2]$$
$$v(x) = (1 + \delta_C x)(1 + \delta_C,x). \qquad (6.2.12)$$

Here there are two spin-wave branches, each resulting from expressions which are similar to the semi-infinite case B result found in (5.5.6). Taking both the thick-film and uniaxial limits we can write (6.2.6) using

$$y(x) = (1 + \delta_A x)(1 + \delta_A,x). \qquad (6.2.13)$$

Here we find two surface spin-wave modes with frequencies opposite in sign but degenerate in magnitude. This is the expected result for a uniaxial system with isolated surfaces on opposite subiattices.

6.2.2 Case B.2: The Nonuniaxial Parameter is Non-zero on one Surface Only

In the present case we take one surface (layer 1) to be nonuniaxial while the other surface is uniaxial, e.g. $F_S \neq 0$, $F_{S'} = 0$. We use (6.2.1) through (6.2.4), removing the terms involving F_S in the equations for $\mathcal{G}_{Nn'}$ and $\mathcal{G}'_{Nn'}$. We eliminate $\mathcal{G}$ and $\mathcal{G}'$ from the equations for G and G' to again find formally the same expressions as in (6.1.5) and (6.1.7). Here we have $\delta_{B'} = 0$ and $\delta_{D'} = 0$ and therefore we may write $\underline{\delta}_B = \delta_B \underline{\nu}'$ and $\underline{\delta}_D = \delta_D \underline{\nu}'$ where $\underline{\nu}'$ is the matrix defined earlier in Section 6.1. The matrices $\underline{\delta}_A$ and $\underline{\delta}_C$ have the form given in (6.1.6).

Parameters δ_A, δ_C, δ_B, and δ_D are defined as in (6.2.5). The others, $\delta_{A'}$ and $\delta_{C'}$, are redefined with $f_{S'} = 0$ as

$$\delta_{A'} = 1 - \frac{(\Omega + d + 8)}{(\Omega + d + 4)}$$

$$\delta_{C'} = 1 - \frac{(\Omega - d - 8)}{(\Omega - d - 4)}. \qquad (6.2.14)$$

We may write the Green functions formally as in (6.1.17) and then G as in (6.1.18). The functions y(x) and v(x) appearing there are now given by

$$y(x) = [r(x)s(x) + (\delta_A + \delta_{A'})q(x) + \delta_A\delta_{A'}h(x)g(x)]$$
$$\times [r(x)s(x) + (\delta_C + \delta_{C'})q(x) + \delta_C\delta_{C'}h(x)g(x)]$$
$$- \delta_B\delta_D[q(x) + \delta_{A'}h(x)g(x)][q(x) + \delta_{C'}h(x)g(x)]$$

$$v(x) = r(x)s(x)\left[r(x)s(x) + (\delta_C + \delta_{C'})q(x) + \delta_C\delta_{C'}h(x)g(x)r(x)s(x)\right] \qquad (6.2.14)$$

where g(x), h(x), r(x), s(x) and q(x) are defined as in (2.3.11) and (2.3.15) with M instead of N. Numerical results are presented in Section 6.3.

In the uniaxial limit we find for the Green functions the same expression as for case B.1, (6.2.11), as expected. If we consider the thick-film uniaxial limit we find (6.2.13), also as expected. However, here the nonuniaxial thick-film limit for G is

$$G = \frac{\sigma\ \mathrm{adj}\underline{P}\ \underline{Q}\ (1 + \delta_C x)}{(1 + \delta_{A'}x)[(1 + \delta_A x)(1 + \delta_C x) - \delta_B\delta_D x^2]}. \qquad (6.2.15)$$

Where one of the denominator terms is related to the layer N uniaxial surface and one is related to the layer 1 nonuniaxial surface.

6.3 Numerical Results

In this section we present numerical results for examples of each of the special cases we have considered above. These include dispersion relations for both surface spin waves and (in most cases) quantized bulk spin waves. As well, for surface modes, examples of the mean-squared amplitude $A_n^+(\mathbf{k}_\parallel)$ (as defined in (4.1.3)) versus the layer index n are provided. In each case we have assumed S = 1.

6.3.1 Dispersion Relations

For films with an odd number of layers and nonuniaxial anisotropy on both surfaces (case B.1), numerical examples of dispersion relations appear in figures 6.1 and 6.2 for seven- and thirteen-layer films respectively. These figures share some common features with those relating to nonuniaxial ferromagnetic films. Specifically, we see that the frequency spectrum for the thicker film has a greater number of branches and the two acoustic surface modes are nearly degenerate for large N, as a consequence of film symmetry. Also the frequency spectrum is symmetric about $\Omega = 0$, containing N spin-wave branches on both the positive- and negative-frequency side (although we have elected in figure 6.2 to show only those with $\Omega > 0$). Finally, comparing figures 6.1 and 6.3 for $F_s \neq 0$ and $F_s = 0$ respectively, we see that nonuniaxial anisotropy leads to spin waves of lower energy. Figure 6.3 depicts the asymmetric dispersion relation for a seven-layer uniaxial film which, in contrast to figure 6.1, has a total of N branches including two positive-frequency surface modes. The number of branches with $\Omega > 0$ and

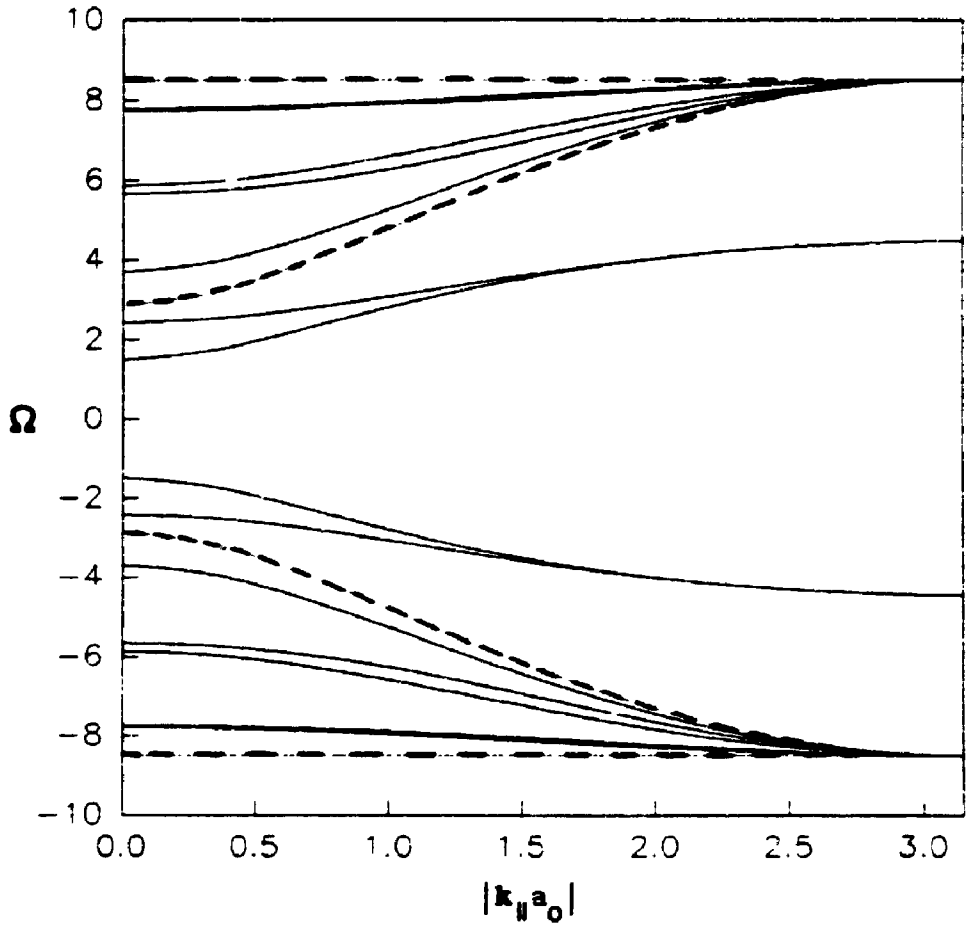

Figure 6.1 The spin-wave frequencies (in units of SJ) plotted against $|k_{\parallel}a_0|$ for a case B.1 antiferromagnetic film. Here we have chosen N = 7, $F_s/J = F_{s'}/J = 0.5$ and $F/J = 0$.

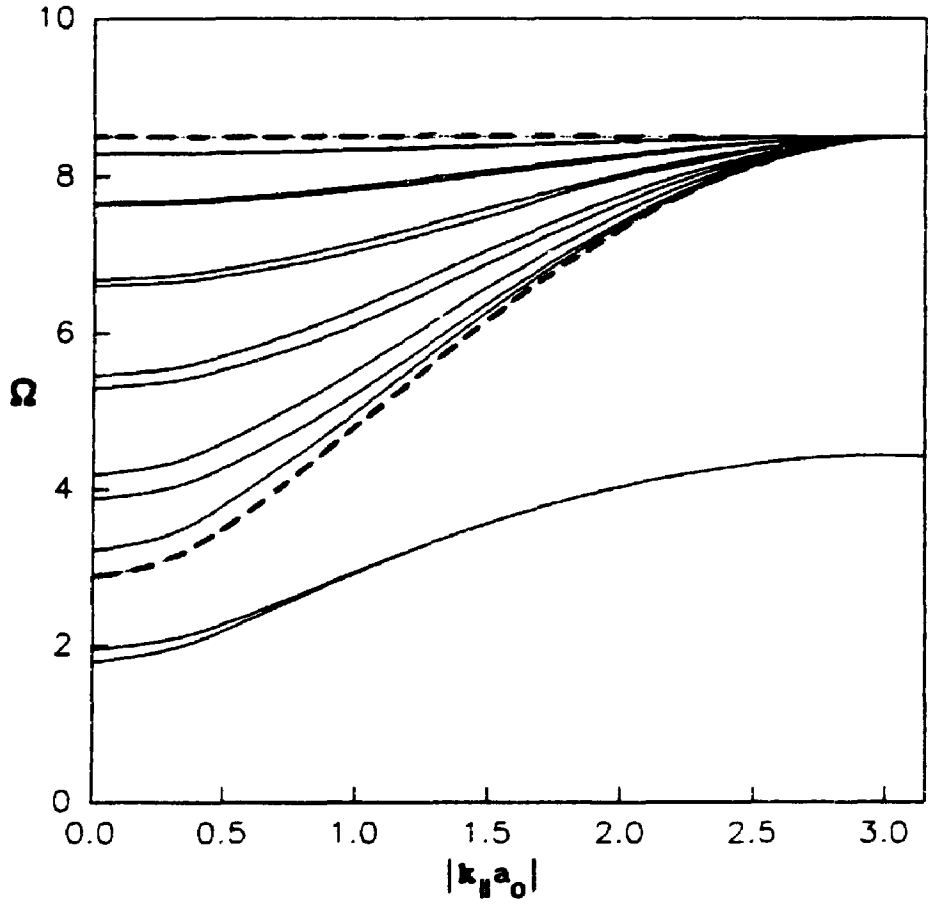

Figure 6.2 The spin-wave frequencies (in units of SJ) plotted against $|k_{\parallel}a_0|$ for a case B.1 antiferromagnetic film. Here we have chosen N = 13 and all other parameters as in figure 6.1.

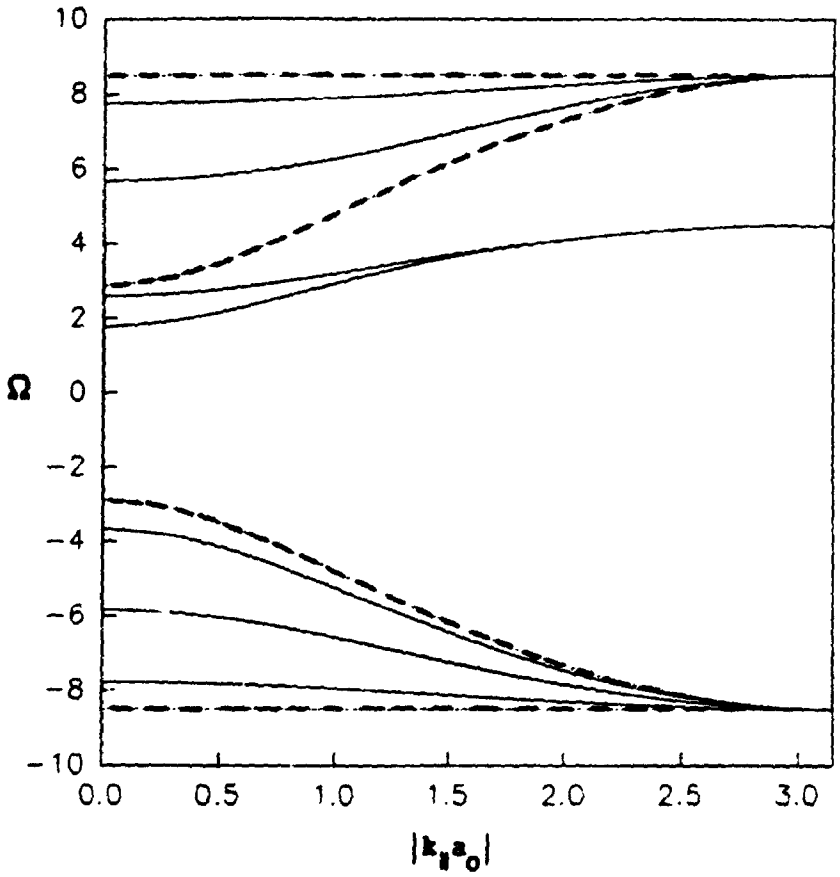

Figure 6.3 The spin-wave frequencies (in units of SJ) plotted against $|k_{\parallel}a_o|$ for a uniaxial antiferromagnetic film. Here we have chosen N = 7 and $F_s/J = F_{s'}/J = 0 = F/J = 0$.

$\Omega < 0$ correspond to the number of layers in the spin-up and spin-down sublattices respectively.

For films with an odd number of layers and nonuniaxial anisotropy on one surface only (case B.2) a numerical example of dispersion relation results appears in figure 6.4 which is qualitatively similar to those produced for case B.1 films above. We note that in the present case the acoustic surface modes are less similar than in the case B.1 plots, a consequence of the asymmetry of the case B.2 films.

For films with an even number of layers numerical examples of dispersion relation results appear in figure 6.5 (case B.1) and figure 6.6 (case B.2). These plots qualitatively resemble those relating to films with an odd number of layers. In the uniaxial limit, when $F_s = 0$, the results for films with N odd and N even are not qualitatively similar as seen in figures 6.7 (N even) and 6.3 (N odd). In the case of N even the two sublattices are equivalent hence spin-wave frequency spectrum is symmetric.

6.3.2 Mean-Squared Amplitude Results

The Green functions for SL1 and SL2 can be used to calculate the spectral intensities and correlation functions as in Chapter 5. In particular we have used equal-time correlation functions to calculate the mean-squared amplitude $A_n^+(\mathbf{k}_\parallel)$ for each layer in the film using Green functions for both SL1 and SL2. The formal results are the same as for the semi-infinite case B systems, e.g. (5.5.10). We provide some

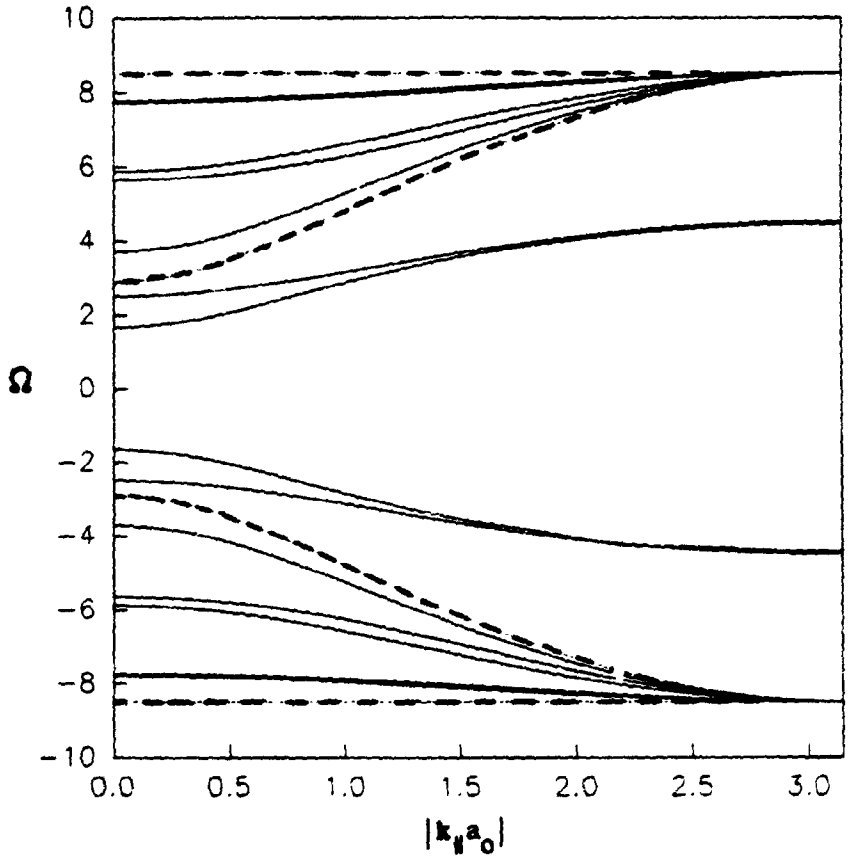

Figure 6.4 The spin-wave frequencies (in units of SJ) plotted against $|k_{\parallel}a_0|$ for a case B.2 antiferromagnetic film. Here we have chosen N = 7, $F_s/J = 0.5$ and $F_{s'}/J = F/J = 0$.

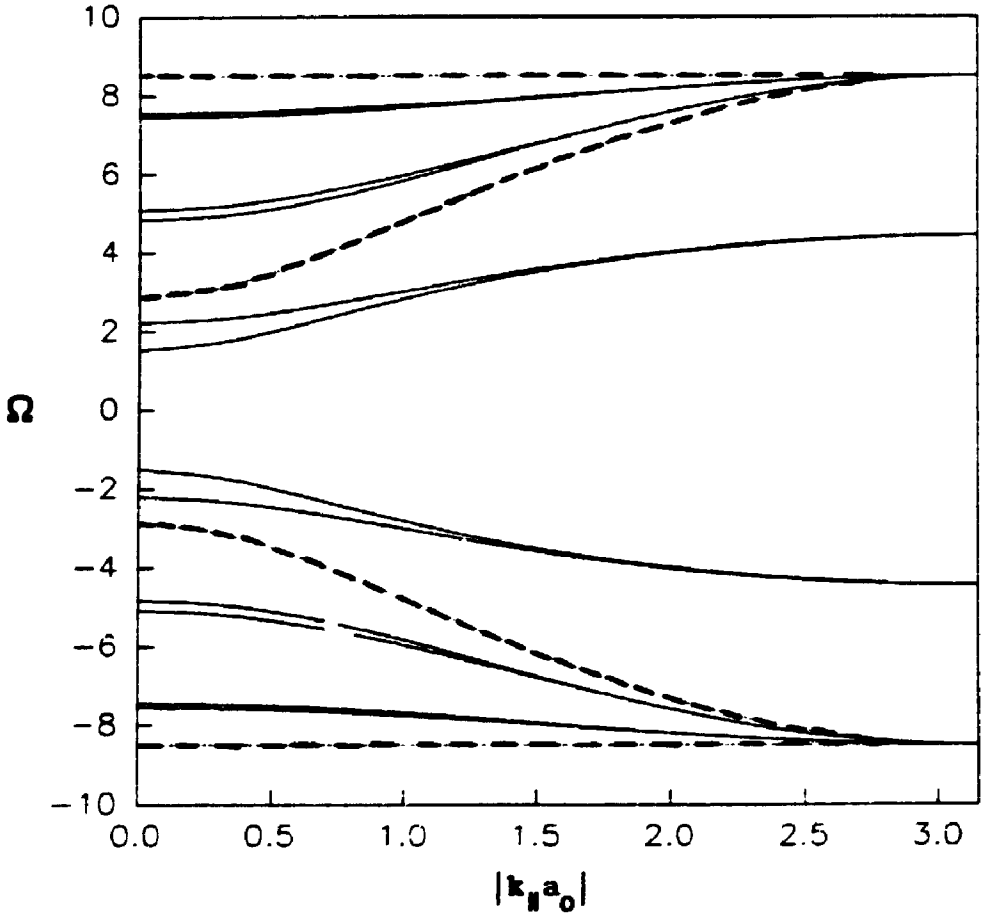

Figure 6.5 The spin-wave frequencies (in units of SJ) plotted against $|k_{\parallel}a_0|$ for a case B.1 antiferromagnetic film. Here we have chosen N = 6, $F_s/J = F_{s'}/J = 0.5$ and $F/J = 0$.

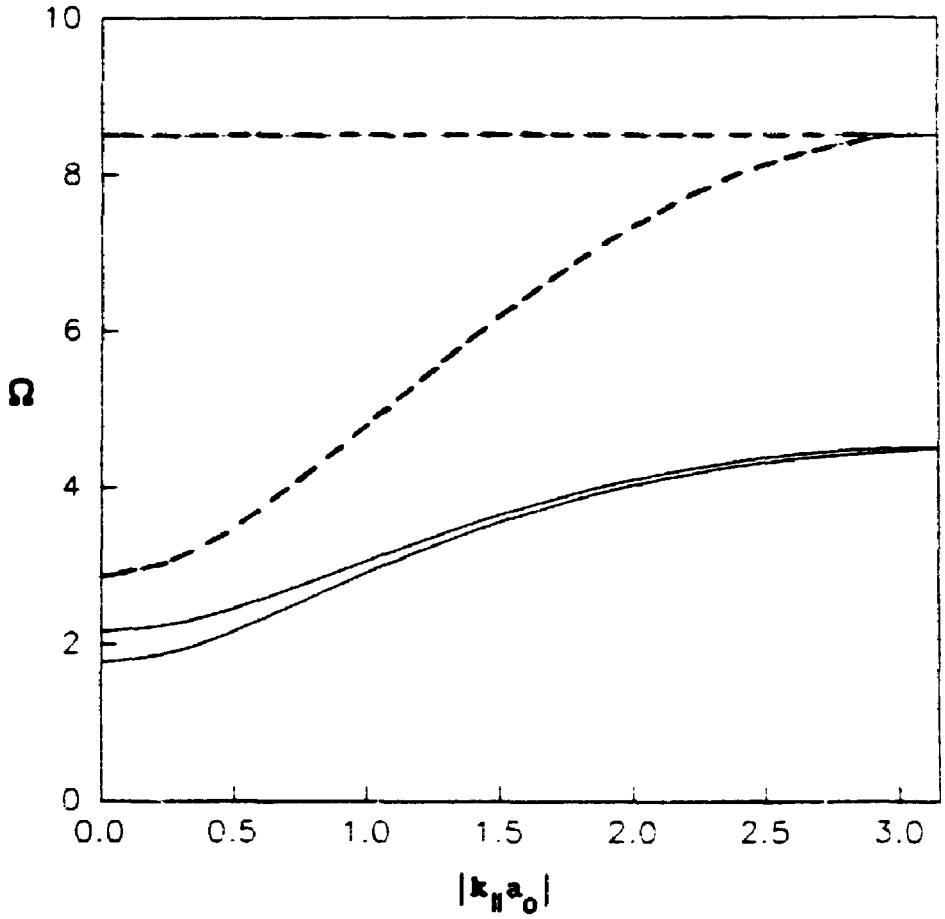

Figure 6.6 The surface spin-wave frequencies (in units of SJ) plotted against $|k_{\parallel}a_0|$ for a case B.2 antiferromagnetic film. Here we have chosen N = 6, $F_s/J = 0.5$ and $F_{s'}/J = F/J = 0$. The quantized bulk modes are omitted.

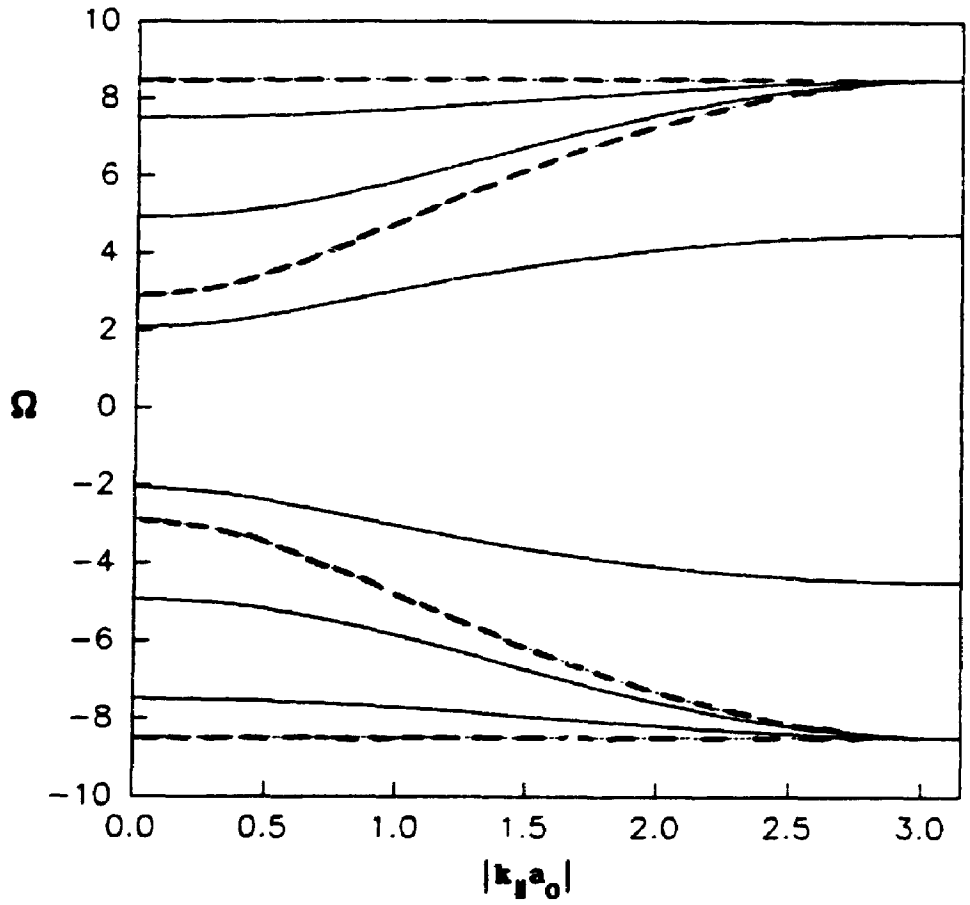

Figure 6.7 The spin-wave frequencies (in units of SJ) plotted against $|k_{\parallel}a_0|$ for a uniaxial antiferromagnetic film with N = 6.

numerical examples for surface spin waves in order to illustrate some features of these films.

We note that the appearance of "extra" branches in the nonuniaxial frequency spectra is analogous to the situation with ferromagnetic films which we have addressed in earlier chapters. In either case we find that a spin-wave having energy proportional to $|\Omega^S|$ is represented in the Green functions by poles at both $+\Omega^S$ and $-\Omega^S$. In the uniaxial limit for antiferromagnetic films where the sublattices are equivalent (N even) we find this still to be the case. In contrast, in this limit for films where the sublattices are not equivalent (N odd), each spin wave will give rise to only one Green function pole, which may be at either $+\Omega^S$ or $-\Omega^S$. As in the earlier ferromagnetic case these mathematical properties of the Green functions are primarily of interest in that they contribute to the correct prediction of physical behaviour.

We have mentioned that in a spin-wave state the (semi-classical) amplitude of precession for spins on SL1 will differ from that on SL2 due to the necessity of maintaining constant phase relationships between the adjacent spins. In the Green function theory this means that the spectral intensities will be dictated by both the sublattice and layer indices, as seen in the numerical results below.

For case B.1 films with N odd, numerical examples for $A_n^+(\mathbf{k}_\parallel)$ versus n for surface modes at $\mathbf{k}_\parallel = 0$ appear in figures 6.8 and 6.9. The layer dependence of this quantity is an irregular function (due to the

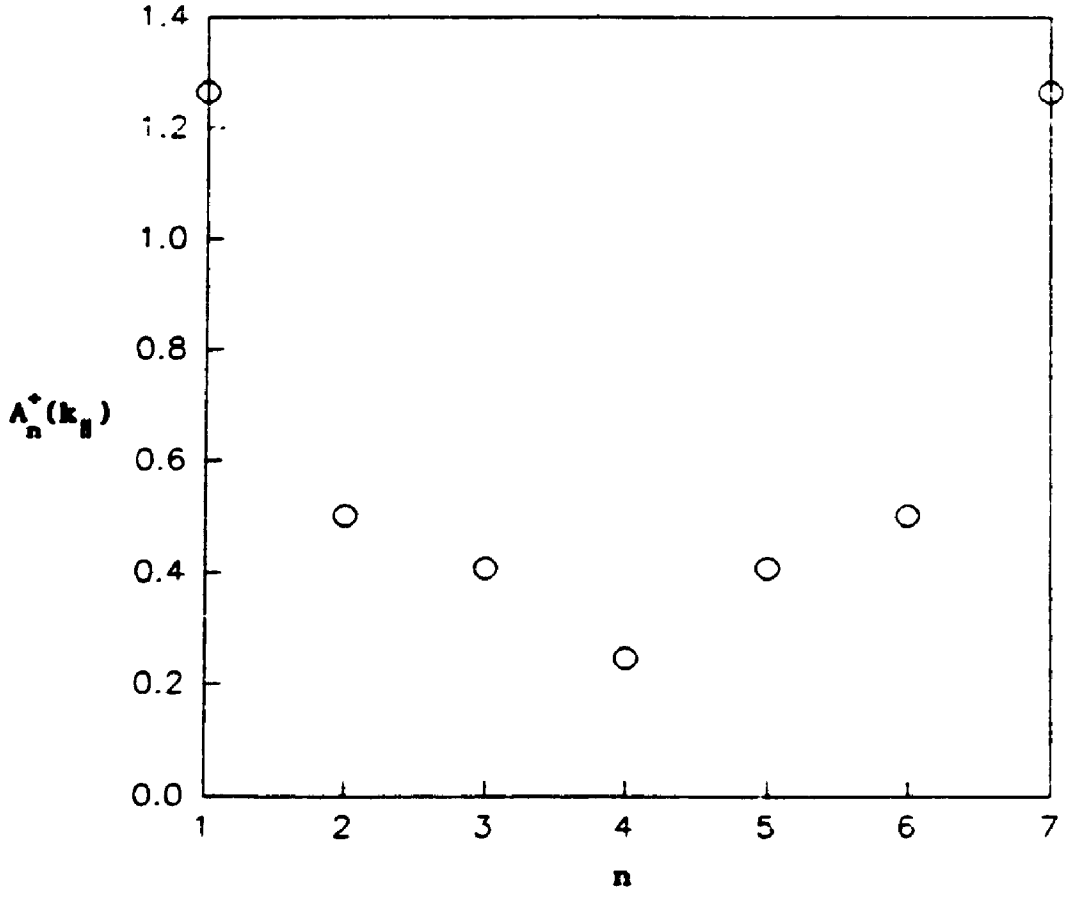

Figure 6.8 $A_n^+(k_\parallel)$ at $k_\parallel = 0$ for surface modes plotted against the layer index n for a case B.1 antiferromagnetic film with the dispersion relation of figure 6.1.

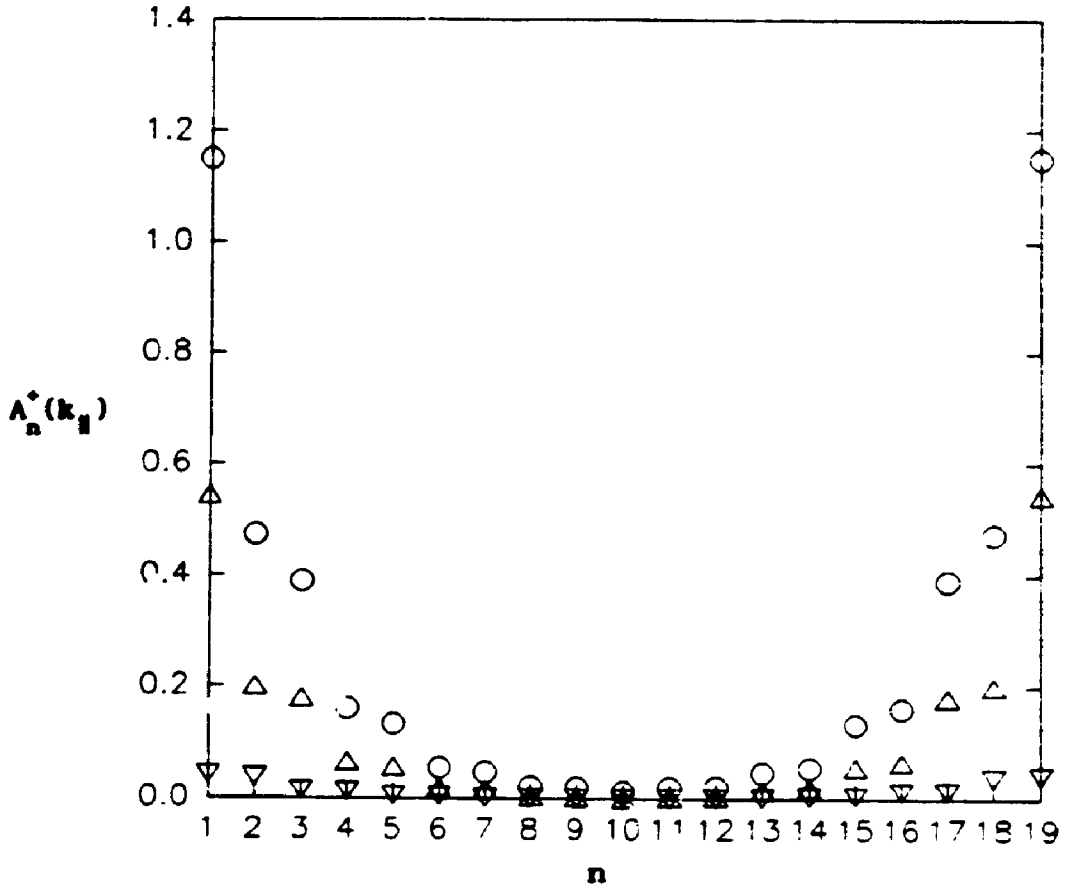

Figure 6.9 $A_n^+(k_\parallel)$ at $k_\parallel = 0$ for surface modes plotted against the layer index n for a case B.1 antiferromagnetic film. Here we have chosen N = 19 and other parameters as in figure 6.1. Contributions at $\Omega > 0$ and $\Omega < 0$ are represented by upright and inverted triangles respectively.

alternation of the sublattices) as it was in the semi-infinite cases of Chapter 5. For a relatively thick film e.g. figure 6.9 for N = 10, on each sublattice $A_n^+(\mathbf{k}_{||})$ is seen to decay in an exponential manner. In figure 6.9 we see that for one of the surface modes the contributions at positive (upright triangles) and negative frequencies (inverted triangles) are non-zero. In contrast, in figure 6.10 for a uniaxial film we see that there is a non-zero contribution at the positive frequency only. [The result for the other (nearly degenerate) surface mode is the same.] This uniaxial film has a dispersion relation resembling figure 6.3 in which it is seen that there are no negative-frequency surface modes. For case B.2 films with N odd, the numerical results for $A_n^+(\mathbf{k}_{||})$ at $\mathbf{k}_{||} = 0$ for the surface modes, seen in figures 6.11 and 6.12, resemble those of case B.1 but reflect the film asymmetry of case B.2.

For case B.1 films with N even, a numerical example of the mean-squared amplitude $A_n^+(\mathbf{k}_{||})$ for surface modes at $\mathbf{k}_{||} = 0$ appears in figure 6.13 which we can compare to figure 6.9 for a film with N odd. For a case B.2 film with N even, figure 6.14 which depicts $A_n^+(\mathbf{k}_{||})$ versus n for the surface modes at the zone centre, reflects the film asymmetry.

6.4 Discussion

In this chapter we have calculated Green functions relating to both sublattices in a bct (001) antiferromagnetic film having surface nonuniaxial anisotropy. We have treated several special cases. For films with an odd number of layers we have seen that the surfaces have

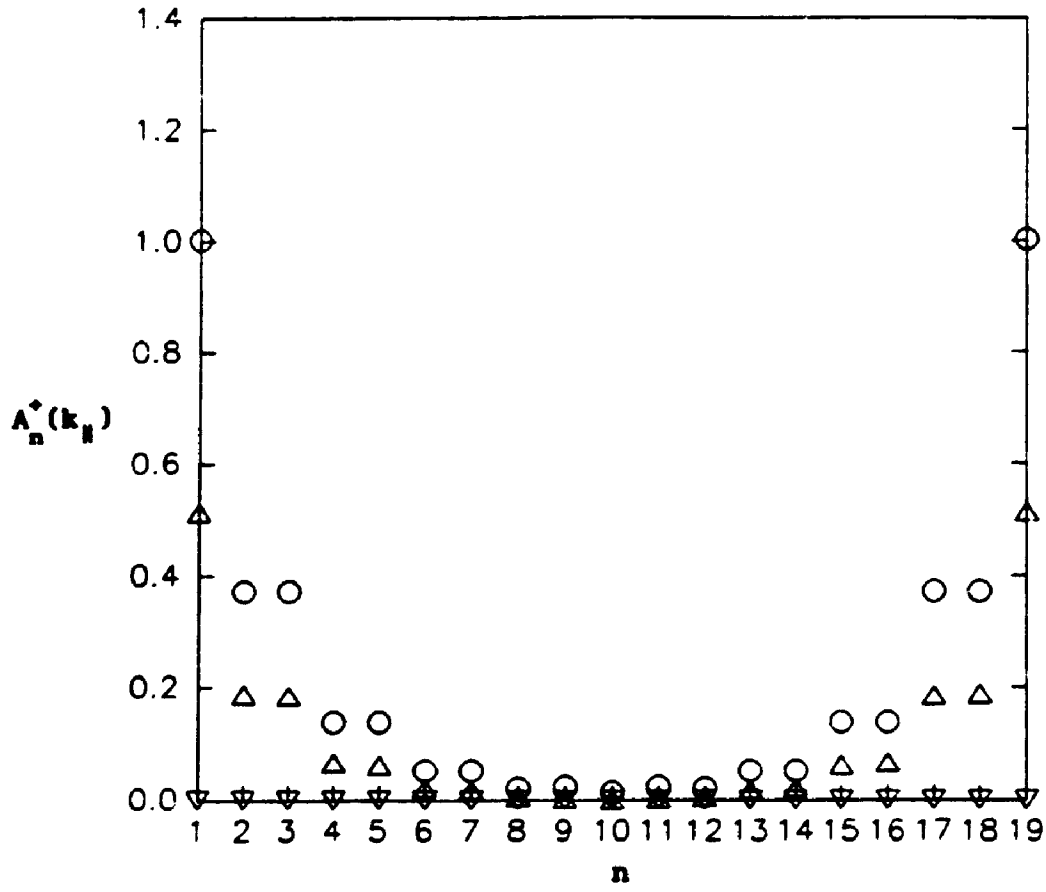

Figure 6.10 $A_n^+(k_\parallel)$ at $k_\parallel = 0$ for surface modes plotted against the layer index n for a uniaxial antiferromagnetic film. Here we have chosen N = 19 and other parameters as in figure 6.1. Contributions at $\Omega > 0$ and $\Omega < 0$ are represented by upright and inverted triangles respectively.

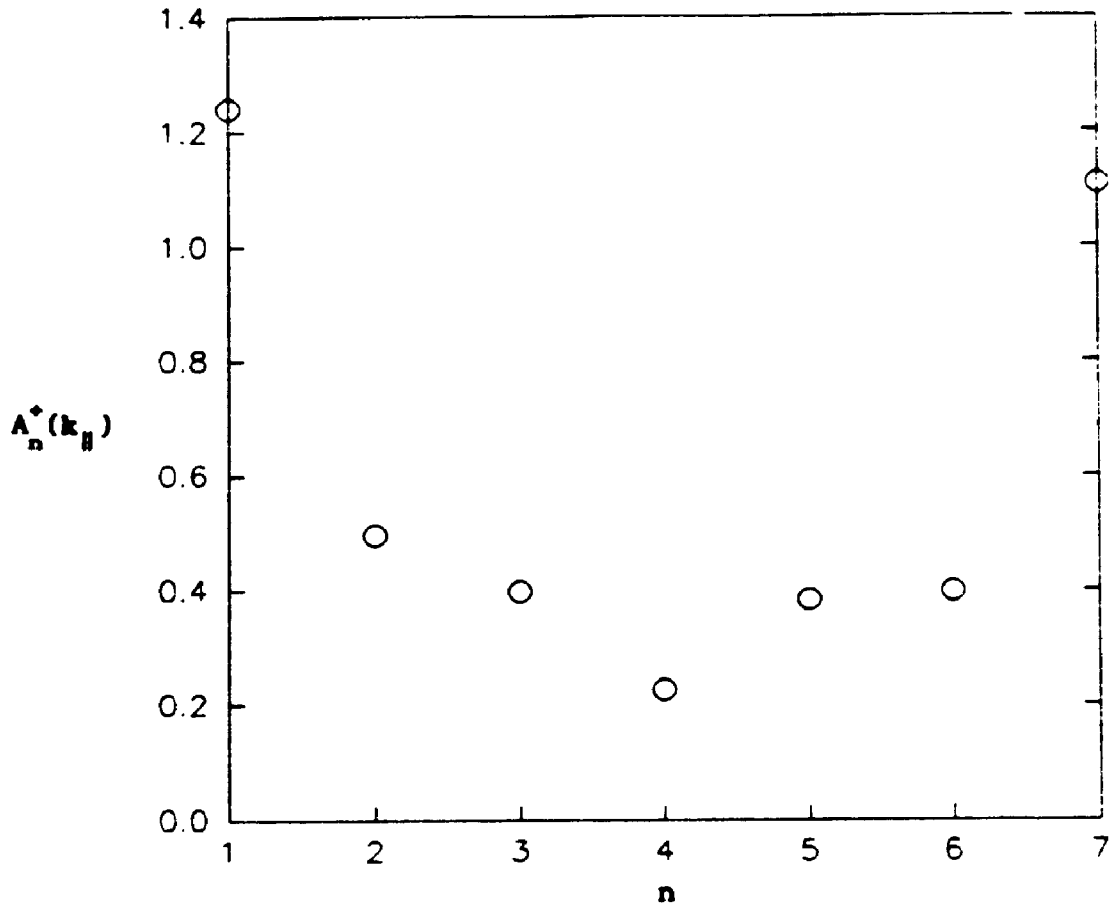

Figure 6.11 $A_n^+(k_{\parallel})$ at $k_{\parallel} = 0$ for surface modes plotted against the layer index n case B.2 film with the dispersion relation of figure 6.4.

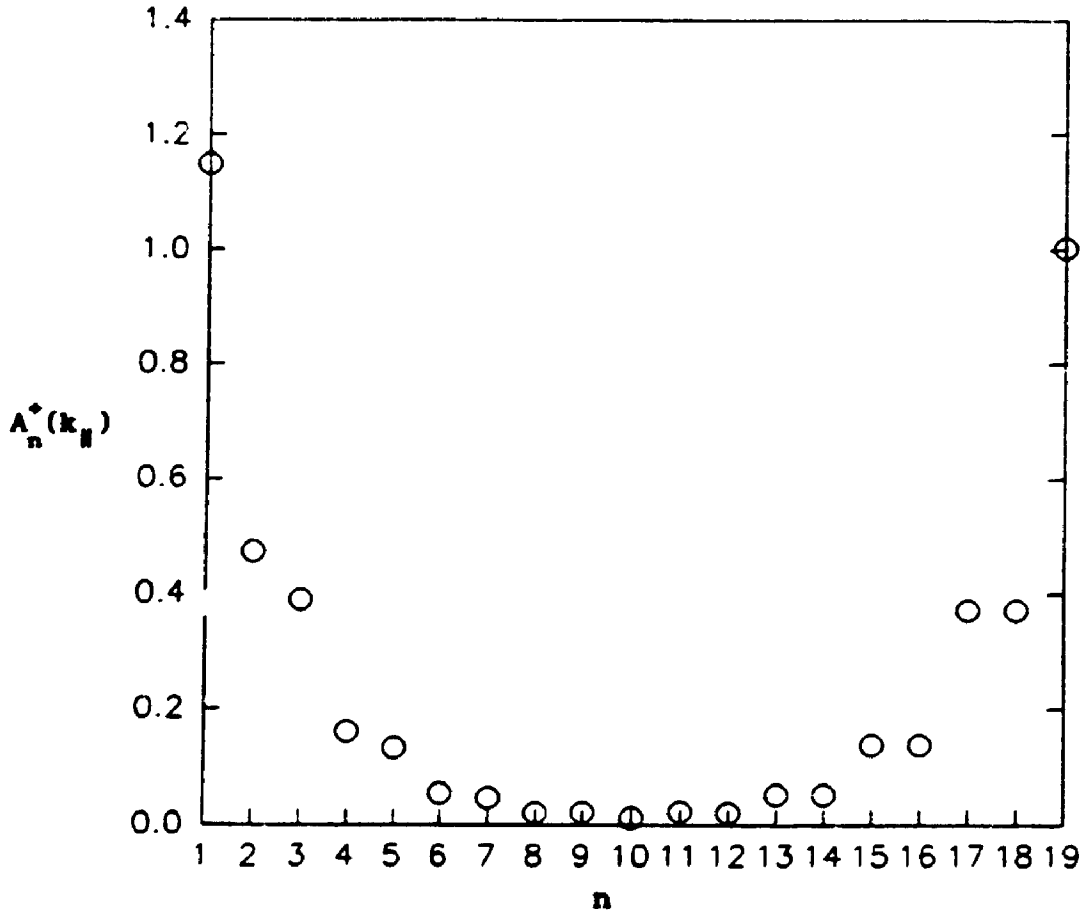

Figure 6.12 $A_n^+(k_\parallel)$ at $k_\parallel = 0$ for surface modes plotted against the layer index n for a case B.2 antiferromagnetic film. Here we have chosen N = 19 and all other parameters as in figure 6.4.

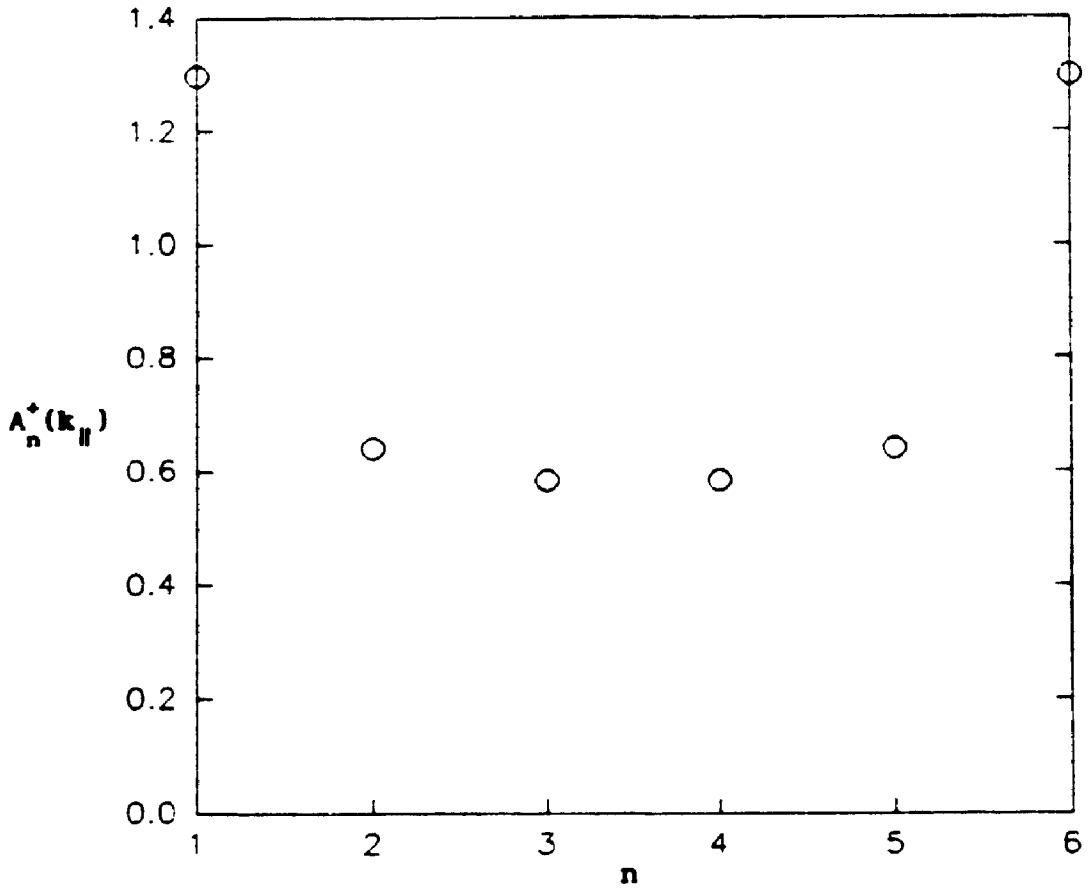

Figure 6.13 $A_n^+(k_{\parallel})$ at $k_{\parallel} = 0$ for surface modes plotted against the layer index n for a case B.1 film with the dispersion relation of figure 6.5.

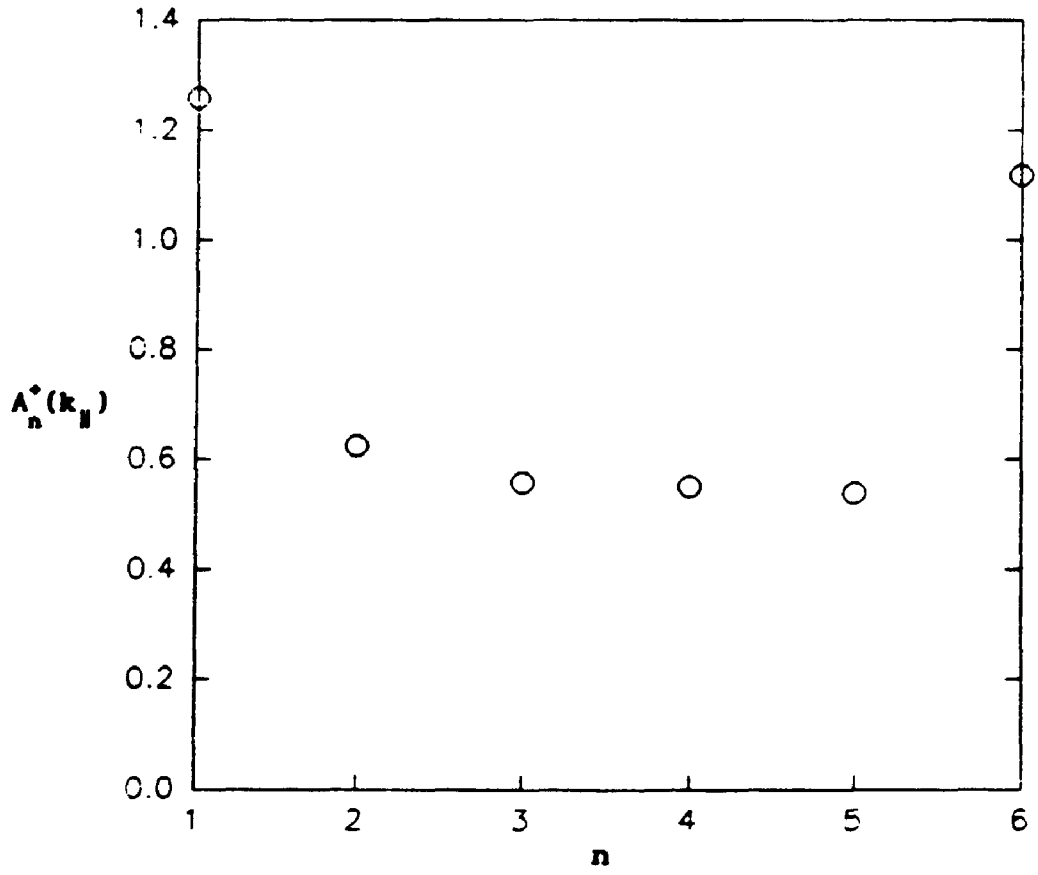

Figure 6.14 $A_n^*(k_{\parallel})$ at $k_{\parallel} = 0$ for surface modes plotted against the layer index n for a case B.2 film with the dispersion relation of figure 6.6.

similar properties as both are associated with the same sublattice while in films with an even number of layers there is instead symmetry between the two sublattices. All of the dispersion relations are symmetric about $\Omega = 0$ for $F_s \neq 0$ and we have used the mean-squared amplitude for surface modes to illustrate the asymmetry in spectral intensities In all cases we recover our results of Chapter 5 in the limit that the number of layers is large. We recover the results of previous work on dispersion relations in uniaxial systems if we take $F_i = 0$. The Green functions for this limiting case represent a generalization of the results of Diep (1991) to arbitrary S and films with an odd number of layers.

The numerical results all refer to the special case in which $D_s = D$ and $J_s = J$. The case of $D_s \neq D$ and $J_s \neq J$ can be accommodated using the more general definition of the surface parameters (δ_A etc.) as in Chapter 5. The Green function results in this chapter may be used to calculate experimentally observable quantities such as the light-scattering cross-section and SWR absorption strength as shown in Chapter 4.

CHAPTER 7

CONCLUSIONS

In this thesis we have presented new results for exchange-dominated linear spin waves in ferromagnetic and antiferromagnetic thin films in which nonuniaxial single-ion anisotropy is either an intrinsic feature of the material or arises as a consequence of lowered local symmetry at surface sites. Our Green function study provides a description of both the frequencies and spectral intensities associated with the spin waves and the relative numbers of surface and bulk modes which occur. We have found both localized surface modes and a set of non-localized quantized bulk modes, all of which have elliptical-precession character as a consequence of the nonuniaxial nature of the systems. Two previous theoretical studies of note will be used as the principal basis for the discussion of what is new in the present work, in terms of both results and methods. Gopalan and Cottam (1990) have considered nonuniaxial anisotropy but in the case of sem -infinite ferromagnetic systems only while Cottam and Kontos (1980) considered ferromagnetic thin films but with uniaxial anisotropy only. We show that the present study is a generalization of these previous ones, encompassing the earlier results for ferromagnets in the appropriate limits and including anisotropic antiferromagnetic systems. Elsewhere in this chapter we consider possible means of experimental verification of our results and finally we suggest some extensions to the present work.

The microscopic Green-function approach we have taken has the advantage

of being applicable throughout the Brillouin zone unlike macroscopic long-wavelength treatments. Our results apply at temperatures well below the critical point where a high degree of long-range order is present and the near-saturation approximation is valid. In Chapter 1 we reviewed basic material on spin waves, as well as theoretical and experimental methods and established the context for the thesis. We introduced the special cases and gave a detailed account of the Hamiltonian we have chosen.

In Chapter 2 we applied the operator equation-of-motion method to the case of ferromagnetic films, finding formal expressions for the dispersion relations which were evaluated numerically for some special cases in Chapter 3. We found the spin-wave dispersion for both the bulk and surface modes to be sensitive to the nonuniaxial anisotropy in the region where $|k_{\parallel}a_0|$ is small. Here the frequencies are generally lower than those corresponding to the uniaxial case calculated by Cottam and Kontos (1980). By setting the nonuniaxial parameter equal to zero we recovered the results of that study. We also showed that a sufficient condition for the appearance of a (weakly localized) surface mode is the surface nonuniaxial parameter F_s being greater in magnitude than the bulk value F (including when F = 0).

A different numerical approach was developed to find, in particular, the bulk dispersion relations in films where the nonuniaxial parameter is non-zero on the surface(s) only. This case requires the location of the roots of a polynomial (of order $\cong$ 2N) in two variables, one of them real

and inside the unit circle, the other complex and on the unit circle. We showed how to deal with this by exploiting the fact that the two variables are not independent, a strategy which should prove helpful in other similar situations, e.g. some of the extensions mentioned below. Although the study by Gopalan and Cottam (1990) of semi-infinite systems led similarly to an expression containing two variables, the *continuum* of bulk modes found there obviated the need for numerical bulk dispersion relation calculations. By allowing the number of layers N in our films to be large we have recovered the surface dispersion relation results of that study.

In Chapter 4 we considered these same ferromagnetic films using the Green function equation-of-motion method from which we determined spin correlation functions and verified that the same dispersion relations as found in Chapters 2 and 3 arise. We demonstrated the use of equal-time correlation functions in finding some layer-dependent magnetic properties. These were the expectation values associated with the square of the amplitude of spin precession for spin waves at a particular value of $|k_{\parallel}a_0|$. In a special case we considered the static magnetization and illustrated the zero-temperature spin deviation with a numerical example. We also illustrated the elliptical nature of the spin precession. In the limits that $N \to \infty$ and/or $F \to 0$ we recovered the results of previous studies. We described how the extraction of the imaginary parts of the analytically continued Green function can be achieved where, unlike the semi-infinite case of Gopalan and Cottam (1990), the poles associated with spin wave frequencies do not appear

explicitly in the denominator. This general approach should also prove useful for some of the suggested extensions mentioned below.

In Chapter 5 we applied a similar Green function method to semi-infinite antiferromagnets with some modifications to accommodate the sublattice structure. We found dispersion relations for the surface modes that were symmetric about $\Omega = 0$ in contrast to the uniaxial case. In the limit that $F \rightarrow 0$ we recovered the results of previous studies on uniaxial systems, e.g. Cottam (1978). We calculated the intensities associated with these modes as a function of layer number and illustrated that a single spin wave mode gives rise to different (elliptical) precessional amplitudes on the two sublattices. We generalized the results to thin films in Chapter 6 for the special case in which nonuniaxial anisotropy is a feature of surface spins only and calculated dispersion relations for surface and quantized bulk modes and the related intensities. For thin films the Green function results in the limiting case of uniaxial anisotropy also represent a generalization of previous work by Diep (1991) on spin 1/2 systems with even numbers of layers.

We have shown that our results may be understood in the context of other theoretical efforts involving simpler systems and in fact constitute a generalization of those studies. Our results could also be evaluated through comparison with experimental observations. To this end it would be of interest to have light scattering experiments performed on thin films of materials which are consistent with the spin Hamiltonian we

have chosen. These experiments should be carried out in a 180° backscattering geometry from one of the surfaces of the film in order to maximize the surface sensitivity. For a specific real material the formal dispersion relations we have found can readily be used to produce numerical data given appropriate experimentally determined constants for the exchange and anisotropy etc. The spin-wave frequencies thus predicted should coincide with the position of the peaks in the measured inelastic light scattering spectrum. A good candidate for such a study would be $CrBr_3$ for which Brillouin light scattering measurements on *bulk* samples are available, dating back to the pioneering work of Sandercock (1974). In this system, where S = 3/2 and T_c = 33 K, the anisotropy parameters F and D are comparable in magnitude and $D/J \cong 0.006$. The hexagonal structure of $CrBr_3$ could be accommodated in the formalism we have developed with a redefinition of some structure factors. Other materials which have bulk nonuniaxial anisotropy and, by virtue of strong magneto-optic coupling are good subjects for light scattering studies, include the antiferromagnets NiO and K_2FeF_4. Bulk exchange and anisotropy parameters are provided by inelastic neutron scattering experiments by Hutchings and Samuelson (1971) for NiO and Thurlings *et al* (1980) for K_2FeF_4. Numerical results relating to the Fe (110) films, in which the anisotropy is cubic in the bulk and nonuniaxial on the surfaces, could also be generated using, for example, the anisotropy constants listed by Heinrich and Cochran (1993) for ultrathin Fe films grown on various substrates. In these films the orientation of the magnetization relative to the surface is seen to depend on the film thickness as a result of surface anisotropy effects (e.g. see Prinz *et*

al 1982, Gradmann *et al* 1986). It would therefore be of interest to consider the situation in which the magnetization is parallel to the surface (as described in Appendix I) as well as perpendicular to the surface.

Further comparisons with experimental measurements could be based on SWR data, in which case the dispersion curves near the zone centre should coincide with the frequencies at which resonant absorption occurs. With an improvement in surface sensitivity, inelastic neutron scattering could (in principle) provide experimental data for spin-wave energies throughout the Brillouin zone. In addition, the cross-sections for light scattering or the absorption strength for SWR could be calculated for the specific real materials as shown in Chapter 4. Finally, the layer dependence of the static magnetization could be verified experimentally by, for example, electron or positron scattering (Gidley *et al* 1982) or neutron scattering (Felcher 1981, 1993).

Straightforward extensions to this work include some of those mentioned in Appendix I, e.g. considering the nonuniaxial Dzialoshinski-Moriya exchange interaction. Further numerical results could be produced, particularly in the antiferromagnetic thin film case where the anisotropy is nonuniaxial throughout the system. Another possibility would be the production of numerical examples of the above-mentioned light scattering cross-sections or SWR absorptions, ideally in some realistic case for which experimental data could readily be produced. A more involved extension would be to consider higher temperatures where

the linear spin-wave approximation does not hold. This could be done using, perhaps, a diagrammatic perturbation method for calculating the Green functions. Our present results would then compare with those found in the first-order of that method. Dipolar interactions could be included in our Hamiltonian in order to compare with results of experiments aimed at very small values of $|k_{\parallel} a_0|$.

For the antiferromagnetic films it would be of interest to include larger applied fields and investigate the spin-flop phase as was done in the case of (effectively) infinite systems by Cottam and Latiff-Awang (1979) (b). In particular, it would be a straightforward matter to examine the dependence of the critical field for this transition, H_{SF}, on the anisotropy parameters and film thickness etc. by looking for field-induced instabilities in the spin-wave spectrum. This procedure resembles that we have used in the case of ferromagnetic films in which instabilities provoked by increasing the nonuniaxial parameter were linked to ground state reordering. In the examples we have studied the lowest-lying spin excitations have been acoustic surface modes having energies determined by a number of factors, the film thickness and the value of the nonuniaxial parameter being of particular interest here. The field required to reduce the energies to zero and bring about the spin-flop transition will therefore also be dependent on these quantities.

Extensions could also be made to some other materials or structures. For instance, the calculations in Chapters 5 and 6 could be extended to

include *canted* antiferromagnetic systems, such as NiF_2, in which the nonuniaxial parameter has a different sign on each sublattice. The approach taken with the antiferromagnets could also be applied relatively straightforwardly to *ferrimagnets* in which the two sublattices are occupied by spins of different species. The basic methods described here could be used in the extension to bilayers, multilayers and superlattices for which the results of the present study could compare in the limit that the separation between magnetic layers is large. The operator method has recently been applied to find dispersion relations in nonuniaxial superlattices (Albuquerque and Cottam 1994), whereas a Green function treatment would allow the calculation of spin correlation functions, as we have shown here. Finally, it would be of interest to incorporate the effects of surface defects, such as impurities or reconstruction, which may occur in experimental situations.

APPENDIX I

Extensions to the Basic Model

Throughout the discussion of ferromagnetic films (Chapters 2 through 4) the formalism has been described for the case of a simple cubic (001) crystal with nearest-neighbour exchange interactions and perpendicular magnetization. It has been stated several times in the text that modifications to accommodate some other systems and other assumptions are relatively straightforward. In this Appendix we describe how other cubic crystal symmetries, surface orientations and magnetization directions could be dealt with, how next-nearest-neighbour interactions could be included and how perturbation of the exchange or anisotropy parameters on layers adjacent to the surfaces could be considered. We also consider the possibilty of anisotropic exchange. These modifications may be important in applications to specific materials and in many cases they may affect the number of surface spin-wave branches (e.g. see Wolfram and DeWames 1972).

Other Cubic Crystal Symmetries

We have so far considered simple cubic symmetry with a (001) surface. If we consider BCC or FCC crystals or even SC with a different choice of surface (e.g. (011)) the effect is seen in the structure factors $u_n(\mathbf{k}_\parallel)$ and $v_n(\mathbf{k}_\parallel)$ defined in (2.2.9). A generalized definition of $\gamma(\mathbf{k}_\parallel)$ in (2.2.10) can be made (following Kontos 1985) with separate functions $\gamma_\parallel(\mathbf{k}_\parallel)$ and $\gamma_\perp(\mathbf{k}_\parallel)$ denoting the cases of summations over in-plane

neighbours and out-of-plane neighbours respectively. Assuming that the interactions are between nearest neighbours only and satisfy (1.2.2) we have

$$u_n(\mathbf{k}_\parallel) = \begin{cases} J_S\gamma_\parallel(\mathbf{k}_\parallel) & \text{if } n = 1 \\ J\gamma_\parallel(\mathbf{k}_\parallel) & \text{if } n = 2,..N-1 \\ J_S,\gamma_\parallel(\mathbf{k}_\parallel) & \text{if } n = N \end{cases} \qquad \text{(AI.1)}$$

and

$$v_n(\mathbf{k}_\parallel) = \begin{cases} J\gamma_\perp(\mathbf{k}_\parallel) & \text{if } n = 1,2,..N-1 \\ 0 & \text{if } n = N \end{cases} \qquad \text{(AI.2)}$$

where the exact form of the structure factors $\gamma_\parallel(\mathbf{k}_\parallel)$ and $\gamma_\perp(\mathbf{k}_\parallel)$ are summarized in Table AI.1 for various cubic crystals of lattice constant a_o (Kontos 1985). The formal results for the dispersion relation expressions described in Chapter 2 are unaffected by the choice of lattice and it is necessary only to substitute the appropriate $u_n(\mathbf{k}_\parallel)$ and $v_n(\mathbf{k}_\parallel)$.

In the case of antiferromagnetic systems the presence of two sublattices complicates the extension to systems with other symmetries. As mentioned in Chapter 5 it may be necessary to define different Green functions, if for example, each layer contains spins of both sublattices. It is therefore simpler to treat different lattice types on an individual basis.

Parallel Magnetization

The magnetization may be taken to be in the plane of the film (rather than perpendicular as we have assumed in the main text) with little difference to the the formalism. This is due to the isotropic nature of the exchange Hamiltonian which involves the scalar product $\mathbf{S}_i \cdot \mathbf{S}_j$. By

contrast, this is not the case for magnetostatic modes (see e.g. Wolfram and DeWames 1972) which have the lower symmetry characteristic of dipole-dipole interactions. If the applied field and the preferred axis for the magnetocrystalline terms are assumed to be in-plane then all that is needed is a simple redefinition of the coordinate axes relative to the film surfaces. For example, we could use z and x axes in the plane of the surface and the y axis normal to it.

Next-Nearest-Neighbour Exchange

The possibility of next-nearest-neighbour exchange also leads to a different evaluation of the factors $u(\mathbf{k}_{\parallel})$, $v(\mathbf{k}_{\parallel})$ and $\gamma(\mathbf{k}_{\parallel})$. If we consider an SC (001) structure and assume that the exchange constant is modified only for spin pairs wherein both spins are in a surface layer then we have

$$J_{ij}^{nn} = \begin{cases} J_s & \text{if both spins are in layer 1} \\ J_{s'} & \text{if both spins are in layer N} \\ J & \text{otherwise} \end{cases} \qquad \text{(AI.3)}$$

$$J_{ij}^{nnn} = \begin{cases} j_s & \text{if both spins are in layer 1} \\ j_{s'} & \text{if both spins are in layer N} \\ j & \text{otherwise.} \end{cases} \qquad \text{(AI.4)}$$

We find

$$u_n(\mathbf{k}_{\parallel}) = \begin{cases} J_s\gamma_{\parallel}(\mathbf{k}_{\parallel}) + j_s\gamma'_{\parallel}(\mathbf{k}_{\parallel}) & \text{if } n = 1 \\ J\gamma_{\parallel}(\mathbf{k}_{\parallel}) + j\gamma'_{\parallel}(\mathbf{k}_{\parallel}) & \text{if } n = 2,..N-1 \\ J_{s'}\gamma_{\parallel}(\mathbf{k}_{\parallel}) + j_{s'}\gamma'_{\parallel}(\mathbf{k}_{\parallel}) & \text{if } n = N \end{cases} \qquad \text{(AI.5)}$$

and

$$v_n(\mathbf{k}_{\parallel}) = \begin{cases} J\gamma_{\perp}(\mathbf{k}_{\parallel}) + j\gamma'_{\perp}(\mathbf{k}_{\parallel}) & \text{if } n = 1,2,..N \\ 0 & \text{if } n = N \end{cases} \qquad \text{(AI.6)}$$

where $\gamma_{\parallel}(\mathbf{k}_{\parallel})$ and $\gamma_{\perp}(\mathbf{k}_{\parallel})$ are given in Table AI.1 and

$$\gamma'_{\parallel}(\mathbf{k}_{\parallel}) = 4\cos(k_x a_o)\cos(k_y a_o)$$
$$\gamma'_{\perp}(\mathbf{k}_{\parallel}) = \gamma_{\parallel}(\mathbf{k}_{\parallel}). \qquad \text{(AI.7)}$$

As in the case of alternate choices of crystal lattice this generalization does not lead to any further complexity on the formalism of Chapter 2.

Exchange Parameter Perturbed in Near-Surface Layers

If we assume nearest-neighbour exchange only but allow that the interaction may be perturbed if even one spin is in the surface layer then we find additional terms in the matrix $\underline{\Delta}$. For symmetric SC (001) films we have

$$J_{ij} = \begin{cases} J_1 & \text{if i and j are both in layer 1 or N} \\ J_2 & \text{if i OR j is in layer 1 or N} \\ J & \text{otherwise} \end{cases} \qquad \text{(AI.8)}$$

Here we find

$$u_n(\mathbf{k}_{\parallel}) = \begin{cases} J_1\gamma_{\parallel}(\mathbf{k}_{\parallel}) & \text{if } n = 1 \\ J\gamma_{\parallel}(\mathbf{k}_{\parallel}) & \text{if } n = 2,..N-1 \\ J_1\gamma_{\parallel}(\mathbf{k}_{\parallel}) & \text{if } n = N \end{cases} \qquad \text{(AI.9)}$$

and

$$v_n(\mathbf{k}_{\parallel}) = \begin{cases} J_2\gamma_{\perp}(\mathbf{k}_{\parallel}) & \text{if } n = 1 \text{ OR } N-1 \\ J\gamma_{\perp}(\mathbf{k}_{\parallel}) & \text{if } n = 2,..N-2 \\ 0 & \text{if } n = N \end{cases} \qquad \text{(AI.10)}$$

The factors $\gamma_{\parallel}(\mathbf{k}_{\parallel})$ and $\gamma_{\perp}(\mathbf{k}_{\parallel})$ are as in Table AI.1. We then find, instead of (2.2.18),

$$\underline{\Delta} = \begin{bmatrix} \Delta_1 & \Delta_3 & & & 0 \\ \Delta_3 & \Delta_2 & \ddots & & \\ \vdots & \vdots & & \vdots & \vdots \\ & 0 & & \Delta_2 & \Delta_3 \\ & & & \Delta_3 & \Delta_1 \end{bmatrix} \qquad \text{(AI.11)}$$

where the quantities Δ_1, Δ_2 and Δ_3 depend on the difference between the perturbed surface parameters and the bulk values. The implications of this for evaluating the Green functions etc. are easy to see, for example in case A.1 the matrix $\underline{P}$ defined in (2.3.8) will have a different block form. The determinant and inverse of this matrix, necessary for evaluating the dispersion relations and Green functions, will be slightly more complicated.

Anisotropy Parameters Perturbed on Near-Surface Layers

If we allow the uniaxial parameter to be perturbed on layers 2 and N-1 as well as 1 and N we find additional diagonal terms in $\underline{\Delta}$. For the case of symmetric films we assume

$$D_i = \begin{cases} D_1 & \text{if i is in layer 1 or N} \\ D_2 & \text{if i is in layer 2 or N-1} \\ D & \text{otherwise} \end{cases} \qquad \text{(AI.12)}$$

and therefore

0

$$\underline{\Delta} = \begin{bmatrix} \Delta_1 & 0 & & & 0 \\ 0 & \Delta_2 & \ddots & & \\ \vdots & \vdots & & \vdots & \vdots \\ & 0 & & \Delta_2 & 0 \\ & & & 0 & \Delta_1 \end{bmatrix} \qquad \text{(AI.13)}$$

where

$$\Delta_2 = 2D(D_2/D - 1)/J. \qquad \text{(AI.14)}$$

As in the case of the exchange parameters being perturbed on

near-surface layers the inclusion of these diagonal terms will complicate the evaluation of the determinant and numerical extraction of frequencies etc.

Some different assumptions concerning the nonuniaxial parameters are straightforwardly incorporated. Special cases A and B have been defined to distinguish between two different situations involving the nonuniaxial anisotropy and the slightly different formalism is required to deal with them. If for example, the nonuniaxial parameter is perturbed from its bulk value on layers 2 and N-1 as well as 1 and N) it could be dealt with within the same formalism as case A.2 by a redefinition of $\underline{\nu}$ in (2.3.1) which would lead to a different (and probably more complicated) version of (2.3.20) through (2.3.25).

Anisotropic Exchange

The anisotropic exchange Hamiltonian of (1.2.2) (Dzialoshinski 1958, Moriya 1960) involves products of the operators S^+, S^- and S^z at different sites. After the Holstein-Primakoff transformation is made as before, there are bilinear terms such as $b_i b_j$ and $b_i^\dagger b_j^\dagger$ with $i \neq j$. These are similar to those appearing in the nonuniaxial part of the anisotropy Hamiltonian (2.1.6) where the operators instead refer to the same site. The Dzialoshinski-Moriya interaction therefore gives rise to nonuniaxial anisotropy effects (e.g. elliptical precession of spins). It is easily treated within the same formalism that we have used. For example, when a 2-D Fourier transform is carried out as in Section 2.2, coupled equations of the same form as (2.2.12) are obtained. However, the definition of the matrix $\underline{f}$ would be modified.

TABLE AI.1 Structure Factors

structure	$\gamma_{\parallel}(\mathbf{k})$	$\gamma_{\perp}(\mathbf{k})$
SC (001)	$2[\cos(k_x a_o)+\cos(k_y a_o)]$	1
SC (011)	$2\cos(k_x a_o)$	$2\cos(k_y a_o/\sqrt{2})$
SC (111)	0	$\exp[-i(k_x/\sqrt{6} + k_y/\sqrt{2})a_o]$ + $\exp[ik_x a_o\sqrt{(2/3)}]$
BCC (001)	0	$4\cos(k_x a_o/2)\cos(k_y a_o/2)$
BCC (011)	$4\cos(k_x a_o/2)\cos(k_y a_o/\sqrt{2})$	$2\cos(k_x a_o/2)$
FCC (001)	$4\cos(k_x a_o/2)\cos(k_y a_o/2)$	$2\cos(k_x a_o/2)+2\cos(k_y a_o/2)$
FCC (111)	$2\cos(k_y a_o/\sqrt{2})$ + $\cos[(k_x/\sqrt{3}+k_y)a_o/2\sqrt{2}]$ + $\cos[(k_x/\sqrt{3}-k_y)a_o/2\sqrt{2}]$	$\exp[i(k_x/2\sqrt{6}+k_y/2\sqrt{2})a_o]$ + $\exp[i(k_x/2\sqrt{6}-k_y/2\sqrt{2})a_o]$

APPENDIX II

The Holstein-Primakoff Transformation of the Anisotropy Hamiltonian

In Chapter 2 we rewrote the ferromagnetic Hamiltonian in terms of boson creation and annihilation operators using the method of Holstein and Primakoff (1940). We made the near-saturation approximation to arrive at the Hamiltonian of (2.1.6) which is quadratic in the boson operators and introduced the spin-dependent quantities η and η' in $\mathcal{H}_A$. Here we will discuss the procedure in more detail. First we use the identities in (2.1.1) to rewrite the Hamiltonian, defined in (1.2.1), as

$$\mathcal{H}_H = -\frac{1}{2}\sum_{ij} J_{ij}\,(S_i^- S_j^+ + S_i^z S_j^z) - g\mu_B H_0 \sum_i S_i^z$$

$$\mathcal{H}_A = -\sum_i D_i (S_i^z)^2 - \frac{1}{2}\sum_i F_i[(S_i^+)^2 + (S_i^-)^2]. \qquad \text{(AII.1)}$$

The spin operators can be written in terms of the boson operators b_i and $b_i^\dagger$ according to (2.1.2). Upon making the near-saturation approximation ($\langle S^z\rangle \cong S$) we expand (2.1.2) and find (2.1.4). For the Heisenberg part of the Hamiltonian the procedure is straightforward. We substitute the expressions for S^+, S^- and S^z into $\mathcal{H}_H$ and find,

$$\mathcal{H}_H \cong -S\sum_{ij} J_{ij}(b_j^\dagger b_i - b_i^\dagger b_i) + g\mu_B H_0 \sum_i b_i^\dagger b_i. \qquad \text{(AII.2)}$$

Here we have simply neglected constant terms and those of quartic or higher order in the boson operators.

The procedure for the terms in the anisotropy Hamiltonian is slightly more involved. Walker (1963) and Hutchings *et al* (1970) argue that certain matrix elements should be preserved under the transformation. For example we see that the factors η and η' arise if this criterion is applied to the operators for the uniaxial and nonuniaxial terms

respectively. The matrix elements of the operators $1/2[(S_i^+)^2 + (S_i^-)^2]$ and $S\eta'[b_i^\dagger b_i^\dagger + b_i b_i]$ are found to be the same for some, but not all spin states. Despite the flaw, this scheme is entirely adequate for our purposes.

We can also demonstrate how these factors arise as a consequence of the expansion of the definitions in (2.1.2). For the uniaxial part of the anisotropy Hamiltonian we have

$$\mathcal{H}_{A,U} = -\sum_i D_i(S^2 - 2Sb_i^\dagger b_i + b_i^\dagger b_i b_i^\dagger b_i). \qquad \text{(AII.3)}$$

The commutation relations of the boson operators (2.1.3) allow us to write $b_i b_i^\dagger$ as $(1 + b_i^\dagger b_i)$ and hence

$$\begin{aligned}\mathcal{H}_{A,U} &= -\sum_i D_i(S^2 - 2Sb_i^\dagger b_i + b_i^\dagger(1 + b_i^\dagger b_i)b_i) \\ &\cong 2S\sum_i D_i b_i^\dagger b_i(1 - 1/2S) \qquad \text{(AII.4)}\end{aligned}$$

where we have again neglected constant and higher order terms. The factor $1 - 1/2S$ is labelled η. For the nonuniaxial term we can write

$$\begin{aligned}\mathcal{H}_{A,N} = -S\sum_i F_i\Big[&b_i b_i - b_i b_i^\dagger b_i b_i/4S - b_i^\dagger b_i b_i b_i/4S - b_i b_i^\dagger b_i b_i^\dagger b_i b_i/32S^2 \ldots \\ &+ b_i^\dagger b_i^\dagger - b_i^\dagger b_i^\dagger b_i^\dagger b_i/4S - b_i^\dagger b_i^\dagger b_i b_i^\dagger/4S - b_i^\dagger b_i^\dagger b_i b_i^\dagger b_i b_i^\dagger/32S^2 \ldots\Big]. \qquad \text{(AII.5)}\end{aligned}$$

Again we write $b_i b_i^\dagger$ as $(1 + b_i^\dagger b_i)$ and find

$$\begin{aligned}\mathcal{H}_{A,N} = -S\sum_i F_i\Big[&b_i b_i - (1 + b_i^\dagger b_i)b_i b_i/4S - b_i^\dagger b_i b_i b_i/4S \\ &- (1 + b_i^\dagger b_i)(1 + b_i^\dagger b_i)b_i b_i/32S^2 \ldots + b_i^\dagger b_i^\dagger - b_i^\dagger b_i^\dagger b_i^\dagger b_i/4S \\ &- b_i^\dagger b_i^\dagger(1 + b_i^\dagger b_i)/4S - b_i^\dagger b_i^\dagger(1 + b_i^\dagger b_i)(1 + b_i^\dagger b_i)/32S^2 \ldots\Big] \qquad \text{(AII.6)}\end{aligned}$$

and so on. We neglect higher order terms in the operators to write

$$\mathcal{H}_{A,N} \cong - S \sum_i F_i \Big[b_i b_i (1 - 1/4S - 1/32S^2 \ldots) + b_i^\dagger b_i^\dagger (1 - 1/4S - 1/32S^2 \ldots) \Big]. \qquad \text{(AII.7)}$$

We note that $(1 - 1/4S - 1/32S^2 \ldots) \cong (1 - 1/2S)^{1/2} = \eta^{1/2} \equiv \eta'$. We have now the Hamiltonian as written in (2.1.6).

APPENDIX III

Some Relationships Involving the Complex Variables x_1 and x_2

We recall that the complex variables x_1 and x_2 are defined by (2.3.7) for case A or (2.4.5) for case B. In either case $|x_1| \leq 1$ and $|x_2| \leq 1$ and all of the parameters upon which they depend are real. We see that (2.4.16)

$$x_1 + x_1^{-1} + x_2 + x_2^{-2} = 2a. \qquad \text{(AIII.1)}$$

applies for either case A or case B. If both x_1 and x_2 are real then the left hand side of (AIII.3) is real and its value is unrestricted. Therefore, regardless of the value of a, for any real x_1 we can use (2.3.7) or (2.4.5) to find a real x_2 which satisfies both (AIII.1) and the localization condition ($-1 < x_2 < 1$). Any combination of x_1 and x_2 (e.g. x_1x_2 or $x_1 + x_2$) will also be real and the spin waves will be localized as shown below.

If on the other hand x_1 and x_2 are both complex and written as $\exp(i\theta)$ and $\exp(i\varphi)$ respectively then (AIII.1) can be written as

$$2\cos(\theta) + 2\cos(\varphi) = 2a. \qquad \text{(AIII.2)}$$

The left hand side of which is real but restricted to the interval $[-4,4]$ so that no solution is possible for $|a| > 2$. However this real variable, defined in (2.2.15), is not physically restricted and for many of the examples we have considered we have $|a| > 2$. Therefore we must have $x_1 = \exp(i\theta)$ and x_2 real (or vice versa). The left hand side is then real and unrestricted in magnitude. In addition, the quantities x_1x_2 etc. are complex and the spin waves will be non-localized as shown below.

Non-localized or bulk spin waves have spatial dependence terms which have wavelike dependence on the z coordinate. The localization of surface spin waves is due to the presence of spatial dependence terms which are not wave-like but exponentially decaying in the z direction. In Chapter 4 it is seen that the Green functions contains various combinations of x_1 and x_2 through the matrices $\underline{A}_1^{-1}$ etc. When x_1 and x_2 are both real they may be written as $x_1 = \exp(-\lambda_1 z)$ and $x_2 = \exp(-\lambda_2 z)$ as explained in Chapter 4. A combination of these variables such as $x_1 x_2$ may then be written as $\exp(-[\lambda_1 + \lambda_2]z)$ which again shows the exponential decay behaviour characteristic of surface modes. In contrast, for bulk modes we have seen that we may have $x_1 = \exp(-ik_z z)$ and $x_2 = \exp(-\lambda z)$ (or vice versa) so that the wavelike behaviour associated with x_1 will be present in combinations of x_1 and x_2.

The method of Gopalan and Cottam (1990) for the semi-infinite ferromagnet exploits the relationship between x_1 and x_2. Here we discuss the generalization of this method to thin films which have non-zero nonuniaxial parameters on the surfaces only (case B.1). We consider the case of N = 3 as an example. The approach is to define a complex variable α such that

$$\alpha = x_1 x_2 \tag{AIII.3}$$

and using (2.4.5)

$$x_1 + x_2 = 2a\alpha / (1 + \alpha). \tag{AIII.4}$$

We then rewrite (2.4.11) in terms of α. For N = 3 we have

$$\begin{aligned} y^{B1}_{1,2}(x_1,x_2) = {} & [x_1x_2 + (x_1x_2)^3 \pm (x_1x_2)(x_1^2 + x_2^2)](\Delta^2 - f_s^2) \\ & + [(x_1 + x_2)(1 + (x_1x_2)^3) \pm (x_1^3 + x_2^3)(1 + x_1x_2)]\Delta \\ & + 1 + (x_1x_2)^4 \pm (x_1^3 + x_2^3). \end{aligned} \tag{AIII.5}$$

Using the following relationships, we rewrite this expression in terms of x_1x_2 and $x_1 + x_2$ (and hence in terms of α):

$$(x_1^2 + x_2^2) = (x_1 + x_2)^2 - 2x_1x_2 = \left(\frac{2ay}{(1 + y)}\right)^2 - 2\alpha \qquad \text{(AIII.6)}$$

$$\begin{aligned}(x_1^3 + x_2^3) &= (x_1 + x_2)^3 - 3\, x_1x_2\, (x_1^2 + x_2^2) - 6x_1x_2 \\ &= (x_1 + x_2)^3 - 3\, x_1x_2 \left[(x_1 + x_2)^2 - 2x_1x_2\right] - 6x_1x_2 \\ &= \left(\frac{2a\alpha}{(1 + \alpha)}\right)^3 - 3\alpha\left[\left(\frac{2a\alpha}{(1 + \alpha)}\right)^2 - 2\alpha\right] - 6\alpha. \qquad \text{(AIII.7)}\end{aligned}$$

We can then write (AIII.5) in terms of α. To find the surface modes we may look for zeroes on the interval $-1 < \alpha < 1$. The same approach can be used for thicker films.

REFERENCES

A.I. Akhiezer, V.G. Bar'Yakhtar, and S.V. Peletminskii, *Spin Waves* (North-Holland, Amsterdam, 1968).

E.L. Albuquerque and M.G. Cottam, Solid State Comm. **89**, 249 (1994).

P.W. Anderson in *Magnetism* Vol. 1 ed. G.T. Rado and M. Suhl (Academic Press, New York, 1963).

S.D. Bader, Ultramicroscopy **47**, 355 (1992).

M.N. Baibich, J.M. Broto, A. Fert, F. Nguyen Van Dau, F. Petroff, P. Eitenne, G. Creuzet, A. Friedrich, and J. Chazelas, Phys. Rev. Lett. **61**, 2472 (1988).

U. Balucani, M.G. Pini, A. Rettori, and V. Tognetti, J. Phys. C **13**, 3895 (1980). (a)

U. Balucani, M.G. Pini, and V. Tognetti, J. Phys. C **13**, 2925 (1980). (b)

G. Binasch, P. Grünberg, F Saurenbach, and W. Zinn, Phys. Rev. B. **39**, 4828 (1989).

J.S. Blakemore, *Solid State Physics* (Cambridge U Press, Cambridge, 1985).

B. Bleaney and K.W.H. Stevens, Rep. Prog. Phys. **16**, 108 (1953).

F. Bloch, Z. Phys. **61**, 206 (1930).

A.S. Borovik-Romanov and S.K. Sinha, eds., *Spin Waves and Magnetic Excitations* (North-Holland, Amsterdam, 1988).

Joseph Callaway, *Quantum Theory of the Solid State* (2nd ed.) (Academic Press Inc., San Diego, 1991).

R.E. Camley, T.S. Rahman, and D.L. Mills, Phys. Rev. B **23**, 1226 (1981).

W.J. Caspers, *Spin Systems* (World Scientific, Singapore, 1989).

Claude Cohen-Tannoudji, Bernard Diu, and Franck Laloë, *Quantum Mechanics* (John Wiley and Sons, New York, 1977).

M.G. Cottam, J. Phys. C **9**, 2121 (1976).

M.G. Cottam, J. Phys. C **11**, 151 (1978).

M.G. Cottam, ed., *Linear and Nonlinear Spin Waves in Magnetic Films and Superlatices* (World Scientific, Singapore, 1994).

M.G. Cottam and A. Latiff Awang, J. Phys. C **10**, 3673 (1977).

M.G. Cottam and A. Latiff Awang, J. Phys. C **12**, 105 (1979).(a)

M.G. Cottam and A. Latiff Awang, J. Phys. C **12**, 121 (1979).(b)

M.G. Cottam and D.E. Kontos, J. Phys. C **13**, 2945 (1980).

M.G. Cottam and D.J. Lockwood, *Light Scattering in Magnetic Solids* (Wiley, New York, 1986).

M.G. Cottam and D.R. Tilley, *Introduction to Surface and Superlattice Excitations* (Cambridge University Press, Cambridge, 1989).

M.G. Cottam and A. Slavin, in *Linear and Nonlinear Spin Waves in Magnetic Films and Superlatices* ed. M.G. Cottam (World Scientific, Singapore, 1994).

L.J. De Jongh and A.R. Miedema, Adv. Phys. **23**, 1 (1974).

S. Demokritov and E. Tsymbal, J. Phys. Condens. Matter **6**, 7145 (1994).

R.E. DeWames and T. Wolfram, Phys. Rev. **185**, 720 (1969).

H.T. Diep, Phys. Rev. B **43**, 8509 (1991).

L. Dobrzynski and D.L. Mills, Phys. Rev. **186**, 538 (1969).

J. R. Dutcher, in *Linear and Nonlinear Spin Waves in Magnetic Films and Superlatices* ed. M.G. Cottam (World Scientific, Singapore, 1994).

I.E. Dzialoshinski, J. Phys. Chem. Solids **4**, 241 (1958).

L.M. Falicov, Daniel T. Pierce, S.D. Bader, R. Gronsky, Kristl B. Hathaway, Herbert J. Hopster, David N. Lambeth, S.S.P. Parkin, Gary Prinz, Myron Salamon, Ivan K. Schuller, and R.H. Victora, J. Mater. Res. **5**, 1299 (1990).

G.P. Felcher, Phys. Rev. B **24**, 1595 (1981).

G.P. Felcher, in *Dynamical Phenomena at Surfaces, Interfaces and Superlattices* eds. F. Nizzoli, K.-H. Rider, and R.F. Willis (Springer, Berlin, 1985).

G.P. Felcher, Physica B **192**, 137 (1993).

B.N. Filipov, Soviet Physics-Solid State vol **9** no. **5**, 1048 (1967).

Sudha Gopalan and M.G. Cottam, Phys. Rev. B **42**, 624 (1990).

D.W. Gidley, A.R. Koymen, and T.W. Capehart, Phys. Rev. Lett. **49**, 1779 (1982).

U. Gradmann, J. Korecki, and G. Waller, Appl. Phys. A **39**, 101 (1986).

U. Gradmann, J. Magn. Magn. Mat. **54-57**, 733 (1986).

W. Heisenberg, Z. Phys. **49**, 619 (1928).

G. Heller and H.A. Kramers, Proc. Roy. Soc. **37**, 378 (1934).

B. Heinrich and J.F. Cochran, Adv. Phys. **42**, 523 (1993).

C. Herring, in *Magnetism* Vol. 4 ed. G.T. Rado and M. Suhl (Academic Press, New York, 1966).

T. Holstein and H. Primakoff, Phys. Rev. **58**, 1098 (1940).

M.T. Hutchings, M.F. Thorpe, R.J. Birgeneau, P.A. Fleury, and H.J. Guggenheim, Phys. Rev. B **2**, 1362 (1970).

M.T. Hutchings and E.J Samuelson, Solid St. Commun. **9**, 1011 (1971).

F. Keffer, H. Kaplan, and Y. Yafet, Am. J. Phys. **21**, 250 (1953).

F. Keffer, in *Handbuch der Physik* Vol. 18 ed. H.P.J. Wijn (Springer, Berlin, 1966).

V.N. Kitaev, M.P. Kaschenko, and L.V. Kurbatov. Sov. Phys. **15**, 1530 (1974).

C. Kittel, Phys. Rev. **110**, 1295 (1958)

C. Kittel, *Quantum Theory of Solids* (Second Revised Printing) (John Wiley and Sons, New York, 1987).

Dimosthenis Kontos, *Microscopic Theory of Spin Wave Dynamics in Ferromagnetic Films* Ph.D. Thesis, University of Essex, 1983.

D. Kontos, Phys. Stat. Sol. (b) **149**, 1 (1985).

J.C.S. Lévy, Surf. Sci. Rep. **1**, 39 (1981).

S.W. Lovesey, *Theory of Neutron Scattering from Condensed Matter Vol.2* (Clarendon Press, Oxford, 1984).

W. Marshall and S.W. Lovesey *Theory of Thermal Neutron Scattering* (Clarendon Press, Oxford, 1971).

D.C. Mattis, *The Theory of Magnetism I* (Springer-Verlag, Berlin, 1981)

D.L. Mills, Phys. Rev. B **40**, 11153 (1989).

T. Moriya, Phys. Rev. **120**, 91 (1960).

R.C. Moul and M.G. Cottam, J. Phys. C. **16**, 1323 (1983).

L. Néel, J. Phys. Radium **15**, 225 (1954).

W.E. Parry, *The Many-Body Problem* (Clarendon Press, Oxford, 1973).

T.G. Phillips and H.M. Rosenberg, Rep. Prog. Phys. **29**, 285 (1966).

Physics Today, April 1995.

G.A. Prinz, G.T. Rado, and J.J. Krebs, J. Appl. Phys. **53**, 2087 (1982).

G.A. Prinz, Ultramicroscopy **47**, 346 (1992).

Proceedings of the Conference on Neutrons and X-rays in Magnetism, Physica B **192** (1993).

H. Puszkarski, Acta Physica Polonica **A38**, 217 (1970).

H. Puszkarski, Acta Physica Polonica **A38**, 899 (1970).

H. Puszkarski, Phys. Stat. Sol. (b) **50**, 87 (1972).

H. Puszkarski, Prog. Surf. Sci. **9**, 191 (1979).

G.T. Rado Phys. Rev. B **26**, 295 (1982).

G.T. Rado, Phys. Rev. B **40**, 407 (1989).

G. Rickayzen, *Green's Functions and Condensed Matter* (Academic Press, London, 1980).

J.R. Sandercock, Solid St. Commun. **15**, 1719 (1974).

J.S. Smart, *Effective Field Theories of Magnetism* (W.B. Saunders, Philadelphia, 1966).

K.W.H. Stevens, in *Magnetism* Vol. 1 ed. G.T. Rado and M. Suhl (Academic Press, New York, 1963).

M.P.H. Thurlings, H.W. De Wijn, and E. Frikkee, J. Magn. & Magn. Mater. **15-18**, 369 (1980).

J.H. Van Vleck, Phys. Rev. **52**, 1178 (1937).

R.F. Wallis, A.A. Maradudin, I.P. Iapatova, and A.A. Klochikin, Solid State Commun. **5**, 89 (1967).

Nelson Wax, *Selected Papers on Noise and Stochastic Processes* (Dover, New York, 1954).

P. Weiss, J. Phys. **6** 661 (1907).

D. Wagner, *Introduction to the Theory of Magnetism* (Pergamon, Oxford, 1972).

L.R. Walker, in *Magnetism* Vol. 1 ed. G.T. Rado and M. Suhl (Academic Press, New York, 1963).

T. Wolfram and R.E. DeWames, Prog. Surf. Sci. **2**, 233 (1972).

T. Wolfram and R.E. DeWames, Phys. Rev. **185**, 762 (1969).

D.N. Zubarev, Soviet Physics - Uspekhi **3**, 320 (1960).